AD-A183 776 THE TRANSITION FROM BRITTLE TO DUCTILE FAILURE IN POLYETHYLENES(U) PENNSYLVANIA UNIV PHILADELPHIA SCHOOL OF ENGINEERING AND APPLIED SCIENCE J L D'ONOFRIO 1/2

UNCLASSIFIED AUG 87 F/G 11/9 NL

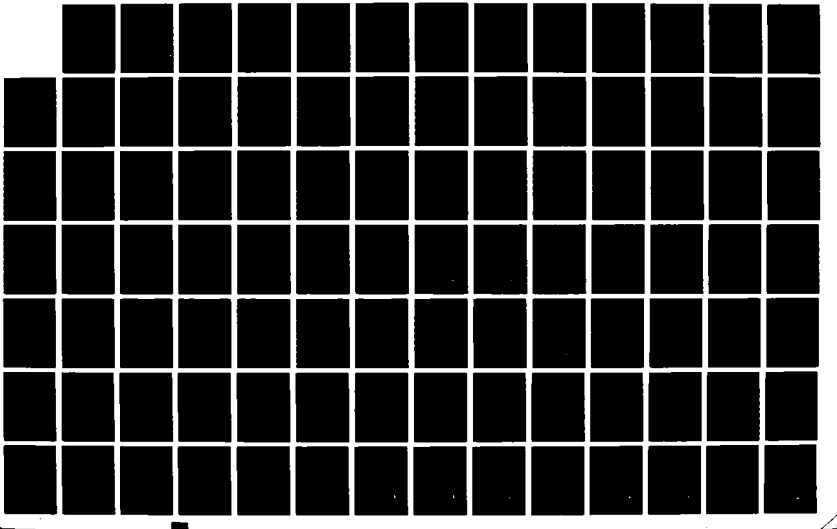

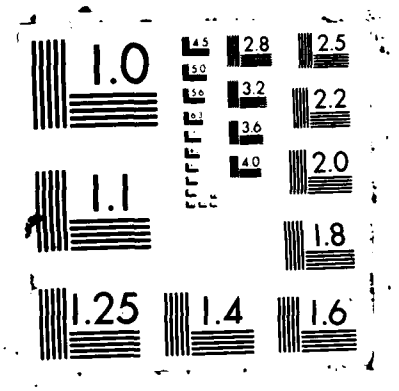
1.0
1.1
1.25
1.4
1.6
1.8
2.0
2.2
2.5
2.8
3.2
3.6
4.0
4.5
5.0
5.6
6.3

UNIVERSITY OF PENNSYLVANIA

SCHOOL OF ENIGINEERING AND APPLIED SCIENCE

THE TRANSITION FROM BRITTLE TO ~~DUTCILE~~ DUCTILE (Correct Spelling) FAILURE IN POLYETHELENE

John L. D'Onofrio

Philadelphia, Pennsylvania

August, 1987

A thesis presented to the Faculty of Enigineering and Applied Science of the University of Pennsylvania in partial fulfillment of the requirements for the degree of Master of Science for graduate work in Mechanical Engineering and Applied Mechanics.

John L. Bassani

Professor John L. Bassani, Thesis Advisor

Professor Norman Brown, Thesis Advisor

Noam Lior

Professor Noam Lior, Graduate Group Chairman

Abstract

The failure characteristics of polyethelene were studied at nominal stresses ranging from one half and up to the yield point, allowing observation of the transition from brittle to ductile failure.

Experiments were performed on Marlex 6006, a linear polyethelene and TR-418, a polyethelene pipe material, exposing single edge notched specimens to plane strain tension. The variable parameters were nominal stress, notch depth and temperature.

The results of the experiments were analyzed both quantitatively by measurement and qualitatively by electron microscope studies. The quantitative data was analyzed and a relationship developed to describe the creep of both materials between initial loading and ultimate failure.

Acknowledgement

The author would like to thank Professor John L. Bassani for his patient advice and assistance in the preparation of this thesis and Professor Norman Brown for his advice, for sharing his expert knowledge in the fields of Polymer Science and experimentation, and for the countless hours spent in his laboratory.

The author would also like to thank Professor Martin Lesser, Professor Ira M. Cohen, and Xici Lu* for their encouragement, confidence, and support, and N. T. Brown for his technical assistance and enthusiasm.

Thanks are also expressed to the United States Navy and the Civil Engineer Corps for the opportunity to pursue a Masters Degree at the University of Pennsylvania and to the Gas Reasearch Institiute for their support of research in this field.

** Visiting scholar from the University of Science and Technology of China, Hefei, People's Republic of China*

Table of Contents

INTRODUCTION

The use of plastics as engineering materials is becoming more and more prevalent. The widespread use of polyethylene is one example. Polyethylene's molecular structure can be designed to provide specific material properties for use in a wide variety of applications. Polyethylene can be molded, drawn, machined, etc., allowing the economical manufacture of products and components traditionally made form more exspensive and difficult to work materials.

Because polyethylene is so versatile and economically advantageous it has been used in various engineering components before the properties of a given material have been fully characterized. One such example is the substitution of polyethylene for iron in the manufacture of pipe for natural gas distribution systems. As a result, municipal gas distribution systems are being installed using polyethylene pipe even though the life of the pipe can not be accurately predicted. Not having the knowledge of when to replace polyethylene pipe before leaks due to systemic material failures begin can have catastrophic consequences. The focus of this thesis is to study the evolution of notch-tip damage to failure of two polyethylenes associated with pipe manufacture, at various stress levels characterizing the competition between brittle and ductile modes of failure. This work extends earlier studies [1,2,3] and particularly those of N. Brown (of the University of Pennsylvania's Material Sciences Department with the support of the Gas Research Institute) [4,5,6,7] that investigate the

mechanisms of failure in polyethylene under stress.

Extensive research on polyethylene failure at low stress levels (below one half the yield point) which normally lead to brittle failure has previously been carried out [4,5,6,7]. This thesis investigates the failure behavior of polyethylene as the stress is increased, approaching the yield point where failure is in the ductile mode. The mechanical behavior of polyethylene is explored as the transition from brittle failure to ductile failure occurs. The behavior of both Marlex 6006, used in previous work [4,5,6,7], and TR 418 a typical gas pipe material is studied.

Owing to the significance of polyethylene as an engineering material, the mechanisms of its failure have been the subject of extensive study. Crissman and Zapas [1] researched creep failure and fracture of polyethylene in uniaxial extension and categorized its ultimate failure as one of three types: by the fracture through a mechansim of crack formation and crack growth, extensive necking and immediate failure, and substantial elongation and eventual fracture. The type of failure observed was found to depend on applied load, temperature, molecular architecture, and environment. The brittle type failure was associated with small initial loadings with the amount of creep failure increasing with load until instantaneous necking and failure occurred.

Hin and Cherry [2] continued with the exploration of creep rupture and pre-rupture phenomenon in linear polyethylene and categorized this behavior in a manner similar to Crissman and Zapas [1]. They classified a Type C failure as a brittle type failure in which neither macro-necking nor tertiary creep occurred and

a Type B failure as one in which some tertiary creep occurred but was otherwise brittle in nature. Types A1 and A2 ruptures occurred just before macro-necking with A2 having the appearance of brittle fracture and A1 being undefinable as a result of cold-drawing the specimen. The type of failure was found to depend on stress similar to the findings of Crissman and Zapas [1].

Chan and Williams [3] studied slow stable crack growth in high density polyethylene. They categorized the mechanisms of brittle failure as being divided into four distinct stages: an incubation period, a period of unsteady crack growth, crack growth, and final instability. They applied fracture mechanics concepts to this type of failure and established a critical stress intensity factor as the controlling factor for crack growth.

Bhattacharya and Brown [4] investigated the micromechanisms of crack initiation in polyethylene (Marlex 6006). They determined that macroscopic crack initiation in polyethylene under plane strain was characterized by a generation of porosity, an increase in the size of the pores, fibrillation and finally, fibril fracture. A method for notching specimens to an accurate depth with no visible damage at the notch tip was developed during this work.

Bhattacharya and Brown [5] continued their research with the study of crack growth in linear polyethylene (Marlex 6006). Single edge notched specimens were examined under plane strain conditions. The microstructure of the damaged zone was found to consist of a porous region around the crack tip, a fibrillated region, a fractured region, and the original notch. It was also found that the initial damage zone grew at a constant velocity which depended on stress.

Bhattacharya and Brown [6] continued with the study of slow crack growth for polyethylene under single edge notch, plane strain tension. The kinetics for the initiation of crack growth were found to begin with an initial deformation which occurs instantly upon loading. A deformation zone then grows at a constant velocity which depends upon stress until fibril fracture occurs, the deformation zone begins to accelerate, and crack growth is initiated. It was also determined that the instantaneous deformation upon initial loading agreed favorably with the time independent Dugdale model.

Lu and Brown [7] explored the relationship of the initiation stage to the rate of slow crack growth in polyethylene. For the first time a relationship was developed that allowed a prediction of the time to ultimate failure from the initial conditions. Another important development of this research was the realization that the length of the damage zone could be determined from measurements of the notch opening, i.e., the relationship between the two is in direct proportion. Now experimental measurements could be taken on the same specimen throughout the failure process allowing for more reliable data. Prior to this, a new sample had to be tested for each time interval from initial loading introducing the added error of a change of specimens.

This project provides for a continuation of earlier research [4,5,6,7] by studying the characteristics of the failure of polyethylene exposed to stress levels from about one half and up to the yield point. In order to provide a continuity in results, experiments were conducted on Marlex 6006, the same material used in previous research [4,5,6,7]. Also studied was TR 418, a branched polyethylene,

typical of the material used in the actual manufacture of gas pipe. Specimens were prepared in a fashion similar to the previous works [4,5,6,7] with the exception that a standard dumbbell shape was used. The specimen was subjected to an axial load in a beam type creep machine placed in a temperature controlled environment. The experimental parameters that were varied were stress, notch depth, temperature, and material. Quantitative measurements were made with an optical microscope fitted with a filar objective, a strain guage extensometer, a thermocouple, timer, and a digital data collector. Specimens were sacrificed and viewed under an electron microscope to allow for qualitative evaluation of the damage zone.

MATERIAL

Pipe manufactured for use in the gas distribution industry is normally made form polyethylene having a branched molecule to allow for toughness. Its molecular design enables it to resist the brittle type failure associated with low stress. Time to failure, even in accelerated conditions amounts to months or even years.

In order to accomplish meaningful research in a reasonable time scale, polyethylene with a linear, non-branched molecule was chosen as the experimental material. Marlex 6006 was used in previous research [4,5,6,7] and for compatibility of data was the material of choice for this work. Individual experiments with Marlex 6006 could be accomplished on a time scale of one day. Additionaly, the molecule being simpler in design is more basic in its mechanical and material properties. It is hoped that the analysis of experiments performed on Marlex 6006 will lead to relationships that can later be extended to actual pipe materials or at very minimum give some insight into their behavior.

The polyethylene, Marlex 6006, is an unpigmented, low additive, linear, commercial resin supplied by the Phillips Petroleum Company. The material was provided in 4 mm thick plaques which were compression molded in accordance with ASTM D1928 and slow cooled from the melt at about 15° C per minute. Marlex 6006 has a density of 964 kgm per m^3, a melt index of 0.75, M_w = 130,000 and M_n = 19,600. Marlex 6006 has a yield point of approximately 25 mpa at 300° K and a strain rate of .02 inches per minute.

In order to gain some insight into the behavior of actual pipe matenal experiments were also conducted on TR 418, a pigmented polyethylene with branched molecules (ethylene-hexene copolymer) produced by Phillips Petroleum. TR 418 is used commercialy in the manufacture of gas pipe and was chosen as the standard pipe material for research purposes at the Workshop on Selection of Standard Piping Materials. [8] It was supplied compression molded in 4 mm thick plaques. TR 418 has a density of 950 kgm per m^3 , a melt index of 0.2, M_w = 150,000 - 200,000, and M_n = 15,000 - 20,000. Tr 418 has a yield point of approximately 13.5 mpa at 300°K and a strain rate of .02 inches per minute.

SPECIMEN DESIGN AND PREPARATION

Since the stress levels to be studied in this work are substantially higher than in the previous works [4,5,6,7], the standard dumbbell shape was the chosen design for the experimental specimens. This shape allows for the isolation of stresses imposed by the experimental apparatus (particularly the creep machine grips). The actual size of the specimen was mostly controlled by the equipment available in the laboratory and the dimensions of the material as supplied by Phillips Petroleum.

Figure (1) presents the design and the approximate dimensions of the specimen. The thickness is approximately 4 mm which was limited by the thickness of the plaques as supplied. A guage length of .5 in was chosen to match the limits of the strain guage extensometer. The specimen width varied between 10 - 11 mm, the maximum width attainable on the specimen router. The width was maximized to ensure that the plane stress conditions which are experienced at the sides of the specimen while under test were negligible across the length of the notch. The overall height of approximately 60 mm was again controlled by the jig used in the specimen router. The specimens were single edge notched to various depths in the center of the gauge length. Notwithstanding the constraints imposed on the specimen design by circumstance, the design was deemed appropriate as the low stress data obtained correlates well with previous work [4,5,6,7].

The plaques as supplied were cut to approximate size on a table saw. The blanks were than milled to the size required by the specimen router on an

industrial milling machine. This step removed and damage caused by the rough cut of the table saw and provided an accurately square blank for routing. The blanks were then machined into a standard dumbbell with a .5 in guage length on the specimen router.

Notching was accomplished on a new piece of apparatus. The new notching machine was constructed from an Instron tensile testing machine fitted with a special jigs to hold the cutting edge (razor blade) and to accurately align the specimen. A head speed of .02 mm per minute was used which was slow enough to notch the specimen and not cause significant damage around the notch tip [4,5,6,7]. To ensure a sharp cutting edge, a fresh razor blade was used for each specimen. Notches were checked for alignment with the specimen face by viewing the depth at the edges with an optical microscope fitted with a filar objective. Several specimens were sacrificed in order to check the accuracy of this method.

Specimens were not polished as done by Hin and Cherry [2] since the possibility on failure initiation due to a surface defect was negligible with the introduction of the stress concentration imposed by the notch.

Experimental

The experimental setup (Figure 2) consisted of a creep machine thermally isolated by an insulated enclosure. The creep machine applied an axial load to the specimen through a lever mechanism with a five to one advantage. The specimen was installed in grips using a jig that prevented movement in order to avoid pre-stressing the specimen and to provide accurate alignment . The strain guage extensometer was installed with its knife edges along the thickness of the guage length. The initial distance between the knife edges was measured to provide an accurate initial guage length. The grips were installed in the creep machine on pin joints to avoid constraint in the application of the load. A pre-load of .5 lbs was applied to the specimen to remove any slack in the setup. Once the specimen was installed in the machine the thermal barrier was sealed and the specimen allowed to stabilize at the experimental temperature for at least 30 minutes. Heat was applied by a low wattage light bulb controlled by a thermocouple sensor and digital controller. Temperature was measured and recorded by a thermocouple attached to the digital controller. Initial measurements were taken of the notch opening using an optical microscope fitted with a filar objective.

The weights necessary to provide the experimental load were placed on a platform supported by a screw jack. The load was released by smoothly lowering the jack. Measurements were taken a appropriate intervals for the time

scale of each experiment. Measurements of the crack opening displacement (COD) were made with an optical microscope fitted with a filar objective. The enlongation of the guage length was measured by the strain guage extensometer and recorded through the digital controller. Temperature and elapsed time were also recorded through the digital controller.

Experiments were ended when failure occurred. Failure was defined depending on the failure mechanism. For experiments where brittle fracture dominated failure occurred when the crack growth rate began to accelerate [4]. When ductile failure predominated failure was defined to have occurred when percent elongation of 10 - 12 percent was reached [9]. Neither elongation beyond 10 - 12 percent nor actual fracture could be allowed to occur in order to prevent damage to the strain guage extensometer.

An equipment listing is provided as Appendix (A)

EXPERIMENTAL RESULTS

Experiments on Marlex 6006 were conducted at 30° C for notch depths of .15, .25, and .40 millimeters at stress levels ranging from 10 through 22 megapascals. Experiments on TR 418 were conducted at 30° C for notch depths of .15, .25, and .40 millimeters at stress levels ranging form 9 through 13 megapascals. For TR 418 experiments were also conducted at 60° C and at a notch depth of .25 millimeters.

Measurements of the initial notch opening and the dynamic COD were taken with an optical microscope using a filar objective and recorded manually. Measurements of temperature were taken with a copper constantan thermocouple through a digital controller card installed in a micro-computer. The controller also provided the reference for the thermocouple measurements. The strain was measured with a strain guage extensometer through the digital controller. The controller also measured the elapsed time of the experiment. Readings of time, temperature, and elongation were recorded by the computer through the controller card. Data for COD was plotted vs time for the various stress levels and notch depths. Both standard and log-log plots were drawn for the percent elongation vs time for the various stress levels and notch depths.

Specimens were sliced on the same apparatus used for notching. The slices were installed in a jig that allowed the specimen to be re-opened to the COD seen at failure. The specimens were then viewed and photographed under

the electron microscope to allow for qualitative analysis.

CONCLUSIONS

The COD vs time curves for Marlex 6006 (Figures 3, 4, and 5) clearly demonstrate an increase in COD growth rate with increasing stress. The shape of the curves suggest that the growth of the COD is governed by different processes at low stresses levels (about one half the yield point) and high stress levels (approaching the yield point). At the lower stress levels the curves indicate a period of initial deformation on loading, followed by slow but steady growth, and finally accelerated growth leading to brittle failure. This behavior is similar to the COD behavior exhibited in the previous studies done on brittle failure of Marlex 6006 [4,5,6]. The high stress curves exhibit an initial deformation upon loading and an almost immediate and steady high COD growth rate. This growth is suspected to be primarily due to creep strain. At stress levels around the transition from brittle to ductile failure (Table 1), the curves exhibit both brittle and creep behavior culminating in brittle fracture below the transition stress and ductile failure above it.

The percent elongation vs time curves (Figures 6, 7, and 8) exhibit typical creep behavior for a linear polyethylene at the high stress levels. At the lower stress levels the behavior is that expected during creep, until a sudden acceleration in elongation takes place. The time of this acceleration coincides with the initiation of fracture on the COD vs time curves. This behavior is even more pronounced when the percent elongation vs time curves are plotted on log-log scales. (figures 9, 10, and 11)

Figures 12 through 17 compare COD vs time and percent elongation vs time at various notch depths for stresses of 12 and 20 mpa. The COD vs time curves for both the low and high stress levels show dependence on notch depth. The percent elongation vs time curves at 12 mpa show no notch dependence until the acceleration associated with brittle fracture is reached. At this point the notch dependence is similar to that of the COD vs time curves. The percent elongation curves at 20 mpa show no dependence for notch depths of .15 and .25 mm as expected since brittle failure does not occur. The curve for a notch depth of .40mm deviates after initial loading. At .40mm the notch depth approaches 10 percent of the material thickness so this notch dependence is likely due to a reduction in cross sectional area.

This data suggests that the failure behavior of a linear polyethylene such as Marlex 6006 is dependent on stress not only for rate but also for mechanism of failure. At the high stress levels failure is predominately ductile in nature. At the low stress levels the material does creep to some extent but the predominant failure mechanism is brittle fracture. As the transition stress is approached both mechanisms of failure are evident with brittle fracture dominant below the transition and ductile failure dominant above.

Figures 18 through 26 present electron microscopic studies for Marlex 6006 with a .15mm notch at 30° C for various stress levels (Please note: in order to obtain similar views of the damage zone magnifications are not all identical). At stresses of 12, 13, and 14 mpa the start of brittle failure is evident, that is, the start of fibril fracture, the growth of new fibrils, and the advancing of the damage

zone. The photographs at stresses of 15, 17, and 18 mpa indicate that the brittle fracture initiation process has begun as evident by the presence of fibrils but the process was halted with a general blunting of the crack tip resulting in slowed COD growth which is now limited to growth induced by creep. At stresses of 19, 20, and 22 mpa there is an immediate blunting of the notch tip with no evidence of fibril growth.

Figures 27 through 30 present electron microscopic studies for Marlex 6006 with a .25 mm notch at 30° C for various stress levels. For 12 and 13 mpa the beginning of brittle fracture is again evident. At 16 mpa there is evidence of fibril formation with blunting of the crack tip and at 18 mpa there is an initial blunting of the notch tip. The photographs for both the .15 and .25 mm notch depths indicate by the shape of the porous damaged area that the shape of the stress field changes from sharp to ballooned. The apparent gradual change in the shape of the stress field is supportative of the transition from brittle to ductile failure.

The electron microscopic studies provided qualitative support for the conclusions made by the analysis of the numerical data.

The COD curves for TR 418 (Figures 31, 32, 33, and 34) exhibit an increase in COD growth rate with increasing stress initially but as time increases the behavior becomes somewhat erratic. There are two possible explanations for the erratic COD growth. First, there is the possibility a mechanism inherrant in the material periodically releases, causing spurts of growth at the microscopic level. This has some validity at the molecular level as TR 418 is composed of branched

molecules which could allow slippage as the branches give way. The second explanation is that the data itself is somewhat faulty. Figure 35 shows the view of the crack tip as seen through the optical microscope during an experimental run with Marlex 6006. The edges of the crack opening are very straight and distinct. Figures 36a and 36b are similar views of TR 418. The edges of the crack opening become more and more deformed with time until it became very difficult to take consistent COD readings. Figures 37a and 37b show the surface of a typical crack front for TR 418 as viewed through the electron microscope. The striations and grooves that form distort the crack edges until the edges become obscure making accurate measurements of COD extremely difficult. Although the second hypothesis is more likely not enough experimentation was done to validate it. Therefore the COD vs time curves for TR 418 were not smoothed as were those for Marlex 6006.

The TR 418 curves at stress levels approaching the yield point exhibit a continuous COD growth rate that decreases slightly with time. This growth pattern suggests that the material is experiencing creep failure. At low stress levels the COD growth almost levels off suggesting that the brittle fracture if any has been arrested and that deformation is primarily by creep. It was hoped that by increasing the temperature that the time scale of the experiments could be reduced but temperature increase only resulted in lowering the yield point with the same results as seen at the lower temperatures with the exception that the experimental stress levels were now lower.

The percent elongation vs time curves for TR 418 are presented as

figures 38 through 41. The rate of elongation decreases with decreasing stress and also decreases with time. These curves are similar to those expected of a strain hardening polymer. The TR 418 percent elongation vs time curves are also presented on log-log scales (Figures 42 through 45).

Although brittle fracture was never realized during the TR 418 experiments, there was a transition from creep predominated failure to at least the initiation state of brittle fracture as the stress was lowered. The transition stress levels for TR 418 are presented as Table 2.

Figures 46, 47, and 48 compare the TR 418 COD curves for various notch depths at stresses of 10, 11, and 13 mpa and a temperature of 30° C. At 10 and 11 mpa there is a definite notch dependence but not at 13 mpa. This indicates that a brittle fracture process is occurring at the lower stress levels.

Figures 49, 50, and 51 compare the TR 418 percent elongation vs time curves for the same conditions and Figures 52, 53, and 54 present these on a log-log scale. At stresses of 10 and 11 mpa there is little dependence on notch depth. At 13 mpa there appears to be some notch dependence which is seen only upon initial loading. This suggests that the elongation of the specimen is only being affected by creep and not the brittle fracture process.

The electron microscopic studies for TR 418 at a notch depth of .25 mm are presented figures 55 through 58. All of the crack tips are blunted even at the low stress levels but there is a damage zone in front of the crack tip that seems to behave in a fashion similar to the crack tip in Marlex 6006. FIgures 59 through 62 present the same views at a higher magnification. Some porosity is exhibited at

all stress levels but it is greater at the lower stresses. The damage zone gets longer and sharper as the stress level decreases and there actually seems to be a blunting in the damage zone at 11 mpa, which is above the transition stress. This indicates that even though the brittle fracture process did not appear as that seen in Marlex 6006, there is some damage process advancing through the material at the lower stress levels.

Figures 63 through 66 present views of TR 418 with a notch depth of .40 mm at stresses of 10.5 and 11 mpa, which are above and below the suspected transition stress. As a second blunted crack front appears within the original blunted crack. The shape of this crack front, though, is similar to that exhibited by fatigue crack growth [10] which probably occurred when the specimen was re-opened to its original COD.

Analyzing the percent elongation vs time curves plotted on log-log scales for Marlex 6006 (Figures 9, 10, and 11) a straight line can be used to approximate the portion of the curve where creep is evident, i.e., between initial loading and ultimate failure. This phenomenon can be represented by the expression

$$\text{Log}\,(\%E) = \text{Log}\,(A) + m\,\text{Log}\,(t) \qquad (1)$$

or

$$\%E = A\,t^{m} \qquad (2)$$

where A and m are constants for a given set of experimental conditions. Tables 3, 4, and 5 present the values of A and m for the various stress levels at notch depths

of .15, .25, and .40 mm respectively. This data is presented graphically as figures 67, 68, and 69.

It is obvious that A depends considerably on stress and that m exhibits slight stress dependence. Comparing the values of A and m for the various notch sizes (Figure 70) shows that neither A nor m depend on notch depth. This again supports the assumption that the elongation of the specimen prior to failure is due primarily to a creep mechanism and not the brittle fracture process until actual fracture occurs, i.e., acceleration.

Equation (2) is plotted against the experimental data in Appendix (B) and demonstrates a good approximation for the creep behavior until failure either by brittle fracture or necking occurs.

Analyzing the stress dependence of A by geometric linear regression gives a relation of the form

$$A = B \sigma^{n} \quad (3)$$

Where B and n are constants for a given set of experimental conditions. The values for B and n are presented as Table 6. Since A and m do not depend on notch depth the analysis was also performed on the combined values at all notch depths.

The relation for percent elongation now becomes

$$\%E = b\,\sigma^{n} t^{m} \quad (4)$$

which can be written as

$$\%E = f_1(\sigma)\, f_2(t) \quad (5)$$

where f_1 can be considered a strain rate dependent term and f_2 a time dependent term.

The creep rate of metals and some polycrystaline materials can often be represented by the Dorn - Weertman relation [11]:

$$E = C\,\sigma^{n} e^{(-Q_f/RT)} \quad (6)$$

where E is the strain rate, C is a constant, Q_f is an activation energy for flow, R is the universal gas constant, and T is absolute temperature. Infact, Clements [12] applied just such a relationship to the creep of Marlex 6009:

$$E = C\,(\sigma / x)^{n} e^{(-Q_f/RT)} \quad (7)$$

where x is a factor representing the temperature dependence of the molecular structure or

$$E = C\,(\sigma / \sigma_c)^{n} e^{(-Q_f/RT)} \quad (8)$$

where (σ / σ_c) represents the structure compensated stress. Since the temperature is a constant for this study equation (8) can be reduced to the form

$$E = B \sigma^n \quad (9)$$

where

$$B = C' e^{(-Q_1 / RT)} = \text{a constant} \quad (10)$$

which is similar to the f_1 term in equation (5).

Since the m dependence on stress appears to be linear, linear least squares approximation was used to analyze the stress dependence of m yielding the relation:

$$m = m_1 + m_2 \sigma \quad (11)$$

where m_1 and m_2 are constants for a given set of experimental conditions. The values for m_1 and m_2 are presented as Table 7. Again a combined value was calculated. Combining equations gives the relation:

$$\%E = B \sigma^n t^{(m_1 + m_2 \sigma)} \quad (12)$$

for elongation of the Marlex 6006 specimens due to creep. Comparisons of

equation (2), equation (12) using the combined values for the constants, and the original data are presented in Appendix (B).

Analyzing the percent elongation curves plotted on log-log scales for TR 418 (Figures 42, 43, 44, and 45) a straight line can again be used to approximate the portion of the curve between initial loading and ultimate failure giving a relationship for creep. Equation (2)

$$\%E = A\,t^{m} \qquad (2)$$

can also be used to represent this relation. A and m are again constants for a given set of experimental conditions and are presented as Tables 8, 9, 10, and 11 and graphically as Figures 71, 72, 73, and 74. Again A is seen to depend considerably on stress with a slight stress dependence being shown for m. Comparing data for A and m at the various notch depths (Figure 75) supports an independence form notch depth.

Equation (2) is plotted against the experimental data for TR 418 in Appendix (B) exhibiting a good approximation for the creep behavior portion of the curves.

Using geometric linear regression again provides the relation

$$A = B\,\sigma^{n} \qquad (3)$$

B and n being constant for a given set of initial conditions. These values are

presented as Table 12.

The relation for percent elongation again becomes

$$\%E = B\,\sigma^{n} t^{m} \qquad (4)$$

Linear least squares approximation was used to analyze the stress dependence of m with good results for notch depths of .15 and .25 mm and fair results for .4 mm and the combined value. These results are given in Table 13. Equation (12)

$$\%E = B\,\sigma^{n} t^{(m_1 + m_2 \sigma)} \qquad (12)$$

therefore, can also be applied to TR 418.

Comparisons of equation (2), equation (12) using the combined values for the constants at 30° C, and the experimental data for TR 418 are presented in Appendix (B).

The reader must be cautioned that equations (2) and (12) do not represent the behavior of either material once yield (necking) has begun and can not therefore be used to accurately predict time to failure. It is at the beginning of ultimate failure that they deviate from the experimental data. More importantly however, they do give insight into the component of creep that influences data developed in previous brittle fracture experiments[5,6,7]. The ability to use equations (2) and (12) to represent both Marlex 6006 and TR 418 demonstrating

that there is some validity to extending some of the findings in studies of Marlex 6006 to TR 418 is also of value. Also noted is the time scale of the TR 418 experiments at medium stress levels which indicates that brittle fracture experiments on this material will require a time scale several orders of magnitude higher than those performed on Marlex 6006.

Two areas limit the usefulness of the data presented in this thesis. First , no tests were done on un-notched specimens which would have provided additional support to the independence of the creep mechanism from notch depth. Secondly, due to the time scale of the experiments it was not possible to perform the experiments a number of times to ensure repeatablity.

SUMMARY

The creep behavior of Marlex 6006 and TR 418 can be described by a power law formula similar to the Dorn-Weertman relation for metals, with power-law strain hardening.

The creep behavior of Marlex 6006 and TR-418 are similar providing evidence that some research done on Marlex 6006 can be applied to a pipe material such as TR 418.

COD and percent elongation curves for Marlex 6006 and TR 418 indicate different failure mechanisms above and below a transition stress. Below the transition stress, brittle fracture is the dominant failure mechansim; ductile failure is dominant above it.

The crack initiation and growth process of TR 418 is much more complex than that of Marlex 6006. The hardening of the material blunts and arrests crack growth making it ideal for pipe manufacture.

REFERENCES

1. J. M. Crissman and L. J. Zapas, CREEP FAILURE AND FRACTURE OF POLYETHYLENE IN UNIAXIAL EXTENSION, *Polym. Eng. Sci.*, Vol. 19, No. 2, pp 99-103, 1979

2. Teoh Swee Hin and B. W. Cherry, CREEP RUPTURE OF A LINEAR POLYETHYLENE: 1. RUPTURE AND PRE-RUPTURE PHENOMENA, *Polymer*, Vol. 25, pp 727-734, May 1984

3. M. K. V. Chan and J. G. Williams, SLOW STABLE CRACK GROWTH IN HIGH DENSITY POLYETHYLENES, *Polymer*, Vol. 24, pp 234-244, Feb 1983

4. Swapan K. Bhattacharya and Norman Brown, MICROMECHANISMS OF CRACK INITIATION IN THIN FILMS AND THICK SECTIONS OF POLYETHYLENE, *J. Matr. Sci.*, Vol. 19, pp 2519-2532, 1984

5. Swapan K. Bhattacharya and Norman Brown, THE INITIATION OF CRACK GROWTH IN LINEAR POLYETHYLENE, Dept. of Mat. Sci., University of Pennsylvania

6. Swapan K. Bhattacharya and Norman Brown, THE INITIATION OF SLOW CRACK GROWTH IN LINEAR POLYETHYLENE UNDER SINGLE EDGE TENSION AND PLANE STRAIN, Dept. of Mat. Sci., University of Pennsylvania

7. Xici Lu and Norman Brown, THE RELATIONSHIP OF THE INITIATION STAGE TO THE RATE OF SLOW CRACK GROWTH IN LINEAR POLYETHYLENE, Dept. of Mat. Sci., University of Pennsylvania

8. J. M. Crissman, REFERENCE POLYETHYLENE RESINS AND PIPING MATERIALS, *Workshop on Selection of Standard polyethylene Piping Materials*, National Bureau of Standards, Sep 1983

9. L. J. Zapas and J. M. Crissman, AN INSTABILITY LEADING TO FAILURE OF POLYETHYLENE IN UNIAXIAL CREEP, *Polym. Eng. Sci.*, Vol. 19, No. 2, pp 104-107, 1979

10. David Broek, ELEMENTARY ENGINEERING FRACTURE MECHANICS, 3rd Revised Edition, *Matinus Nijhoff Pub.*, Sec 2.4, 1984

11. H. W. Hayden, William G. Moffatt, and John Wulf, THE STRUCTURE AND PROPERTIES OF MATERIALS, VOLUME III, *John Wiley & Sons*, Sec 6.8, 1965

12. Linda L. Clements and Oleg D. Sherby, STRAIN - RATE / TEMPERATURE BEHAVIOR OF HIGH DENSITY POLYETHYLENE IN COMPRESSION, *Ames Research Center Tech. Memorandum*, NASA TM-78544

Appendix A

Equipment Listing

Specimen Router	TensilcuT
Notching Machine	Custom built in Professor Brown's Laboratory
Creep Machine	Custom built in Professor Brown's Laboratory
Strain Guage Extensometer	Instron G-51-16
Transducer-Amplifier	Daytronic Model 300D
Microscope	Bauch & Lomb, modified
Objective	Bauch & Lomb Filar Micrometer Model 31-16-50
Temperature Controller	RFL Industries Model 70A
Thermocouple	Iron-Constantan (Type J)
Controller Board	Omega WB-A10-B White Box
Computer	IBM PC-XT

Appendix B

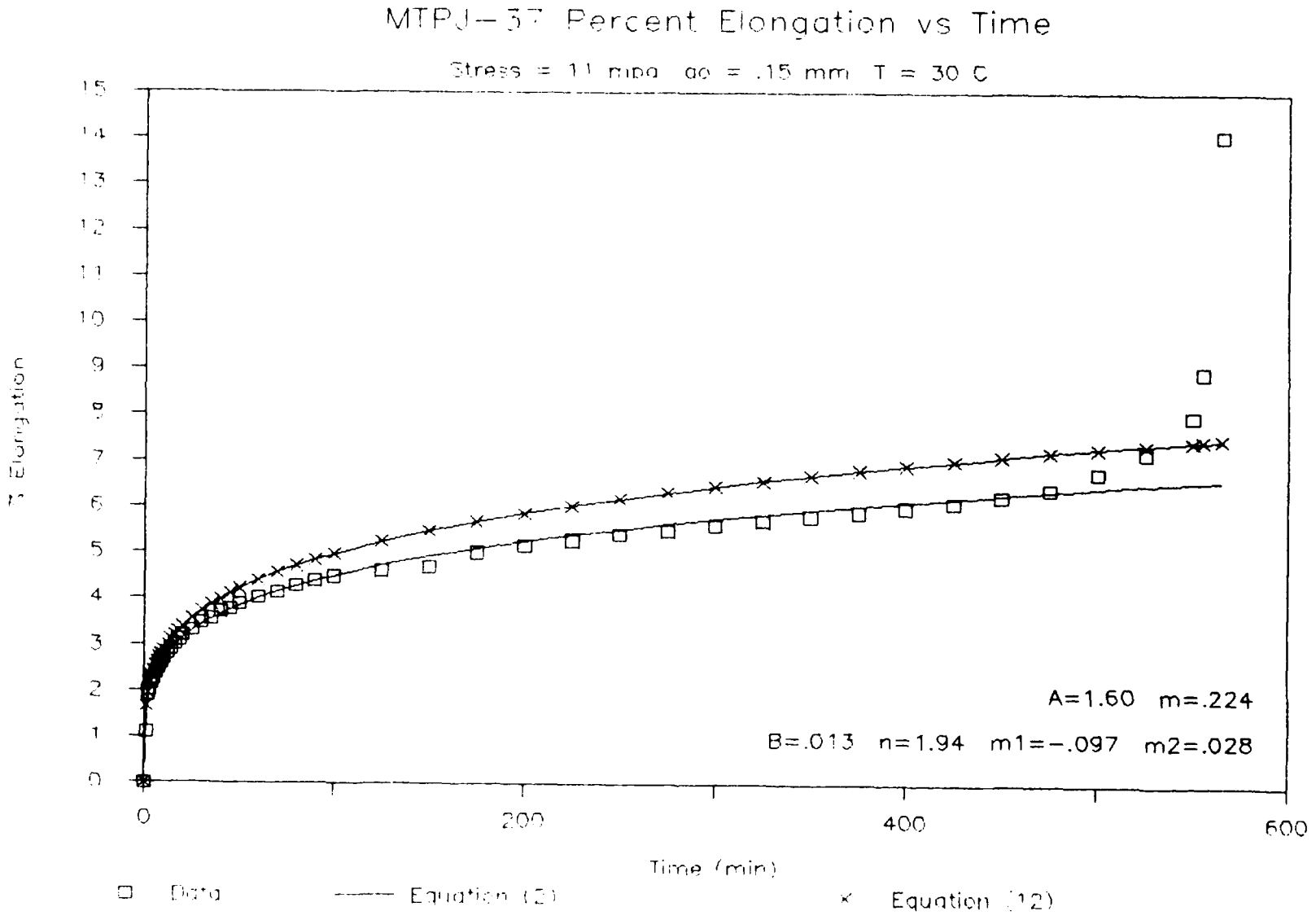
MTPJ-37 Percent Elongation vs Time
Stress = 11 mpa ao = .15 mm T = 30 C
% Elongation
0
1
2
3
4
5
6
7
8
9
10
11
12
13
14
15
0
200
400
600
Time (min)
A=1.60 m=.224
B=.013 n=1.94 m1=-.097 m2=.028
Data
Equation (2)
Equation (12)

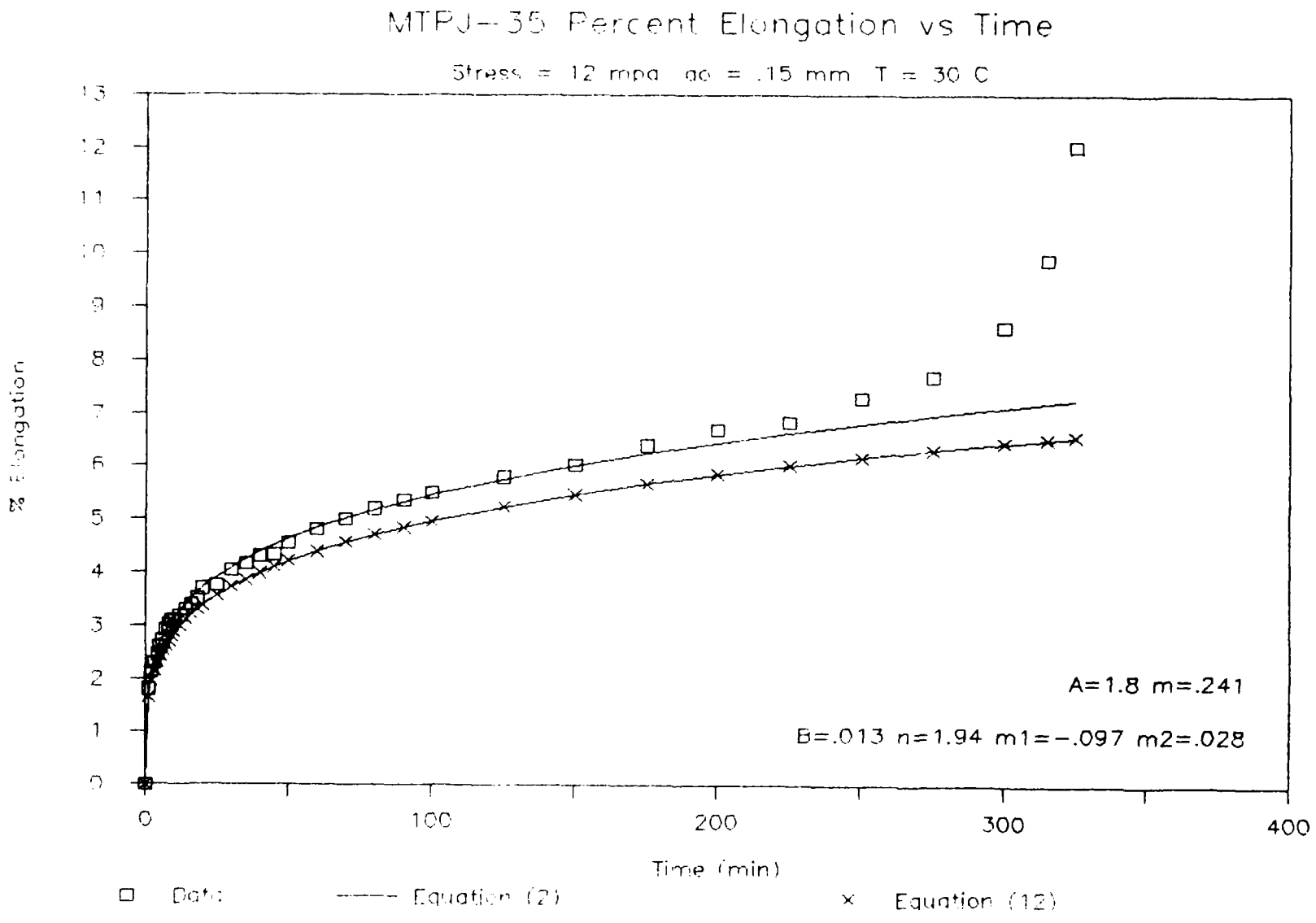
MTPJ-35 Percent Elongation vs Time
Stress = 12 mpa ao = .15 mm T = 30 C
% Elongation
Time (min)
0
100
200
300
400
A=1.8 m=.241
B=.013 n=1.94 m1=-.097 m2=.028
Data
Equation (2)
Equation (12)

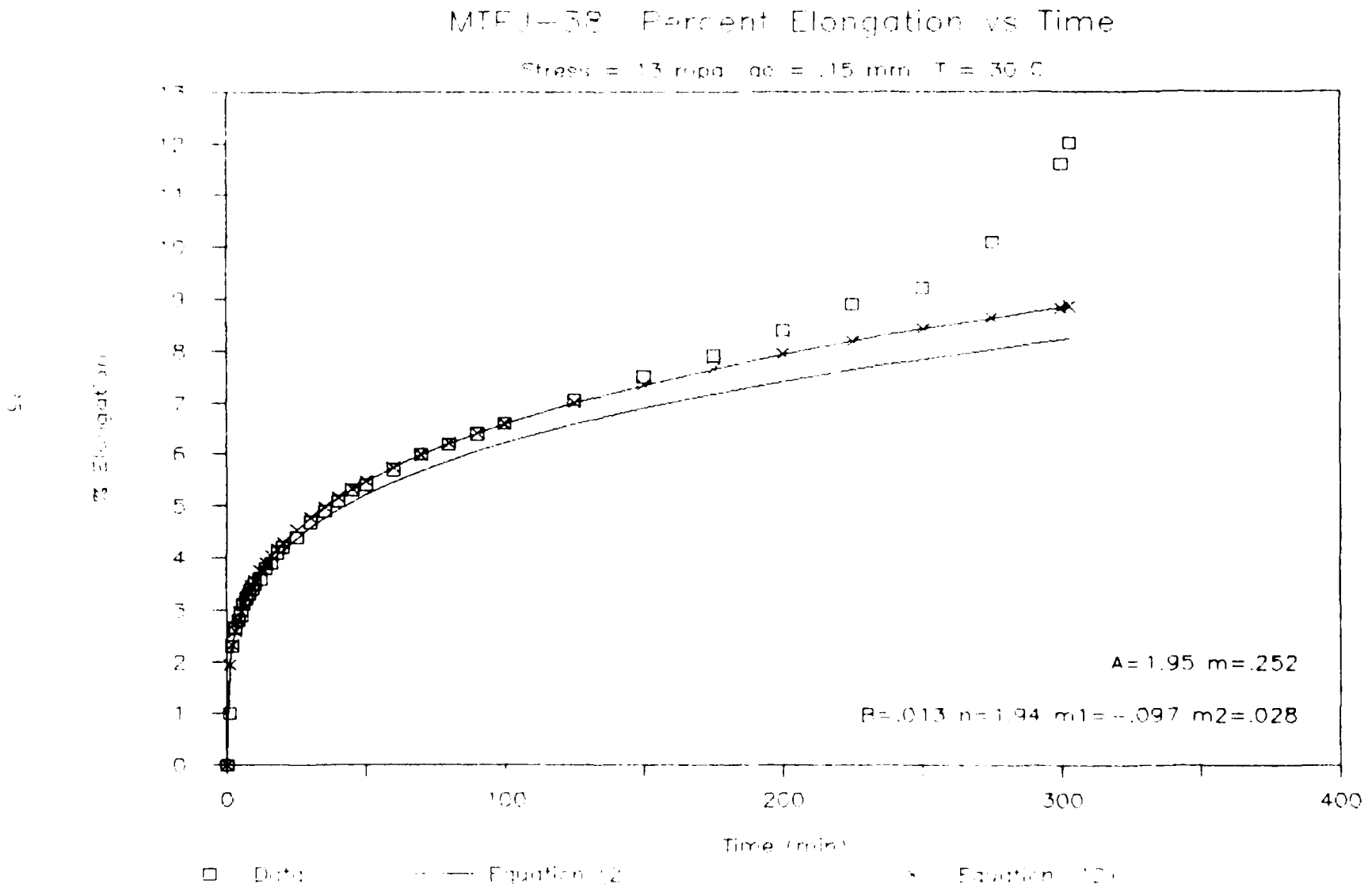
MTF J-38 Percent Elongation vs Time
Stress = 13 mpa ao = .15 mm T = 30 C
% Elongation
0
1
2
3
4
5
6
7
8
9
10
11
12
13
0
100
200
300
400
Time (min)
A=1.95 m=.252
B=.013 n=1.94 m1=-.097 m2=.028
Data
Equation (2)
Equation (3)

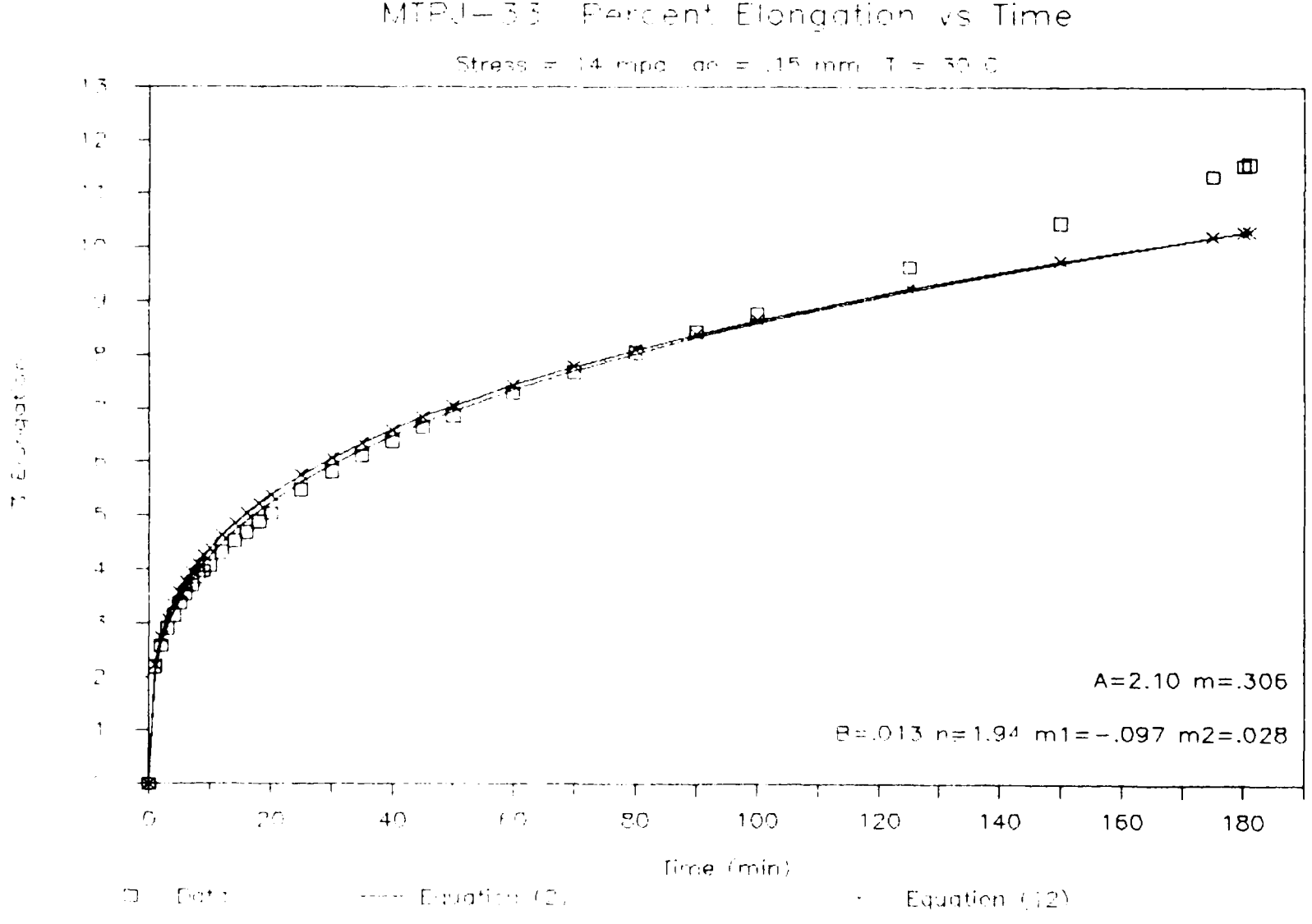
MTPJ-33 Percent Elongation vs Time
Stress = 14 mpa dc = .15 mm T = 30 C
A=2.10 m=.306
B=.013 n=1.94 m1=-.097 m2=.028
0
20
40
60
80
100
120
140
160
180
Time (min)
Data
Equation (2)
Equation (12)

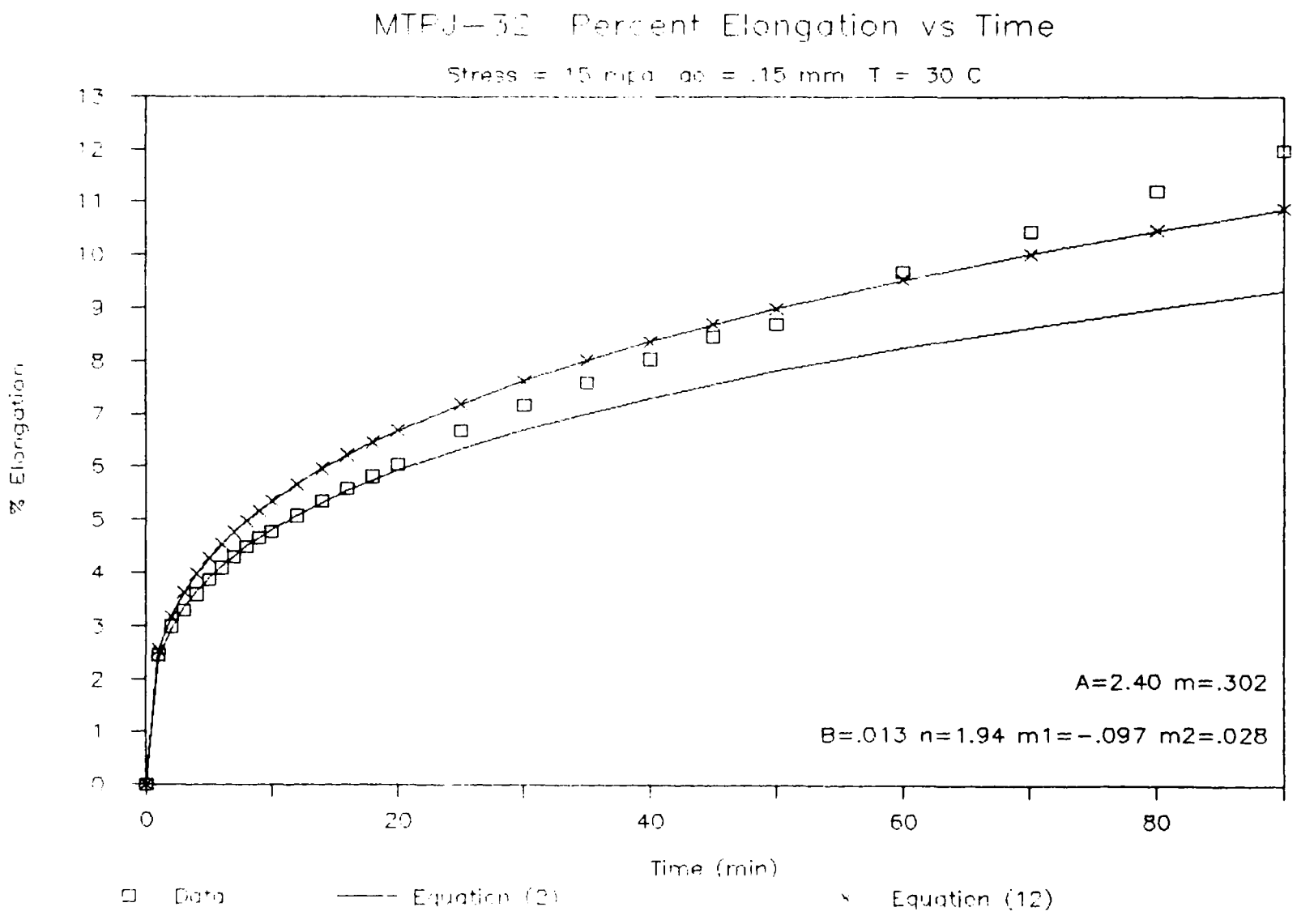
MTPJ-3E Percent Elongation vs Time
Stress = 15 mpa ao = .15 mm T = 30 C
% Elongation
0
1
2
3
4
5
6
7
8
9
10
11
12
13
0
20
40
60
80
Time (min)
A=2.40 m=.302
B=.013 n=1.94 m1=-.097 m2=.028
Data
Equation (2)
Equation (12)

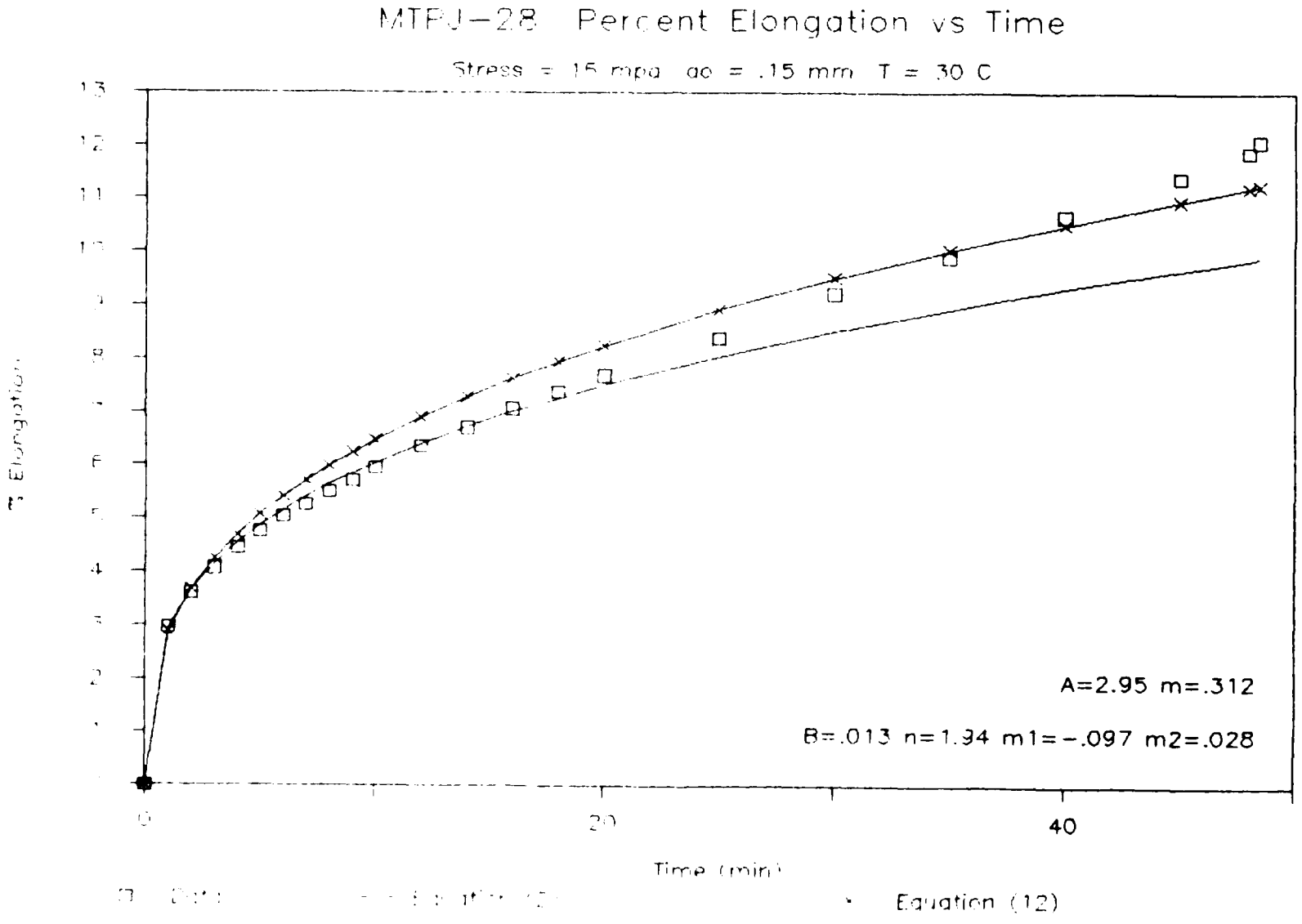
MTPJ-28 Percent Elongation vs Time
Stress = 15 mpa ao = .15 mm T = 30 C
% Elongation
Time (min)
A=2.95 m=.312
B=.013 n=1.94 m1=-.097 m2=.028
40
Equation (12)

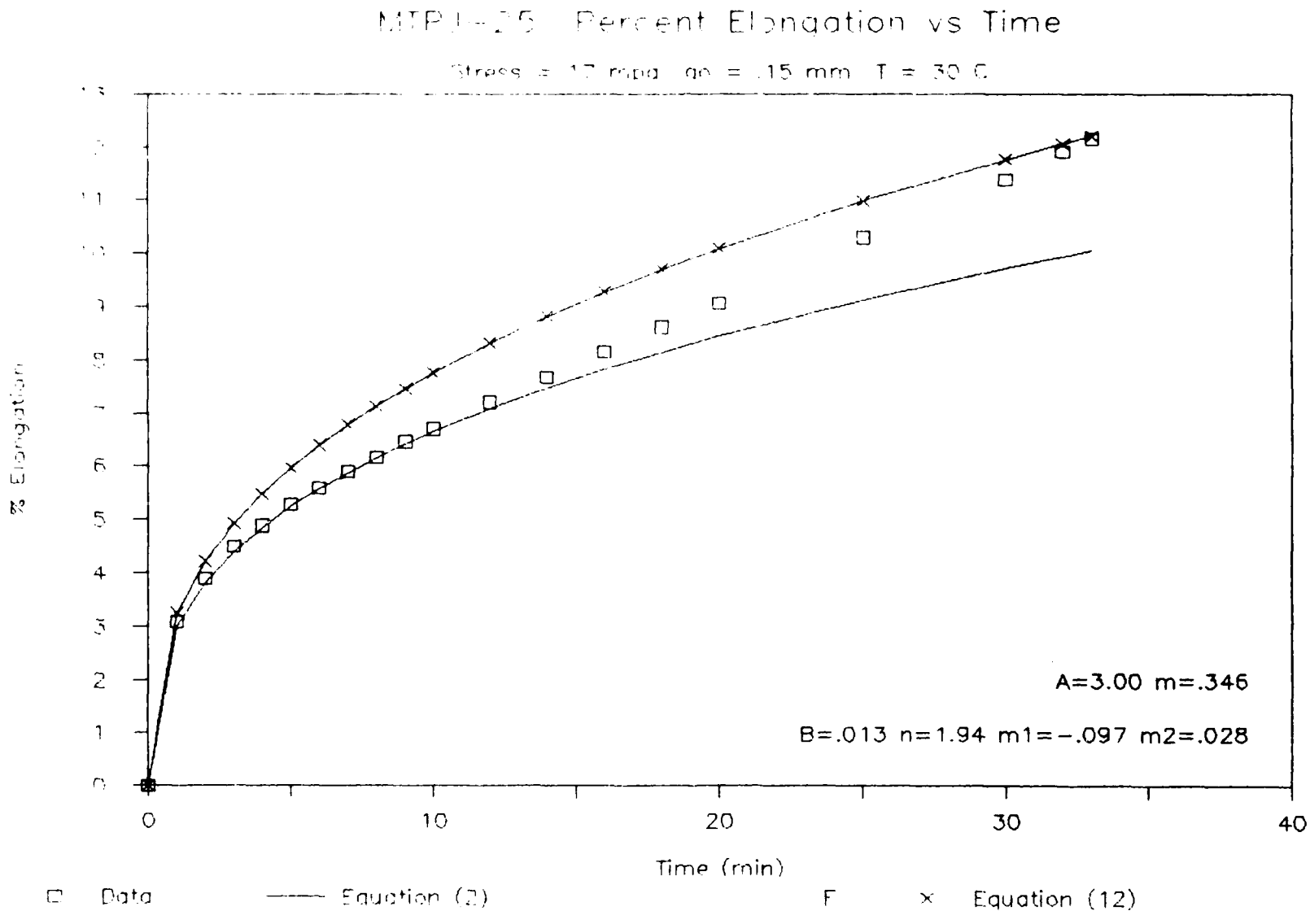
MTPL-25 Percent Elongation vs Time
Stress = 17 mpa go = .15 mm T = 30 C
% Elongation
0
1
2
3
4
5
0
10
20
30
40
Time (min)
A=3.00 m=.346
B=.013 n=1.94 m1=-.097 m2=.028
Data
Equation (2)
F
Equation (12)

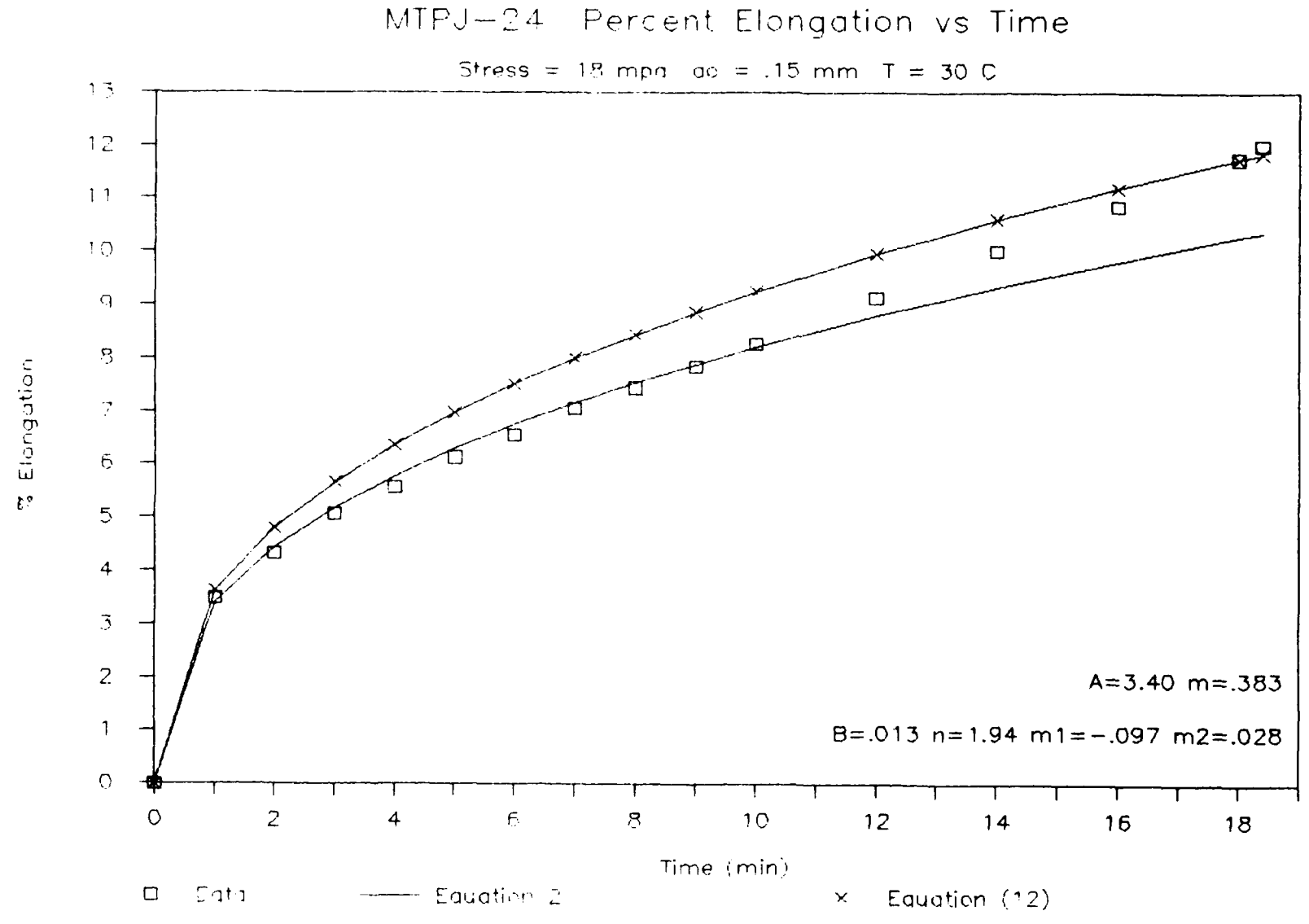
MTPJ-24 Percent Elongation vs Time
Stress = 18 mpa ao = .15 mm T = 30 C
% Elongation
Time (min)
A=3.40 m=.383
B=.013 n=1.94 m1=-.097 m2=.028
Data
Equation 2
Equation (12)

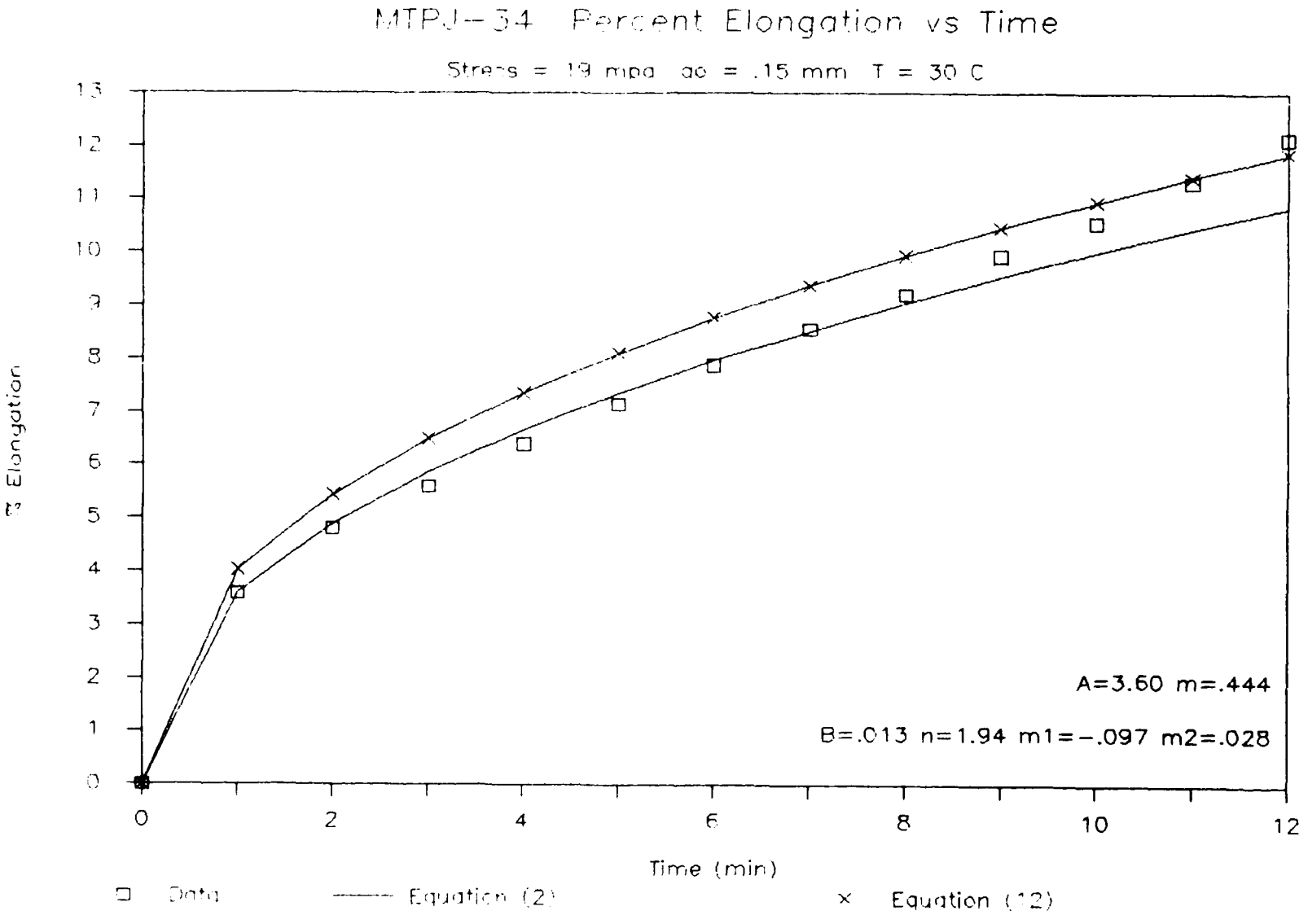
MTPJ-34 Percent Elongation vs Time
Stress = 19 mpa ao = .15 mm T = 30 C
% Elongation
Time (min)
A=3.60 m=.444
B=.013 n=1.94 m1=-.097 m2=.028
Data
Equation (2)
Equation (12)

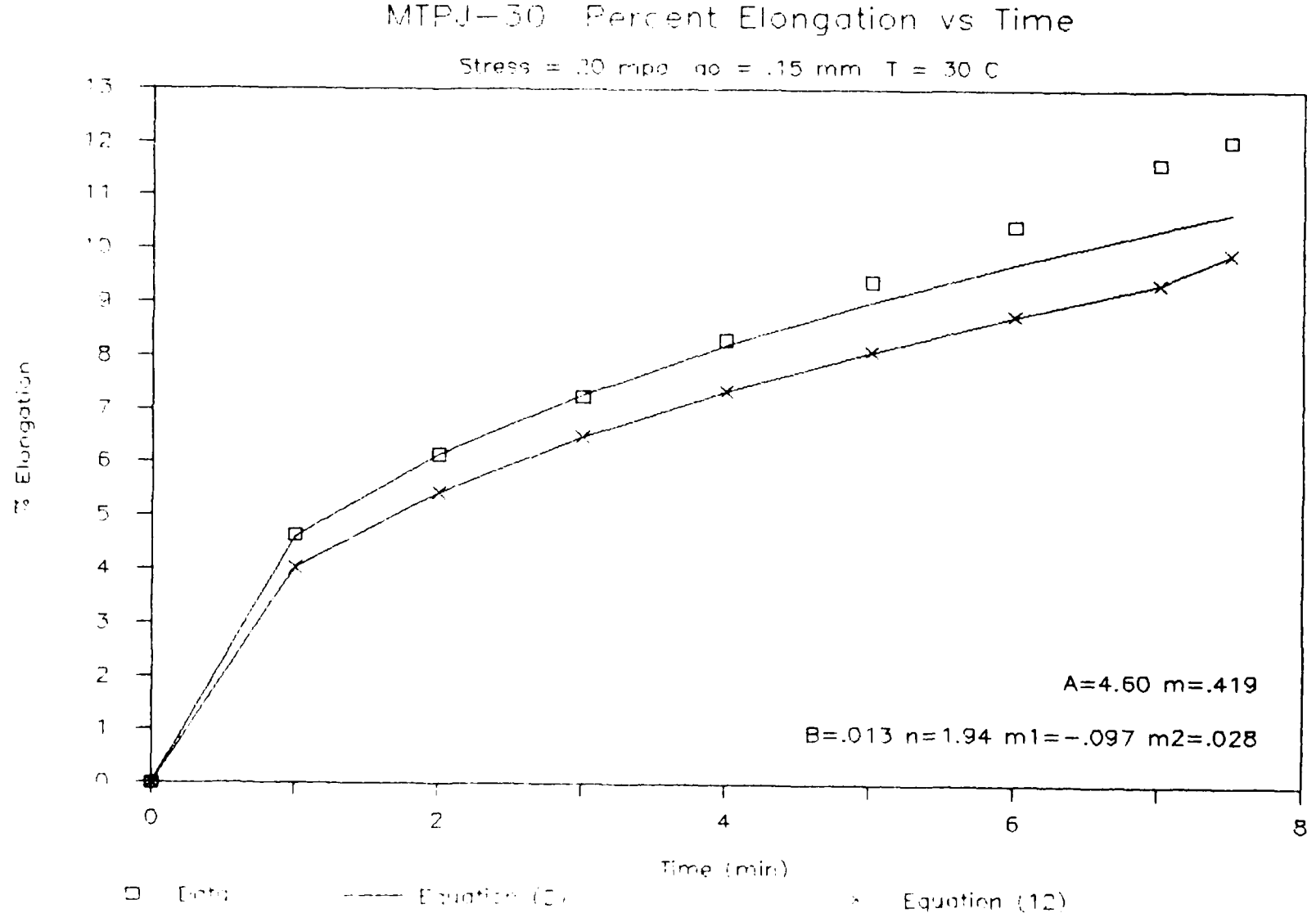
MTPJ-30 Percent Elongation vs Time
Stress = .20 mpa ao = .15 mm T = 30 C
% Elongation
Time (min)
A=4.60 m=.419
B=.013 n=1.94 m1=-.097 m2=.028
Data
Equation (12)

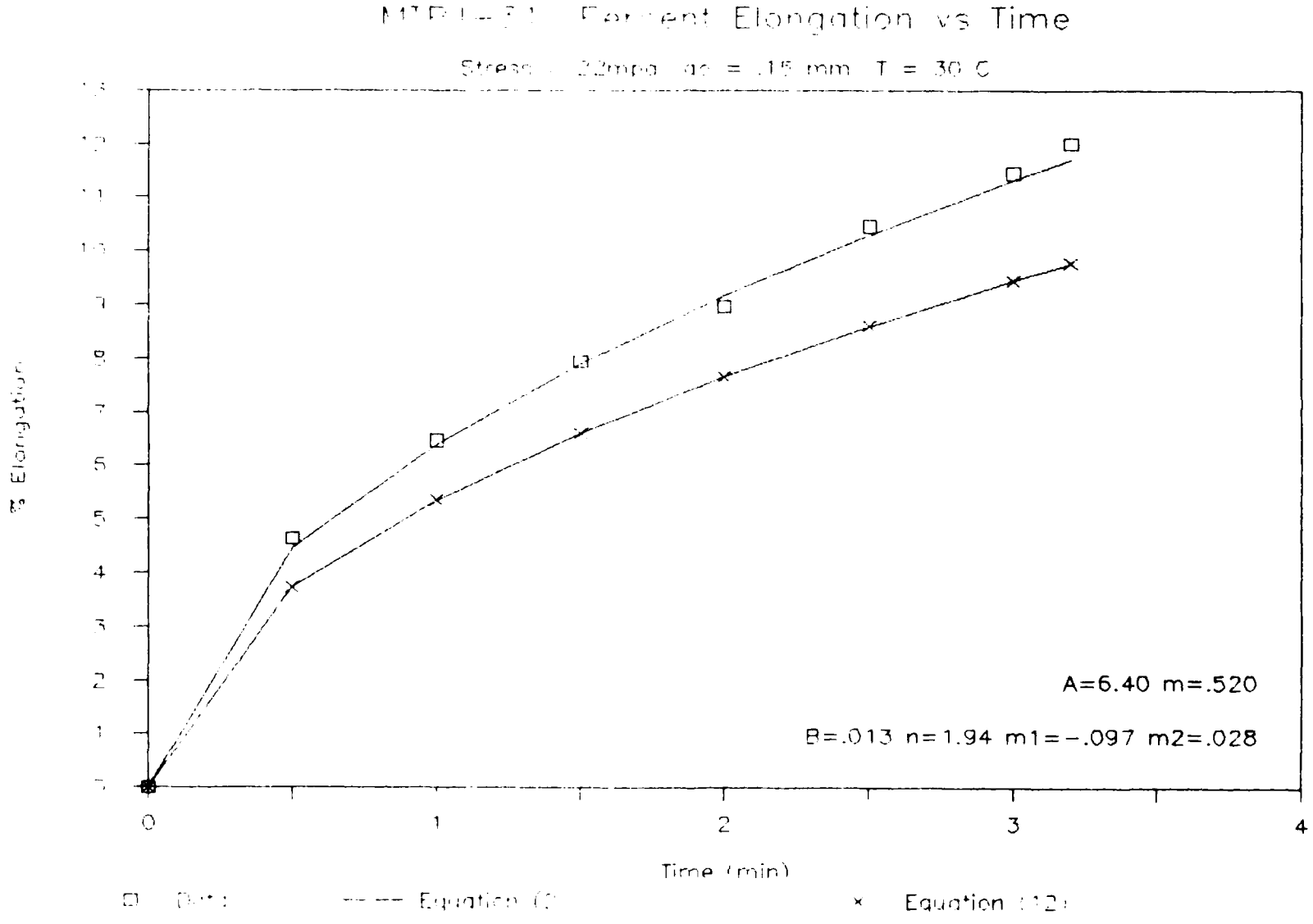
Permanent Elongation vs Time
Stress = .32mpa dc = .15 mm T = 30 C
% Elongation
0
1
2
3
4
Time (min)
A=6.40 m=.520
B=.013 n=1.94 m1=-.097 m2=.028
Equation (12)

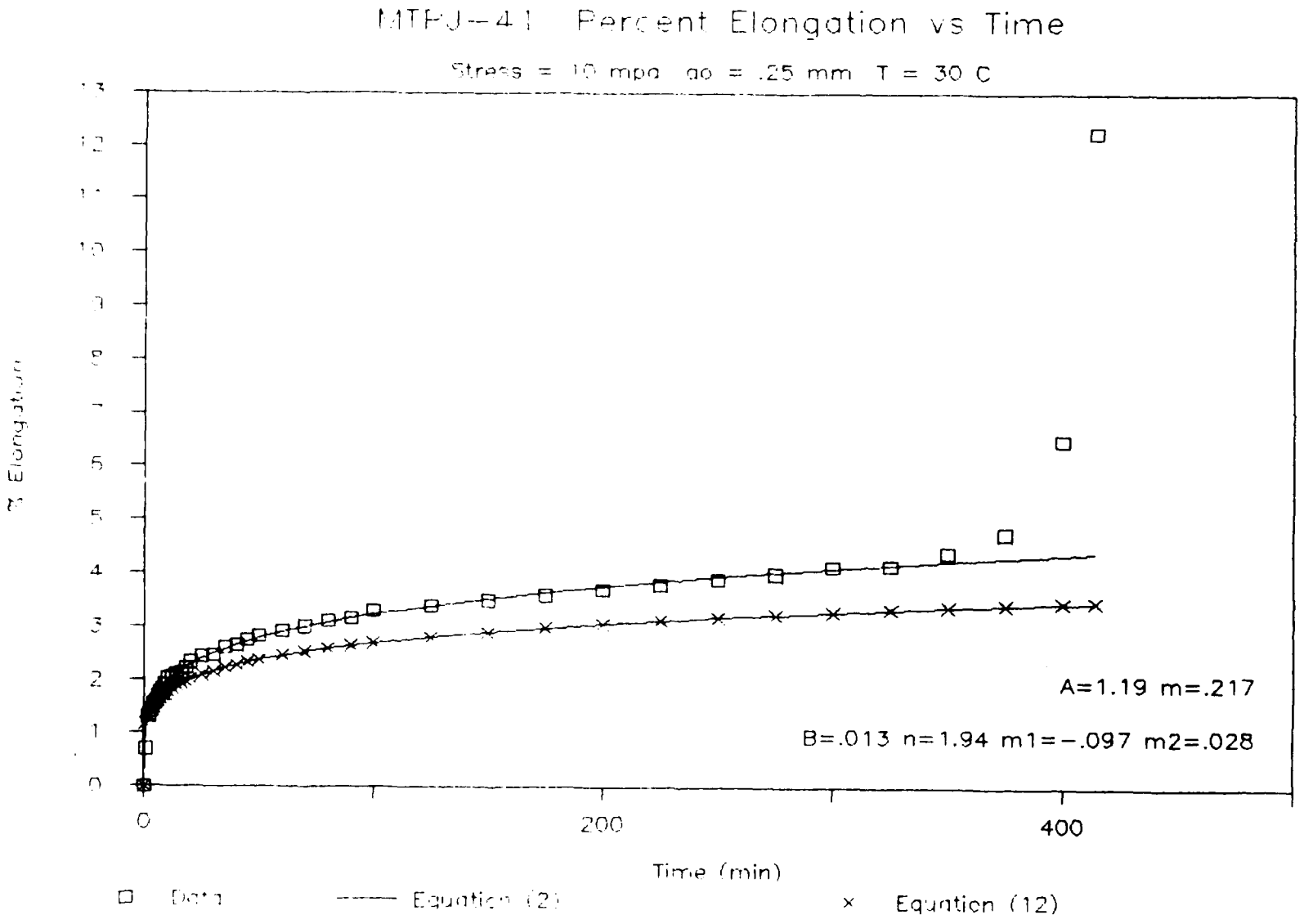
MTPJ--41 Percent Elongation vs Time
Stress = 10 mpa ao = .25 mm T = 30 C
% Elongation
0
1
2
3
4
5
0
200
400
Time (min)
A=1.19 m=.217
B=.013 n=1.94 m1=-.097 m2=.028
Data
Equation (2)
Equation (12)

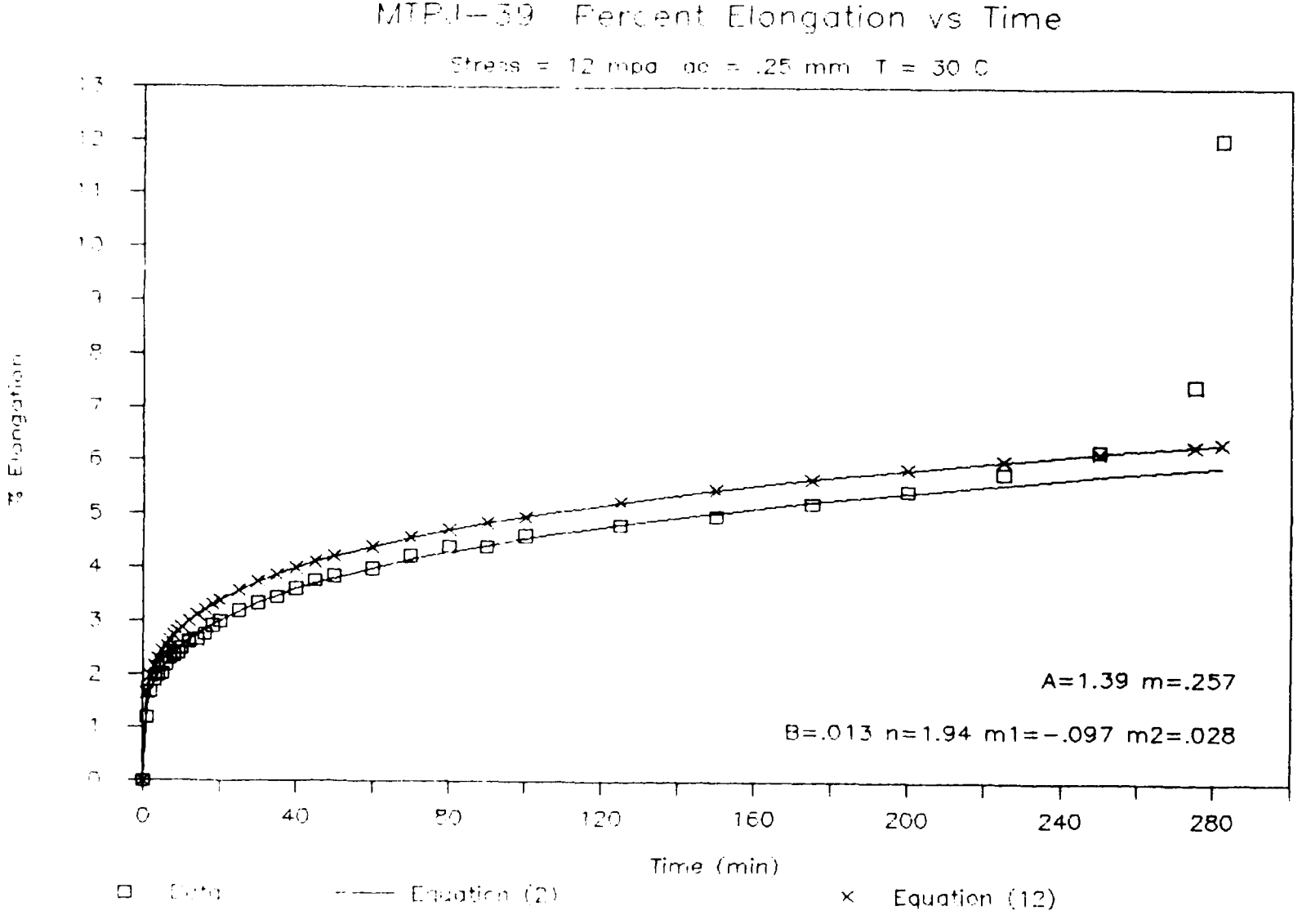
MTPJ-39 Percent Elongation vs Time
Stress = 12 mpa ao = .25 mm T = 30 C
% Elongation
Time (min)
0
40
80
120
160
200
240
280
A=1.39 m=.257
B=.013 n=1.94 m1=-.097 m2=.028
Data
Equation (2)
Equation (12)

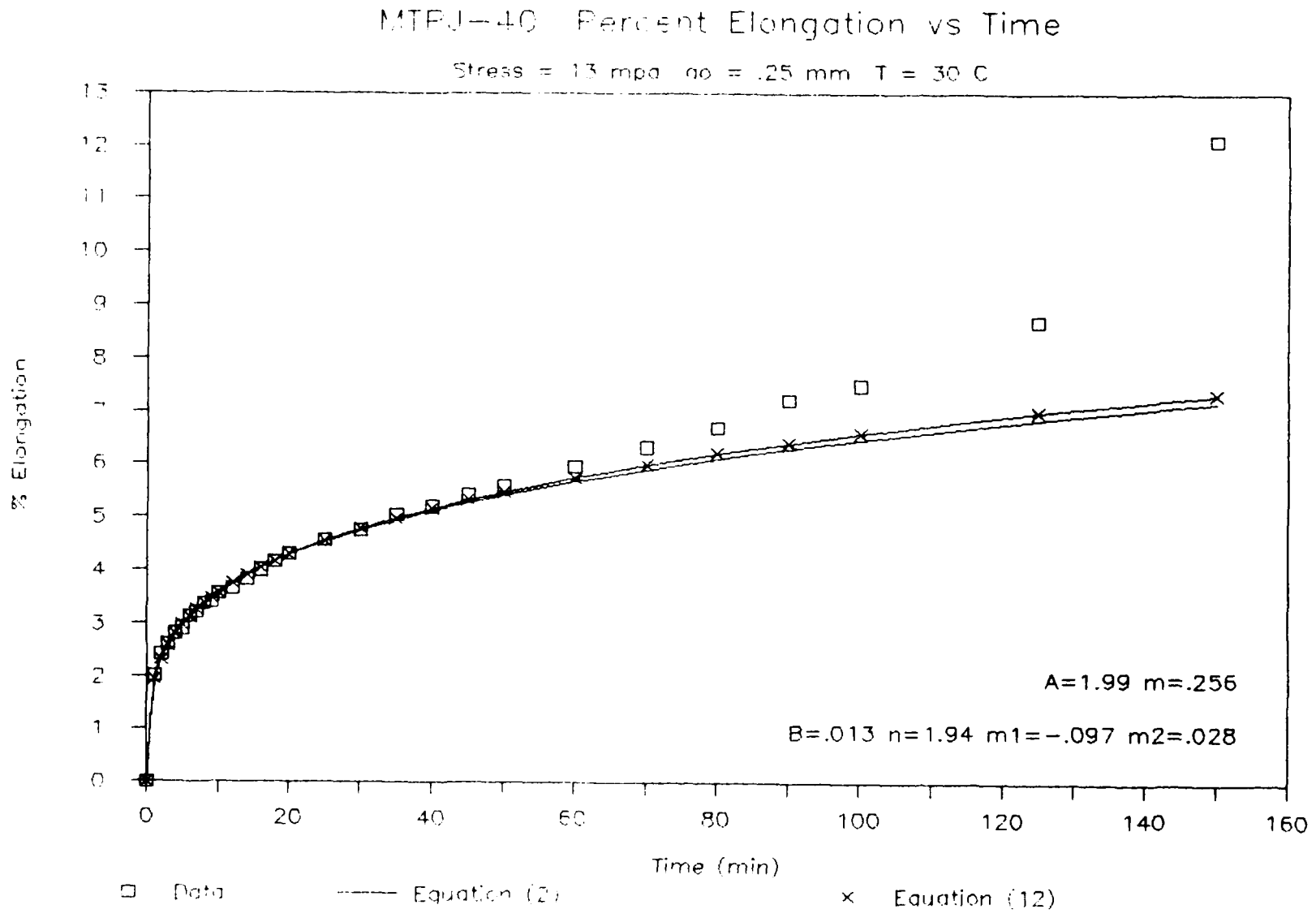
MTPJ-40 Percent Elongation vs Time
Stress = 13 mpa ao = .25 mm T = 30 C
% Elongation
Time (min)
A=1.99 m=.256
B=.013 n=1.94 m1=-.097 m2=.028
Data
Equation (2)
Equation (12)

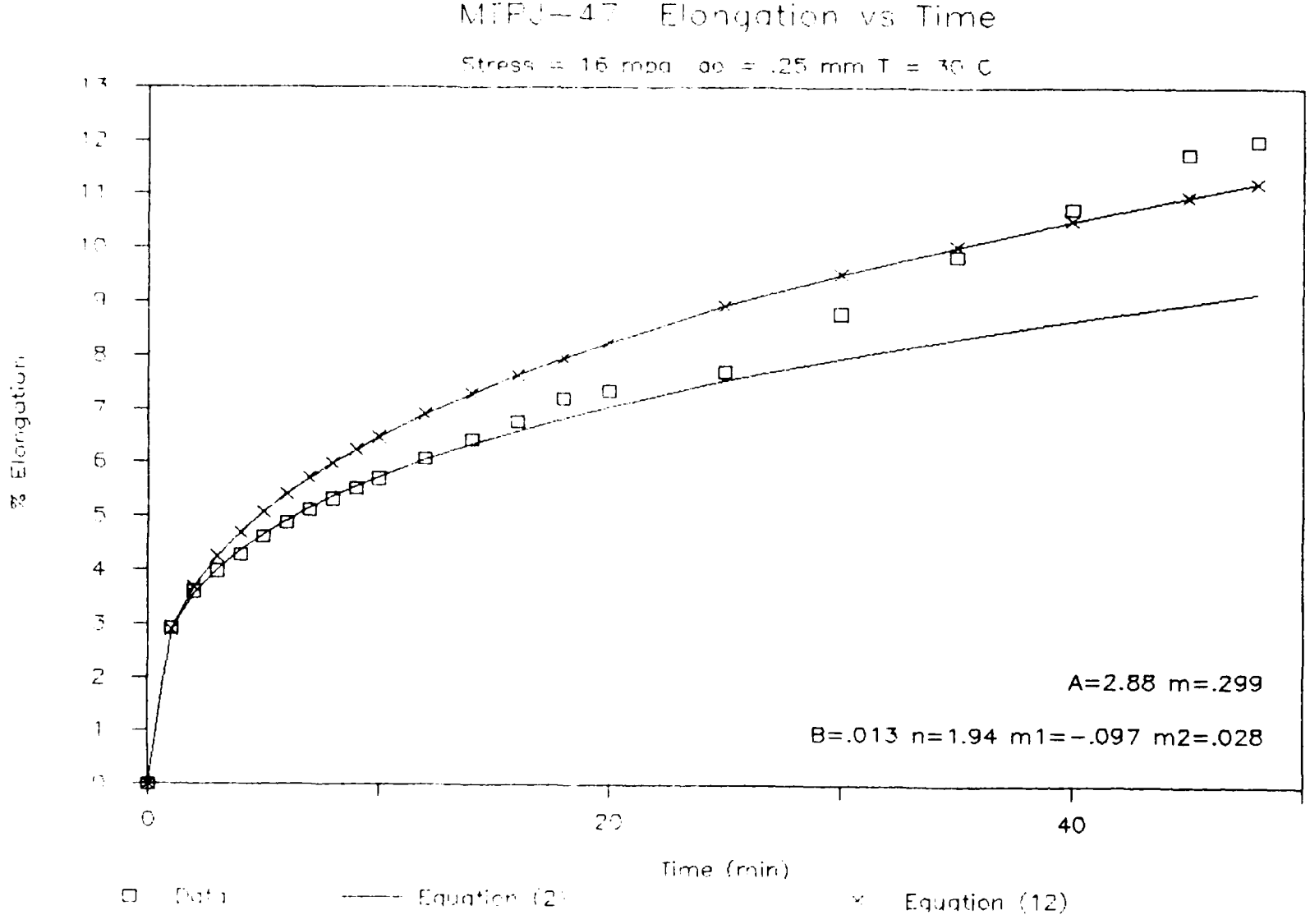
MTPJ-47 Elongation vs Time
Stress = 15 mpa ao = .25 mm T = 30 C
% Elongation
Time (min)
0
20
40
A=2.88 m=.299
B=.013 n=1.94 m1=-.097 m2=.028
Data
Equation (12)

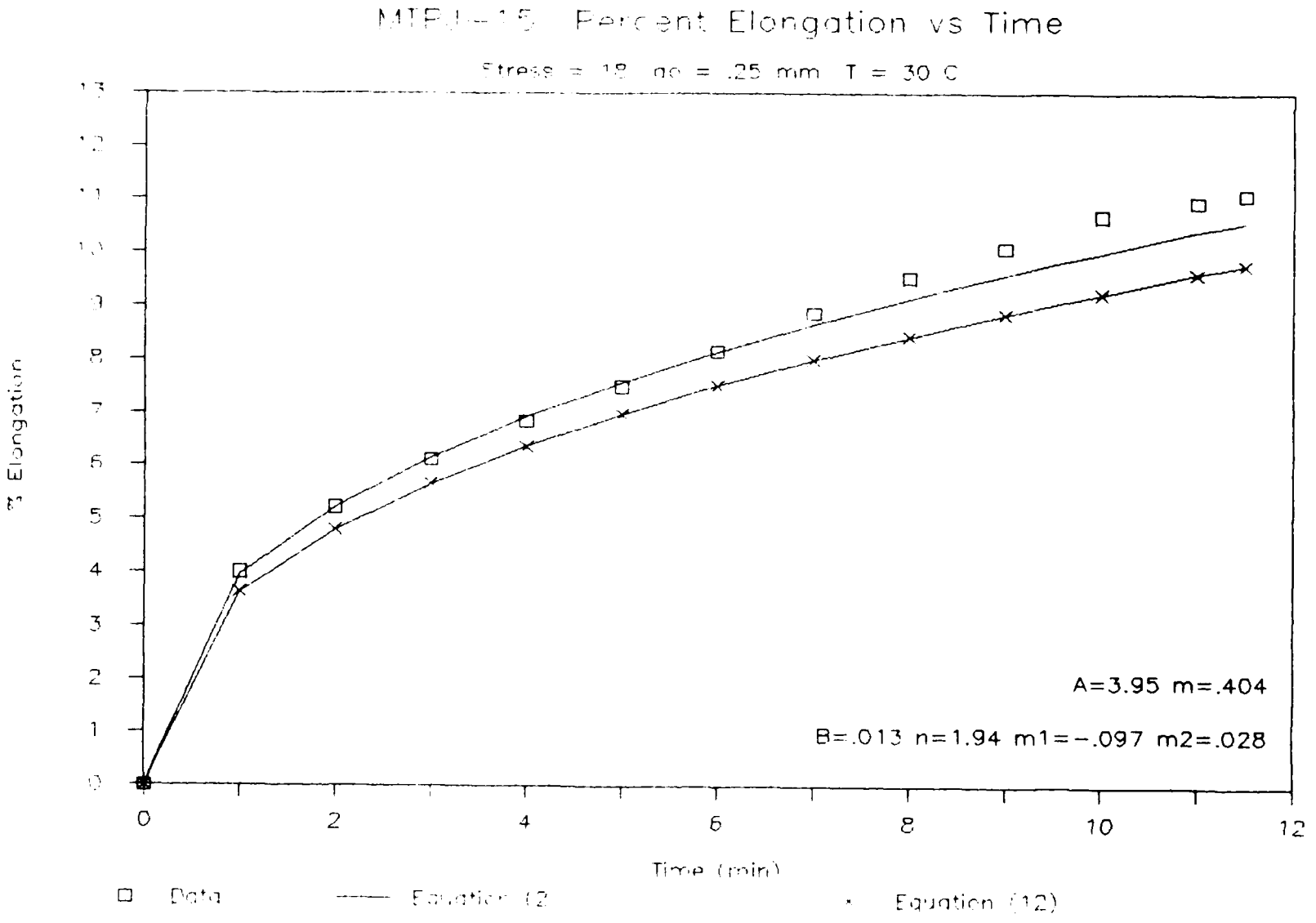
MTP1-15 Percent Elongation vs Time
Stress = 18 ao = .25 mm T = 30 C
% Elongation
Time (min)
0
2
4
6
8
10
12
A=3.95 m=.404
B=.013 n=1.94 m1=-.097 m2=.028
Data
Equation (12)

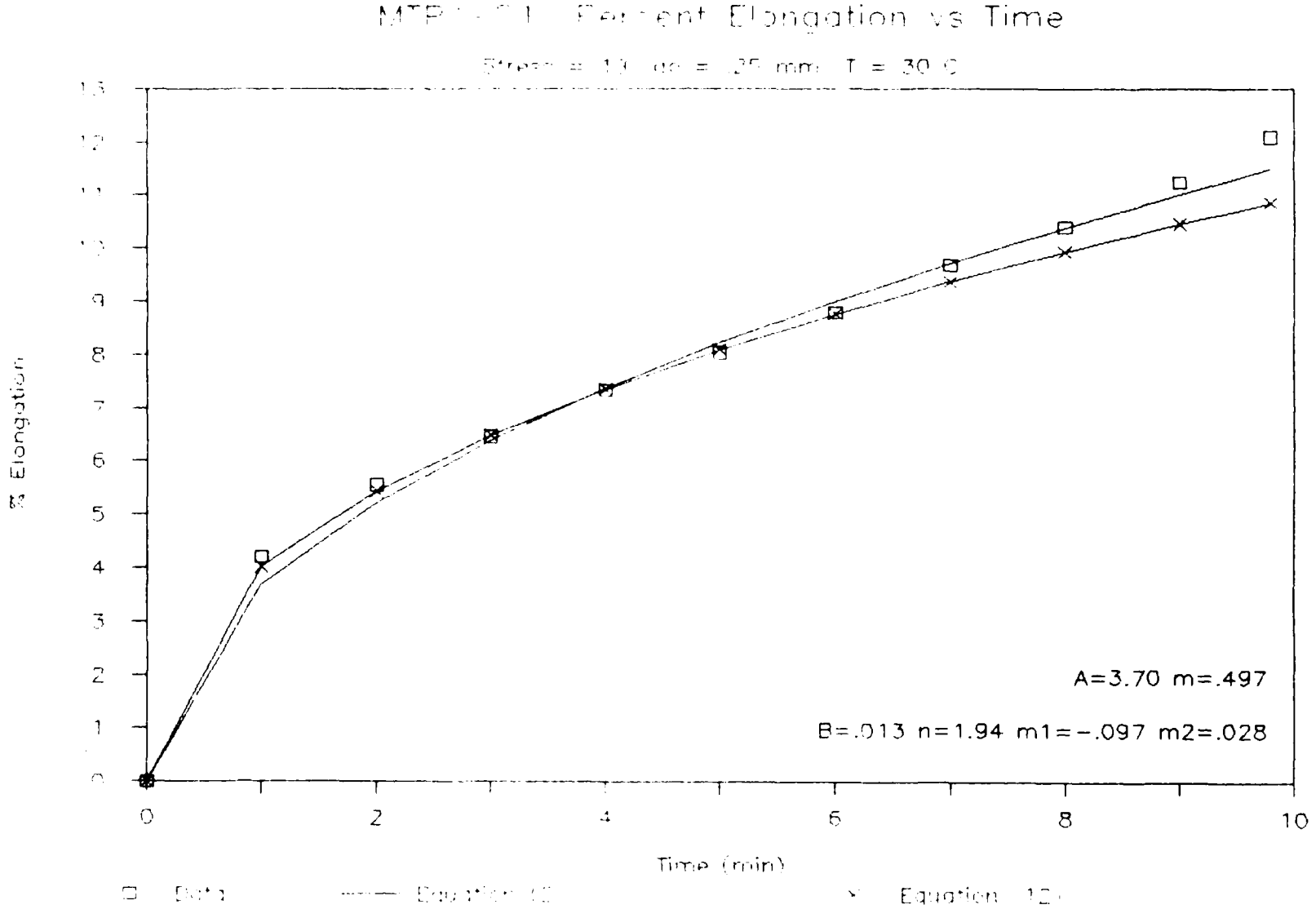
Percent Elongation vs Time
% Elongation
Time (min)
0
2
4
6
8
10
A=3.70 m=.497
B=.013 n=1.94 m1=-.097 m2=.028
Data
Equation (1)
Equation (2)

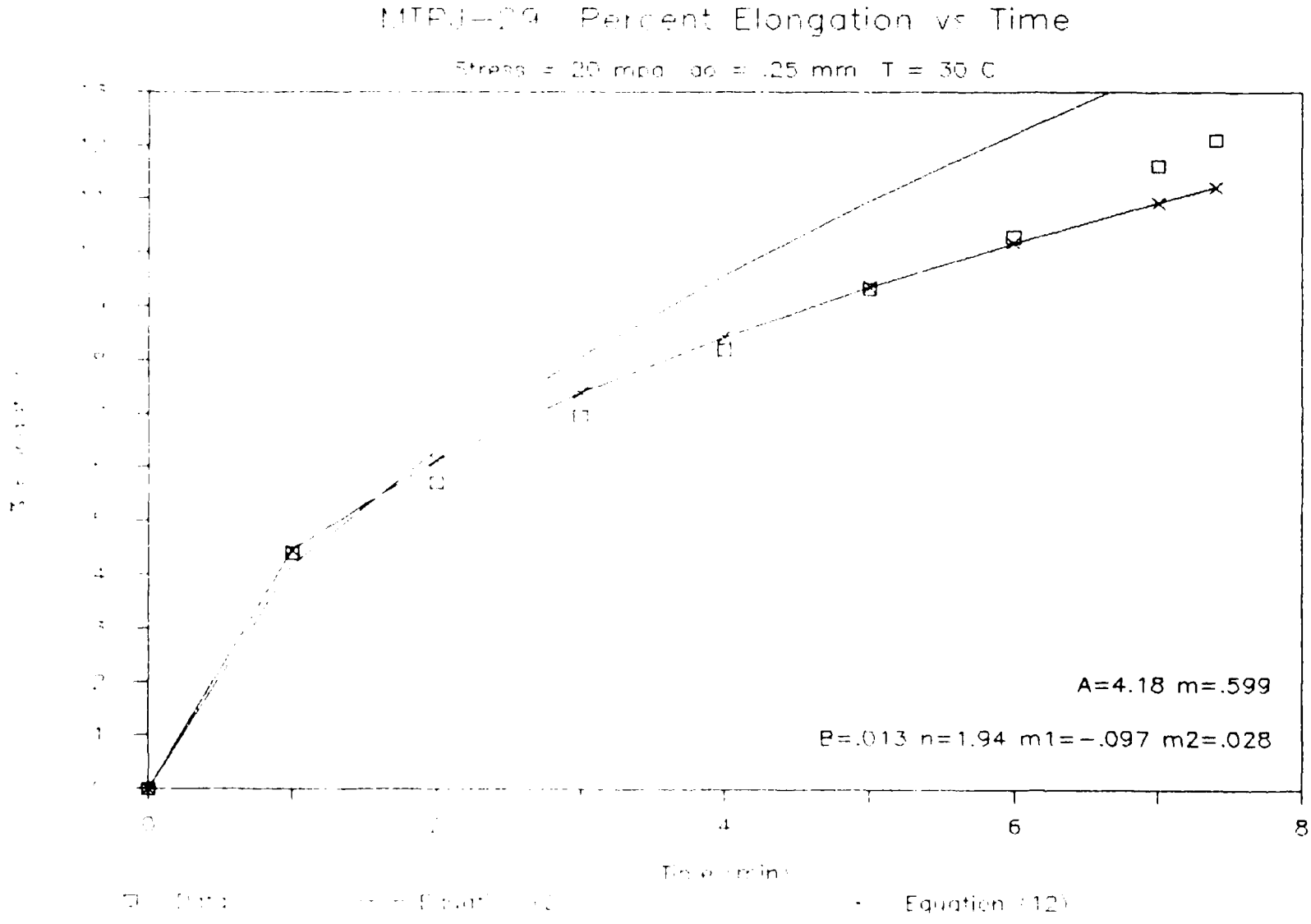
Stress = 20 mpa ao = .25 mm T = 30 C
A=4.18 m=.599
B=.013 n=1.94 m1=-.097 m2=.028
6
8
Equation (12)

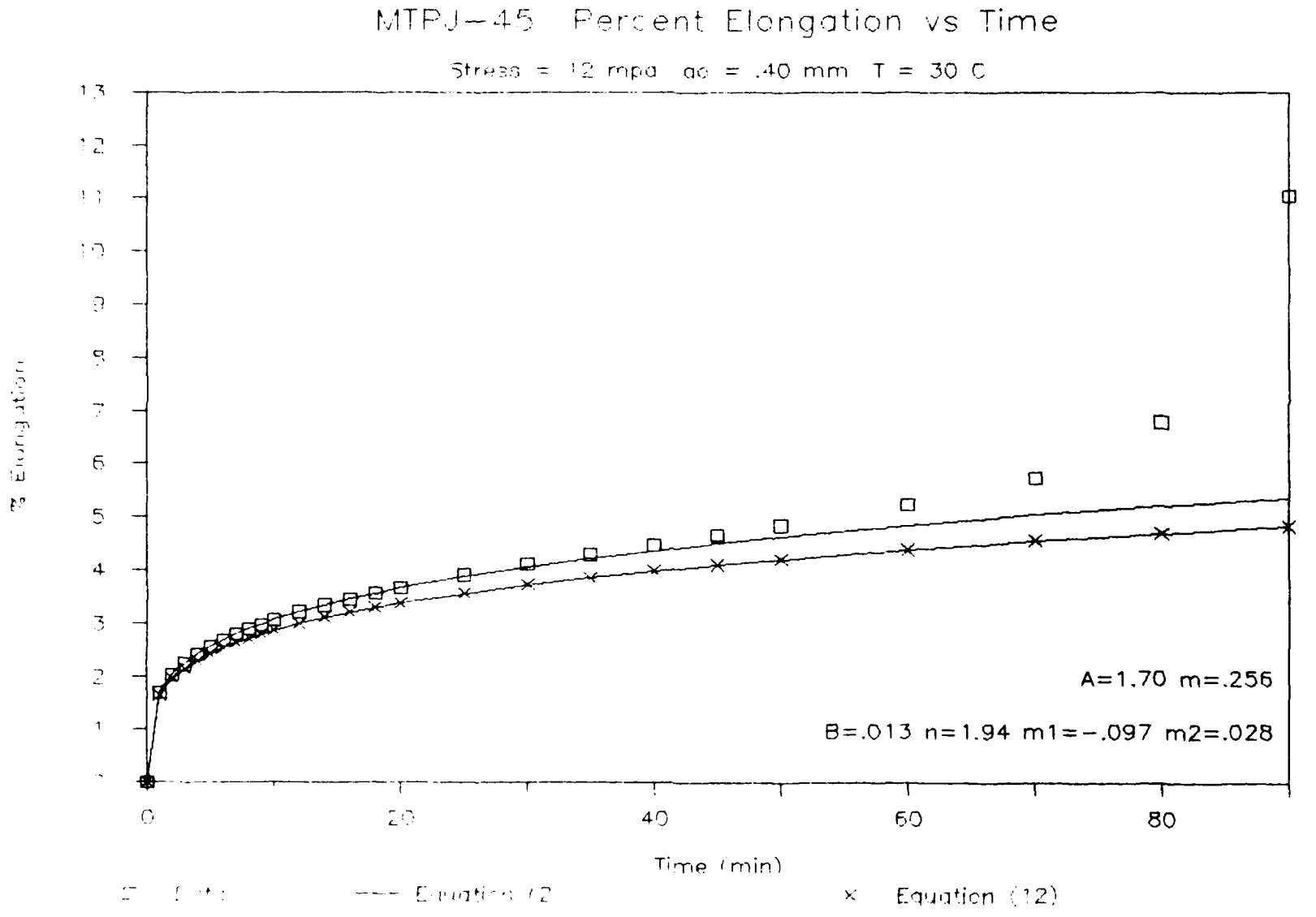
MTPJ–45 Percent Elongation vs Time
Stress = 12 mpa ao = .40 mm T = 30 C
% Elongation
Time (min)
0
20
40
60
80
A=1.70 m=.256
B=.013 n=1.94 m1=–.097 m2=.028
Equation (12)

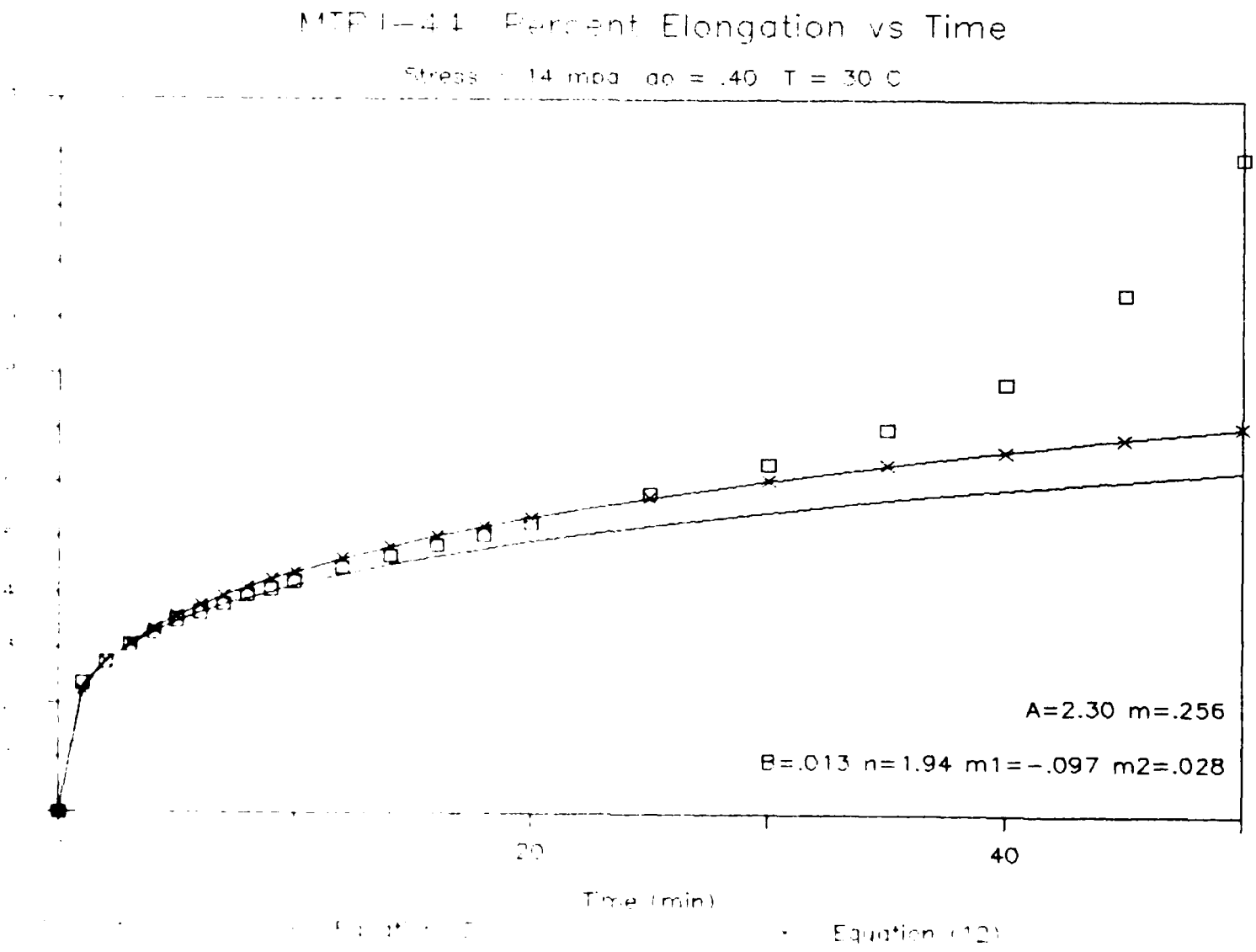
MTP 1-4.1 Percent Elongation vs Time
Stress = 14 mpa ao = .40 T = 30 C
A=2.30 m=.256
B=.013 n=1.94 m1=-.097 m2=.028
20
40
Time (min)
Equation (12)

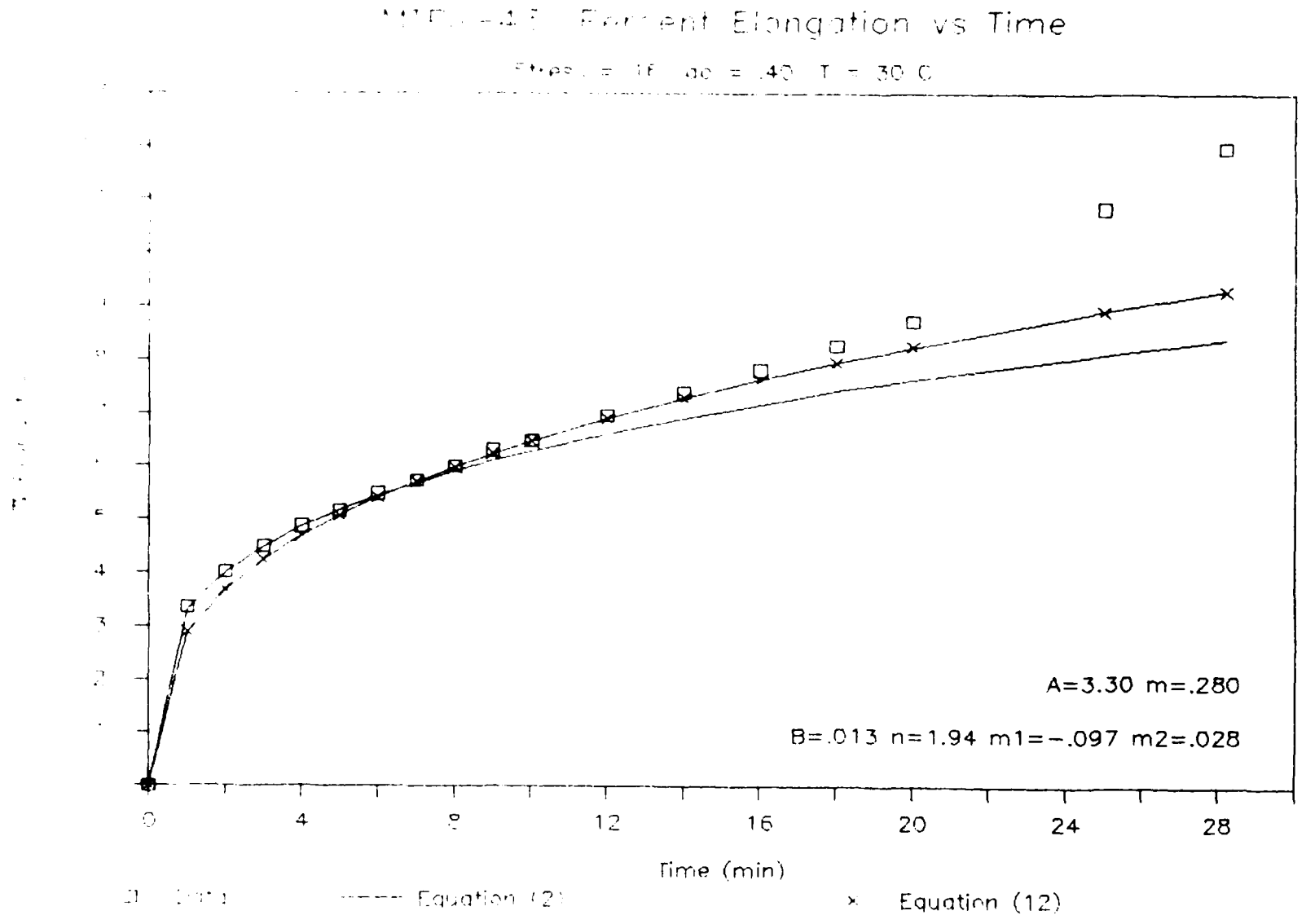
Percent Elongation vs Time
A=3.30 m=.280
B=.013 n=1.94 m1=-.097 m2=.028
0
4
8
12
16
20
24
28
Time (min)
Equation (12)

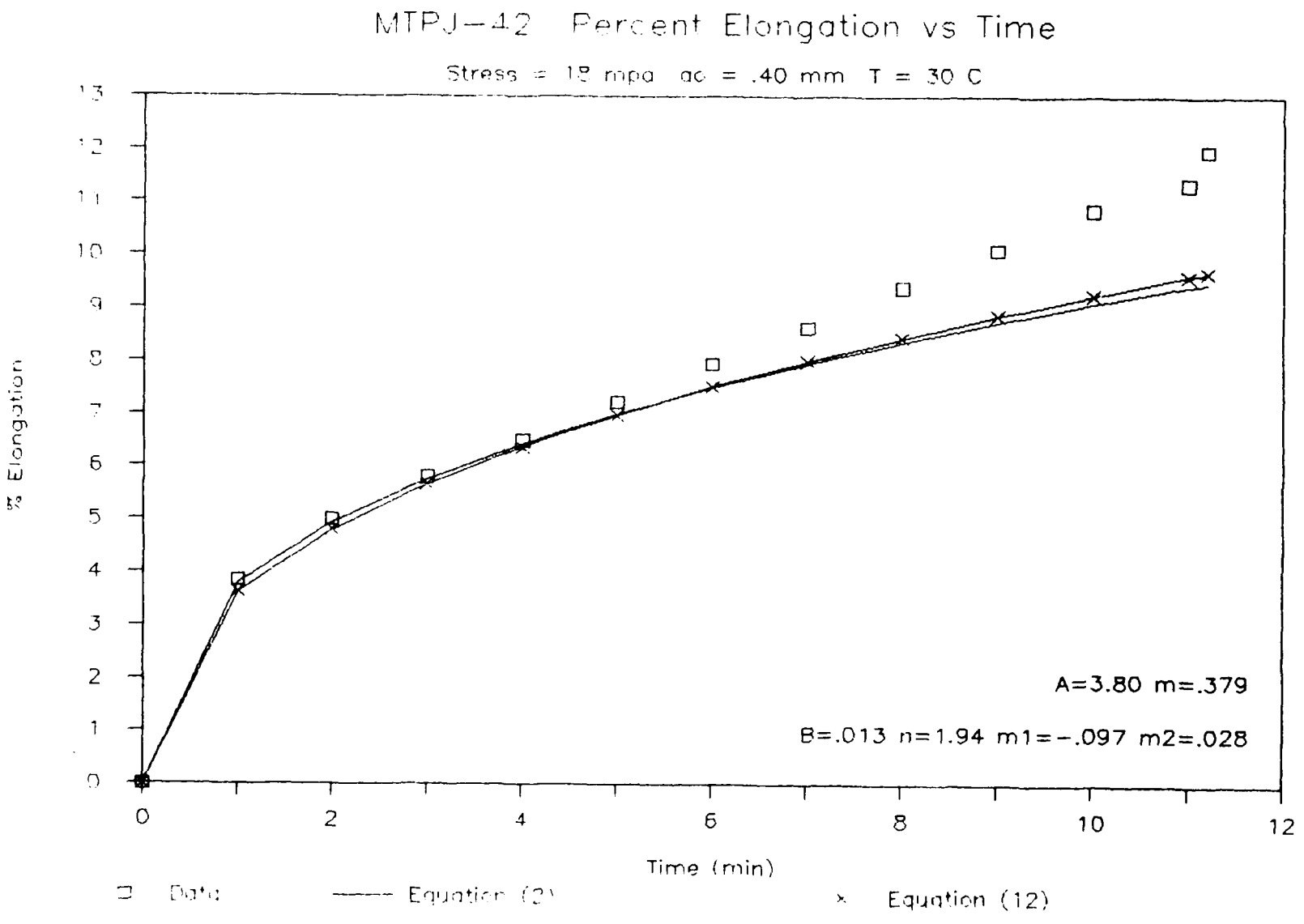
MTPJ—42 Percent Elongation vs Time
Stress = 18 mpa ao = .40 mm T = 30 C
% Elongation
Time (min)
A=3.80 m=.379
B=.013 n=1.94 m1=-.097 m2=.028
Data
Equation (12)

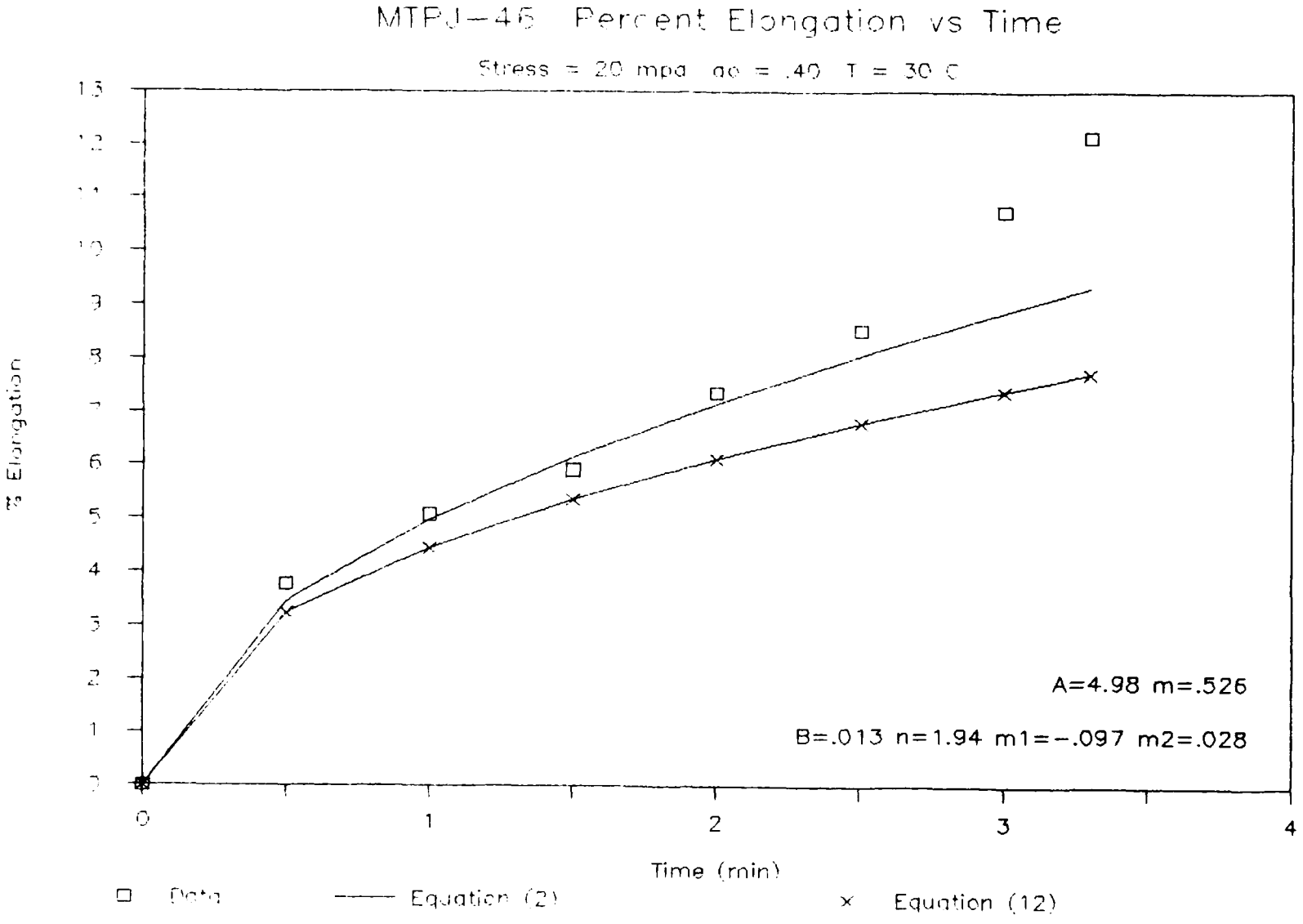
MTPJ-46 Percent Elongation vs Time
Stress = 20 mpa ao = .40 T = 30 C
% Elongation
Time (min)
0
1
2
3
4
A=4.98 m=.526
B=.013 n=1.94 m1=-.097 m2=.028
Data
Equation (2)
Equation (12)

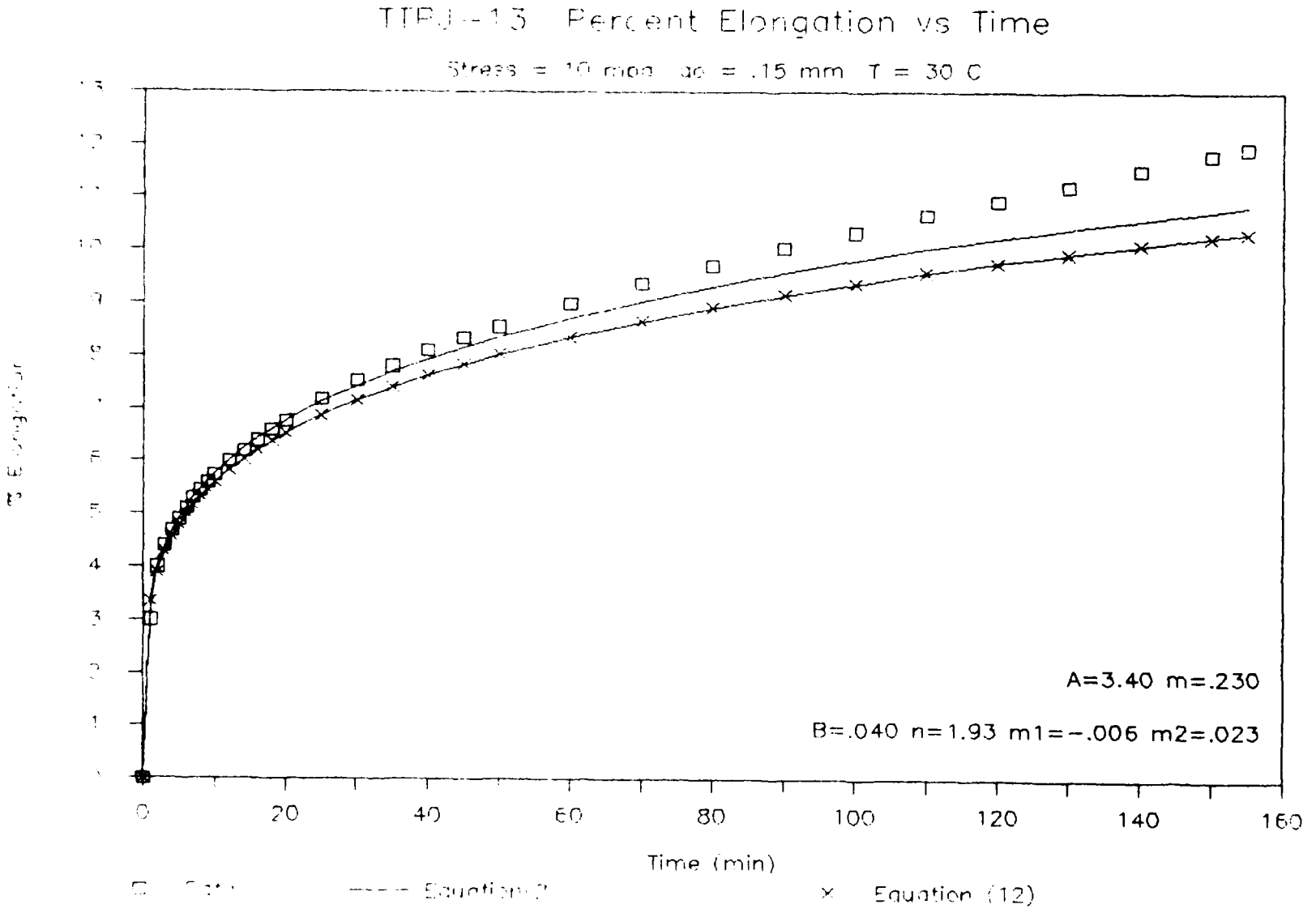
TTBJ--13 Percent Elongation vs Time
Stress = 10 mpa ao = .15 mm T = 30 C
A=3.40 m=.230
B=.040 n=1.93 m1=-.006 m2=.023
0
20
40
60
80
100
120
140
160
Time (min)
Equation (12)

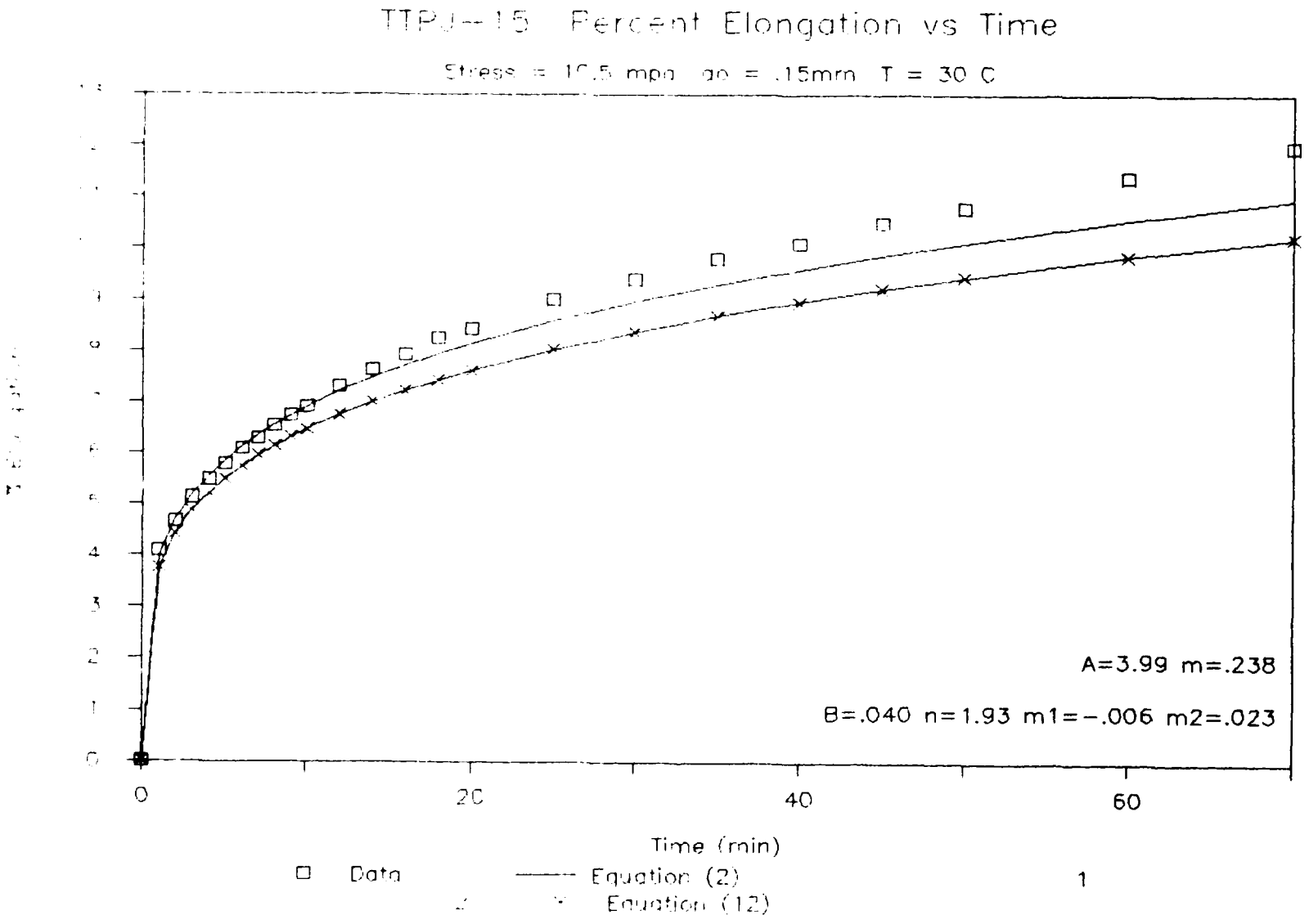
TTPJ--15 Percent Elongation vs Time
Stress = 10.5 mpa go = .15mm T = 30 C
A=3.99 m=.238
B=.040 n=1.93 m1=-.006 m2=.023
0
20
40
60
Time (min)
Data
Equation (2)
Equation (12)

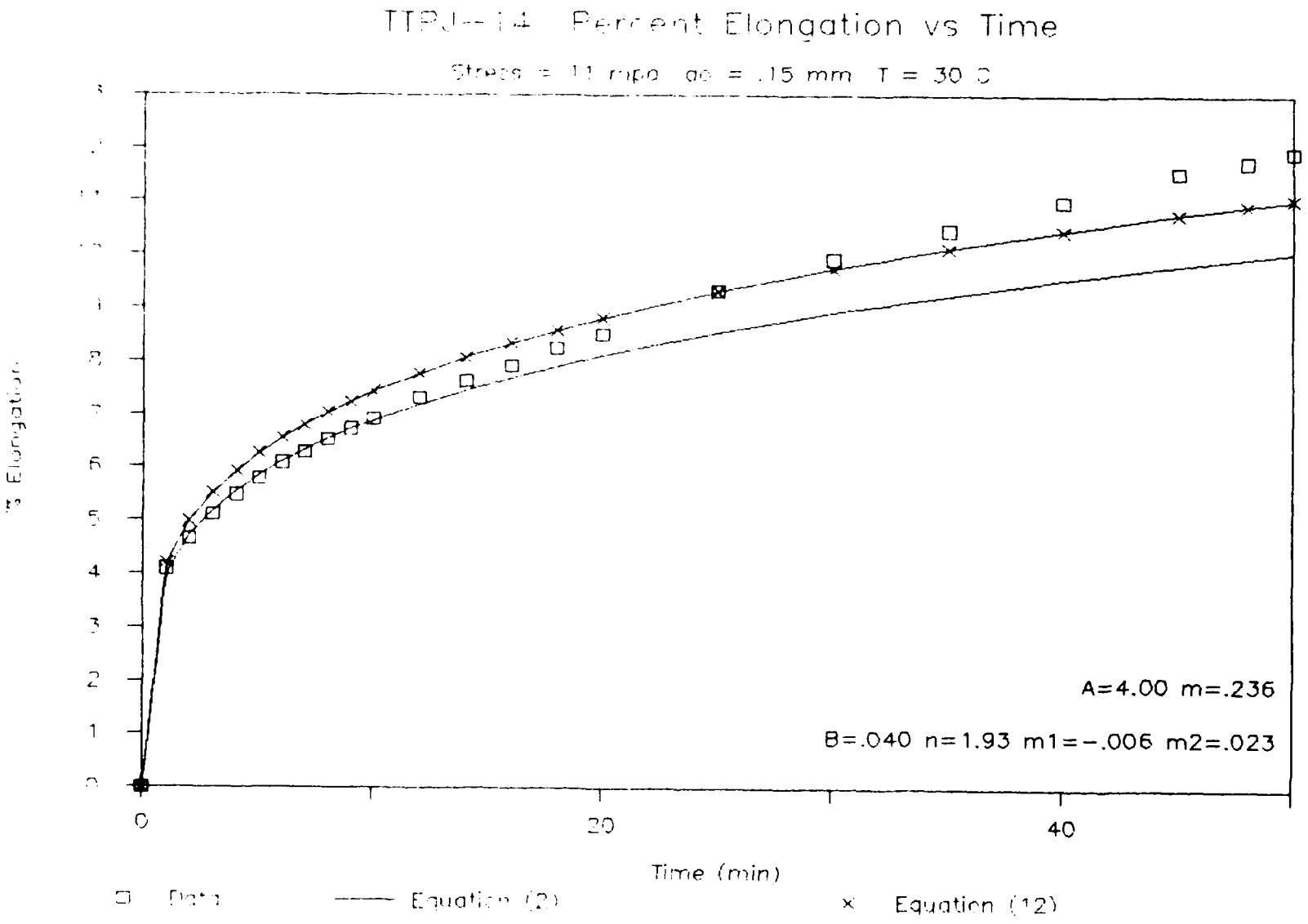
TTRJ--14 Percent Elongation vs Time
Stress = 11 mpa ao = .15 mm T = 30 C
% Elongation
0
20
40
Time (min)
A=4.00 m=.236
B=.040 n=1.93 m1=-.006 m2=.023
Data
Equation (2)
Equation (12)

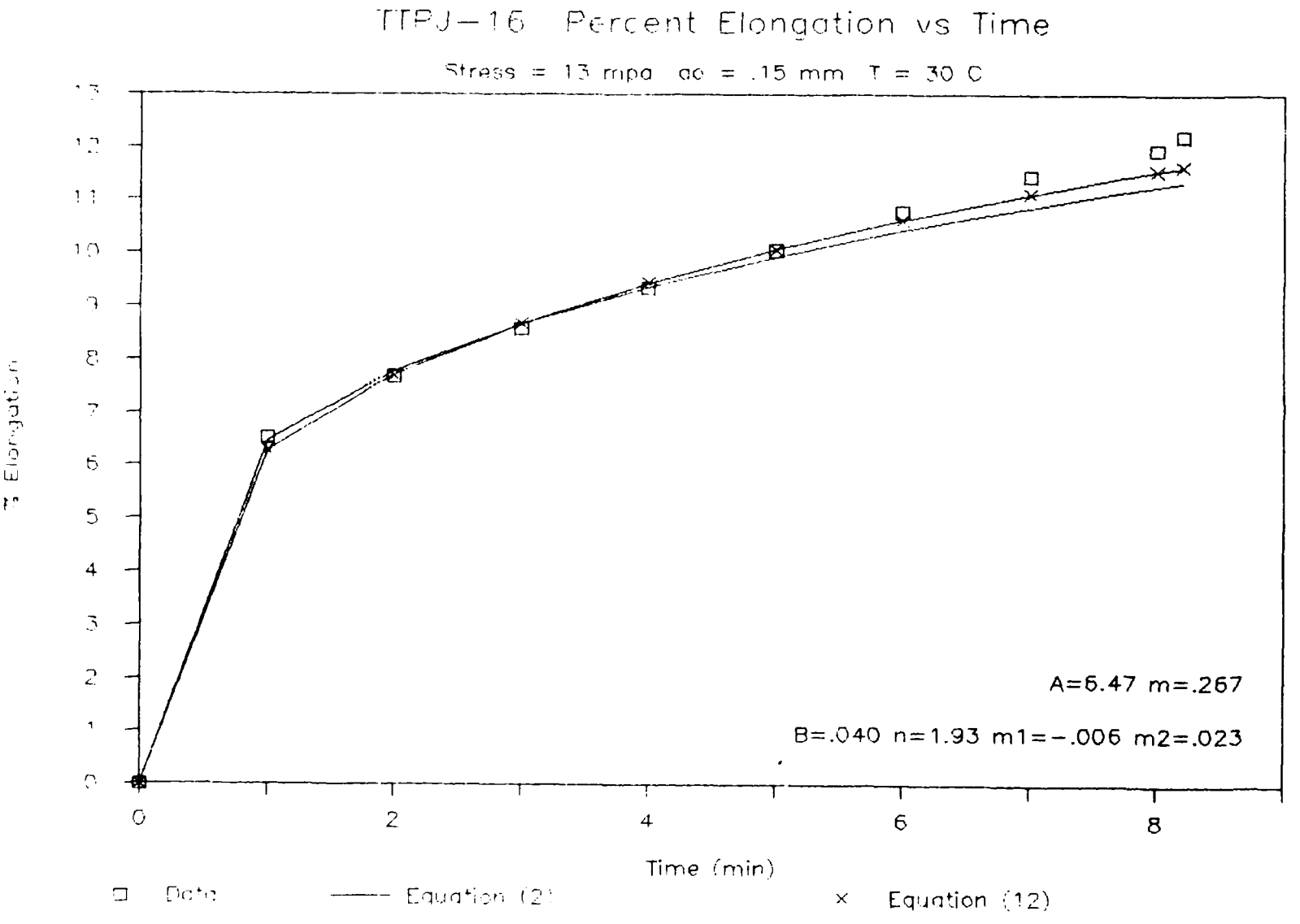
TTPJ—16 Percent Elongation vs Time
Stress = 13 mpa ao = .15 mm T = 30 C
% Elongation
0
2
4
6
8
Time (min)
A=6.47 m=.267
B=.040 n=1.93 m1=-.006 m2=.023
Data
Equation (2)
Equation (12)

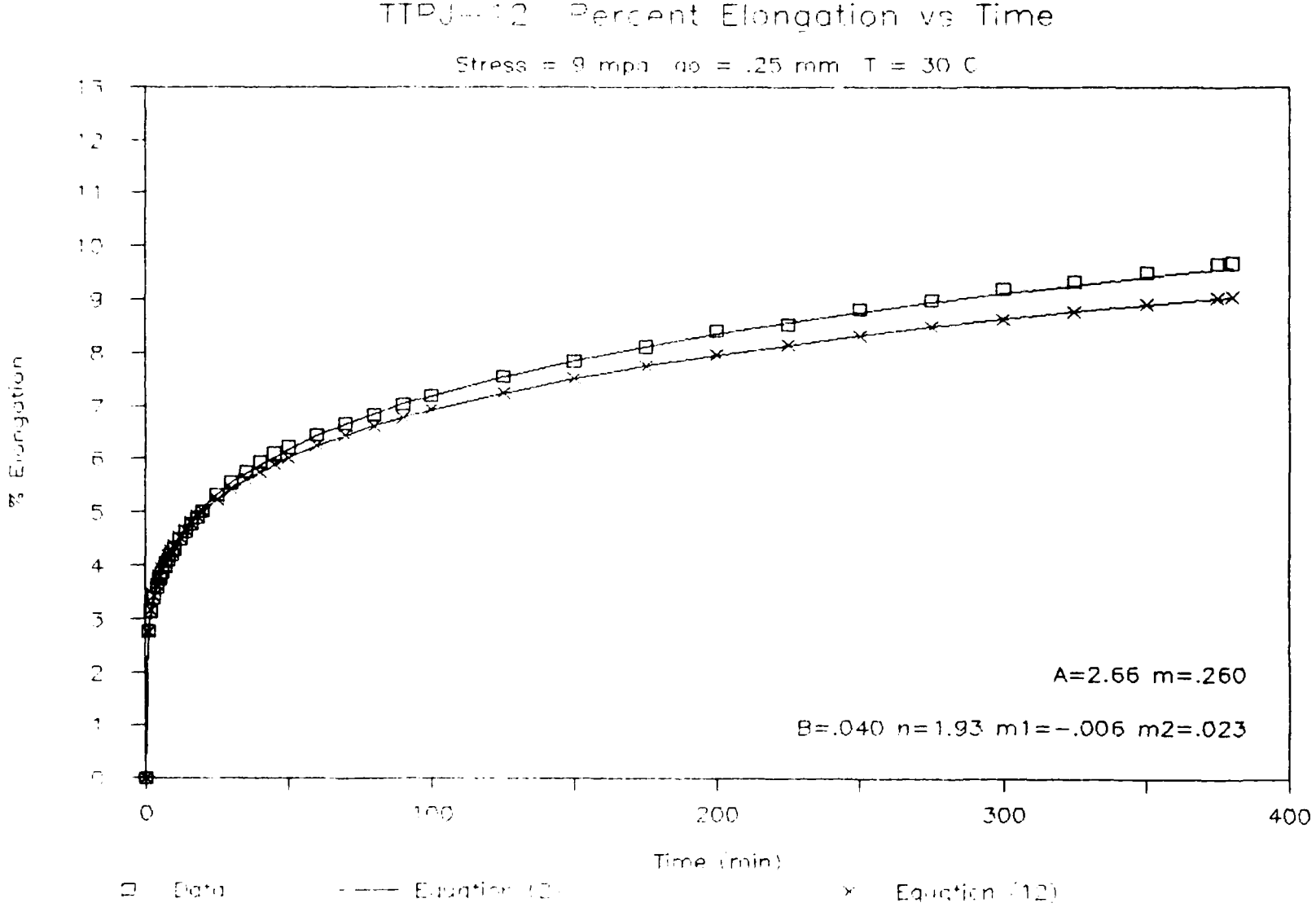
TTPJ-12 Percent Elongation vs Time
Stress = 9 mpa a0 = .25 mm T = 30 C
% Elongation
0
1
2
3
4
5
6
7
8
9
10
11
12
13
0
100
200
300
400
Time (min)
A=2.66 m=.260
B=.040 n=1.93 m1=-.006 m2=.023
Data
Equation (12)

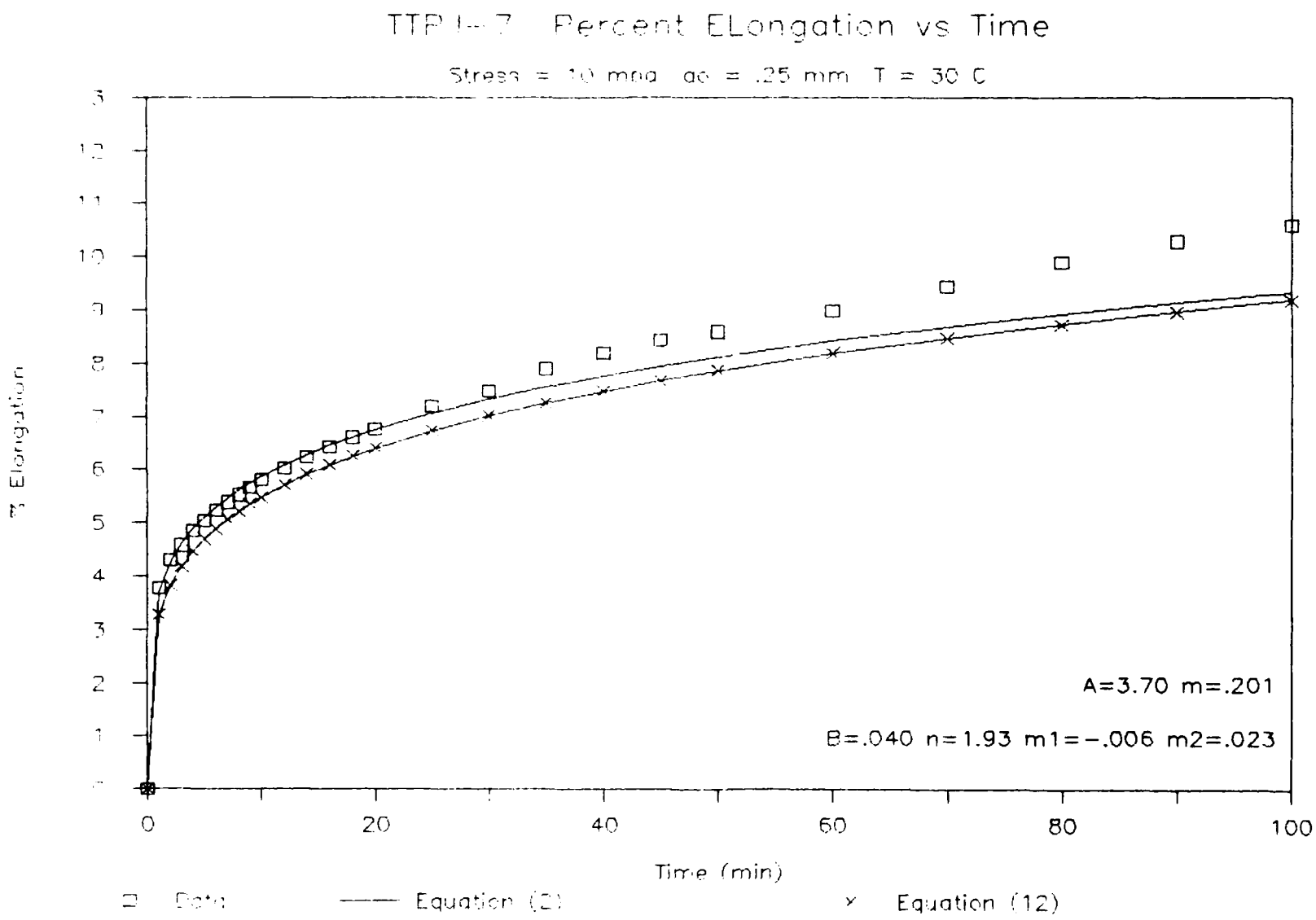
TTP I-7 Percent ELongation vs Time
Stress = 10 mpa ao = .25 mm T = 30 C
% Elongation
0
20
40
60
80
100
Time (min)
A=3.70 m=.201
B=.040 n=1.93 m1=-.006 m2=.023
Data
Equation (2)
Equation (12)

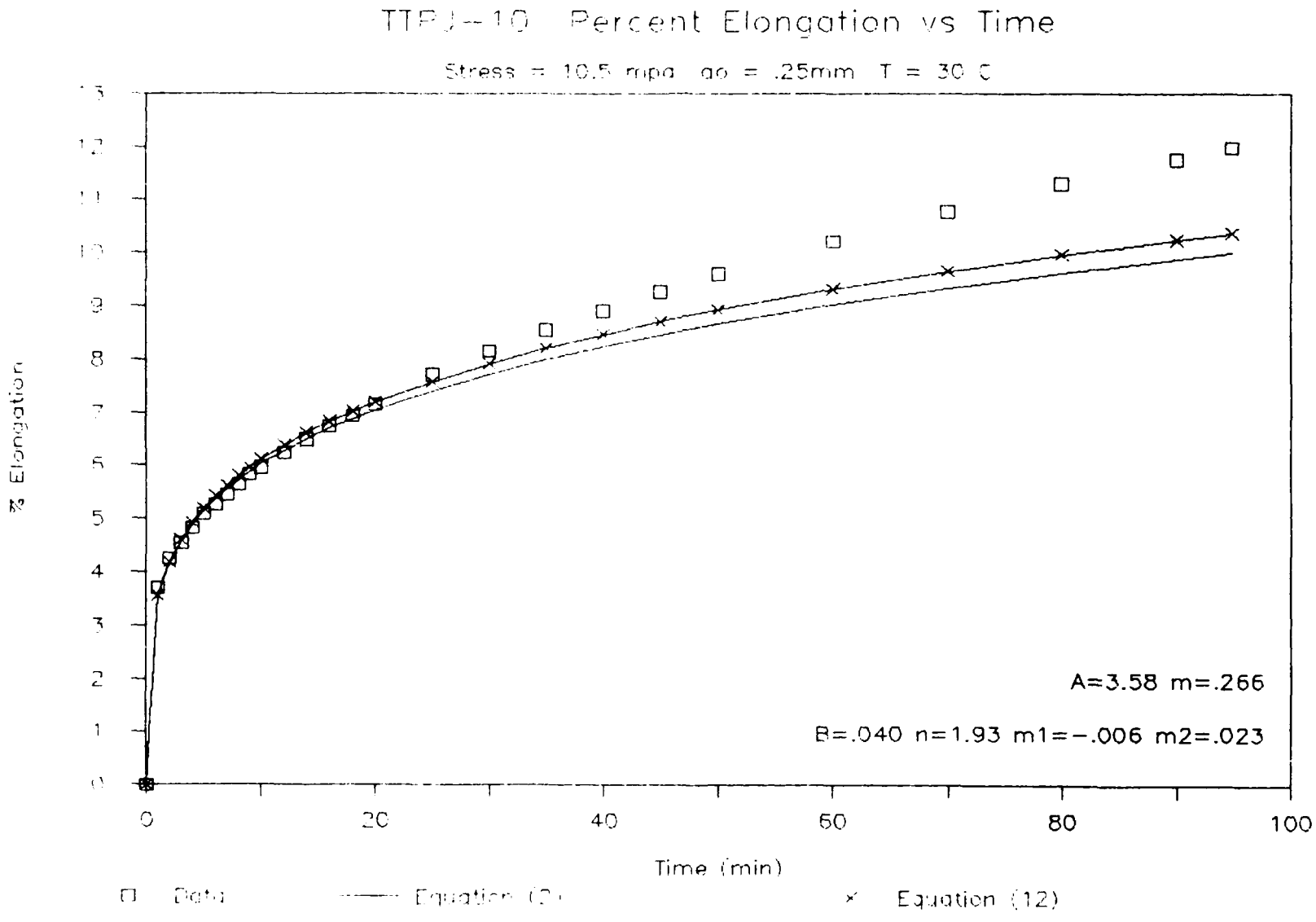
TTPJ--10 Percent Elongation vs Time
Stress = 10.5 mpa go = .25mm T = 30 C
% Elongation
Time (min)
0
20
40
60
80
100
A=3.58 m=.266
B=.040 n=1.93 m1=-.006 m2=.023
Data
Equation (12)

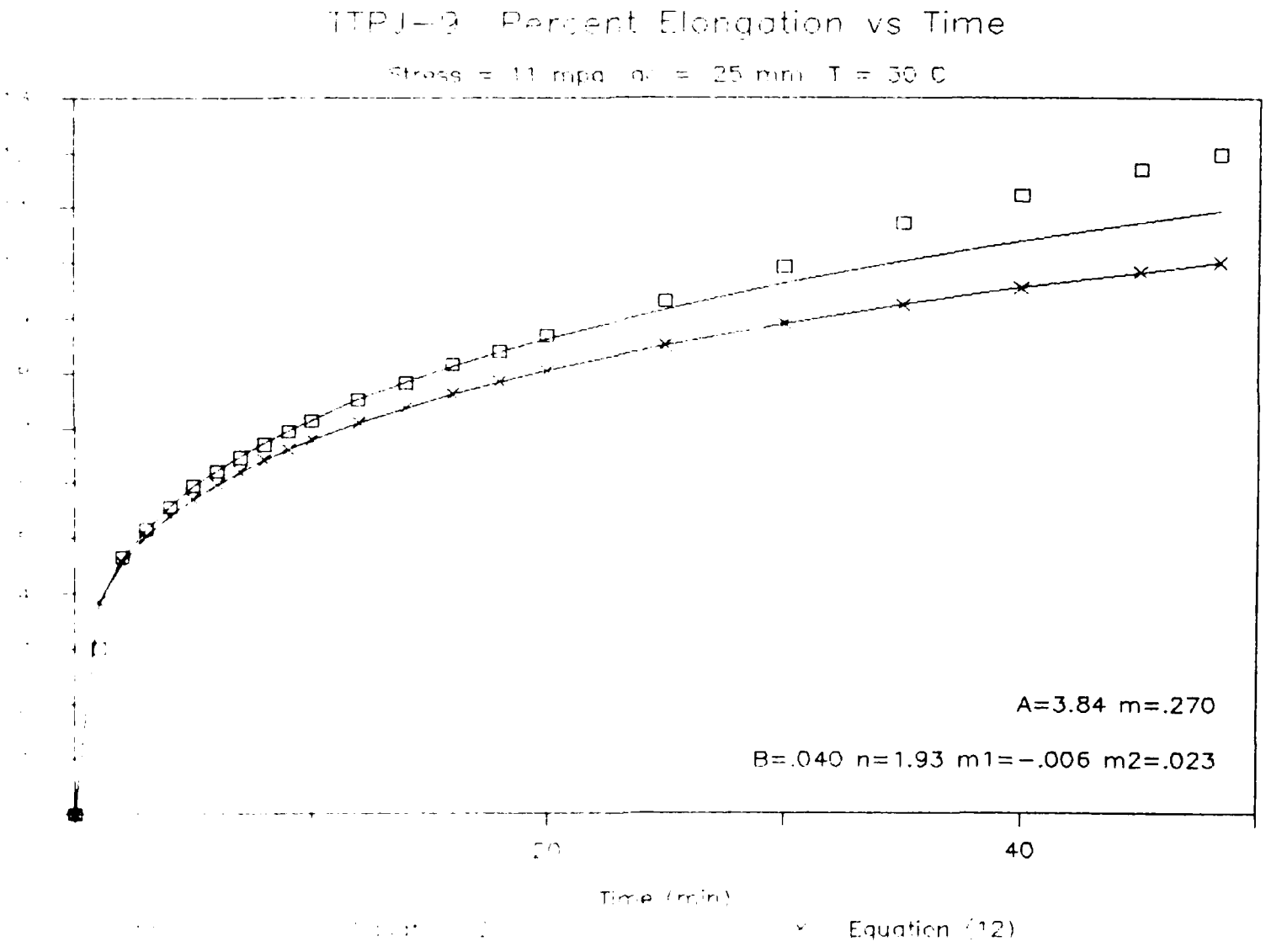
ITPJ-9 Percent Elongation vs Time
Stress = 11 mpa
= 25 mm T = 30 C
A=3.84 m=.270
B=.040 n=1.93 m1=-.006 m2=.023
40
Time (min)
Equation (12)

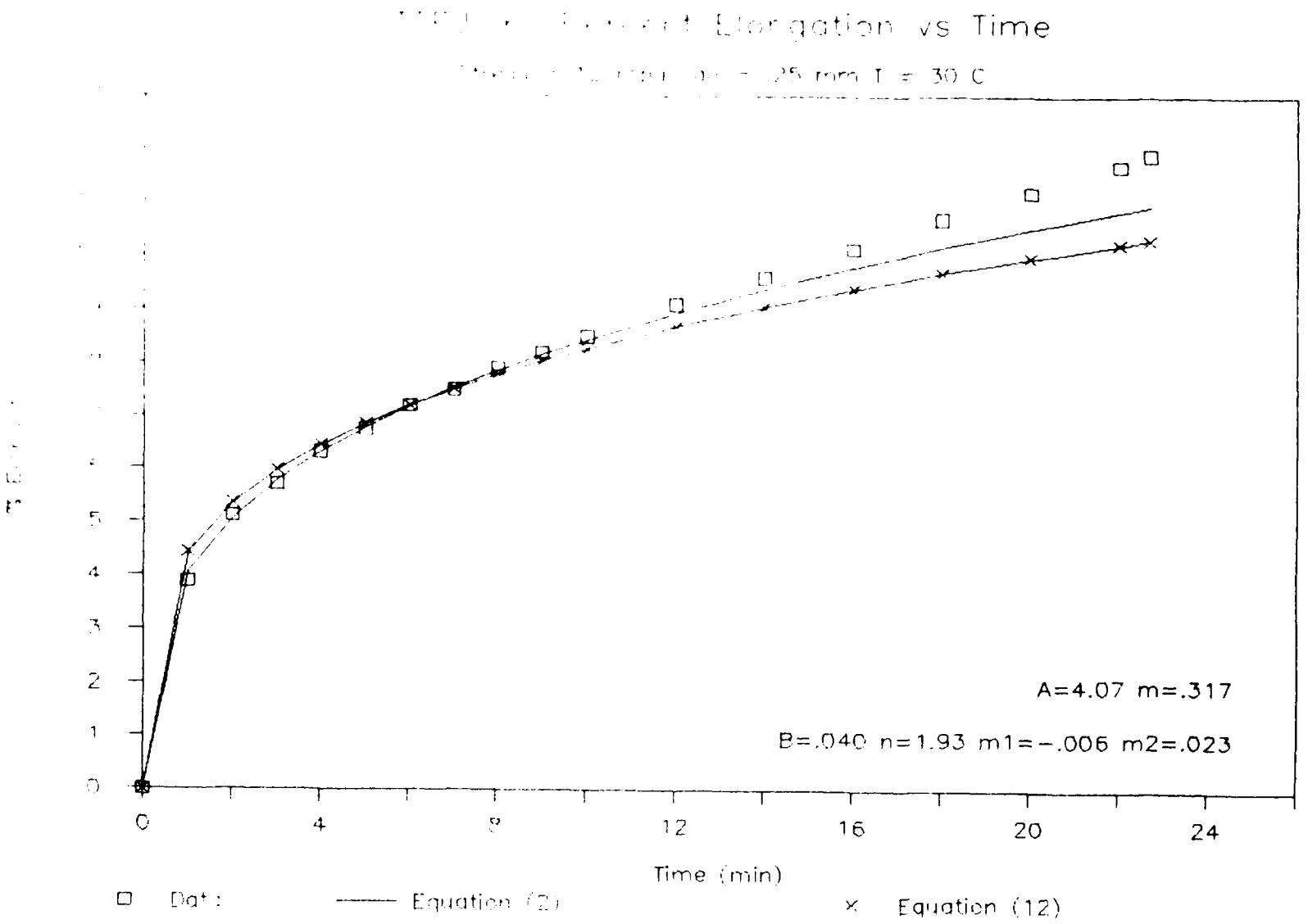
Elongation vs Time
A=4.07 m=.317
B=.040 n=1.93 m1=-.006 m2=.023
0
1
2
3
4
0
4
8
12
16
20
24
Time (min)
Data
Equation (2)
Equation (12)

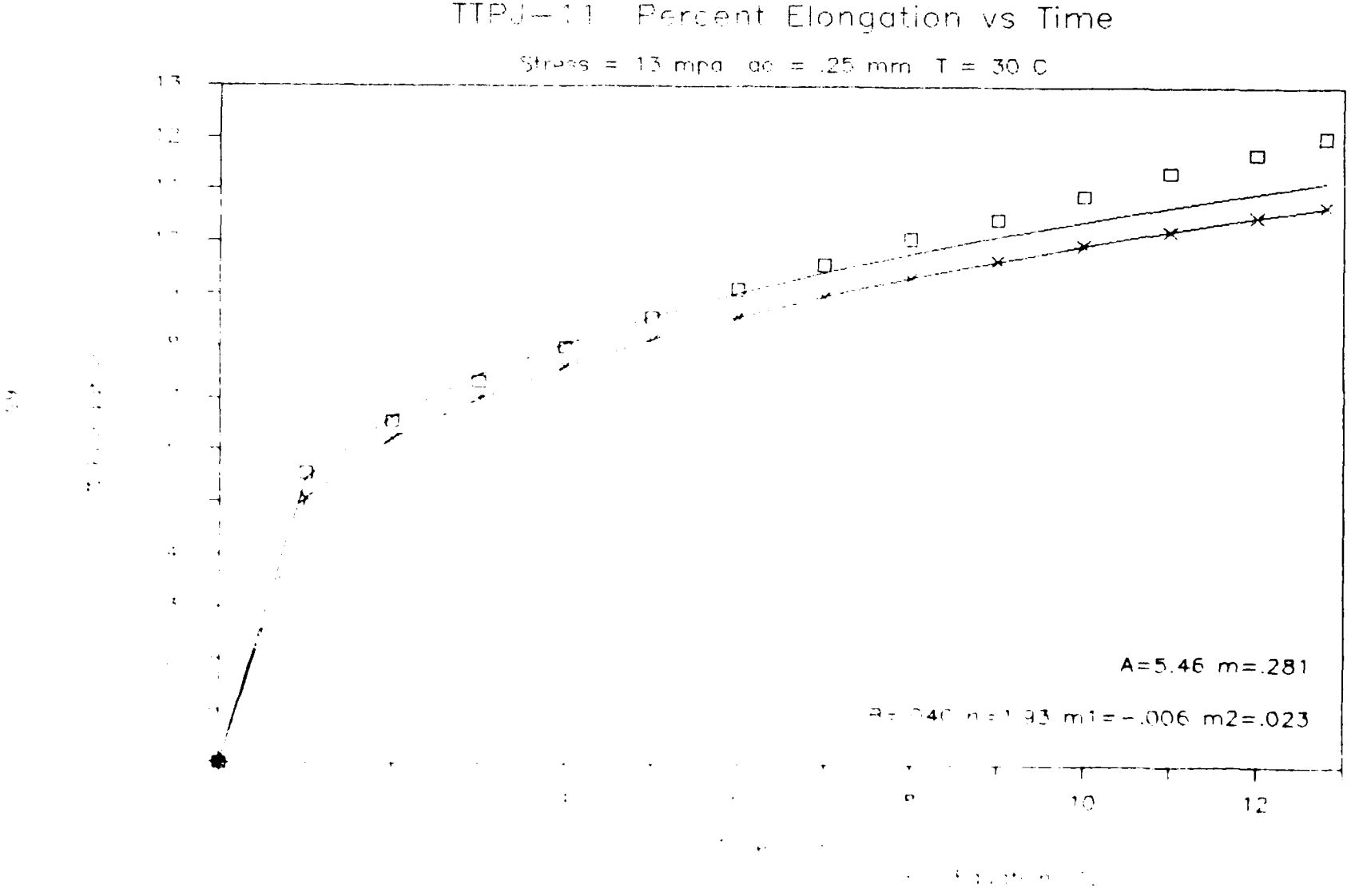
TTPJ-11 Percent Elongation vs Time
Stress = 13 mpa ao = .25 mm T = 30 C
A=5.46 m=.281
B= .240 n=1.93 m1=-.006 m2=.023
10
12

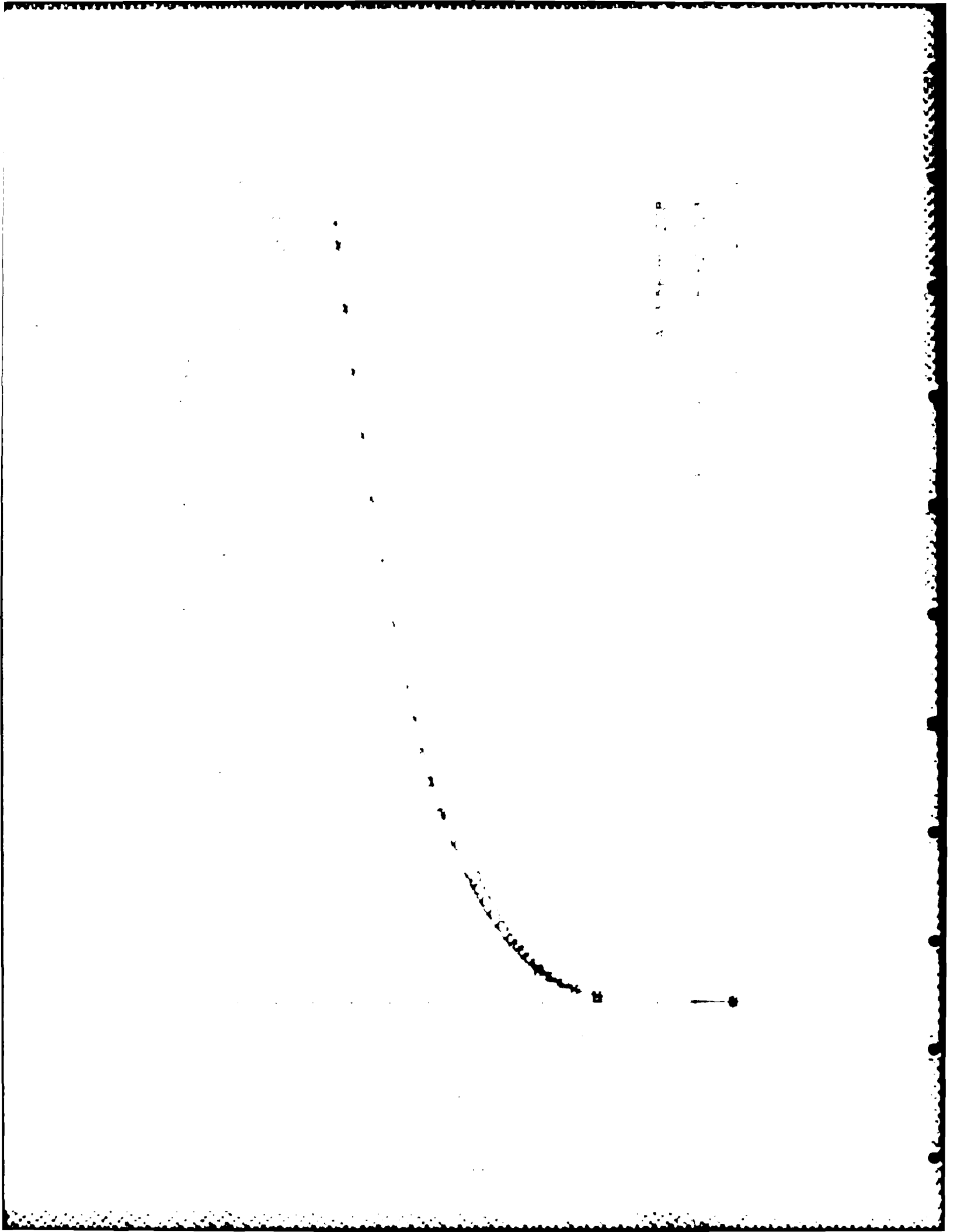

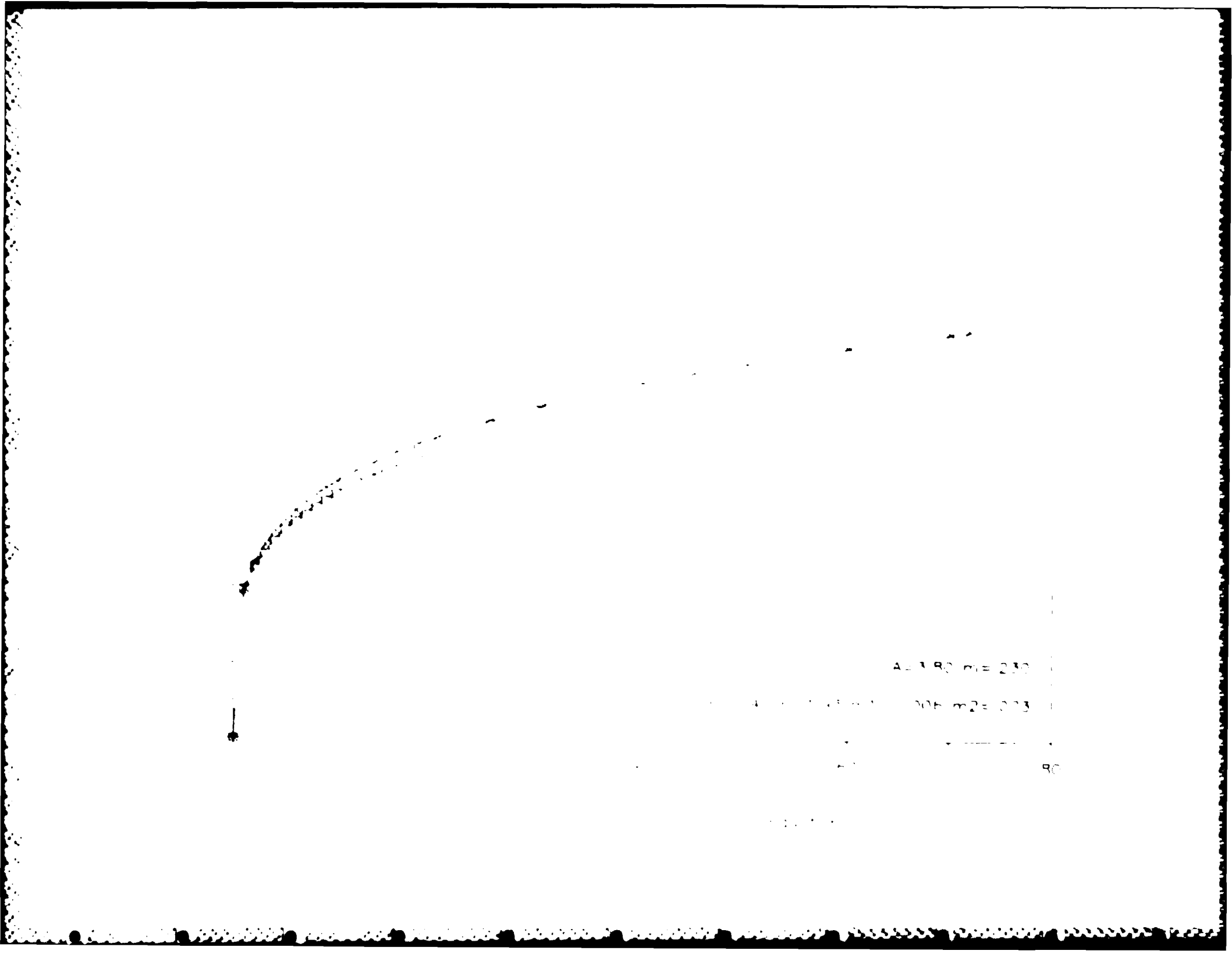

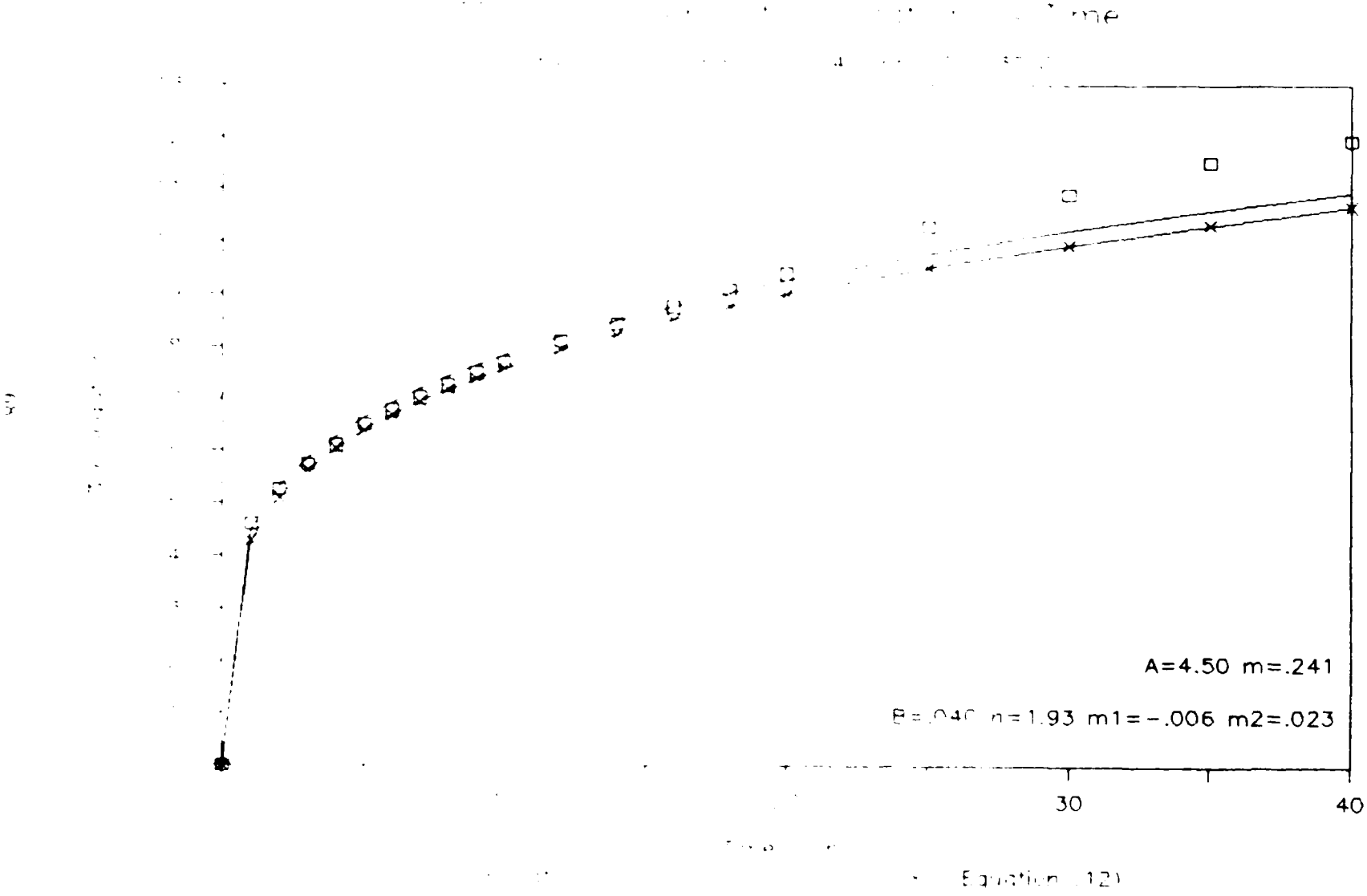
A=4.50 m=.241
B=.040 n=1.93 m1=-.006 m2=.023
30
40

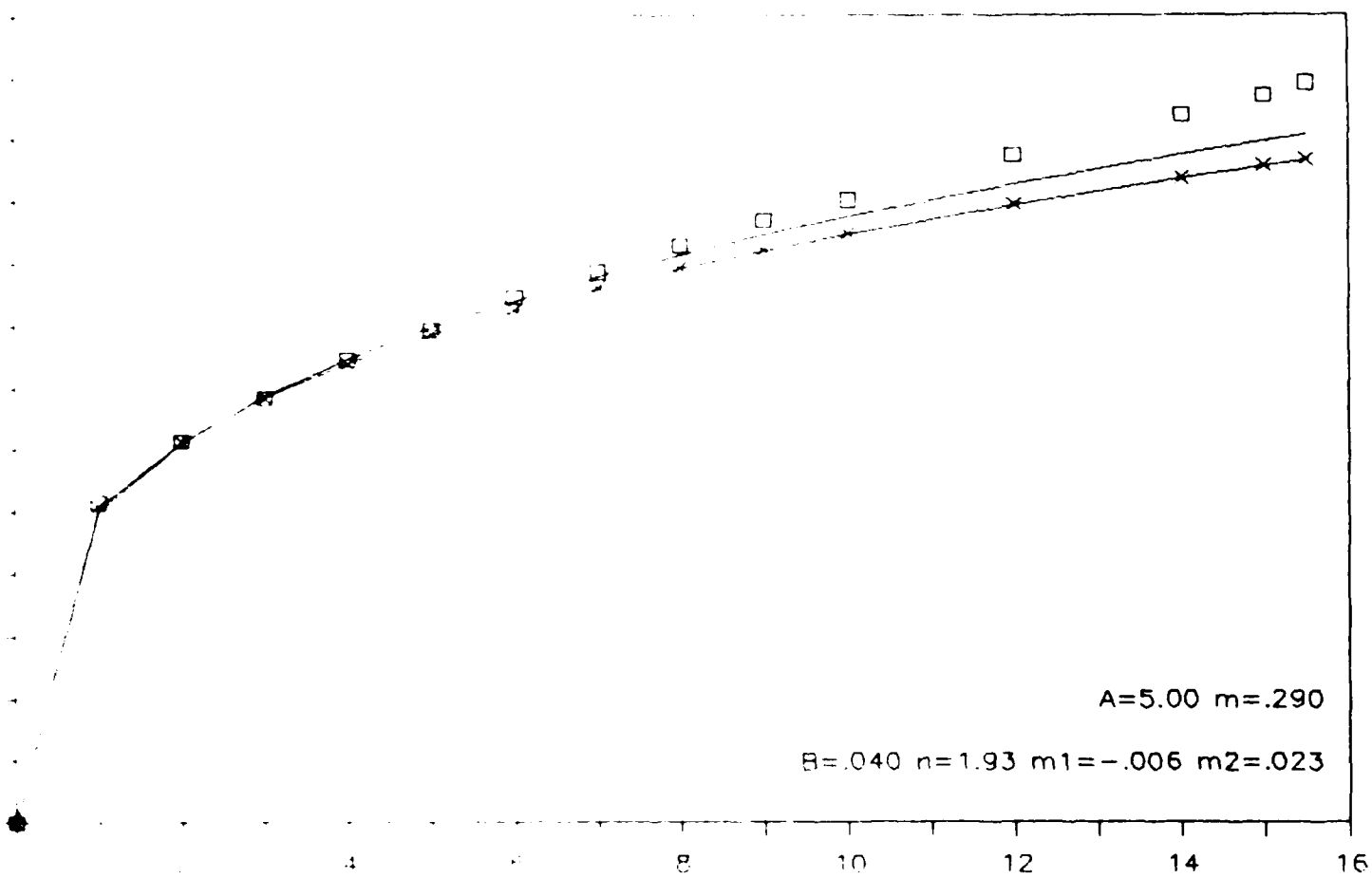

Equation (12)

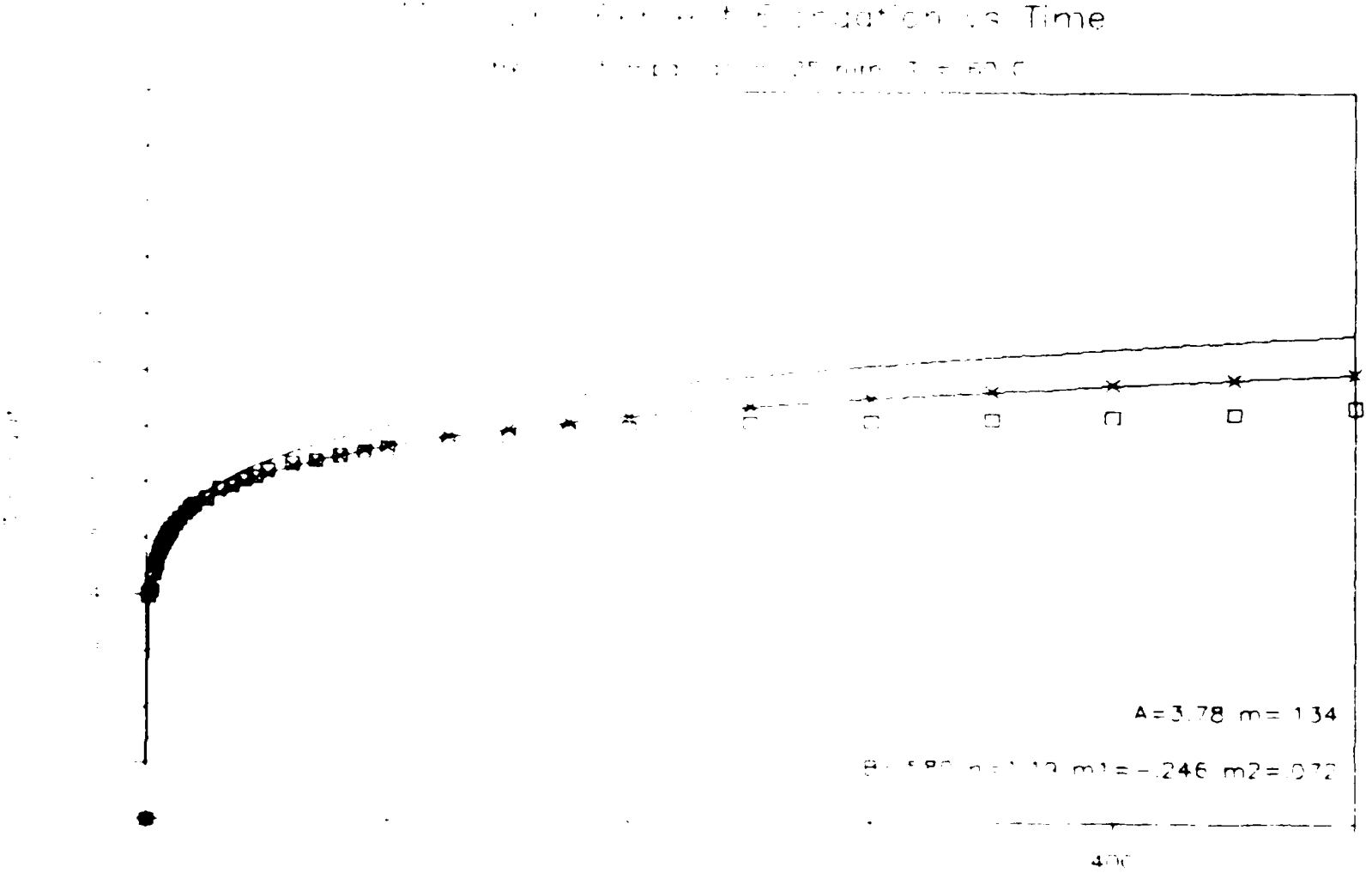
Time
A=3.78 m= 1.34
m1= -.246 m2=
400

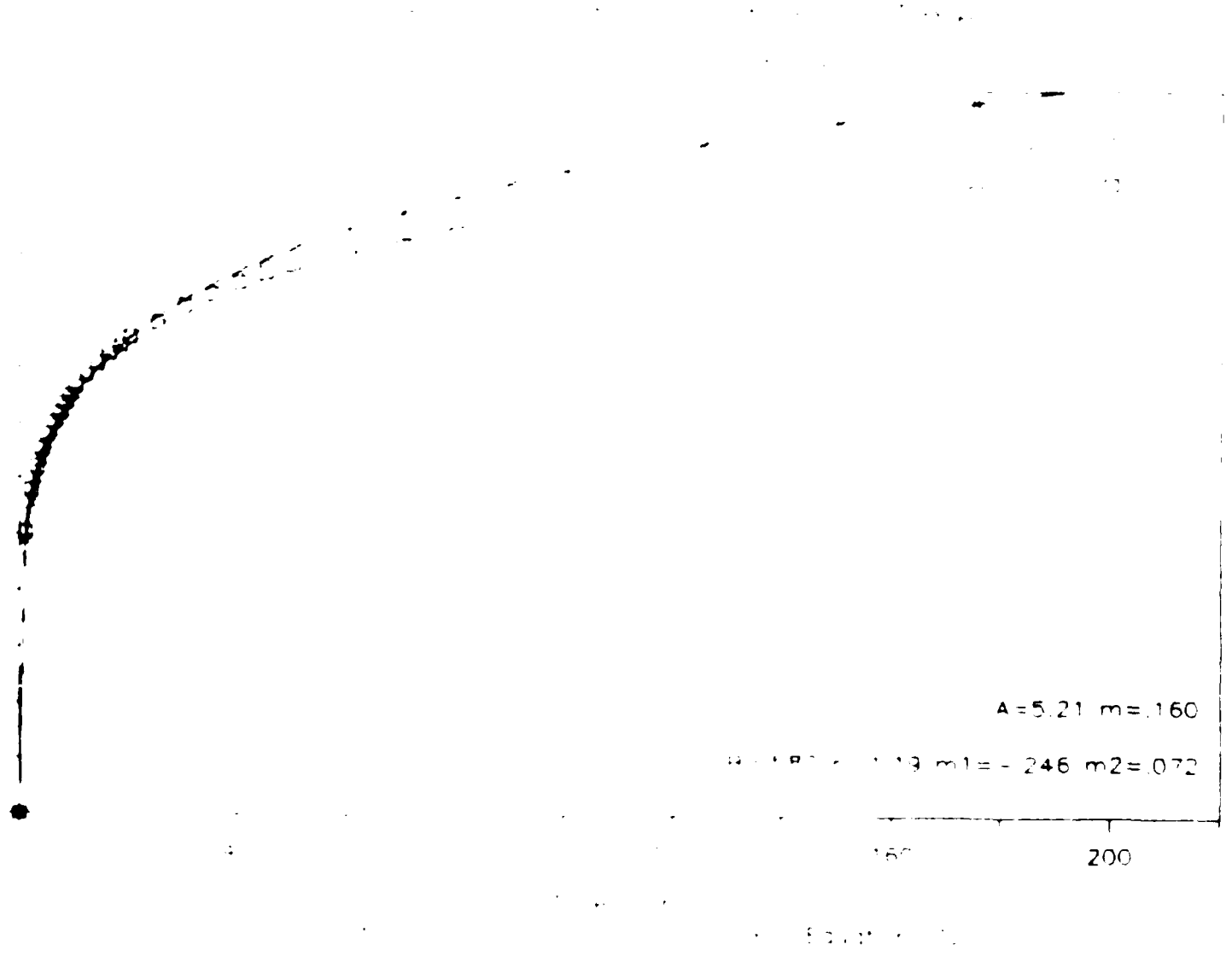
A=5.21 m=.160
m1=-.246 m2=.072
200

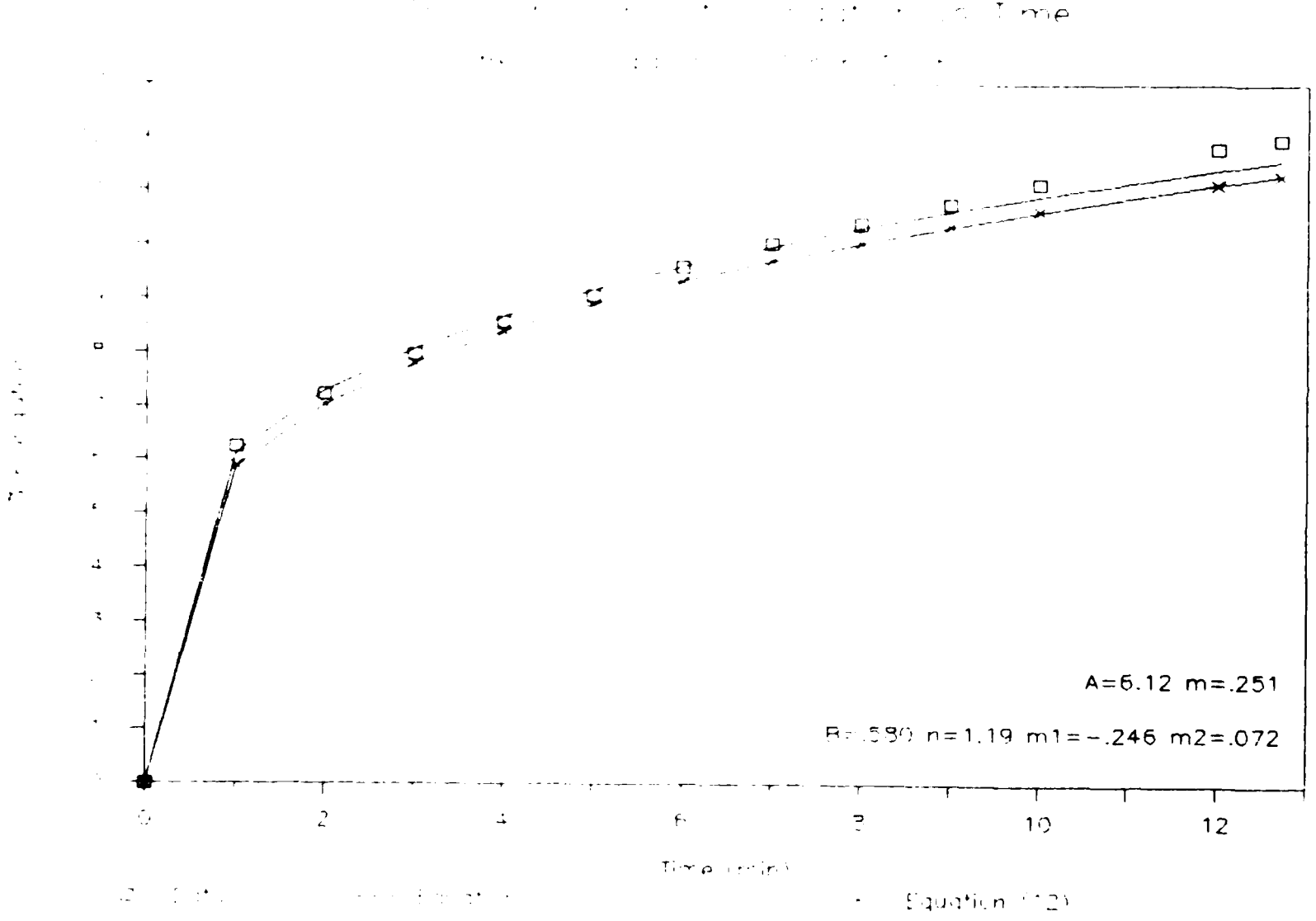
A=6.12 m=.251
B=.590 n=1.19 m1=-.246 m2=.072
0
2
4
6
8
10
12

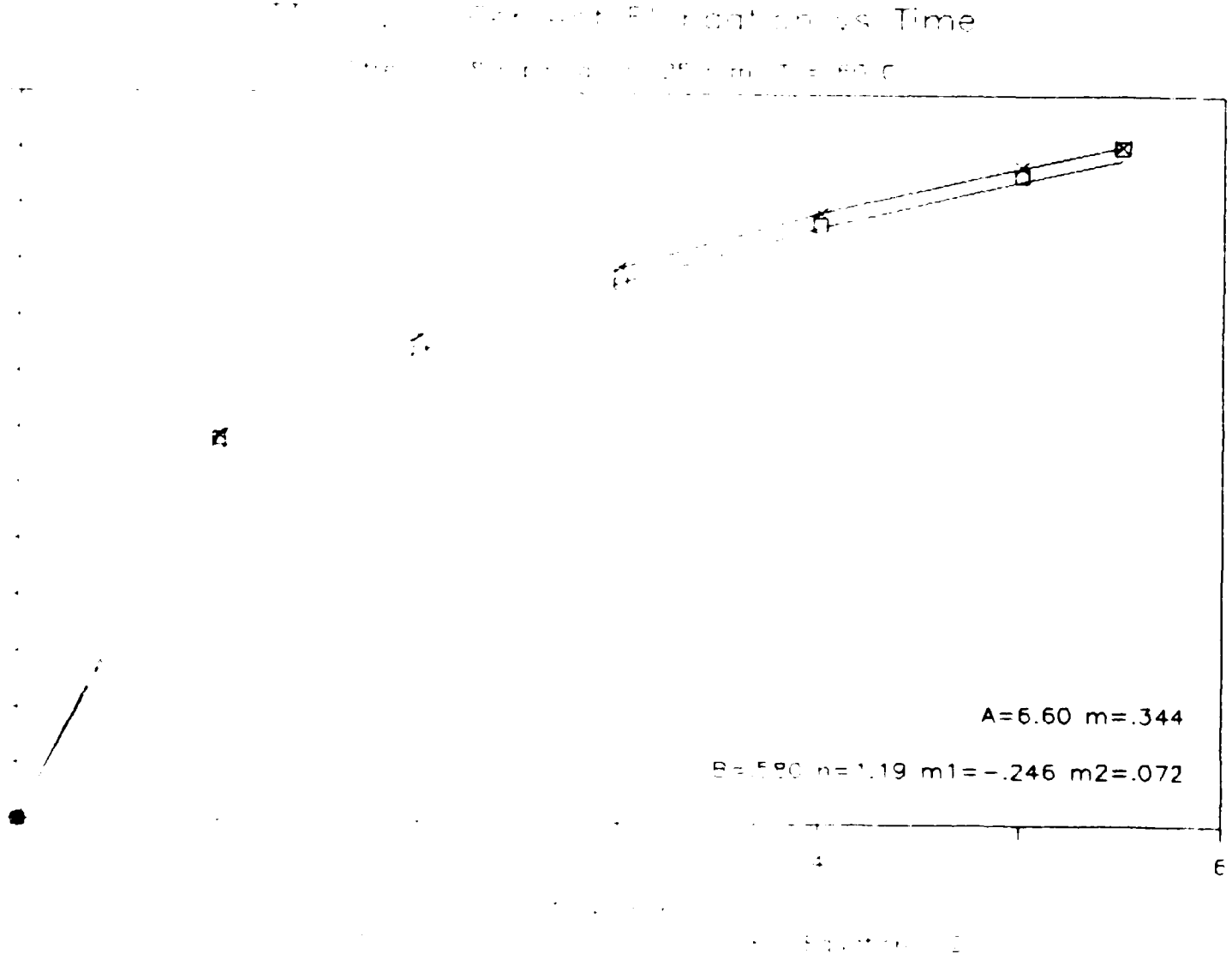
Time
A=6.60 m=.344
m1=-.246 m2=.072
6

Tables

TABLE 1

Transition Stress Levels for Marlex 6006 (30°C)

Notch Depth (mm)	Stress Range (mpa)
0.15	12 - 14
0.25	14 - 16
0.04	16 - 18

TABLE 2

Transition Stress Levels for TR 418

Notch Depth (mm)	Stress Range (mpa)
(30°C)	
0.15	10 0 - 13
0 25	10 5 - 11
0 04	10 5 - 11
(60°C)	
0 25	6 - 7

TABLE 3

Values of A and m for Marlex 6006
A_o = .15 mm T = 30° C

Experiment	φ	A	m
MTPJ - 37	11	1.60	0.224
MTPJ - 35	12	1.80	0.241
MTPJ - 38	13	1.95	0.252
MTPJ - 33	14	2.10	0.306
MTPJ - 32	15	2.40	0.302
MTPJ - 28	16	2.95	0.312
MTPJ - 25	17	3.00	0.346
MTPJ - 24	18	3.40	0.383
MTPJ - 34	19	3.60	0.444
MTPJ - 30	20	4.60	0.419
MTPJ - 31	22	6.40	0.520

TABLE 4

Values of A and m for Marlex 6006
A_o = .25 mm T = 30° C

Experiment	φ	A	m
MTPJ - 41	12	1.19	0.241
MTPJ - 39	14	1.39	0.257
MTPJ - 42	15	1.99	0.256
MTPJ - 43	16	2.88	0.299
MTPJ - 45	18	3.95	0.424
MTPJ - 47	19	3.70	0.497
MTPJ - 49	22	4.18	0.594

TABLE 5

Values of A and m for Marlex 6006
A_o = 40 mm T = 30° C

Experiment	σ	A	m
MTPJ 45	12	1.70	0.256
MTPJ 44	14	2.30	0.256
MTPJ 43	16	3.30	0.280
MTPJ 42	18	3.87	0.319
MTPJ 41	20	4.98	0.520

TABLE 6

Values for B and n for Marlex 6006 (30° C)

Notch Depth (mm)	B	n	Correlation Coefficient
0.15	0.016	1.87	0.98
0.25	0.013	1.94	0.98
0.40	0.010	2.09	0.99
Combined Values	0.013	1.94	0.98

TABLE 7

Values of m_1 and m_2 for Marlex 6006 (30° C)

Notch Depth (mm)	m_1	m_2	Correlation Coefficient
0.15	-0.078	0.026	0.95
0.25	-0.174	0.035	0.85
0.40	-0.191	0.033	0.82
Combined Values	-0.097	0.028	0.91

TABLE 8

Values of A and m for TR 418
A_o = .15 mm T = 30° C

Experiment	σ	A	m
TTPJ - 13	10.0	3.40	0.230
TTPJ - 15	10.5	3.99	0.238
TTPJ - 14	11.0	4.00	0.236
TTPJ - 16	13.0	6.47	0.267

TABLE 9

Values of A and m for TR 418
A_o = .25 mm T = 30° C

Experiment	σ	A	m
TTPJ - 12	9.0	2.66	0.260
TTPJ - 7	10.0	3.70	0.201
[illegible]	10.5	3.58	0.266
[illegible]	11.0	3.84	0.270
[illegible]	12.0	4.07	0.317
[illegible]	13.0	5.46	0.281

TABLE 10

Values of A and m for TR 418
A_o = .40 mm T = 30° C

Experiment	σ	A	m
TTPJ - 25	10.0	3.56	0.208
TTPJ - 23	10.5	3.80	0.230
TTPJ - 22	11.0	4.50	0.241
TTPJ - 24	12.0	5.00	0.290

TABLE 11

Values of A and m for TR 418
A_o = .25 mm T = 60° C

Experiment	σ	A	m
TTPJ - 26	5.0	3.78	0.134
TTPJ - 18	6.0	5.21	0.160
TTPJ - 19	7.0	6.12	0.251
TTPJ - 20	8.0	6.60	0.344
TTPJ - 17	10.0	0.00	∞

TABLE12

Values of B and n for TR 418

Temp (°C)	Notch Depth (mm)	B	n	Correlation Coefficient
30	0.15	0.013	2.41	0.99
30	0.25	0.070	1.67	0.95
30	0.40	0.040	1.95	0.95
60	0.25	0.580	1.19	0.95
30	Combined Value	0.040	1.93	0.93

TABLE 13

Values of m_1 and m_2 for TR 418

Temp (°C)	Notch Depth (mm	m_1	m_2	Correlation Coefficient
30	0.15	-0.106	0.012	0.95
30	0.25	-0.025	0.025	0.66
30	0.40	-0.196	0.040	0.98
60	0.25	-0.246	0.072	0.95
30	Combined Values	-0.006	0.023	0.65

Figures

Figure 1

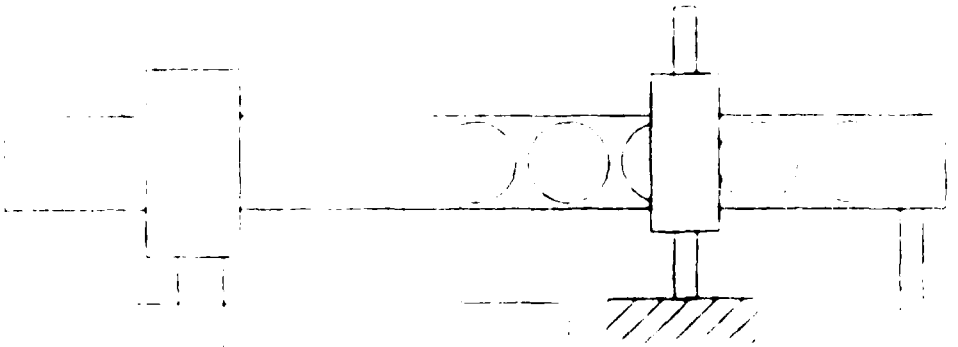

Figure 2

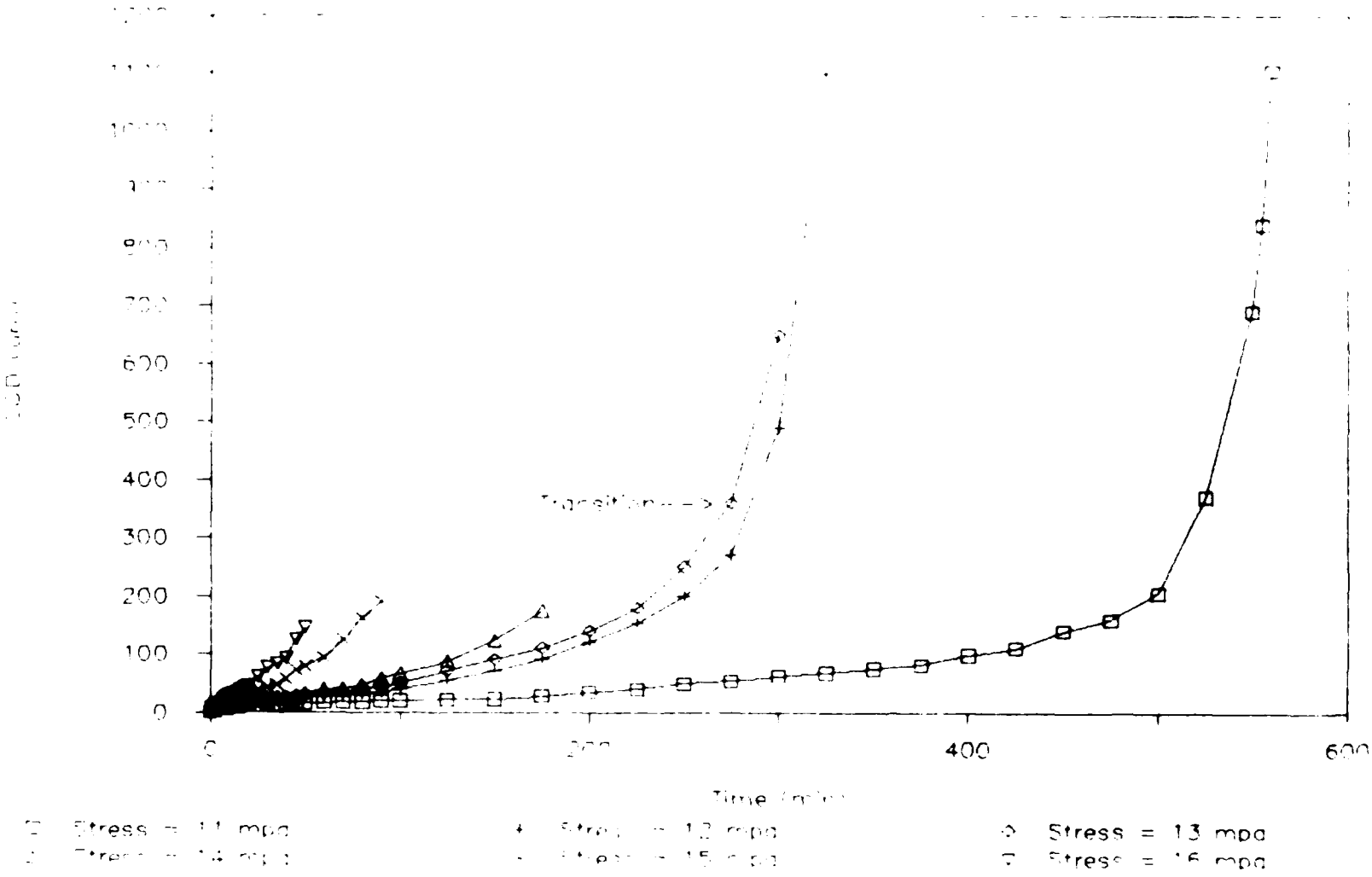

Figure 3A

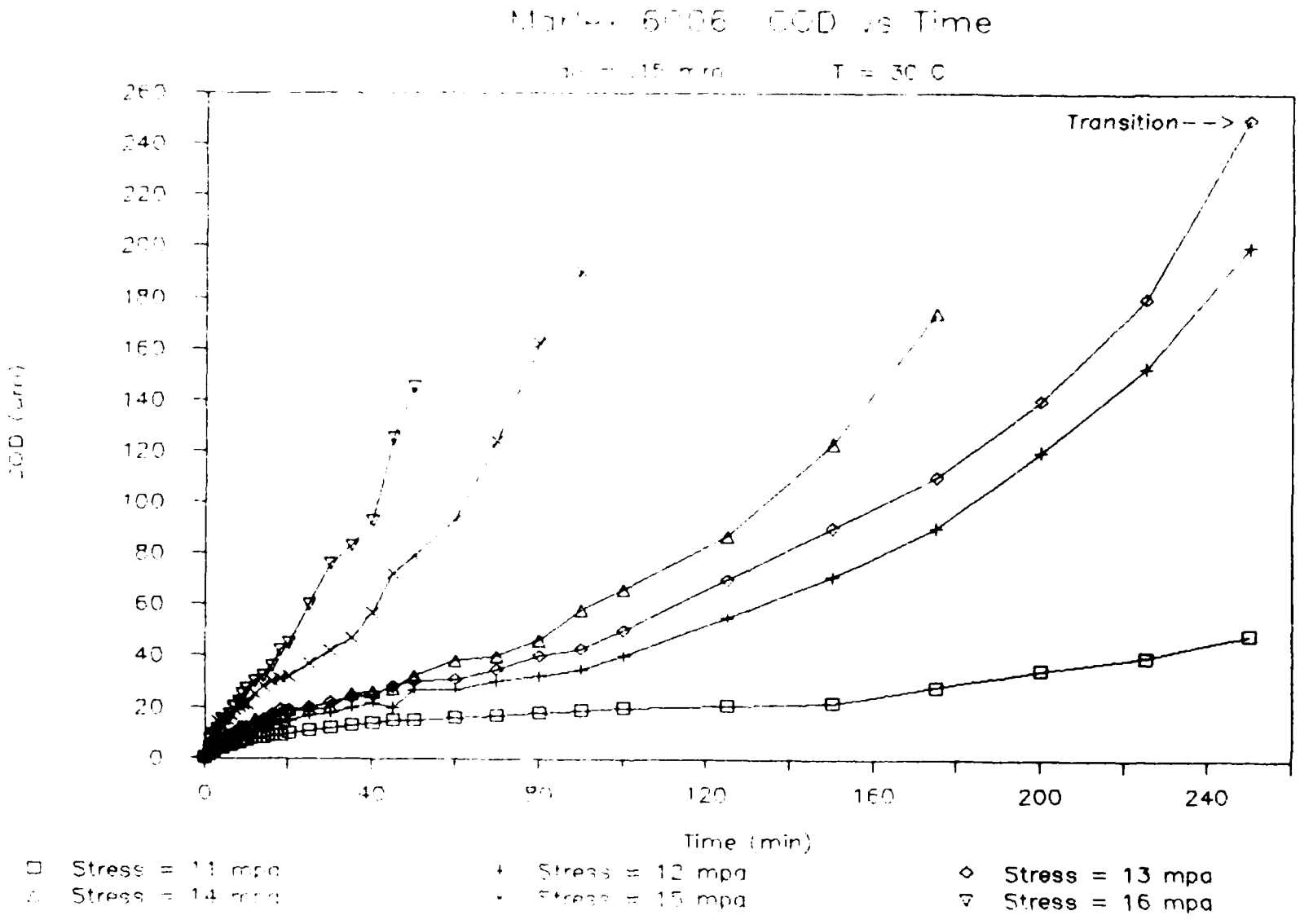
Transition--->
0
20
40
60
80
100
120
140
160
180
200
220
240
260
0
40
120
160
200
240
Time (min)
Stress = 12 mpa
Stress = 13 mpa
Stress = 16 mpa

Figure 3B

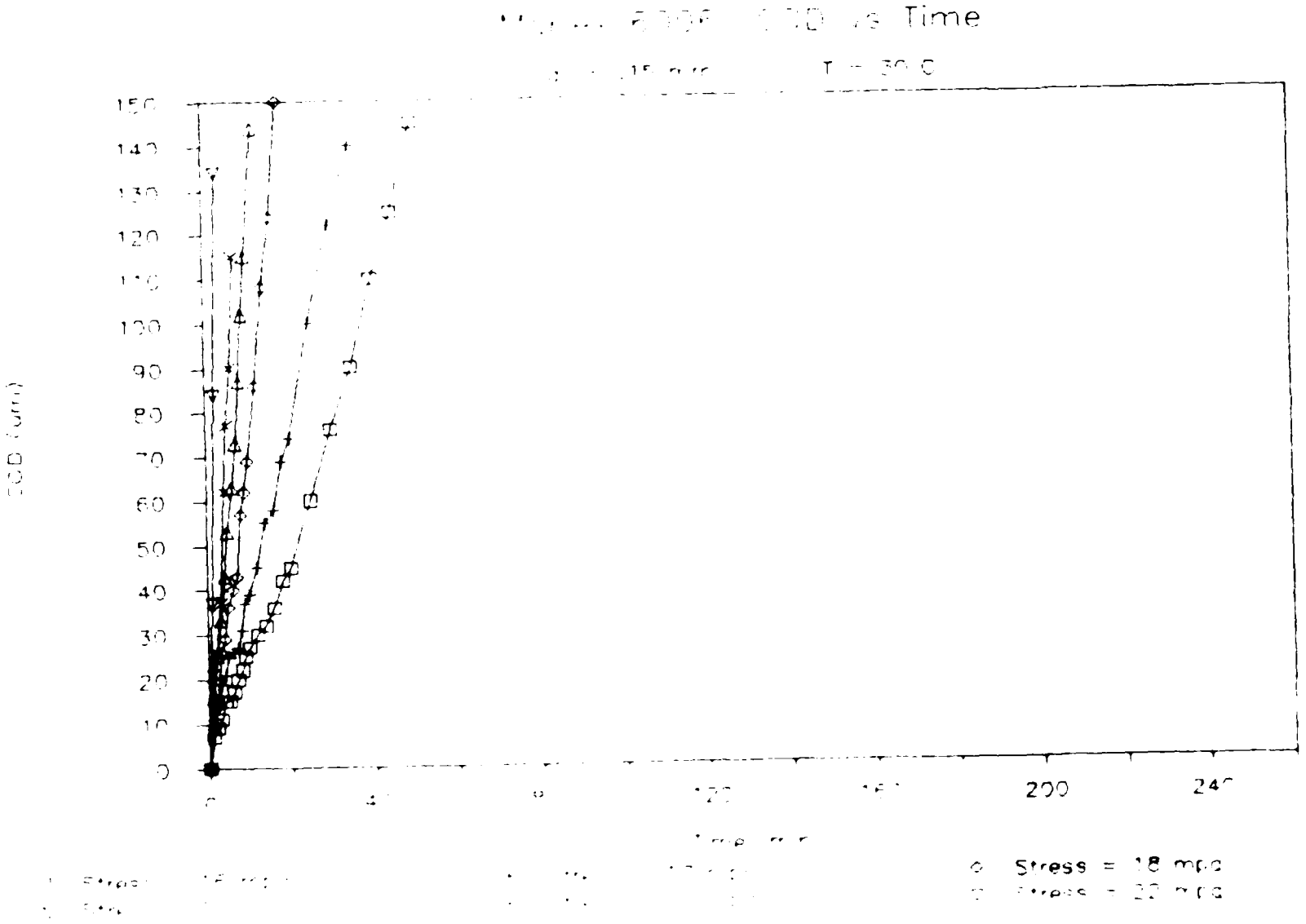
Time
150
140
130
120
110
100
90
80
70
60
50
40
30
20
10
0
200
Stress = 18 mpa

Figure 3C

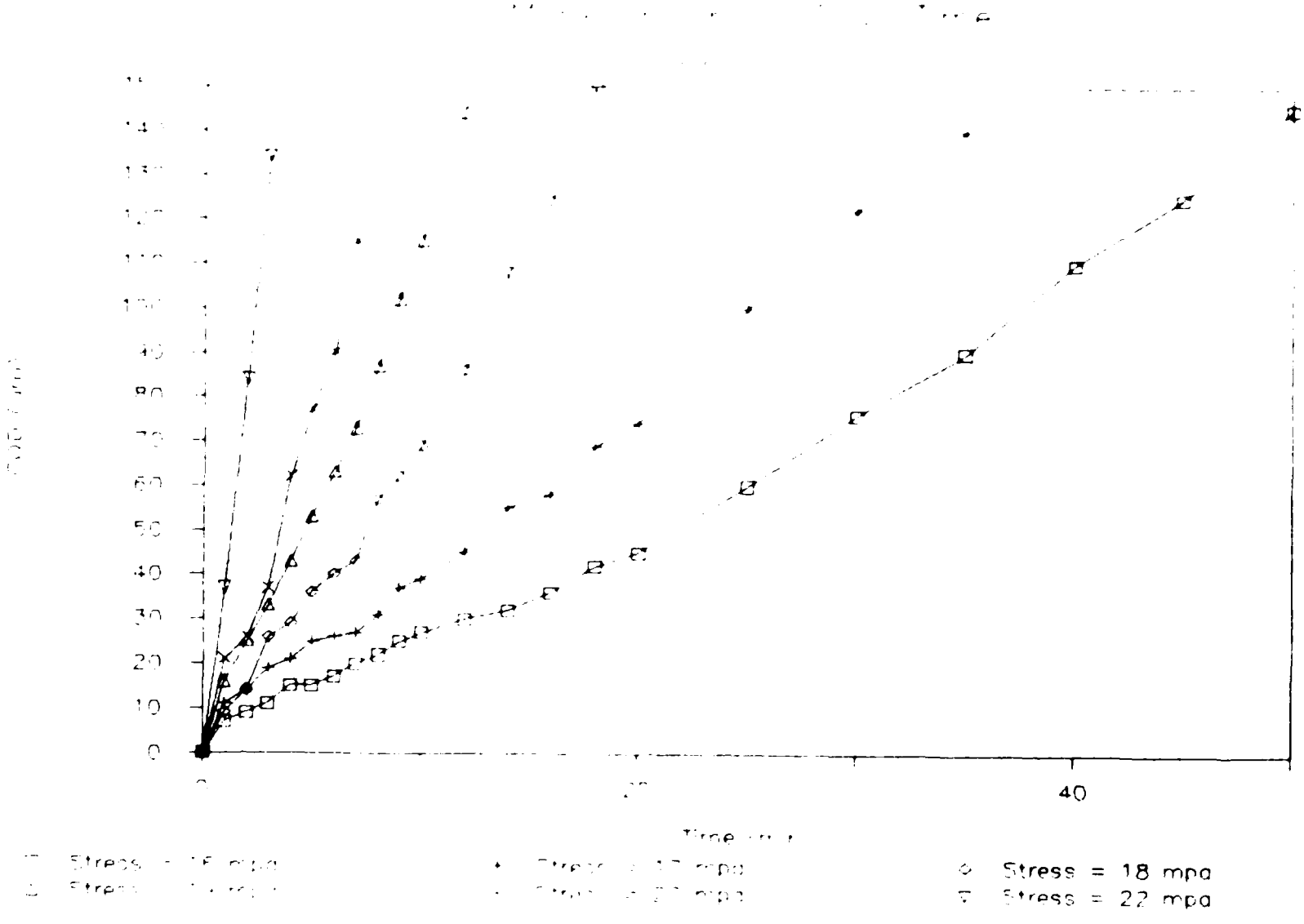

Figure 3D

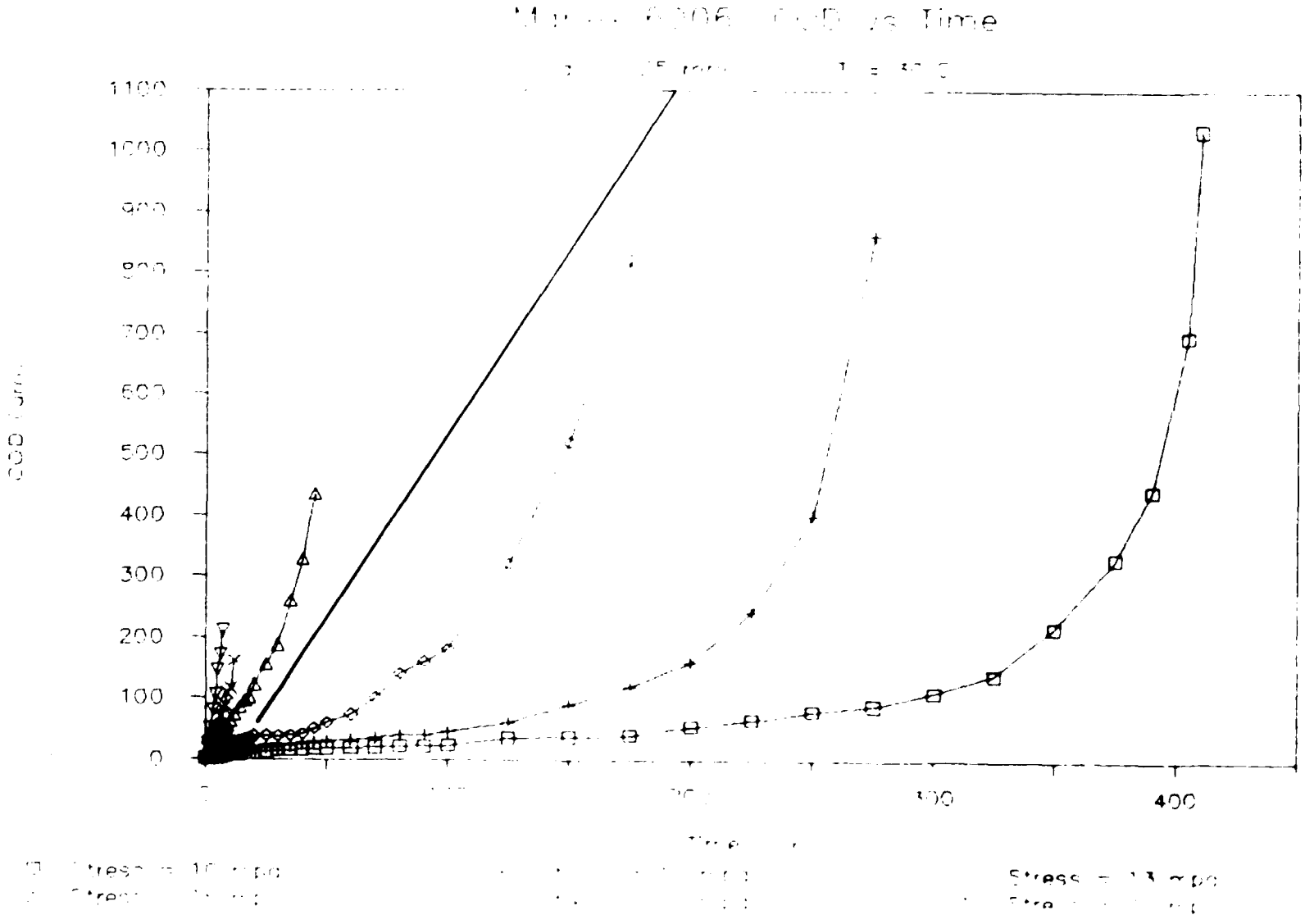
1100
1000
900
800
700
600
500
400
300
200
100
0
400

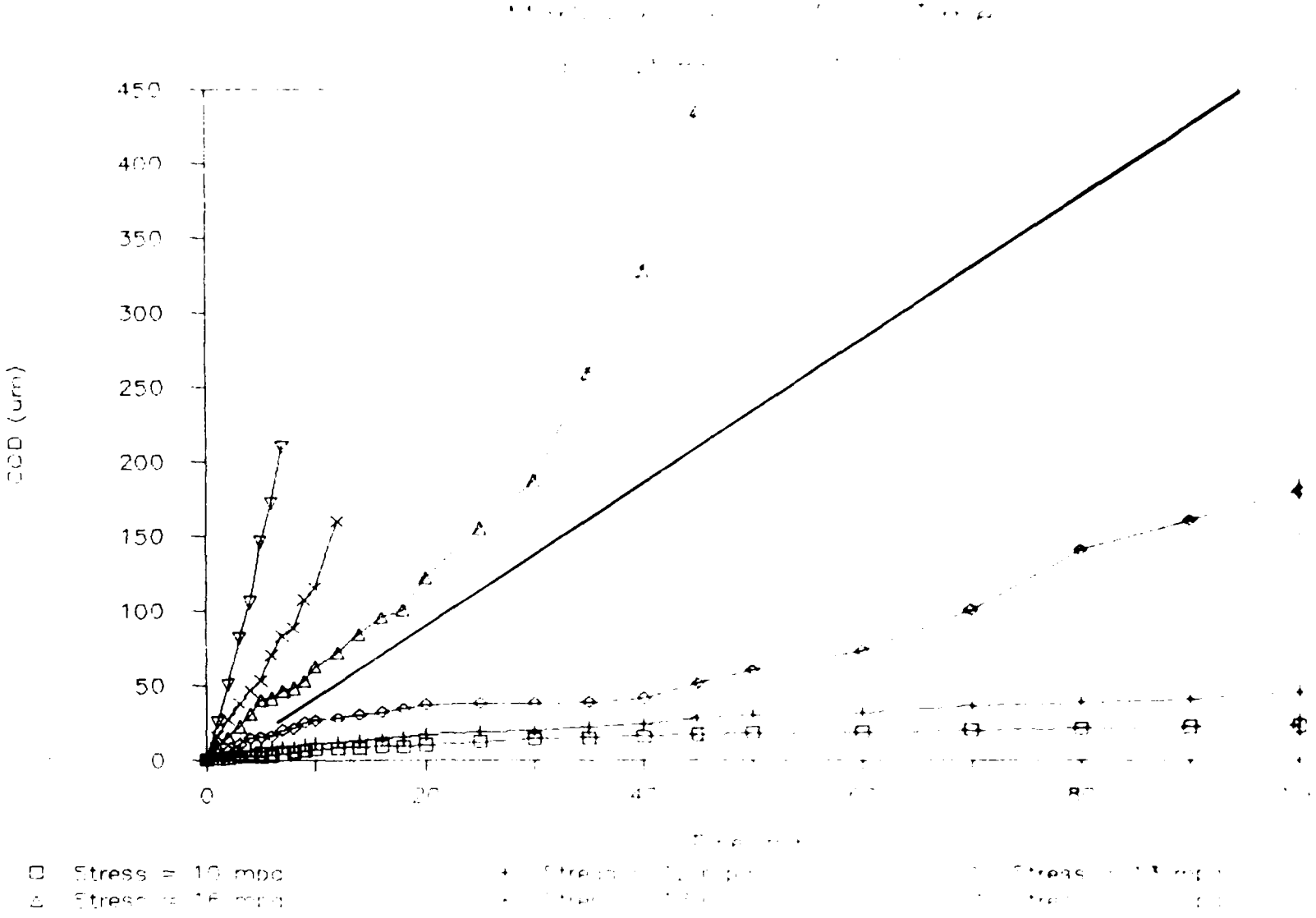

Figure 4B

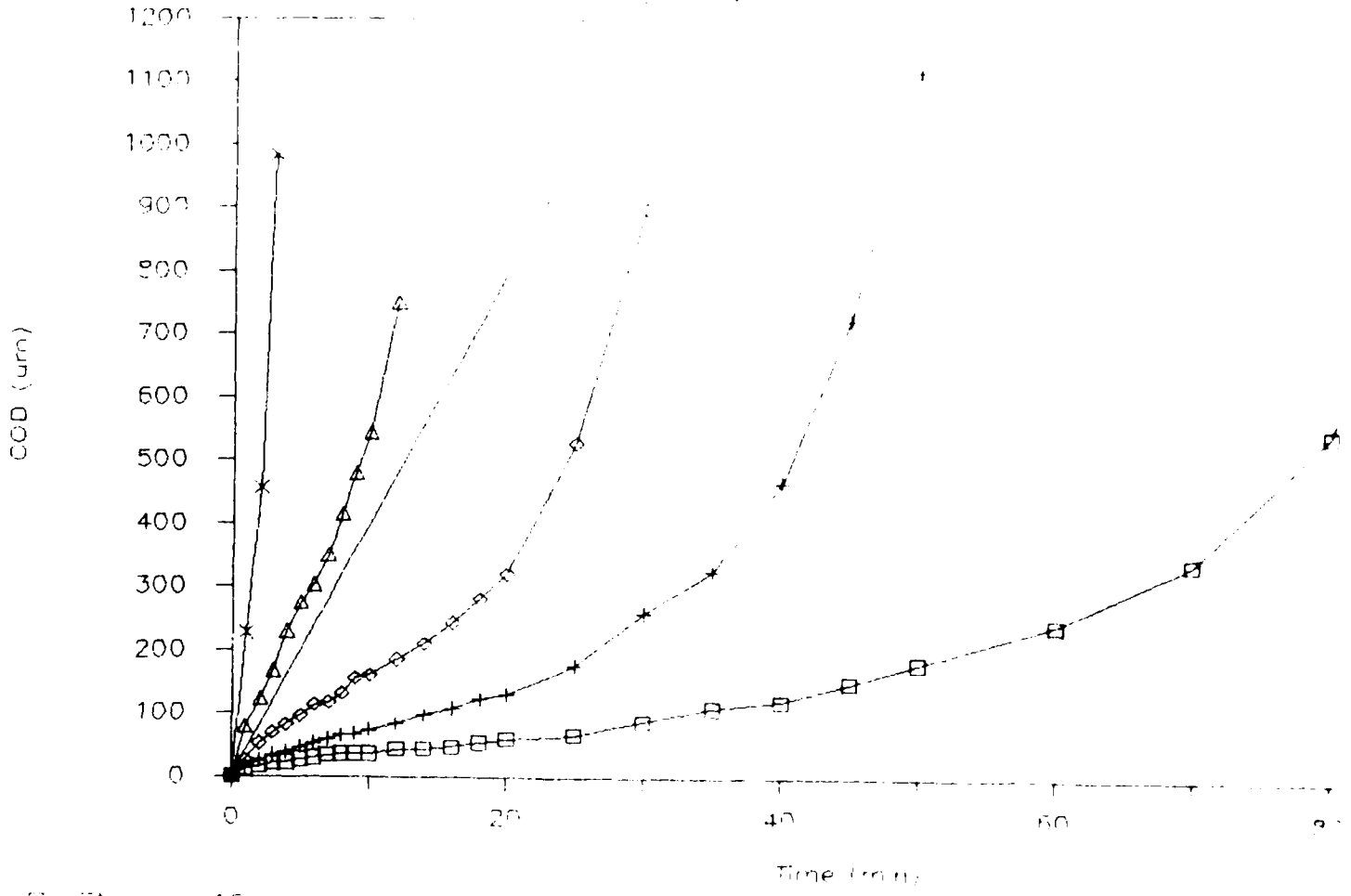
1200
1100
1000
900
800
700
600
500
400
300
200
100
0
COD (um)
0
20
40
60
Time (min)

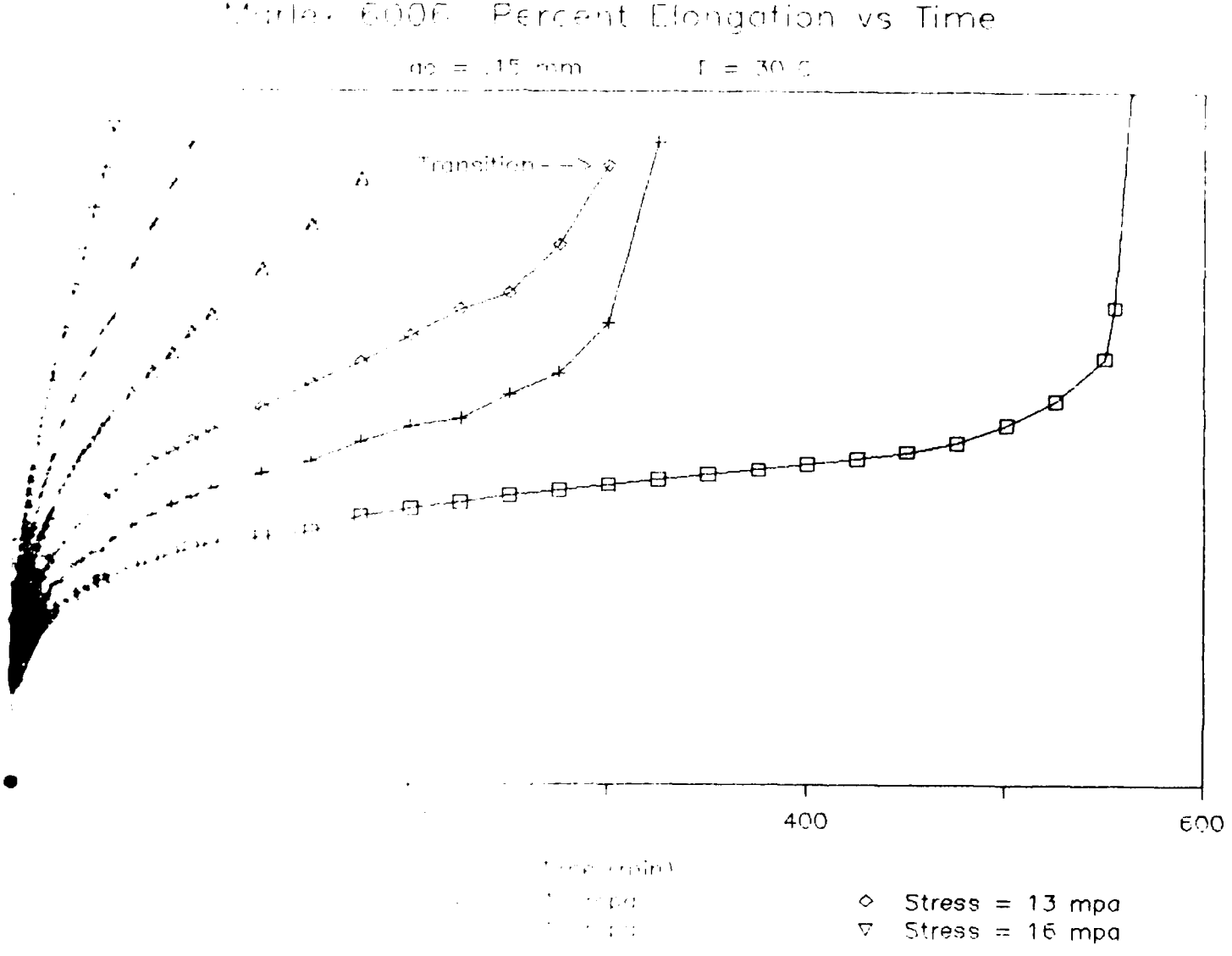
Transition
400
600
◇ Stress = 13 mpa
▽ Stress = 16 mpa

AD-A183 776 THE TRANSITION FROM BRITTLE TO DUCTILE FAILURE IN POLYETHYLENES(U) PENNSYLVANIA UNIV PHILADELPHIA SCHOOL OF ENGINEERING AND APPLIED SCIENCE J L D'ONOFRIO 2/2

UNCLASSIFIED AUG 87 F/G 11/9 NL

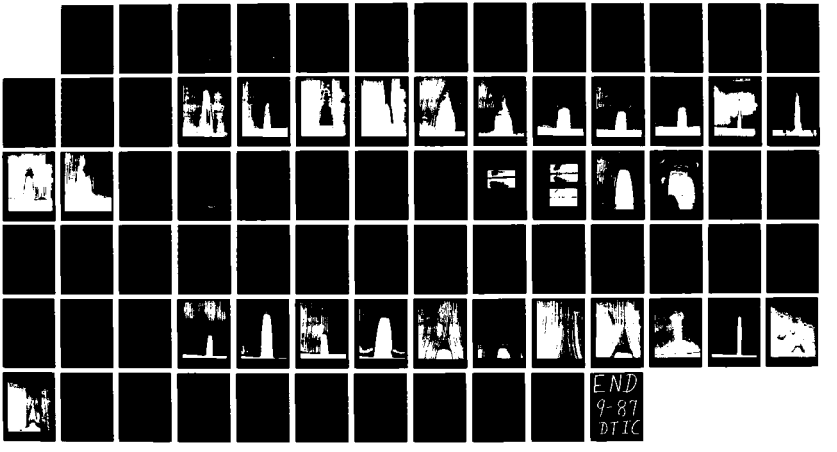

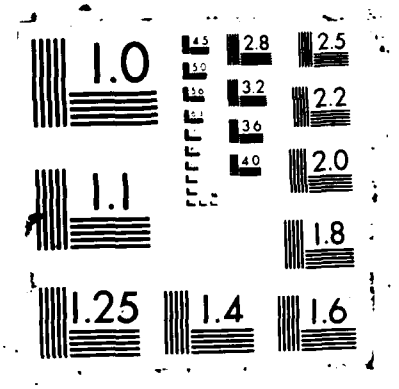
1.0
1.1
1.25
1.4
1.6
1.8
2.0
2.2
2.5
2.8
3.2
3.6
4.0
4.5
5.0
5.6

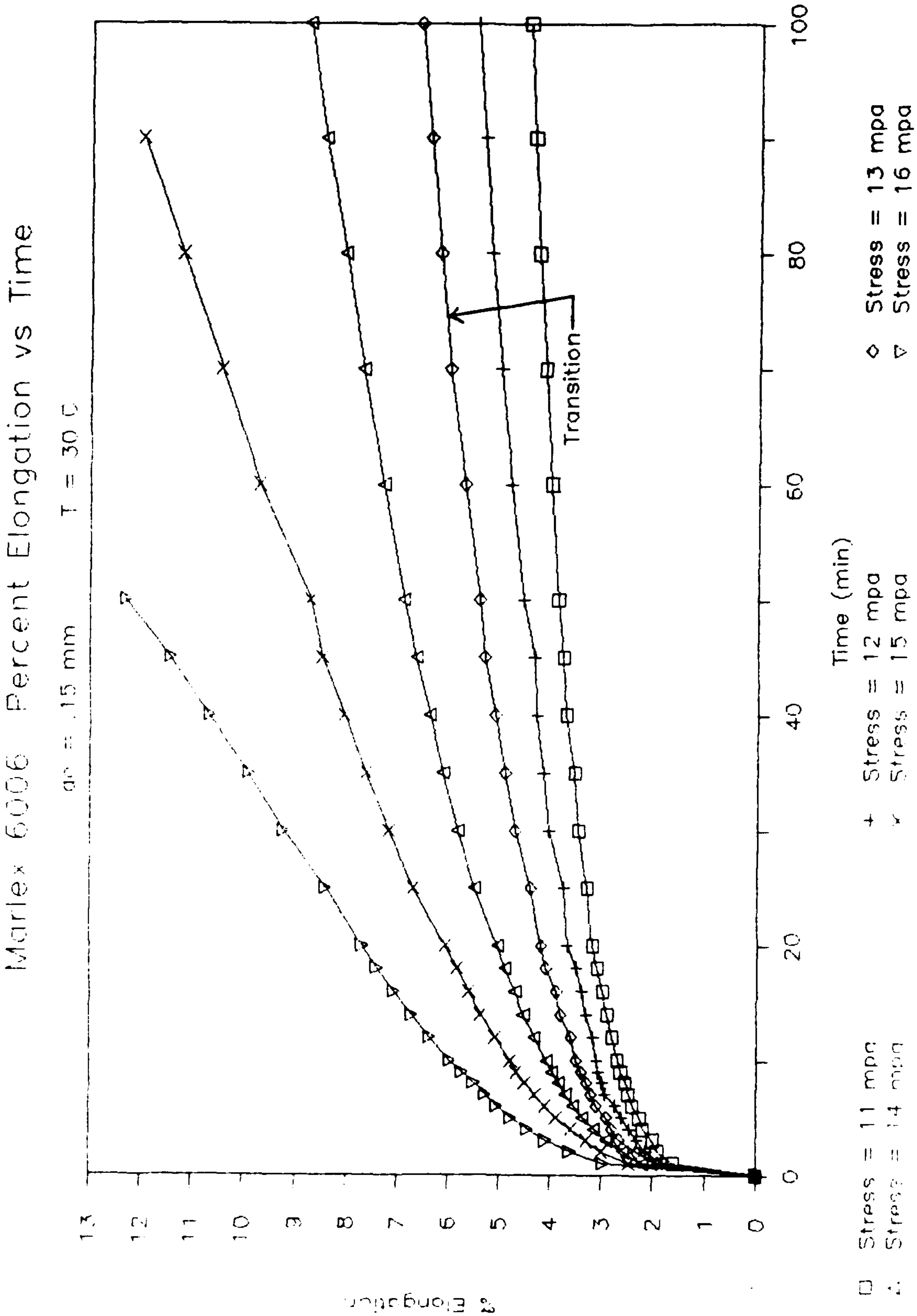

Marlex 6006 Percent Elongation vs Time
T = 30 C
% Elongation
Time (min)
0
20
40
60
80
100
0
1
2
3
4
5
6
7
8
9
10
11
12
13
Transition
Stress = 11 mpa
Stress = 12 mpa
Stress = 13 mpa
Stress = 15 mpa
Stress = 16 mpa

Figure 6B

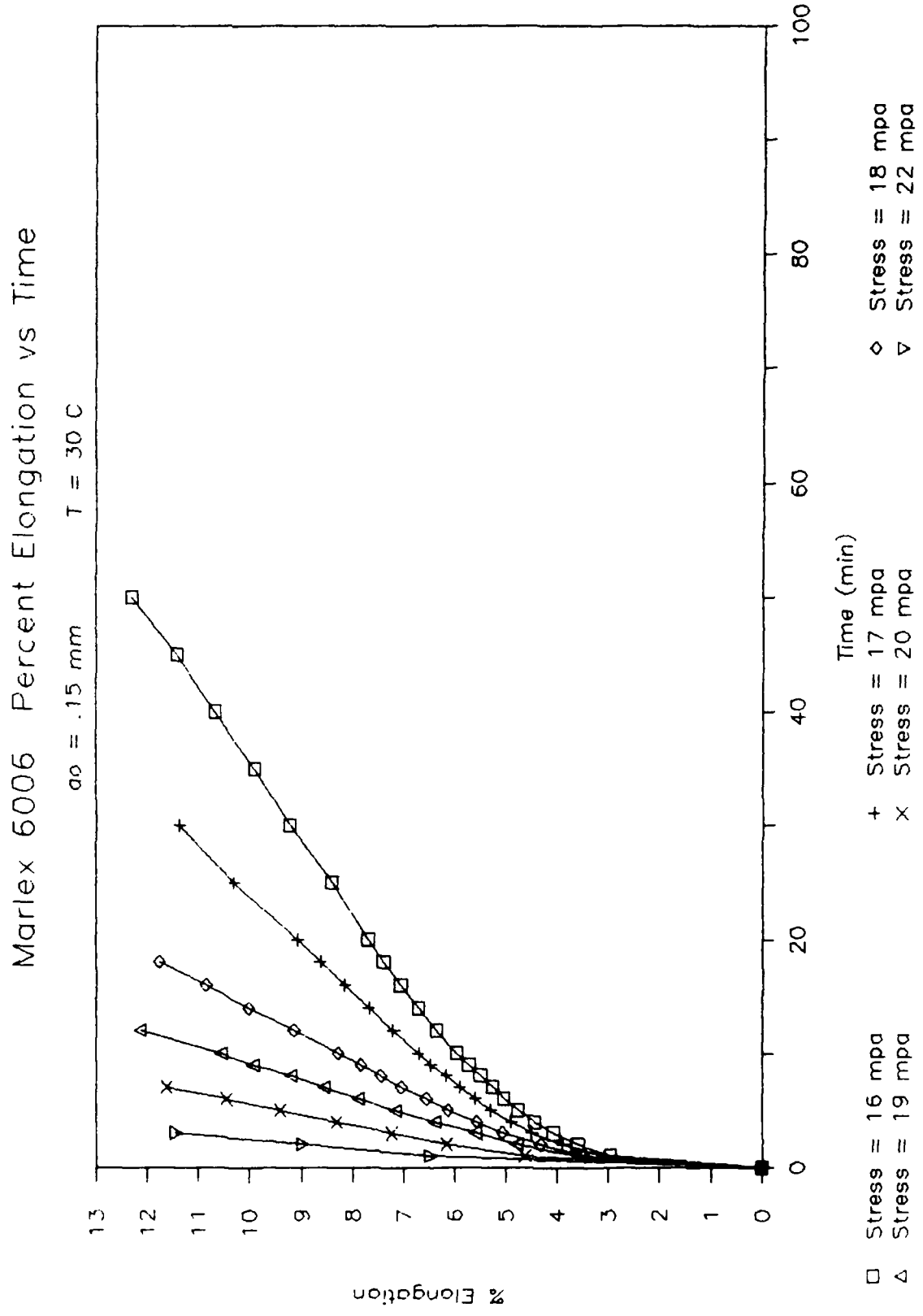
Marlex 6006 Percent Elongation vs Time
ao = .15 mm
T = 30 C
% Elongation
Time (min)
0
1
2
3
4
5
6
7
8
9
10
11
12
13
0
20
40
60
80
100
□ Stress = 16 mpa
△ Stress = 19 mpa
+ Stress = 17 mpa
× Stress = 20 mpa
◇ Stress = 18 mpa
▽ Stress = 22 mpa

Figure 6C

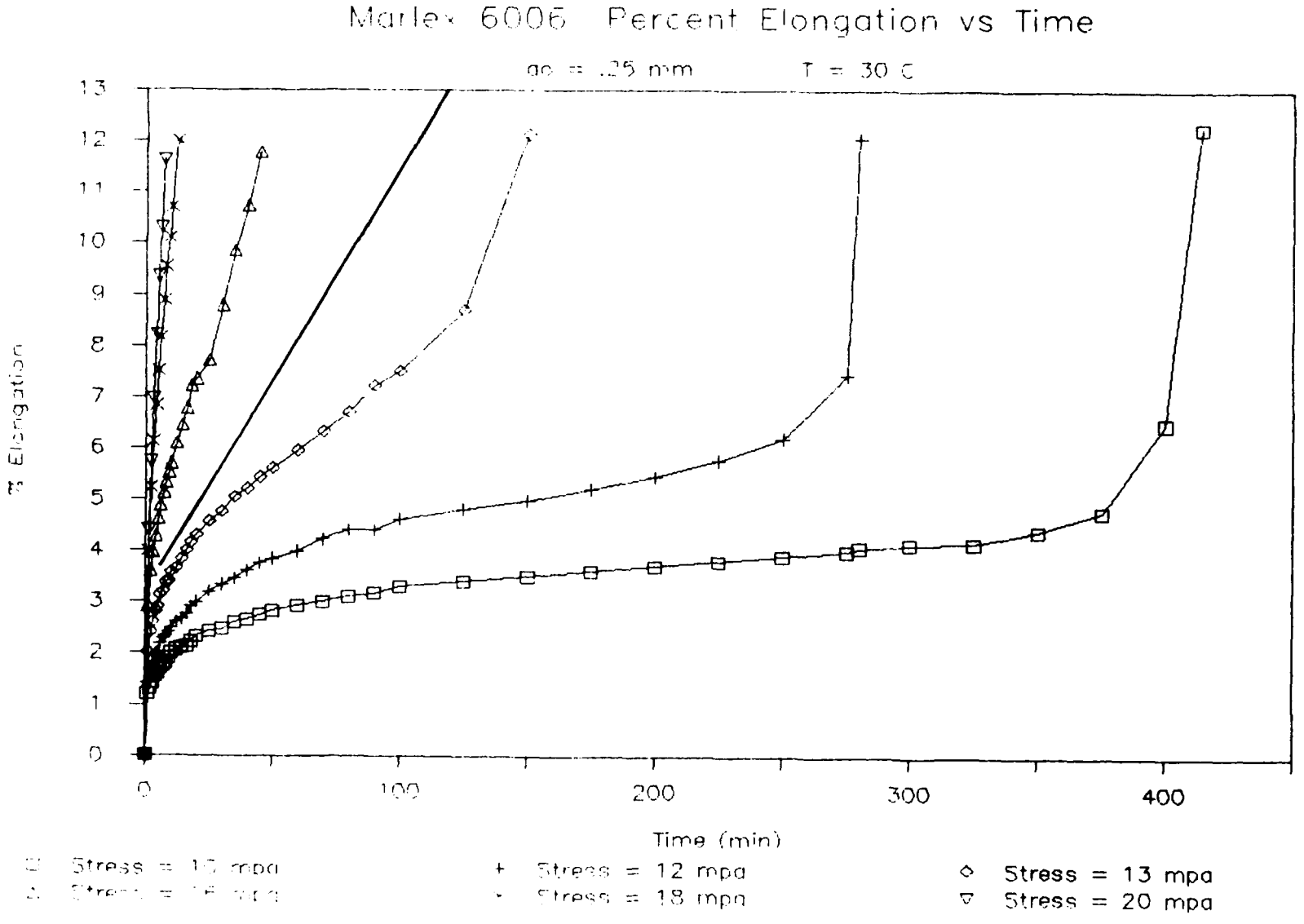
Marlex 6006 Percent Elongation vs Time
go = .25 mm
T = 30 C
% Elongation
Time (min)
0
100
200
300
400
0
1
2
3
4
5
6
7
8
9
10
11
12
13
Stress = 12 mpa
Stress = 13 mpa
Stress = 18 mpa
Stress = 20 mpa

Figure 7A

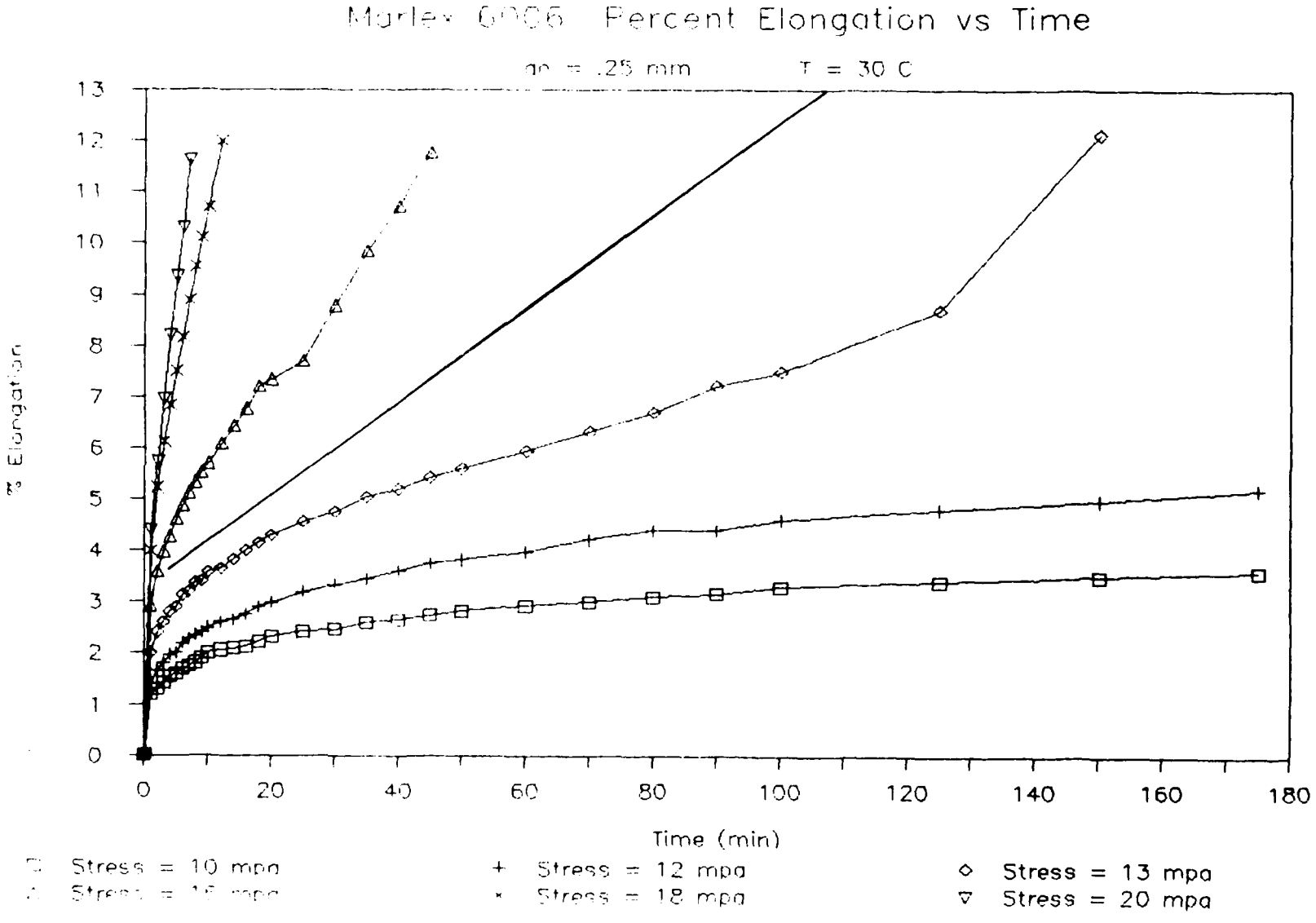
Marlex 6006 Percent Elongation vs Time
T = 30 C
% Elongation
Time (min)
0
20
40
60
80
100
120
140
160
180
1
2
3
4
5
6
7
8
9
10
11
12
13
Stress = 10 mpa
Stress = 12 mpa
Stress = 13 mpa
Stress = 18 mpa
Stress = 20 mpa

Figure 7B

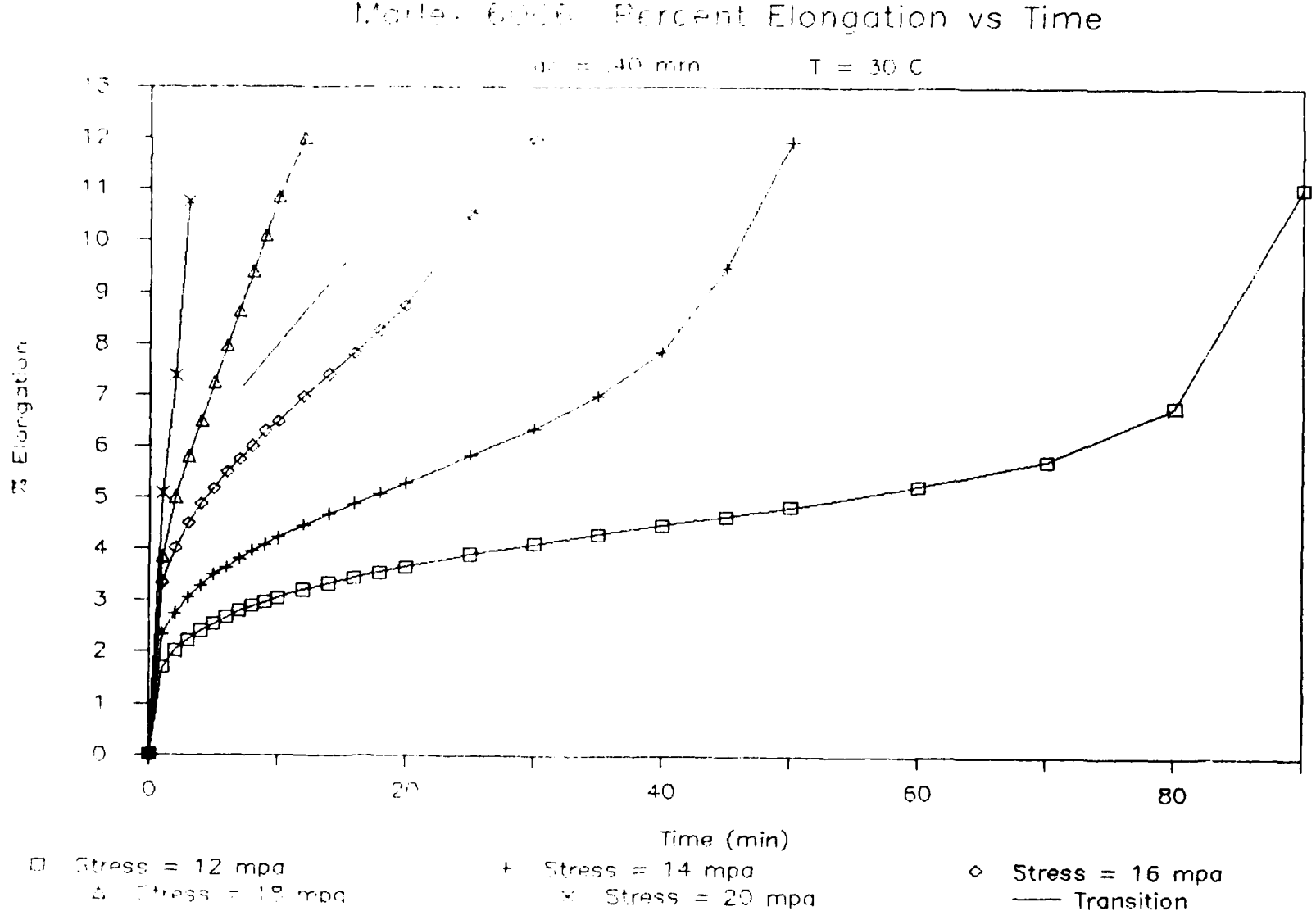
Percent Elongation vs Time
T = 30 C
% Elongation
0
1
2
3
4
5
6
7
8
9
10
11
12
0
20
40
60
80
Time (min)
Stress = 12 mpa
Stress = 14 mpa
Stress = 16 mpa
Stress = 20 mpa
Transition

Figure 8

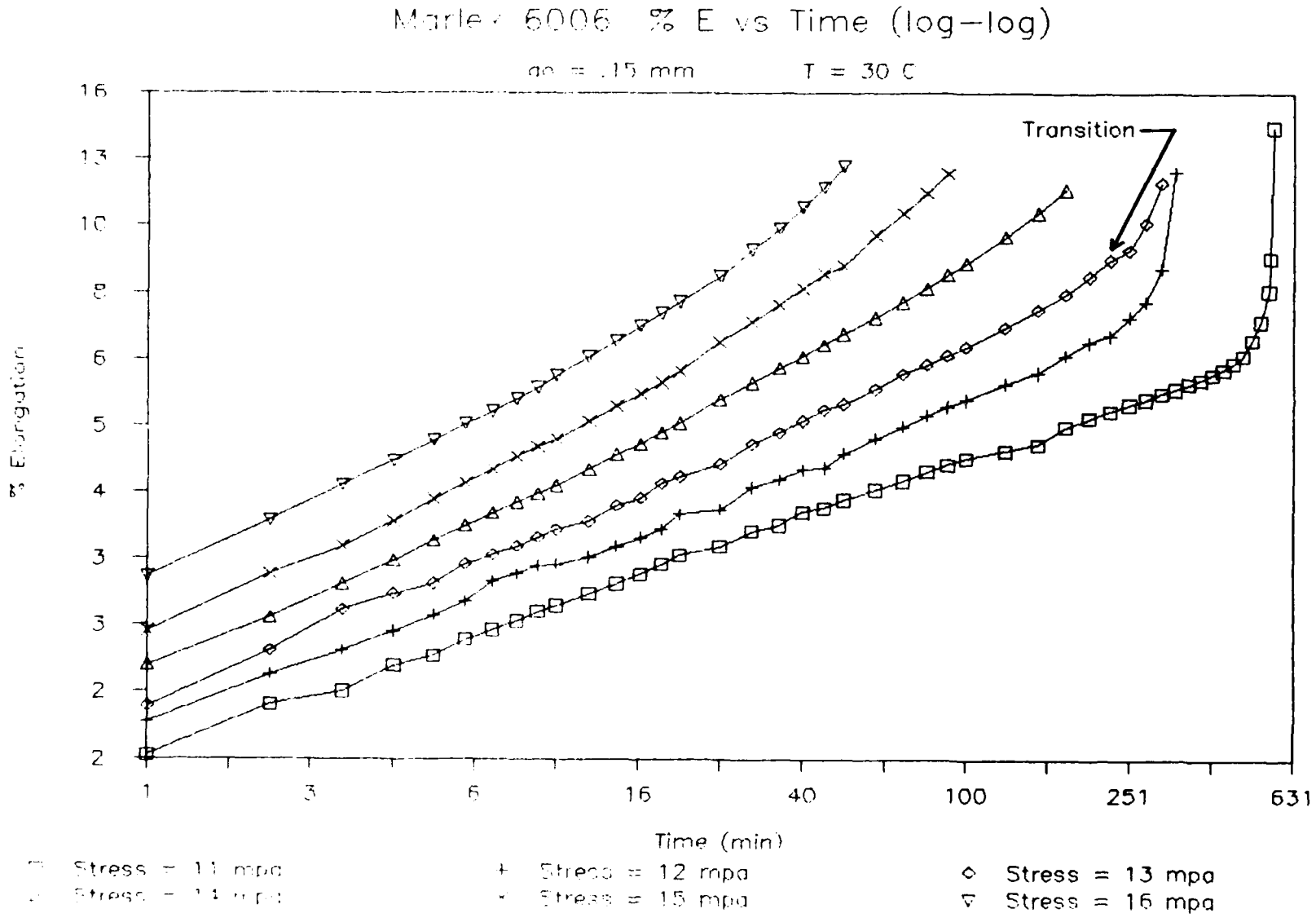
Marlex 6006 % E vs Time (log–log)
T = 30 C
Transition
% Elongation
Time (min)
16
13
10
8
6
5
4
3
3
2
1
3
6
16
40
100
251
631
Stress = 11 mpa
Stress = 12 mpa
Stress = 13 mpa
Stress = 15 mpa
Stress = 16 mpa

Figure 9A

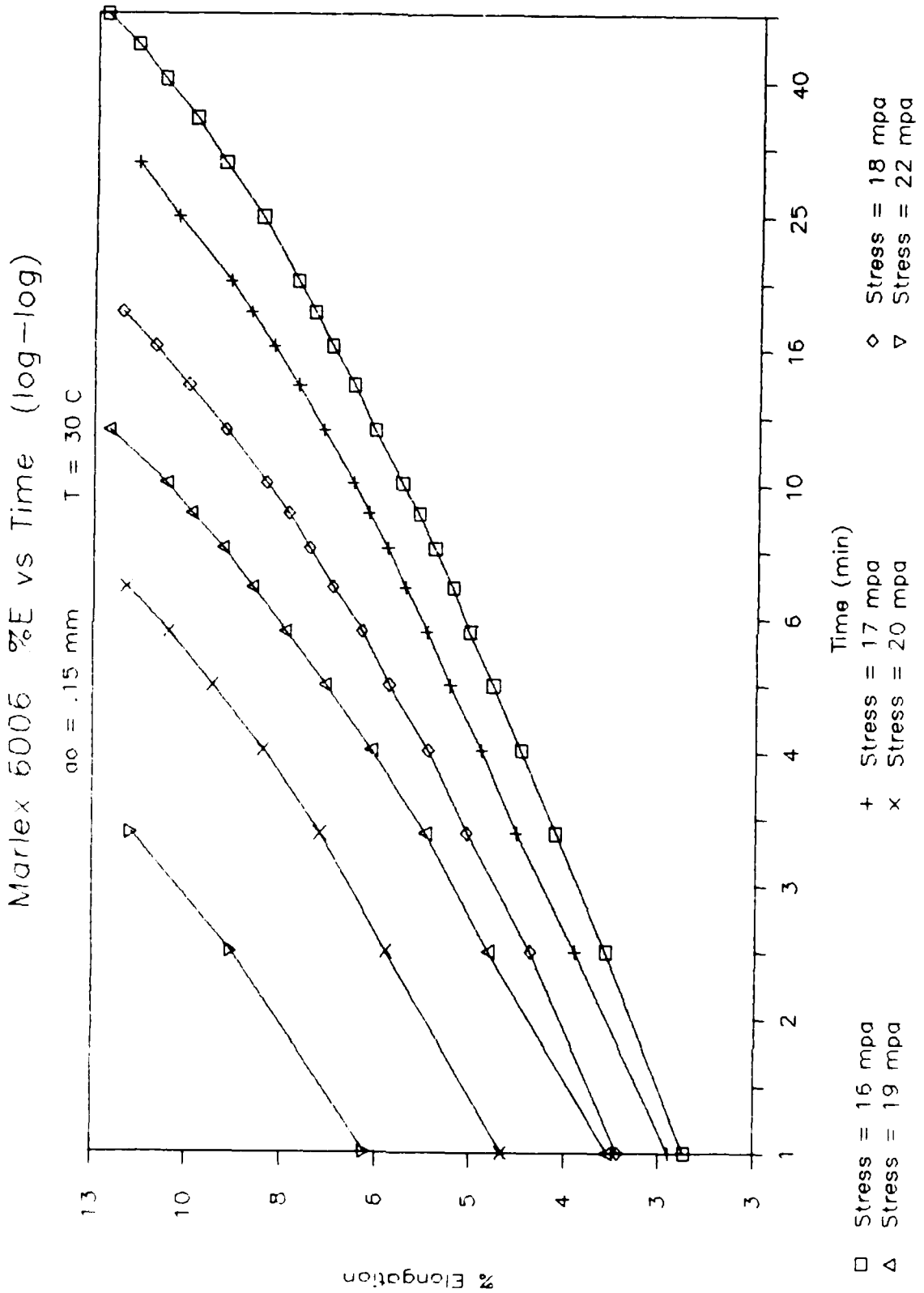
Marlex 6006 %E vs Time (log-log)
ao = .15 mm
T = 30 C
% Elongation
Time (min)
Stress = 16 mpa
Stress = 17 mpa
Stress = 18 mpa
Stress = 19 mpa
Stress = 20 mpa
Stress = 22 mpa

Figure 9B

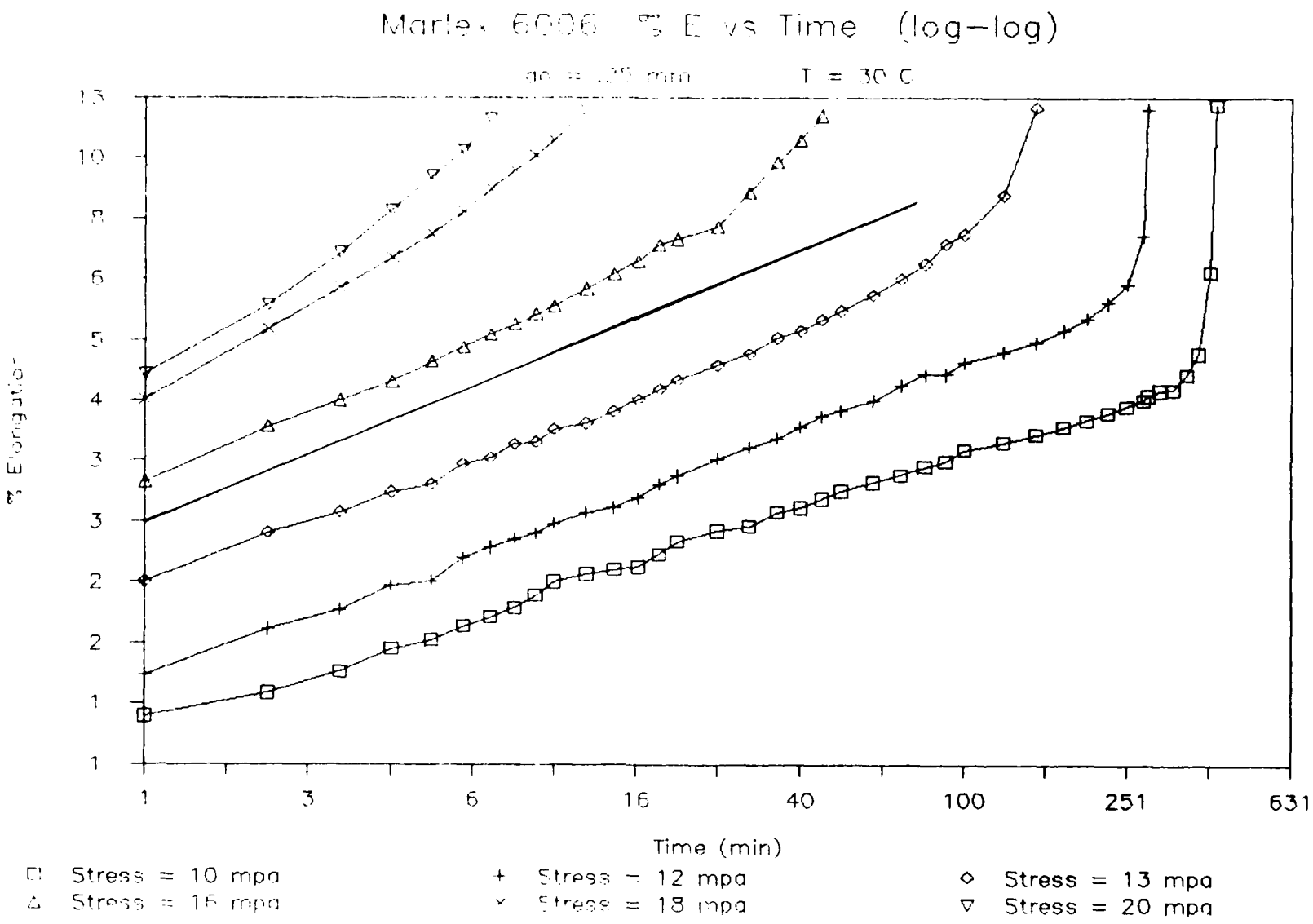
Marlex 6006 % E vs Time (log–log)
T = 30 C
% Elongation
13
10
8
6
5
4
3
3
2
2
1
1
1
3
6
16
40
100
251
631
Time (min)
Stress = 10 mpa
Stress = 12 mpa
Stress = 13 mpa
Stress = 15 mpa
Stress = 18 mpa
Stress = 20 mpa

Figure 10

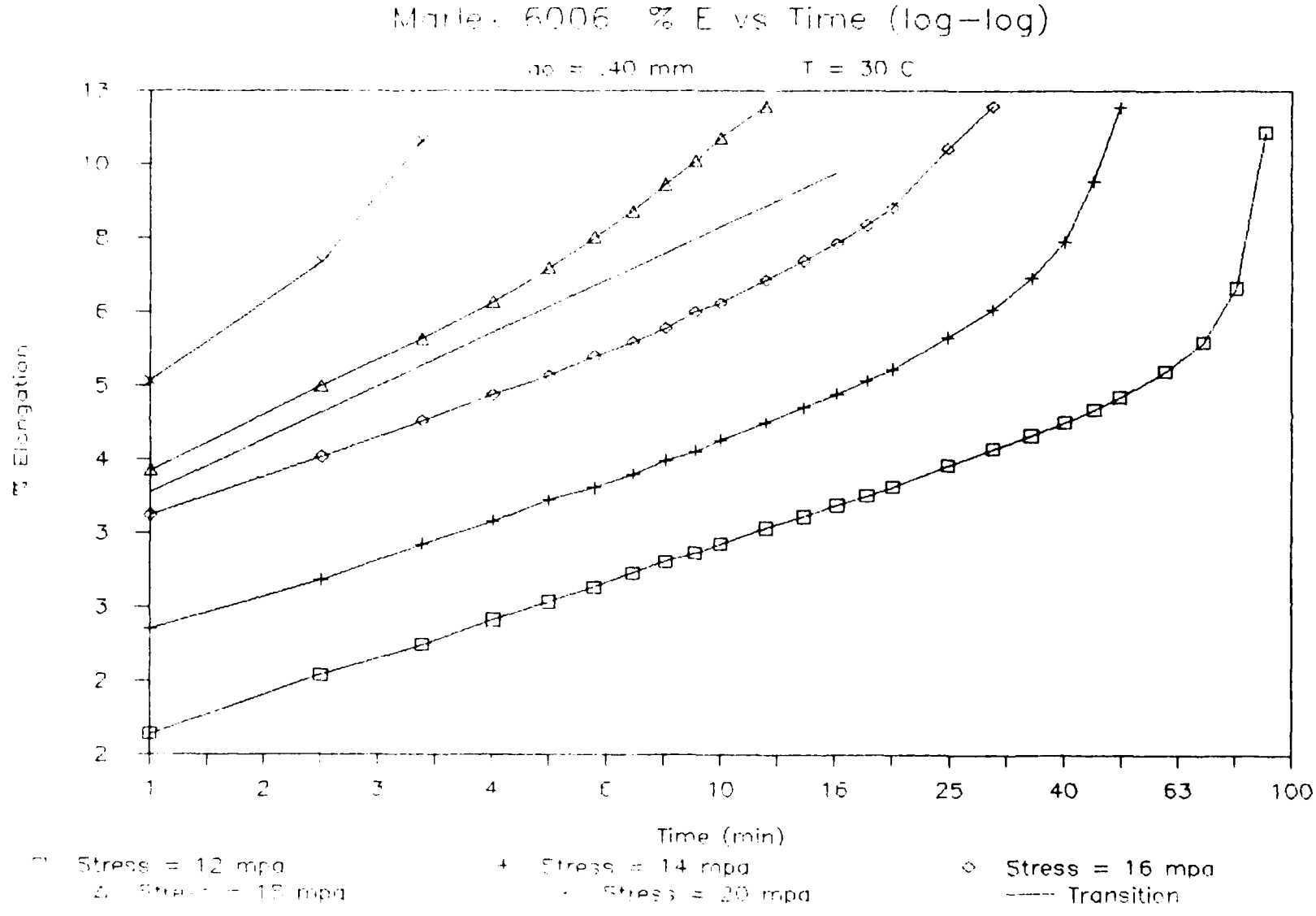
Marlex 5006 % E vs Time (log–log)
T = 30 C
% Elongation
Time (min)
Stress = 16 mpa
Transition

Figure 11

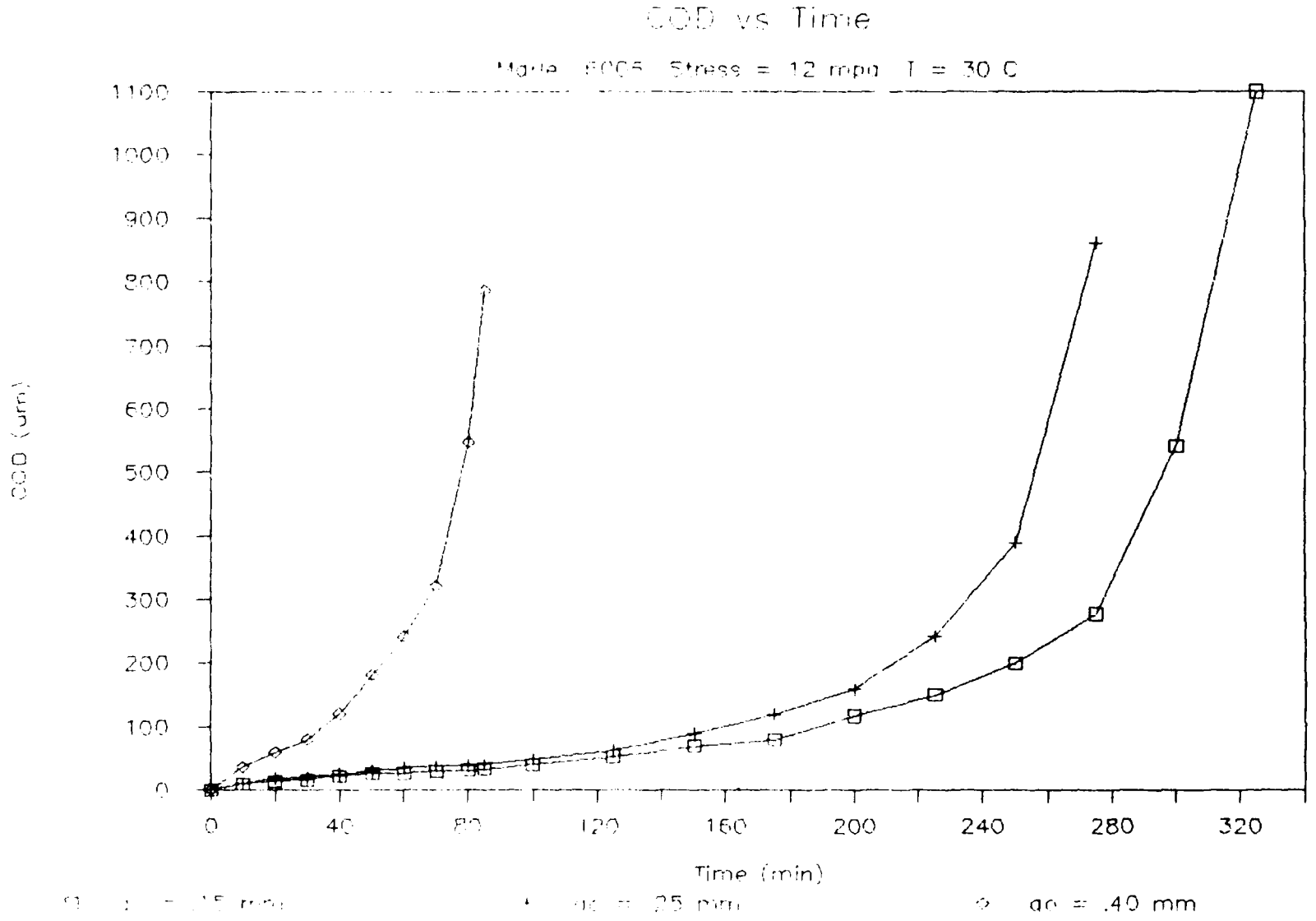
COD vs Time
Mgrde 6005 Stress = 12 mpa T = 30 C
COD (um)
1100
1000
900
800
700
600
500
400
300
200
100
0
0
40
80
120
160
200
240
280
320
Time (min)
ao = .40 mm

Figure 12

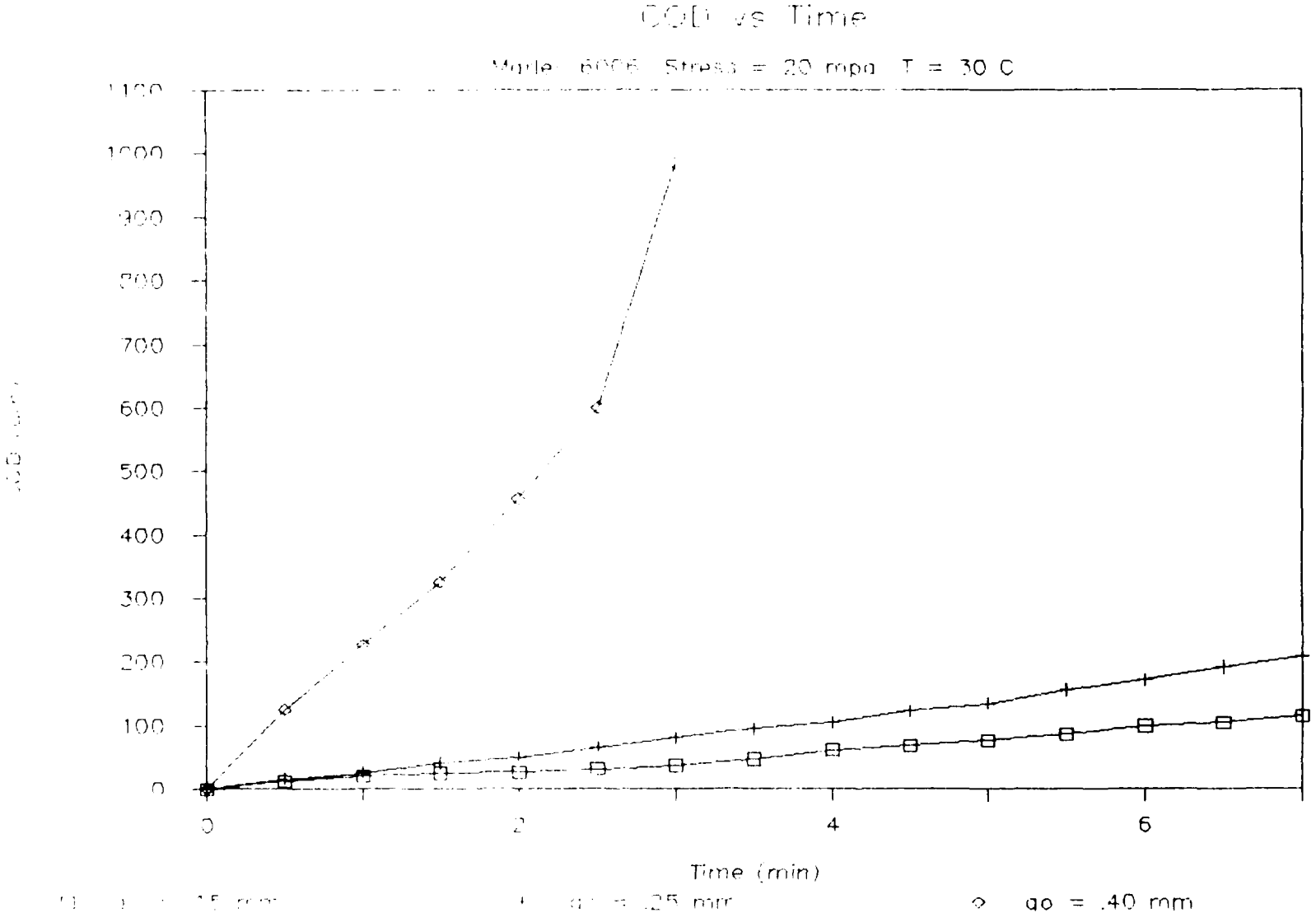
CCD vs Time
Matrix: 6006 Stress = 20 mpa T = 30 C
1100
1000
900
800
700
600
500
400
300
200
100
0
0
2
4
6
Time (min)
ao = .40 mm

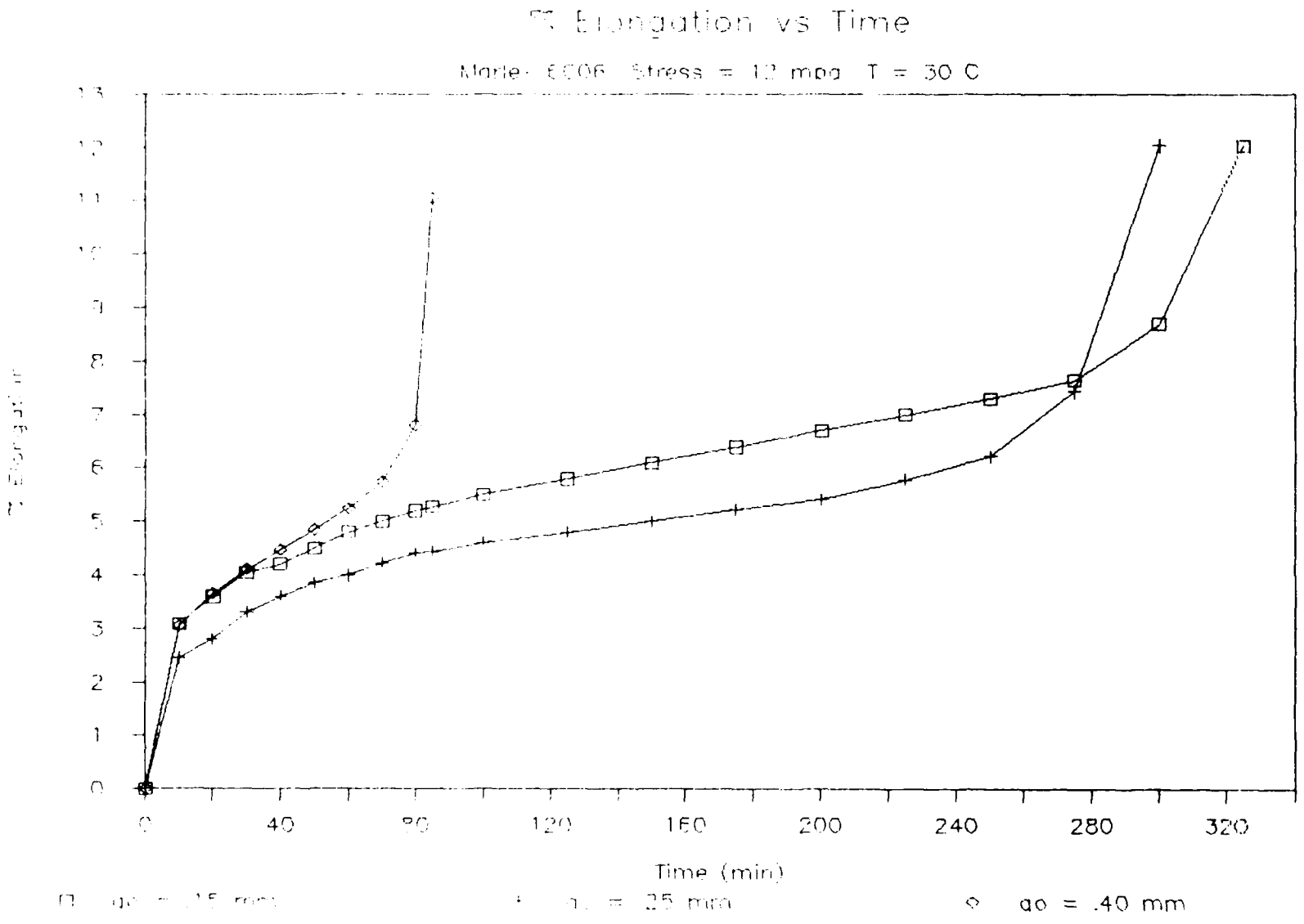
% Elongation vs Time
Matrix: 5506 Stress = 12 mpa T = 30 C
% Elongation
0
1
2
3
4
5
6
7
8
9
10
11
12
13
0
40
80
120
160
200
240
280
320
Time (min)
ao = .40 mm

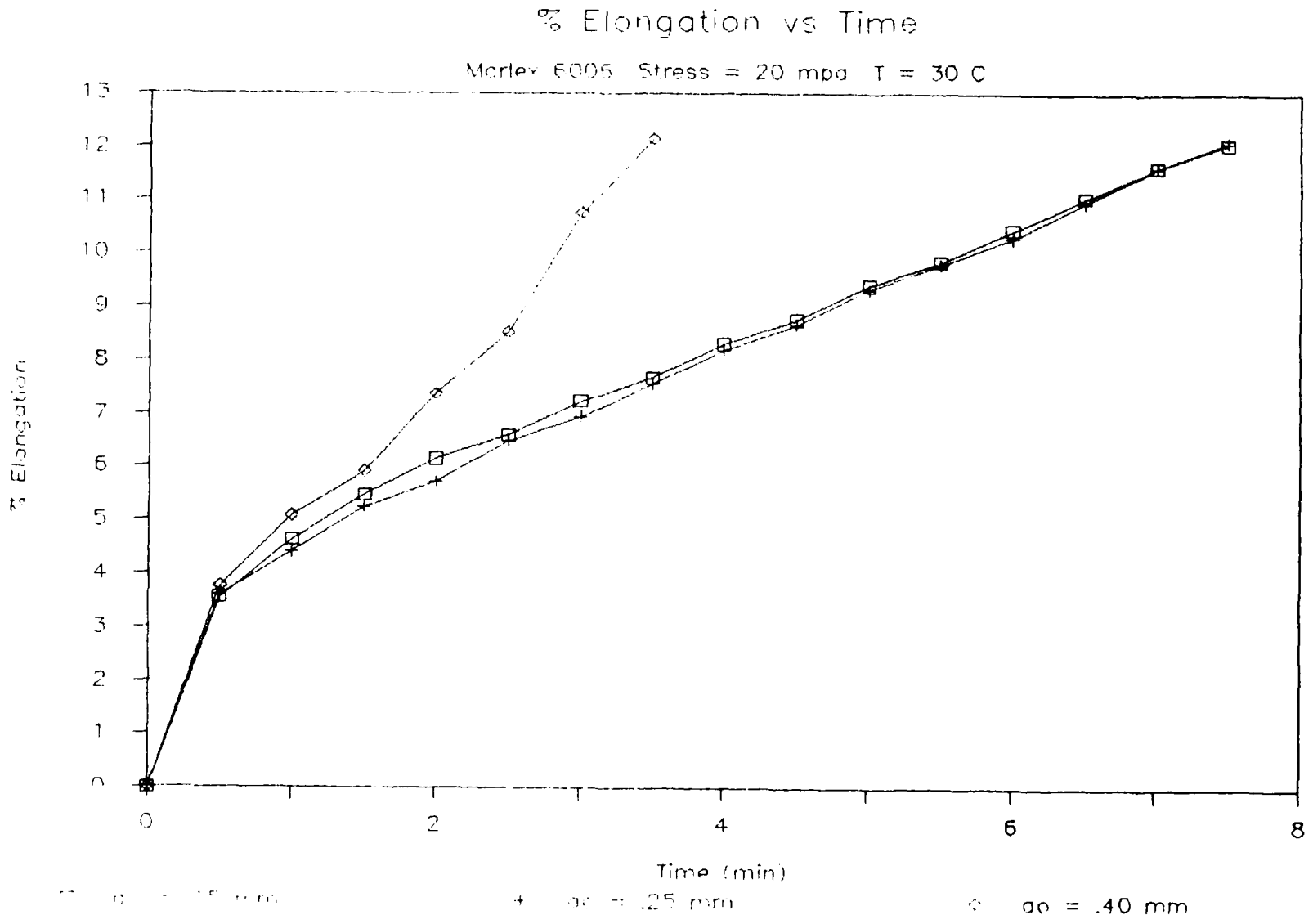
% Elongation vs Time
Marlex 6005 Stress = 20 mpa T = 30 C
% Elongation
Time (min)
0
2
4
6
8
0
1
2
3
4
5
6
7
8
9
10
11
12
13
go = .40 mm

Figure 15

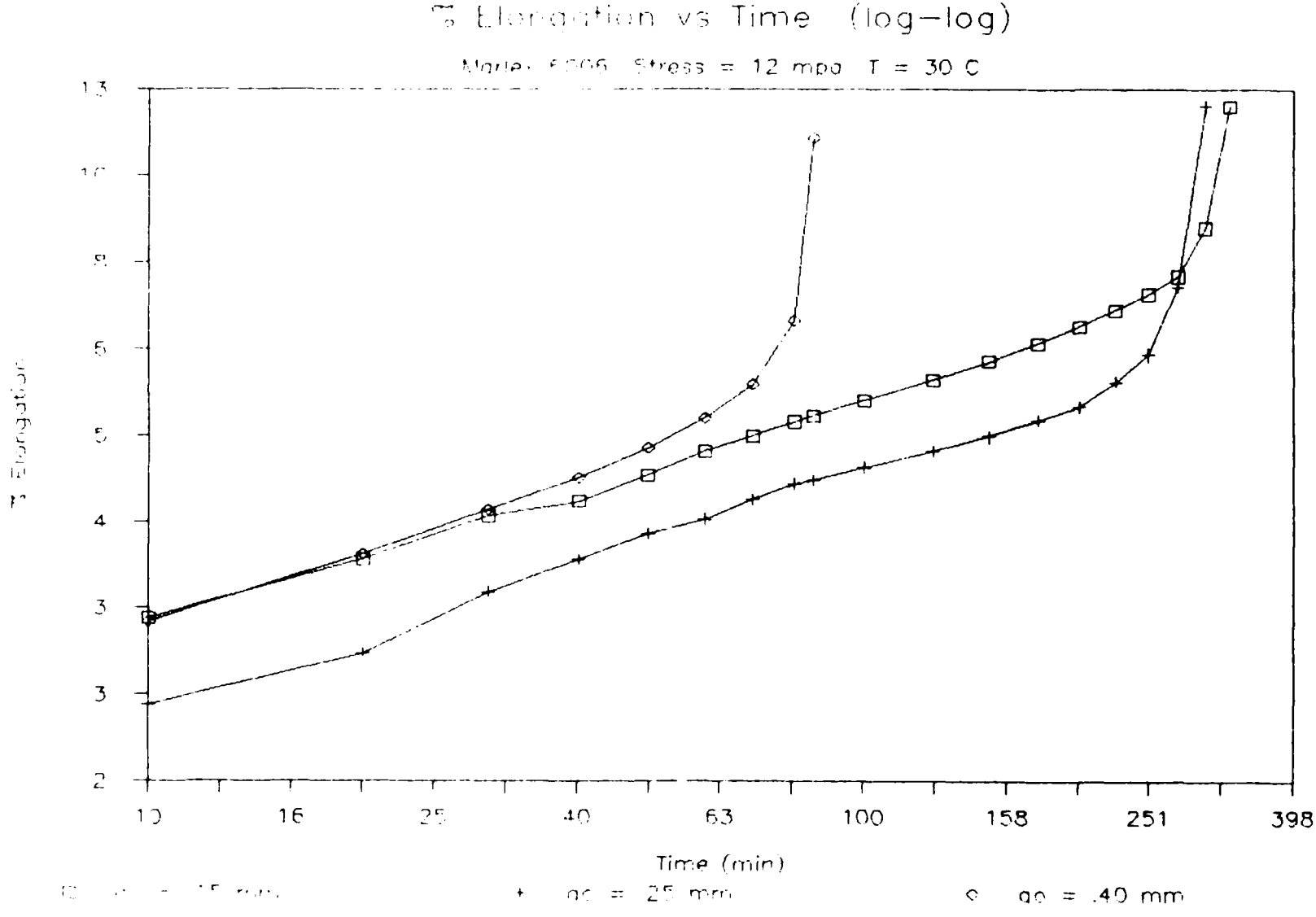
% Elongation vs Time (log–log)
Stress = 12 mpa T = 30 C
% Elongation
Time (min)
10
16
25
40
63
100
158
251
398
2
3
4
5
9
13
+ gg = 25 mm
◇ gg = .40 mm

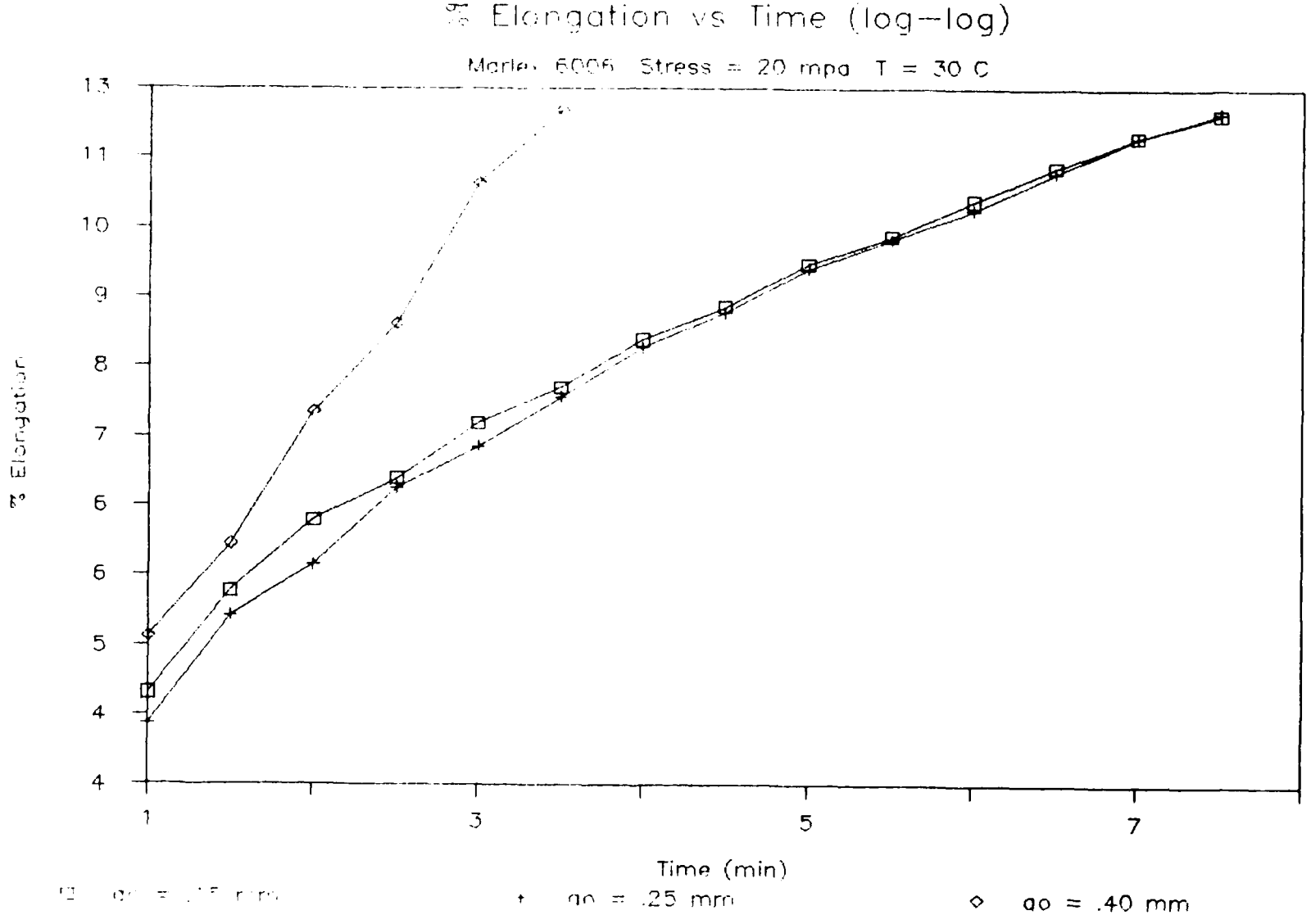
% Elongation vs Time (log–log)
Marlex 6006 Stress = 20 mpa T = 30 C
% Elongation
13
11
10
9
8
7
6
6
5
4
4
1
3
5
7
Time (min)
ao = .25 mm
ao = .40 mm

Figure 1

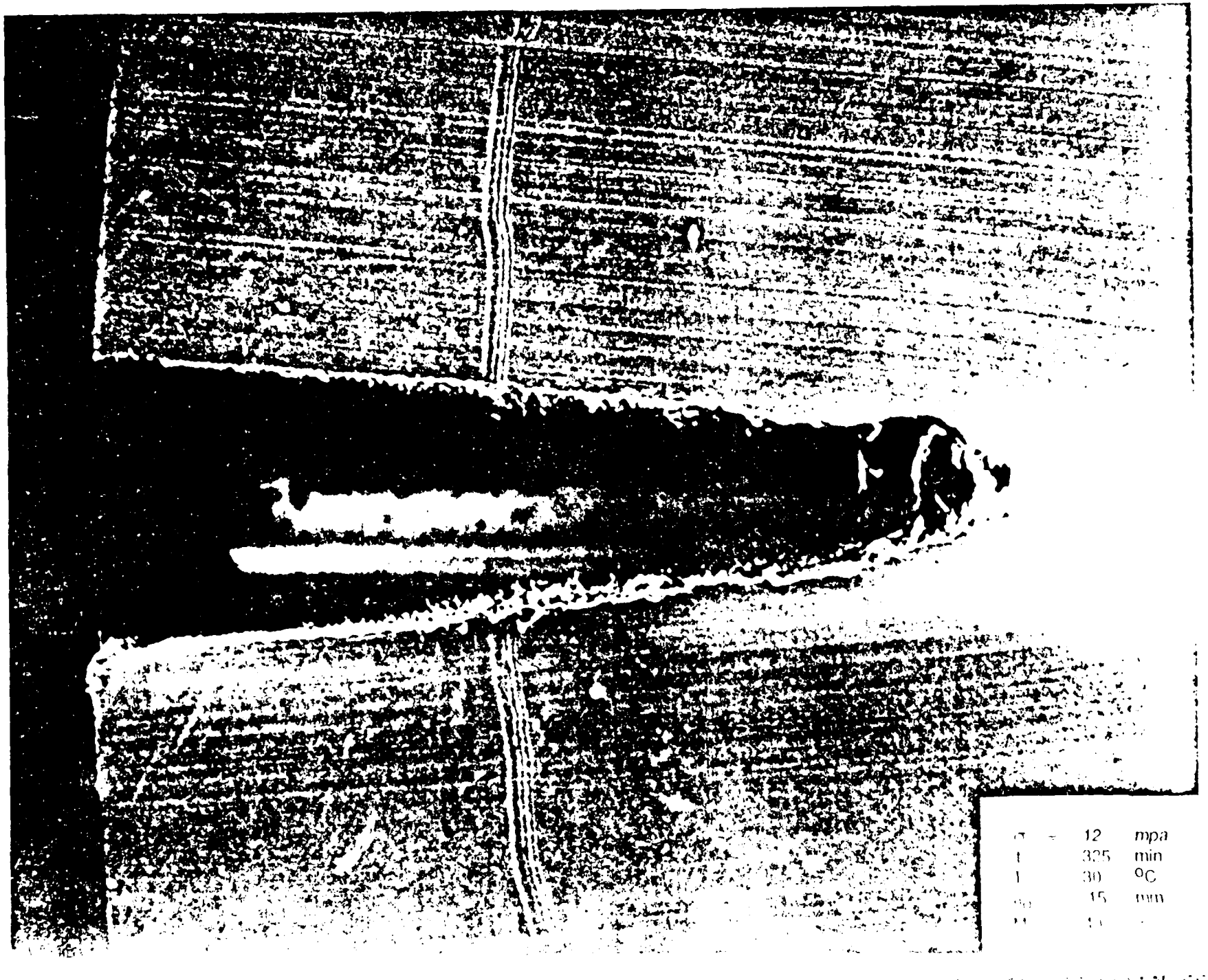
12 mpa
325 min
30 °C
15 mm

Figure 19

mpa
mm
psi

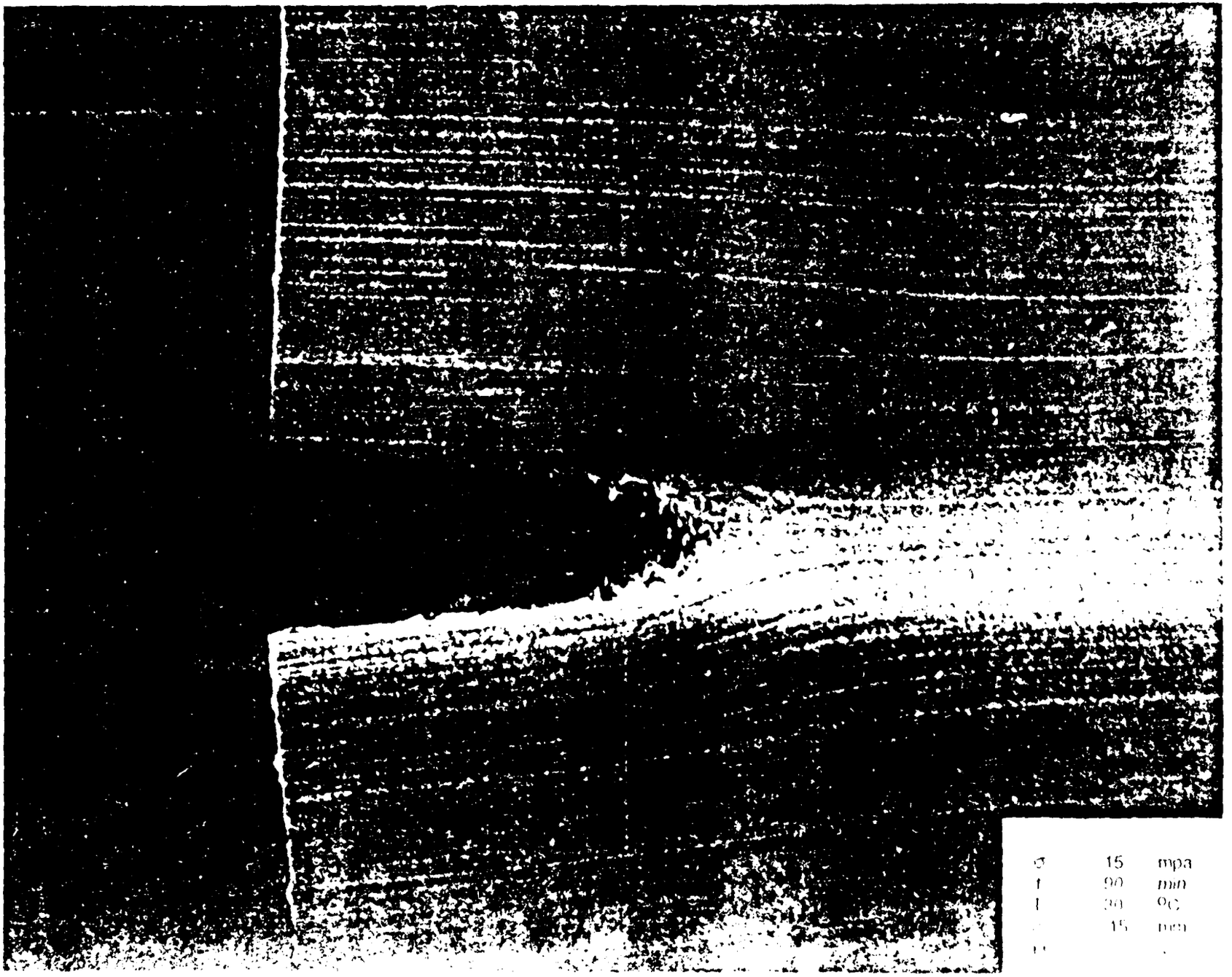
σ 15 mpa
t 90 min
T 90 °C
15 mm

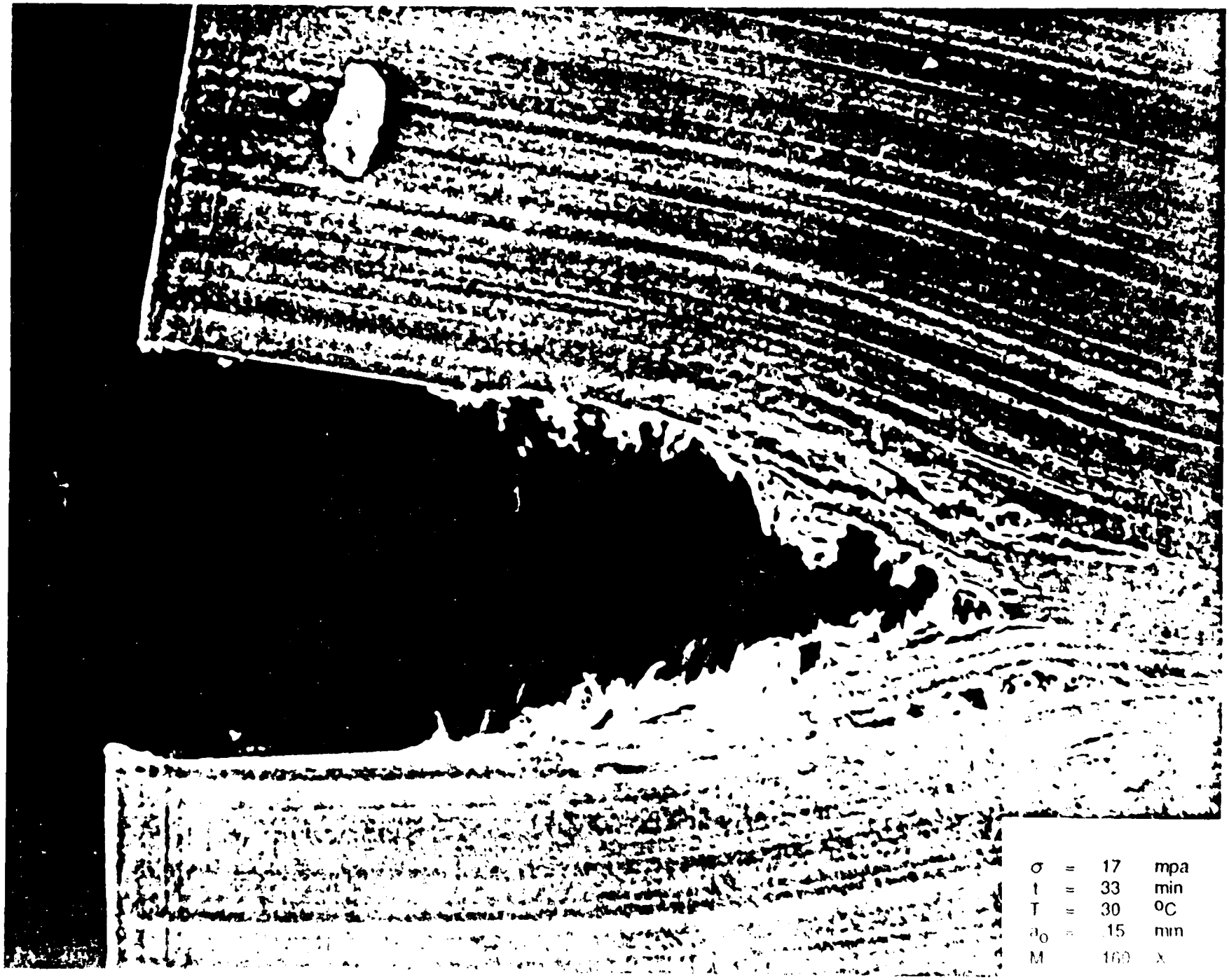
σ = 17 mpa
t = 33 min
T = 30 °C
a_0 = 15 mm
M 160 x

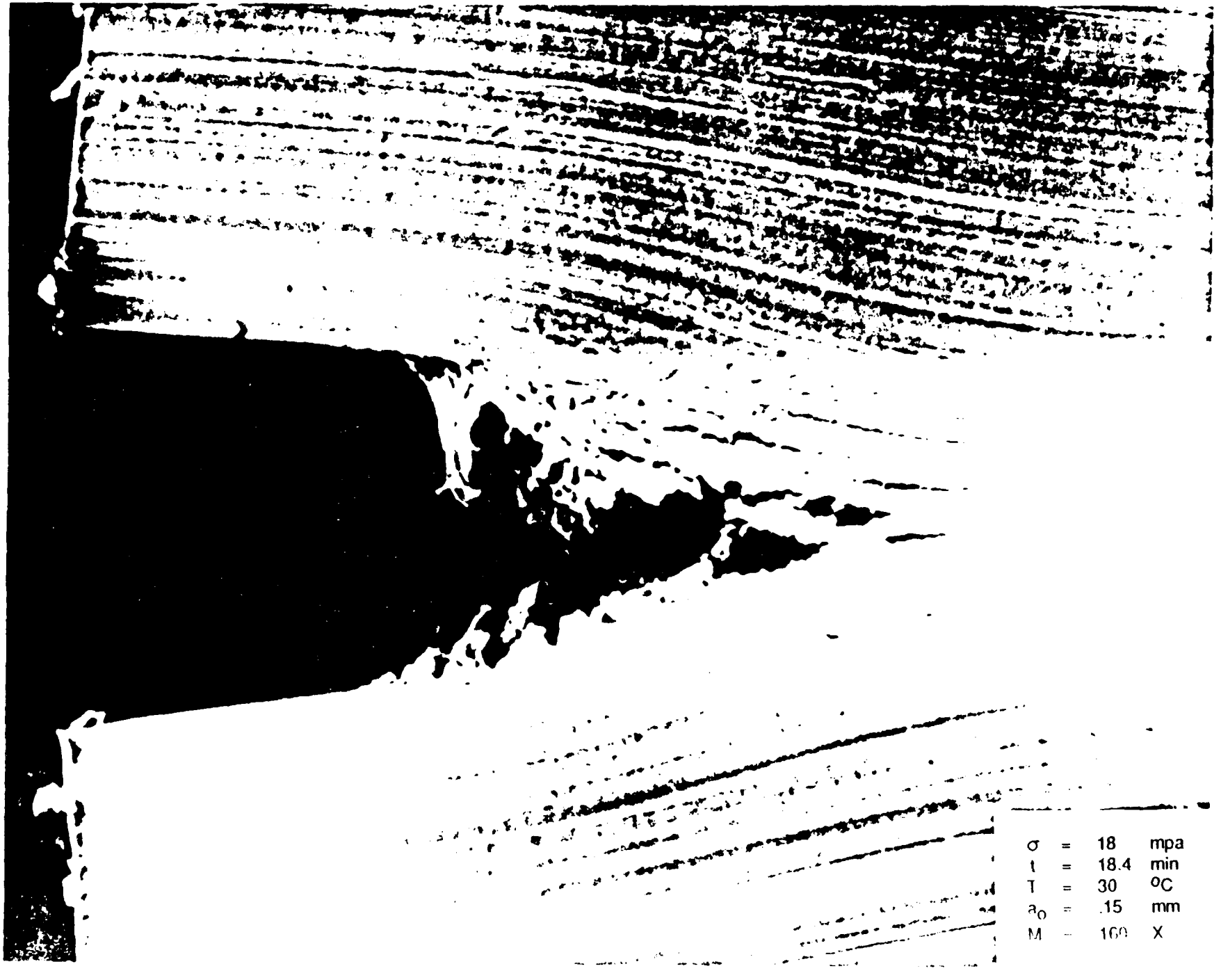

Figure 23

Figure 2.

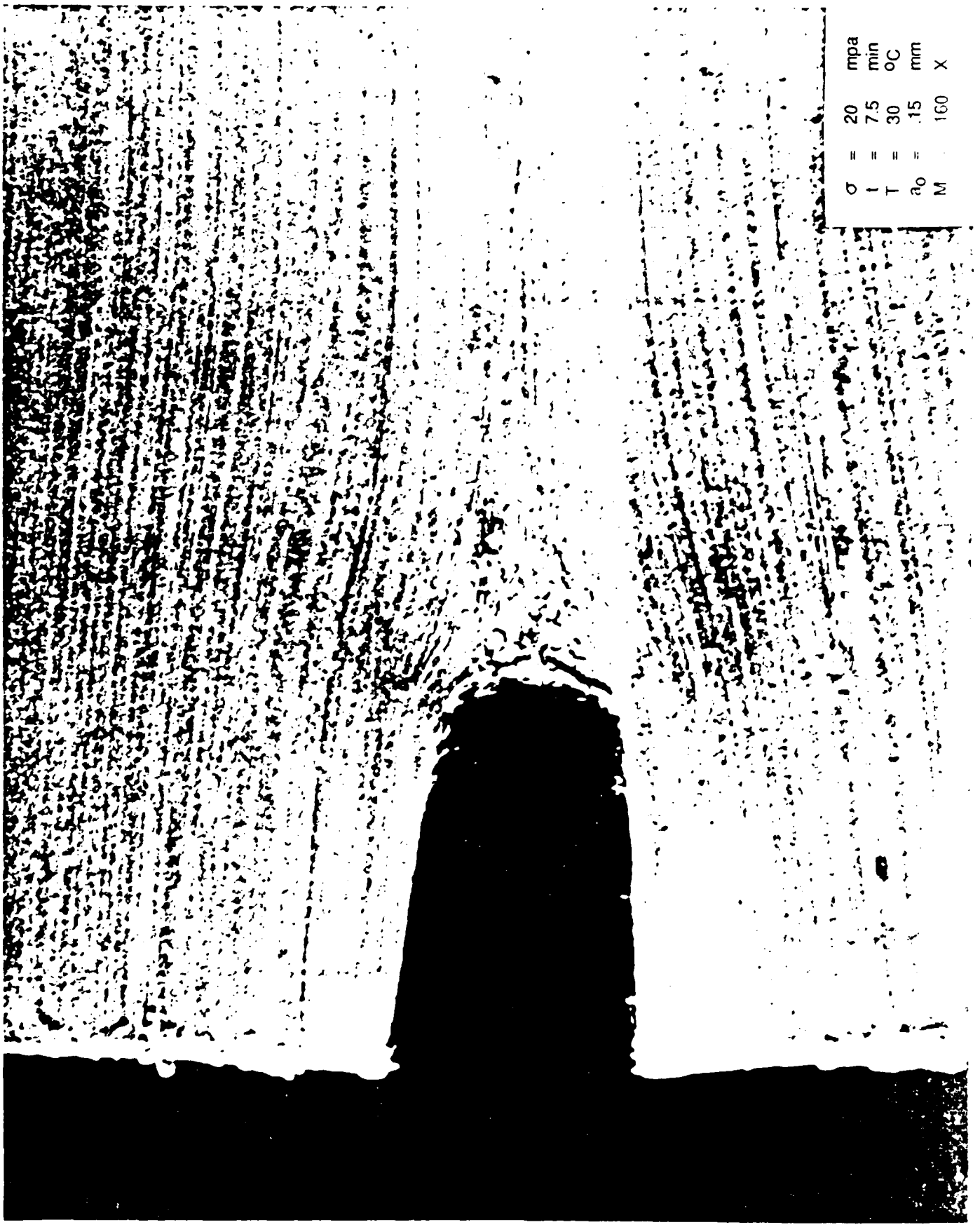

Figure 25

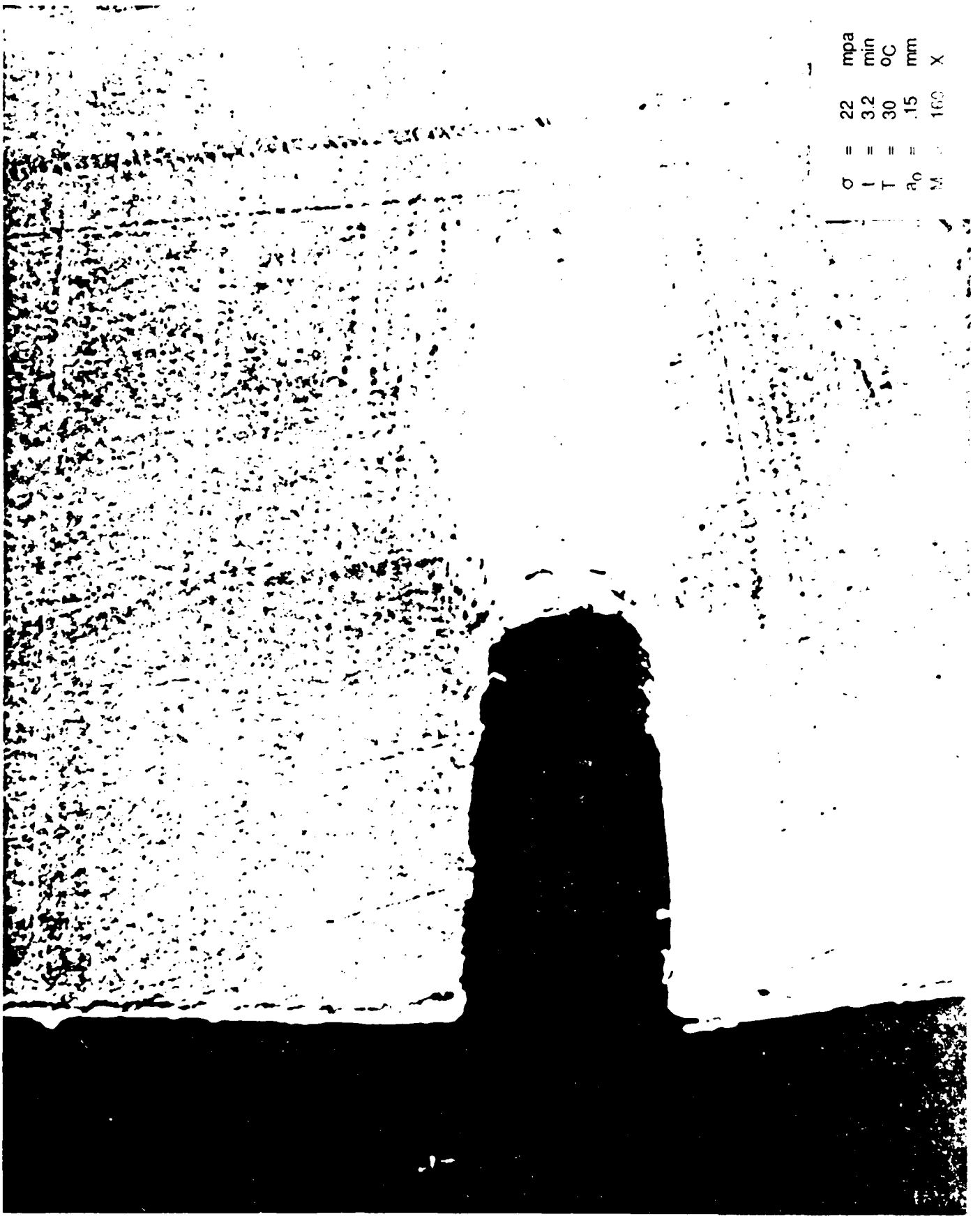

Figure 26

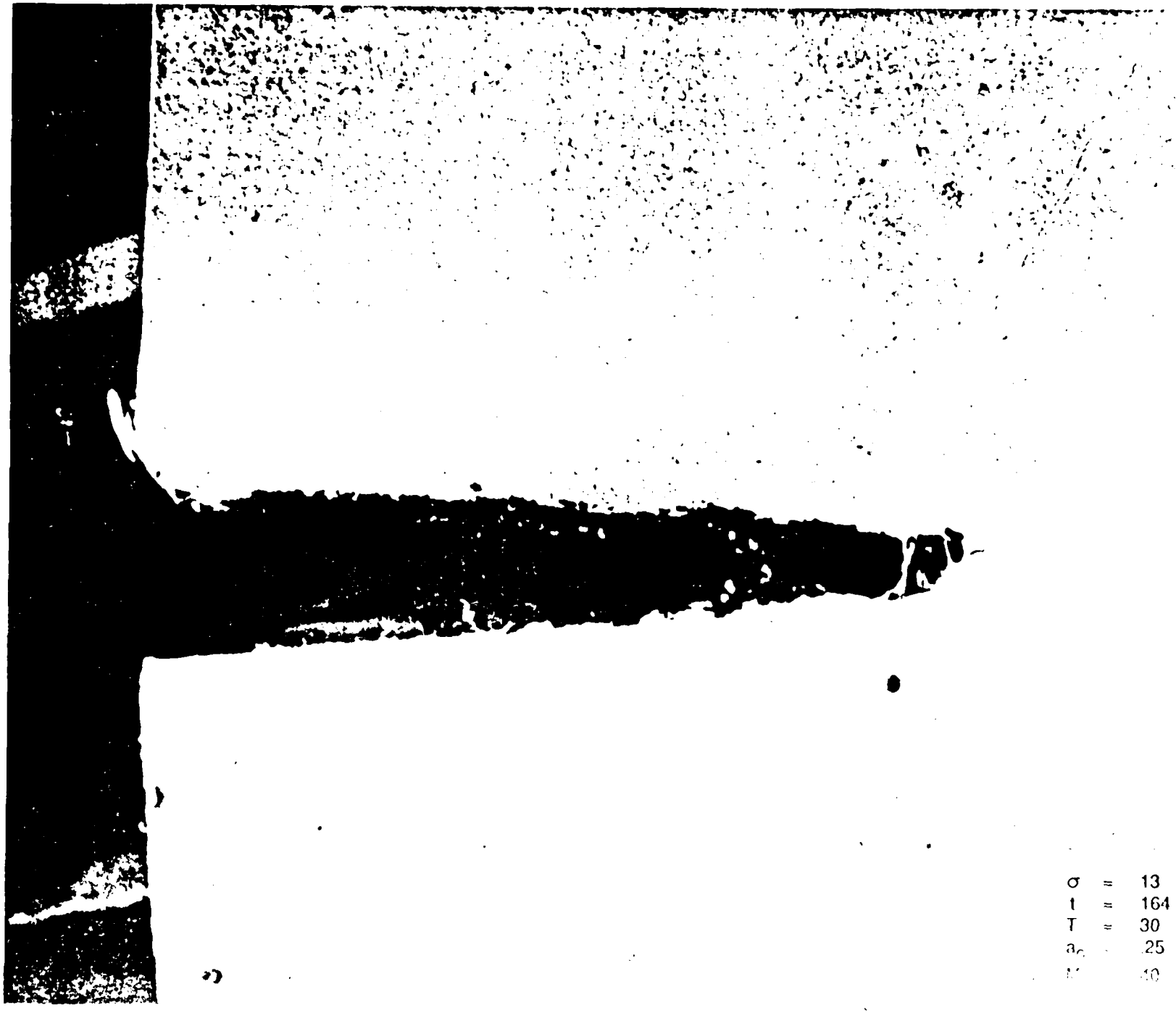
σ = 13 mpa
t = 164 min
T = 30 °C
a = .25 mm
M = 10 X

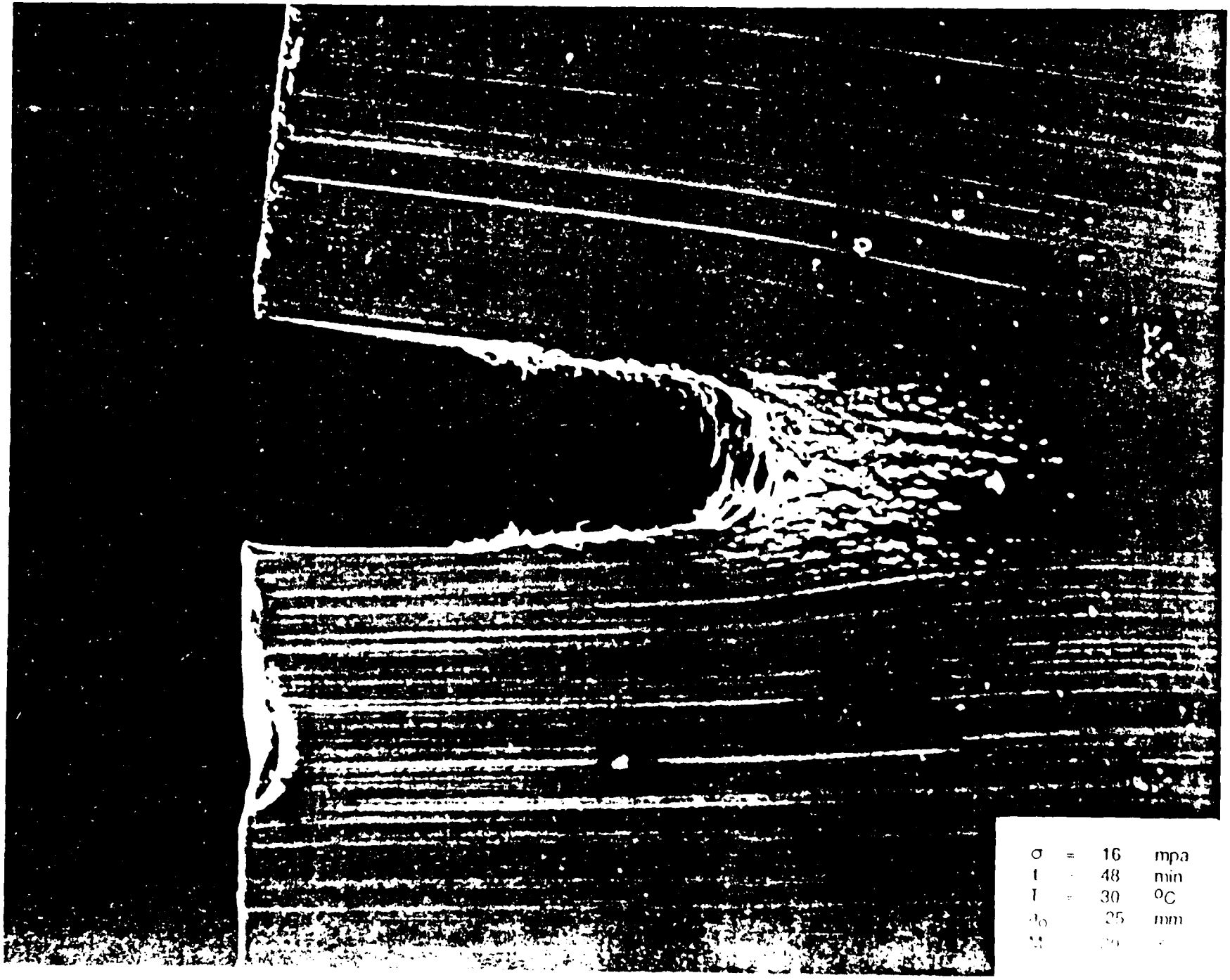
σ = 16 mpa
t = 48 min
T = 30 °C
d_0 = 25 mm

Figure 30

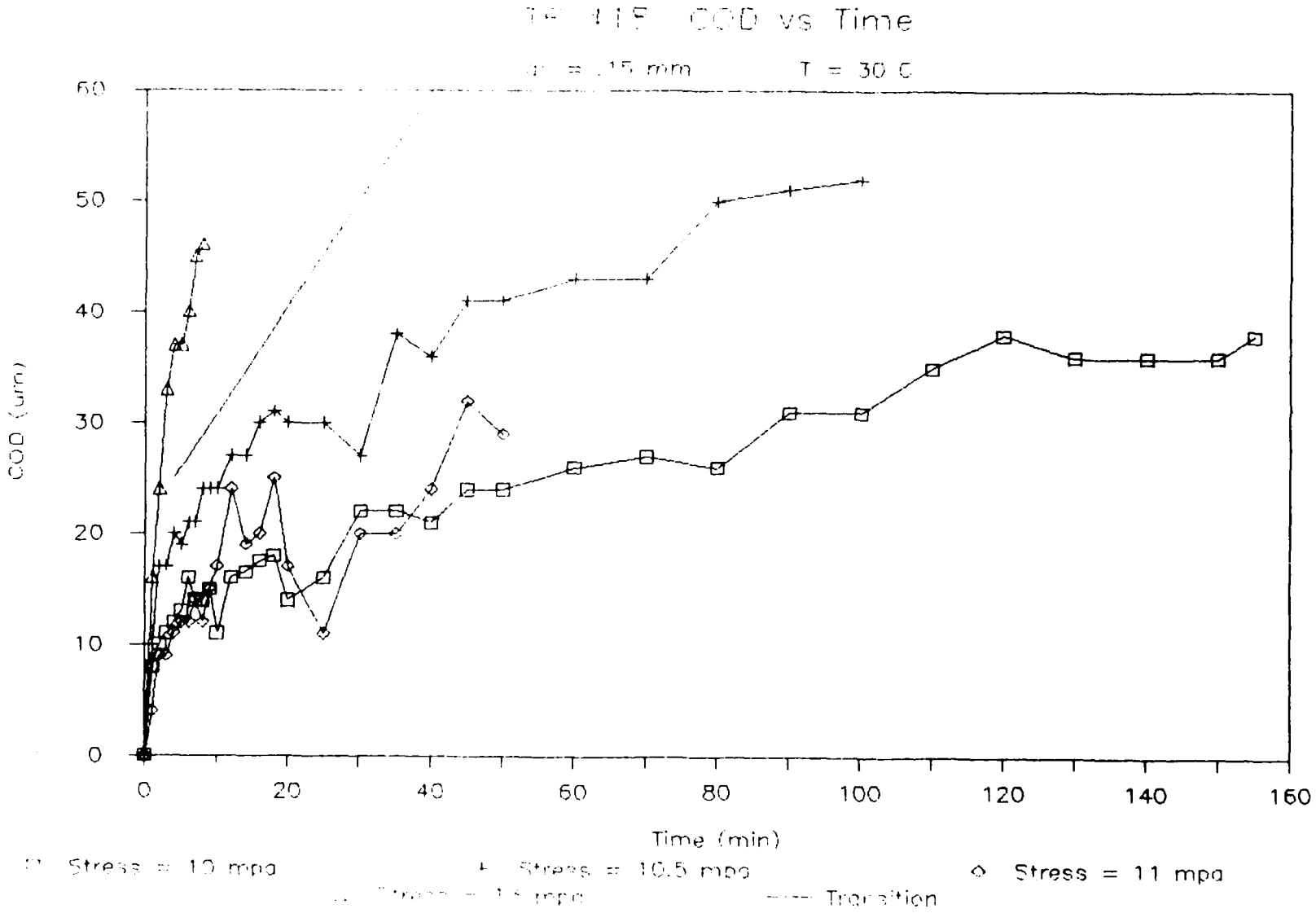
COD vs Time
T = 30 C
COD (um)
Time (min)
0
10
20
30
40
50
60
0
20
40
60
80
100
120
140
160
Stress = 10 mpa
Stress = 10.5 mpa
Stress = 11 mpa
Transition

Figure 31

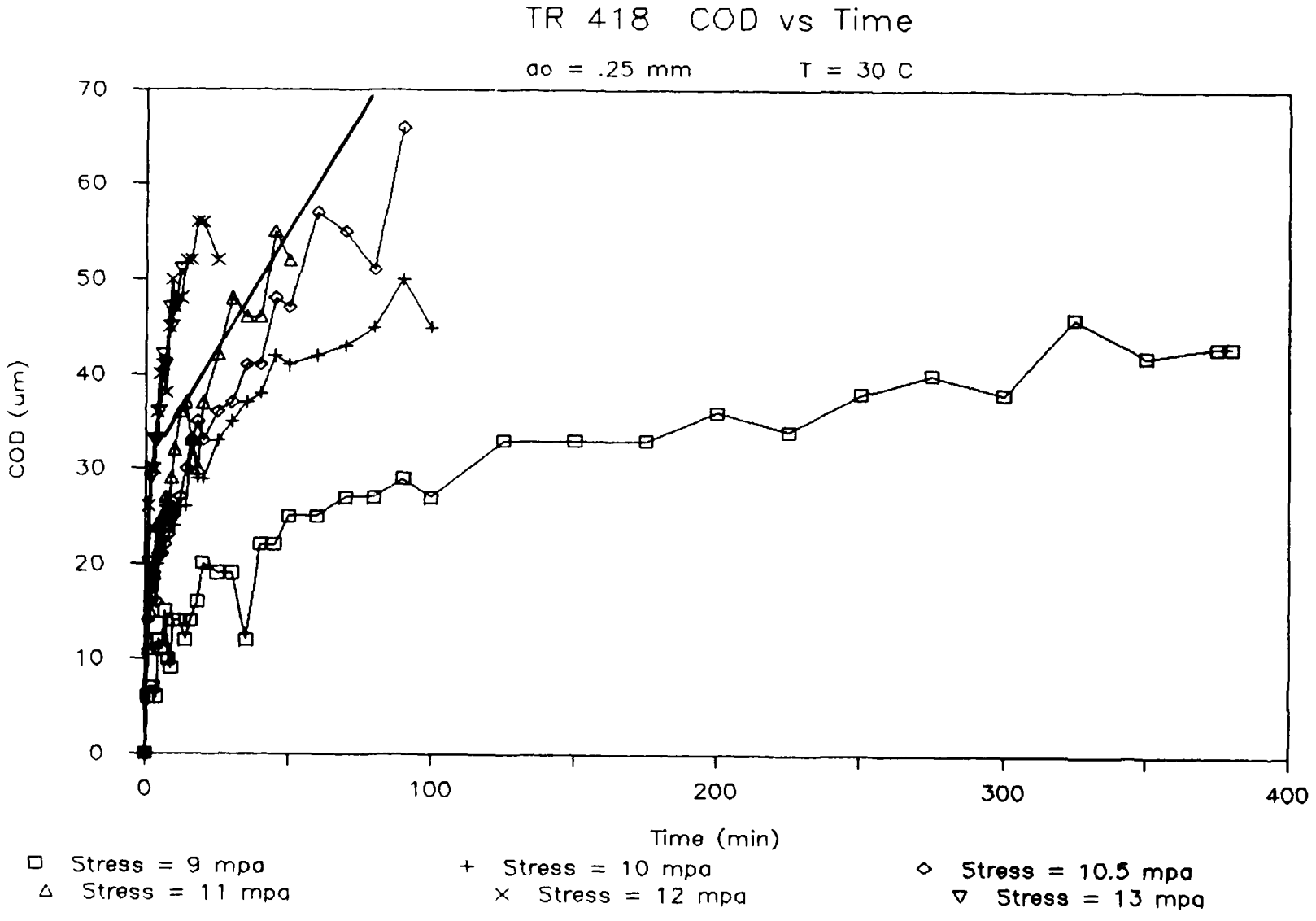
TR 418 COD vs Time
ao = .25 mm
T = 30 C
COD (um)
70
60
50
40
30
20
10
0
0
100
200
300
400
Time (min)
Stress = 9 mpa
Stress = 10 mpa
Stress = 10.5 mpa
Stress = 11 mpa
Stress = 12 mpa
Stress = 13 mpa

Figure 32A

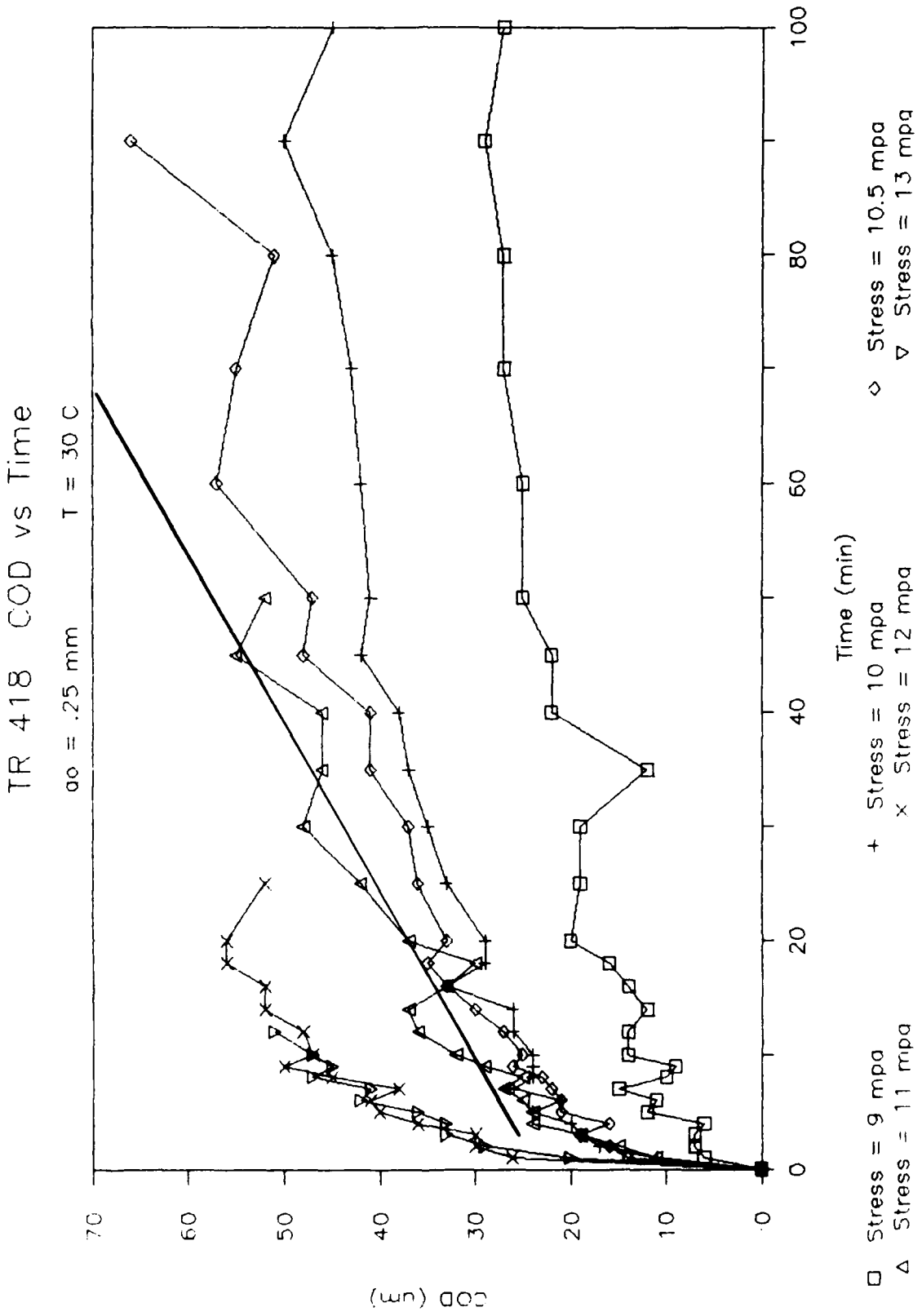
TR 418 COD vs Time
ao = .25 mm
T = 30 C
COD (um)
Time (min)
0
10
20
30
40
50
60
70
0
20
40
60
80
100
□ Stress = 9 mpa
△ Stress = 11 mpa
+ Stress = 10 mpa
× Stress = 12 mpa
◇ Stress = 10.5 mpa
▽ Stress = 13 mpa

Figure 32B

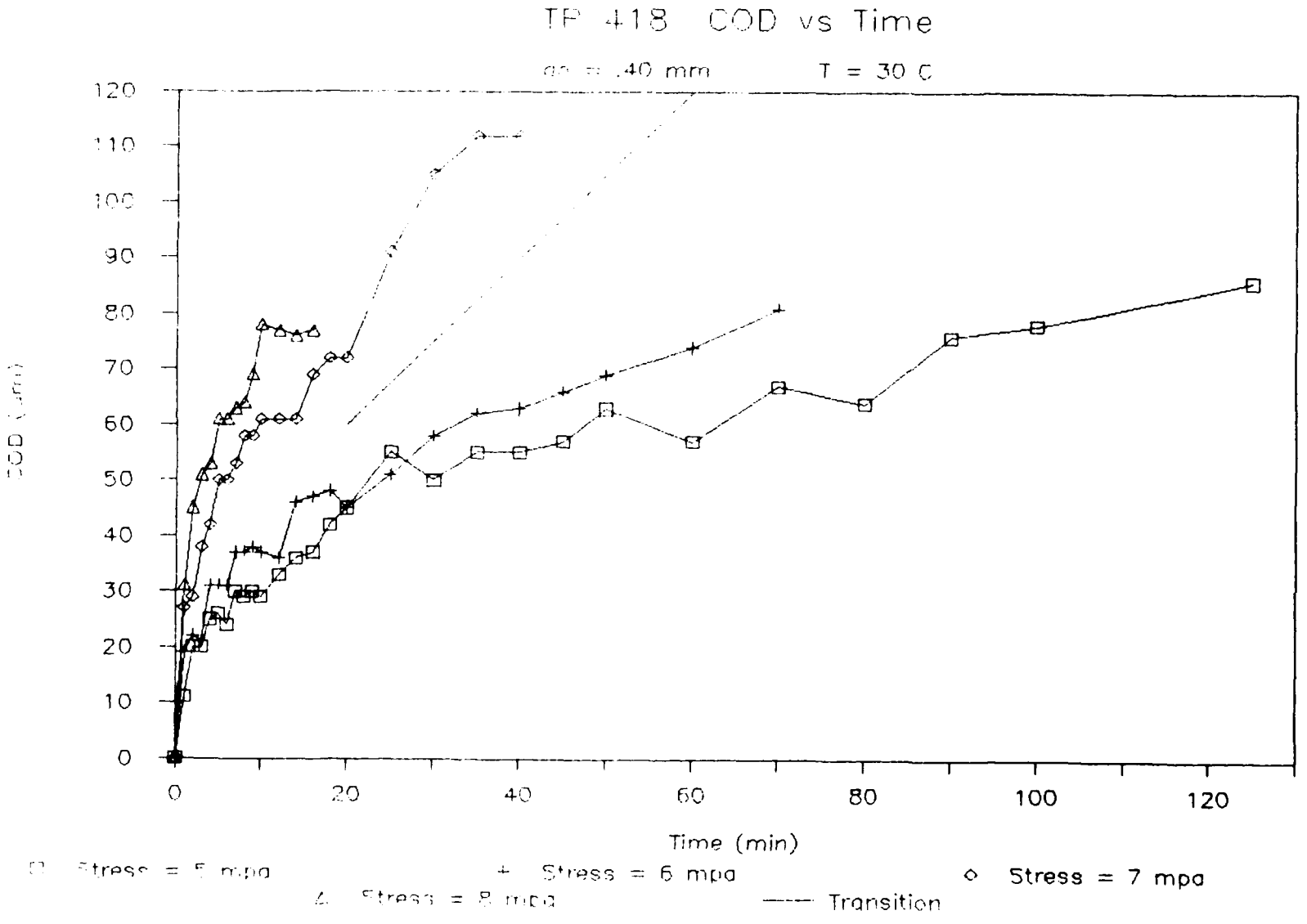
TP 418 COD vs Time
T = 30 C
120
110
100
90
80
70
60
50
40
30
20
10
0
0
20
40
60
80
100
120
Time (min)
Stress = 6 mpa
Stress = 7 mpa
Transition

Figure 33

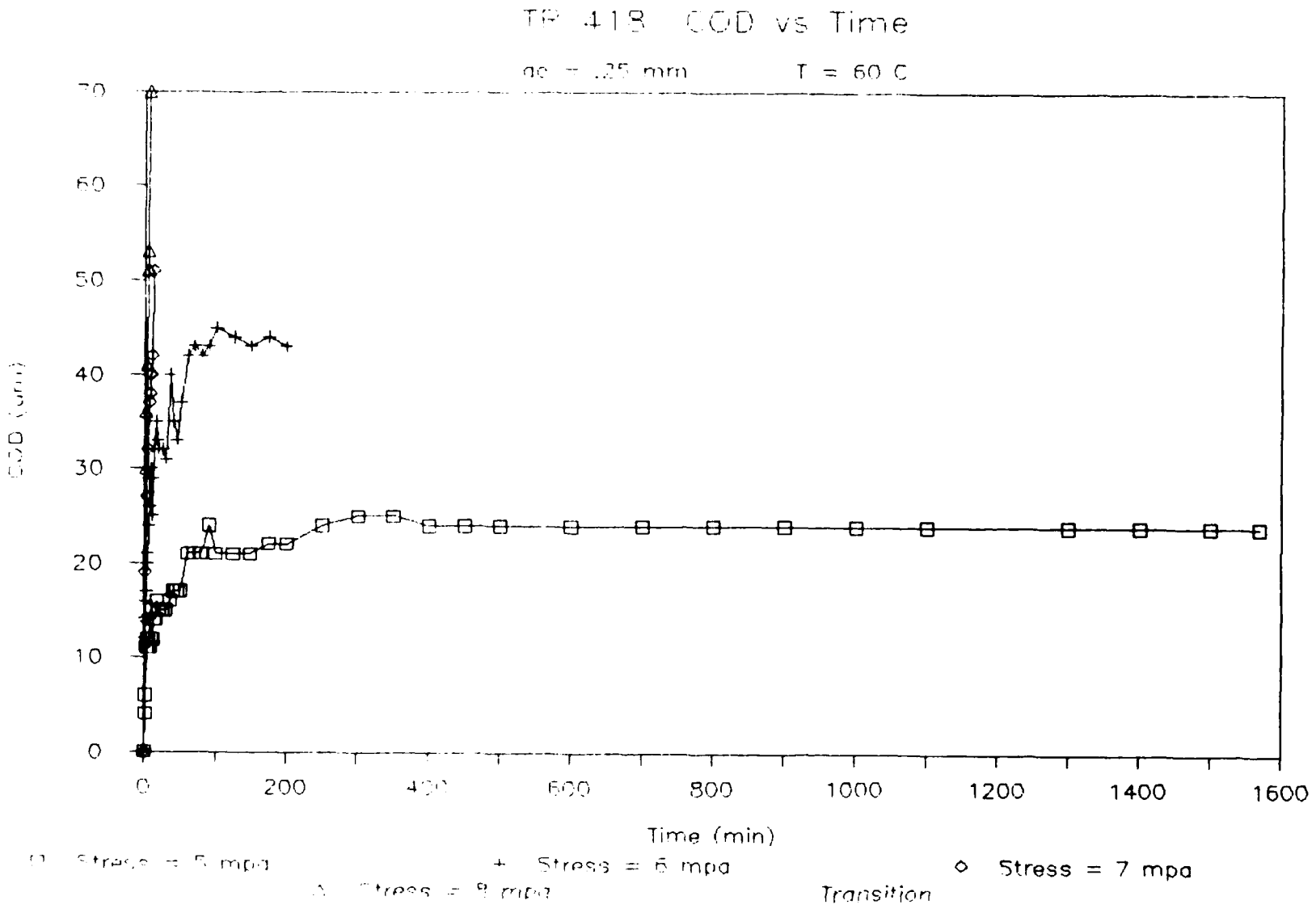
TP 418 COD vs Time
as = .25 mm
T = 60 C
70
60
50
40
30
20
10
0
COD (cm)
0
200
400
600
800
1000
1200
1400
1600
Time (min)
Stress = 5 mpa
Stress = 6 mpa
Stress = 7 mpa
Stress = 8 mpa
Transition

Figure 3-4A

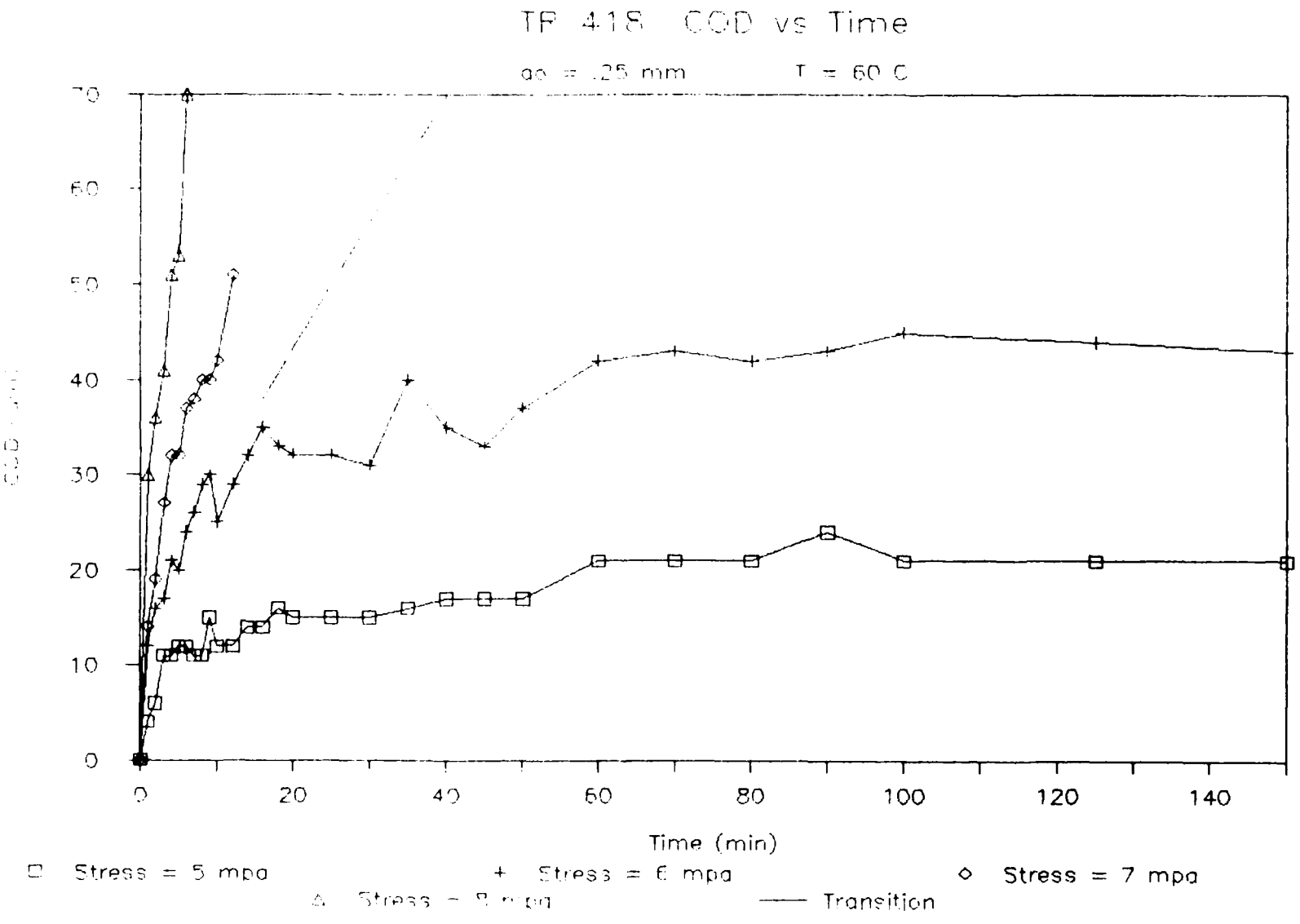
TP 418 COD vs Time
T = 60 C
70
60
50
40
30
20
10
0
0
20
40
60
80
100
120
140
Time (min)
Stress = 5 mpa
Stress = 6 mpa
Stress = 7 mpa
Transition

Figure 4-8

Marlex 6006

Figure 33

(A)

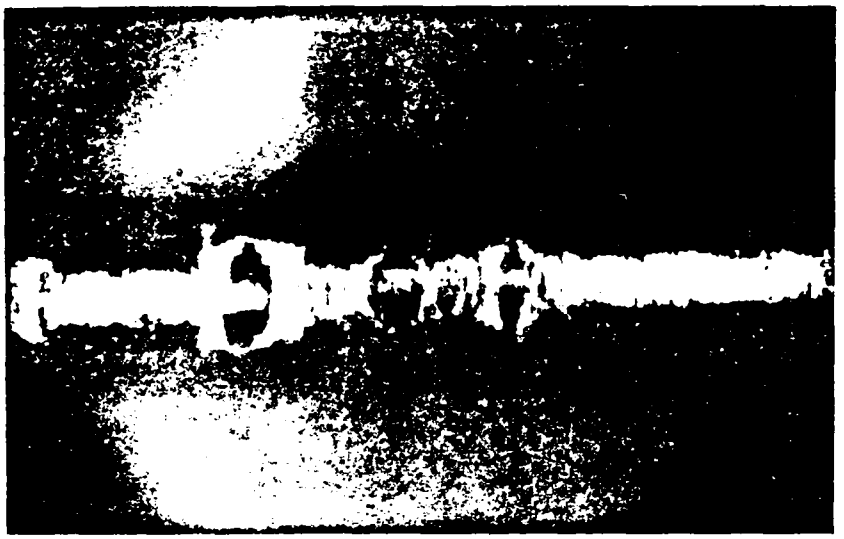

(B)

Figure 36

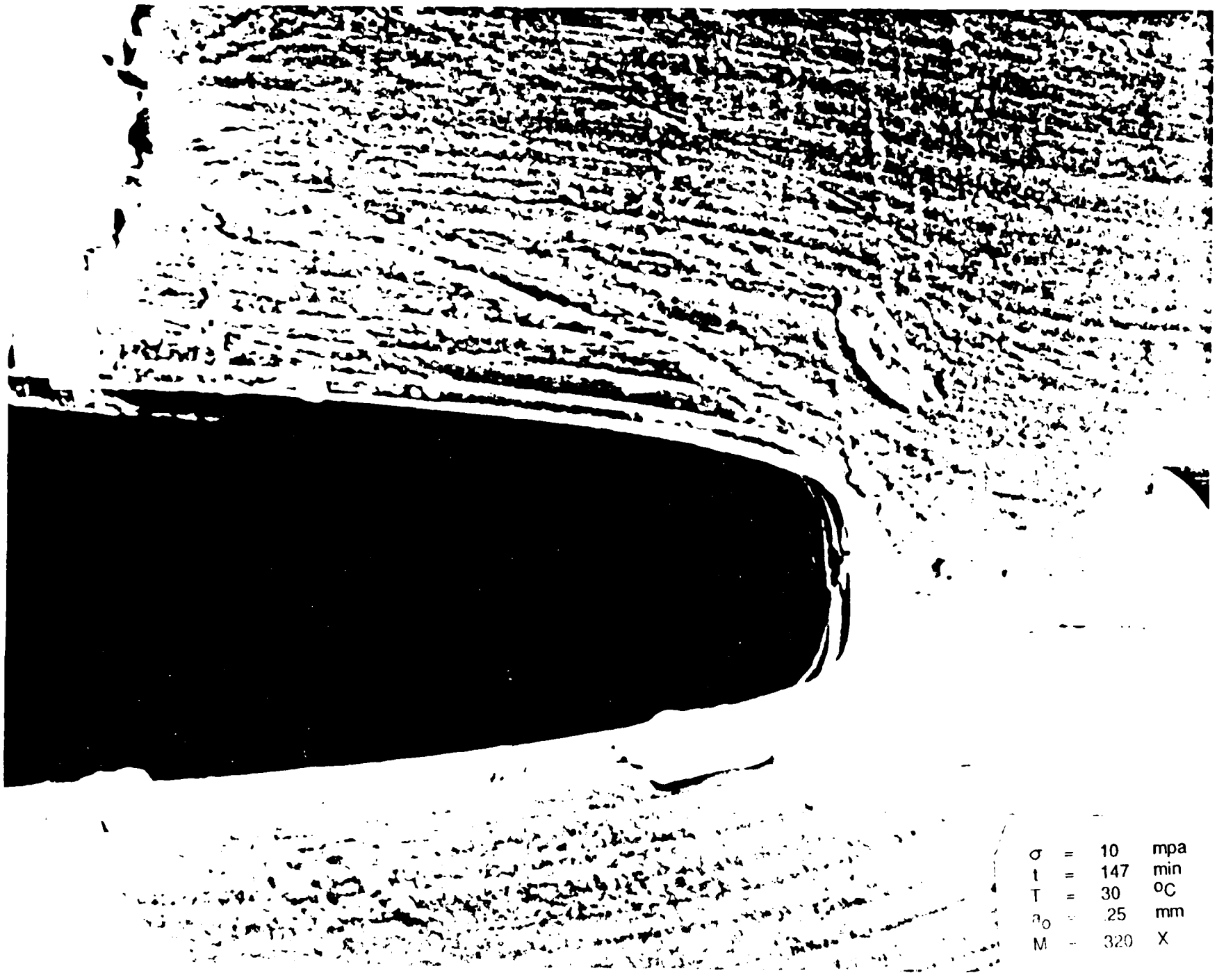
σ = 10 mpa
t = 147 min
T = 30 °C
a_o = .25 mm
M = 320 X

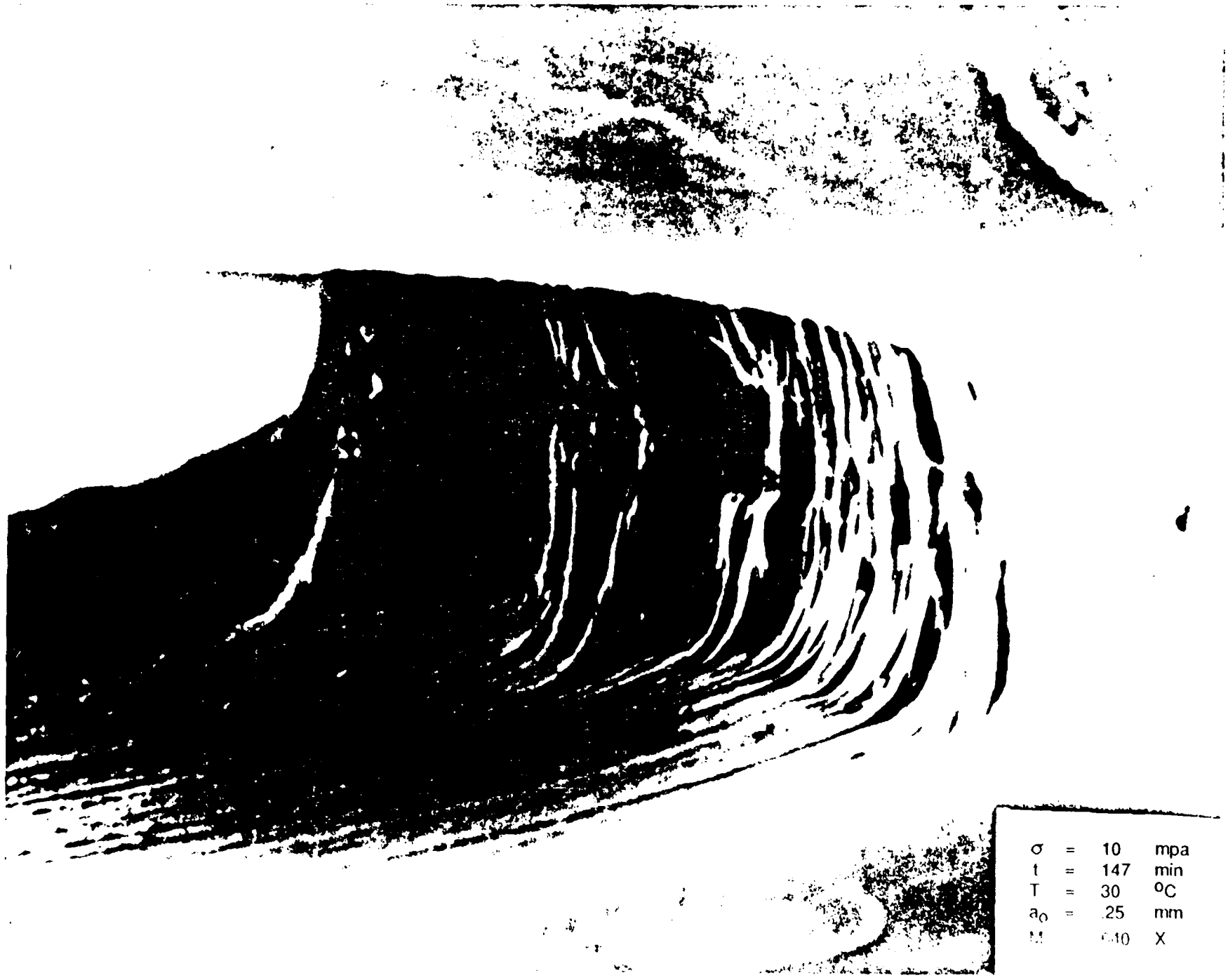
σ = 10 mpa
t = 147 min
T = 30 °C
a_0 = .25 mm
M .10 X

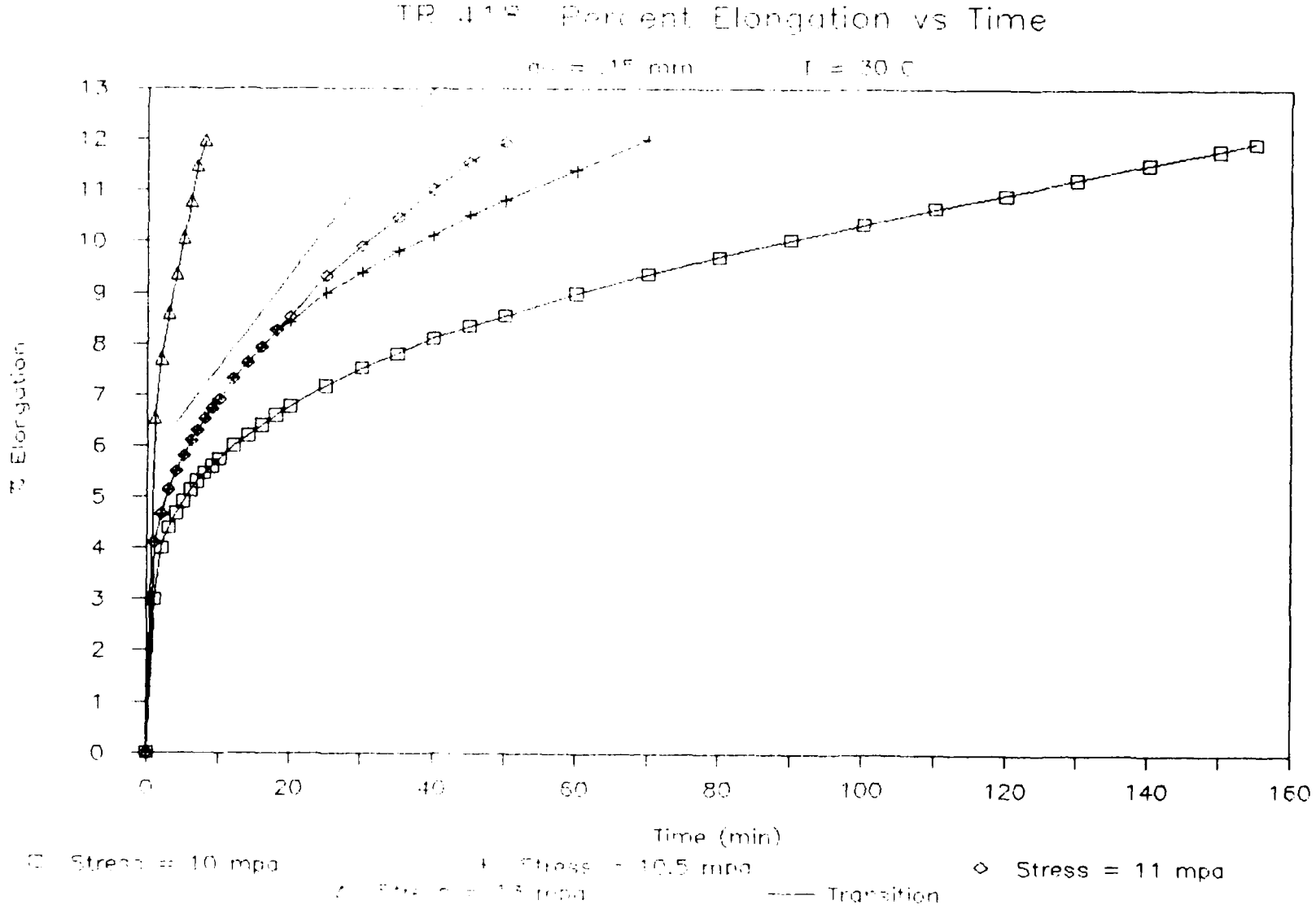
Percent Elongation vs Time
% Elongation
Time (min)
0
1
2
3
4
5
6
7
8
9
10
11
12
13
0
20
40
60
80
100
120
140
160
Stress = 10 mpa
Stress = 11 mpa
Transition

Figure 38

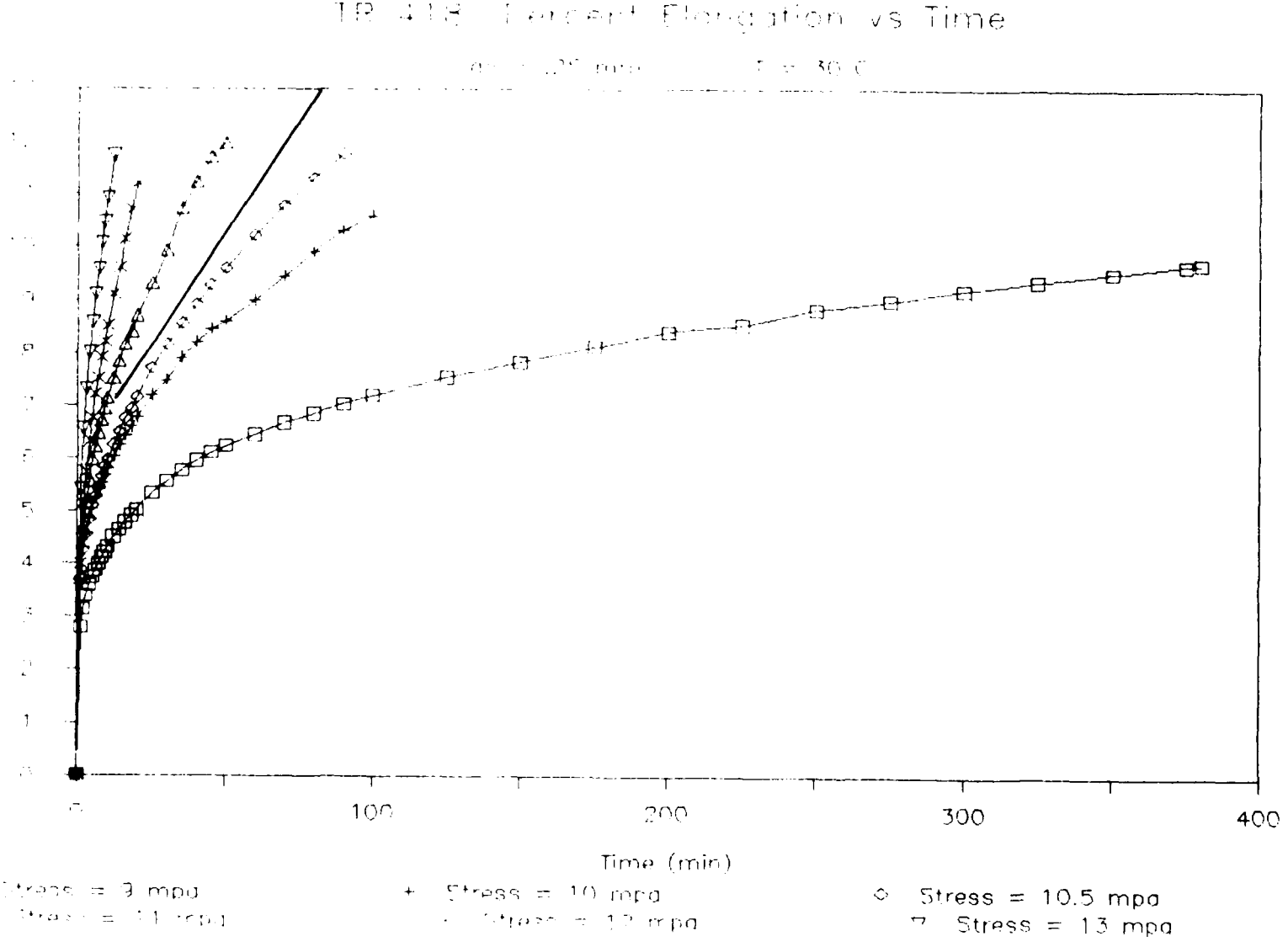
TP 418 Percent Elongation vs Time
% Elongation
0
1
2
3
4
5
100
200
300
400
Time (min)
Stress = 9 mpa
Stress = 10 mpa
Stress = 10.5 mpa
Stress = 13 mpa

Figure 39A

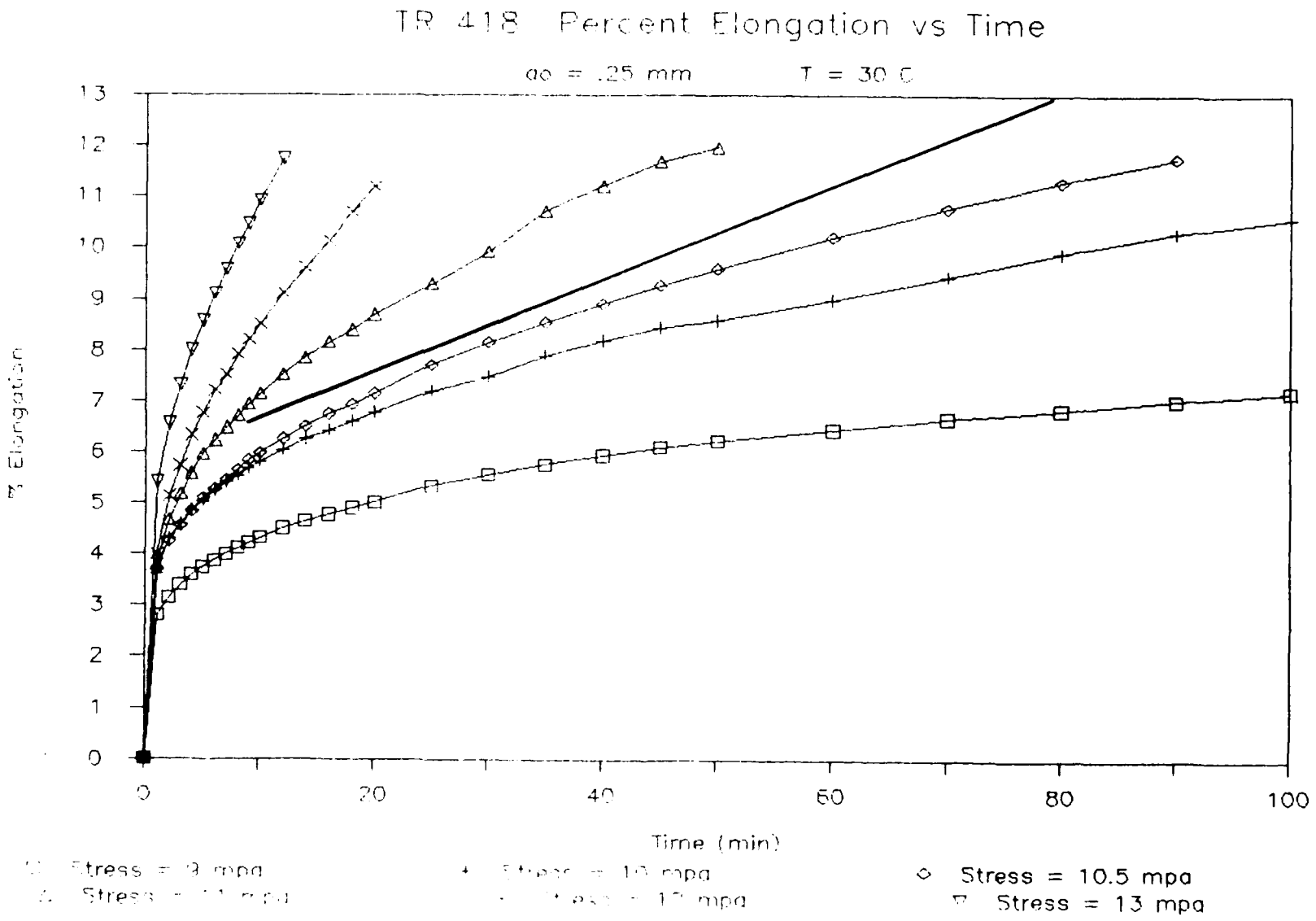
TR 418 Percent Elongation vs Time
ao = .25 mm
T = 30 C
% Elongation
Time (min)
0
20
40
60
80
100
1
2
3
4
5
6
7
8
9
10
11
12
13
Stress = 10.5 mpa
Stress = 13 mpa

Figure 39B

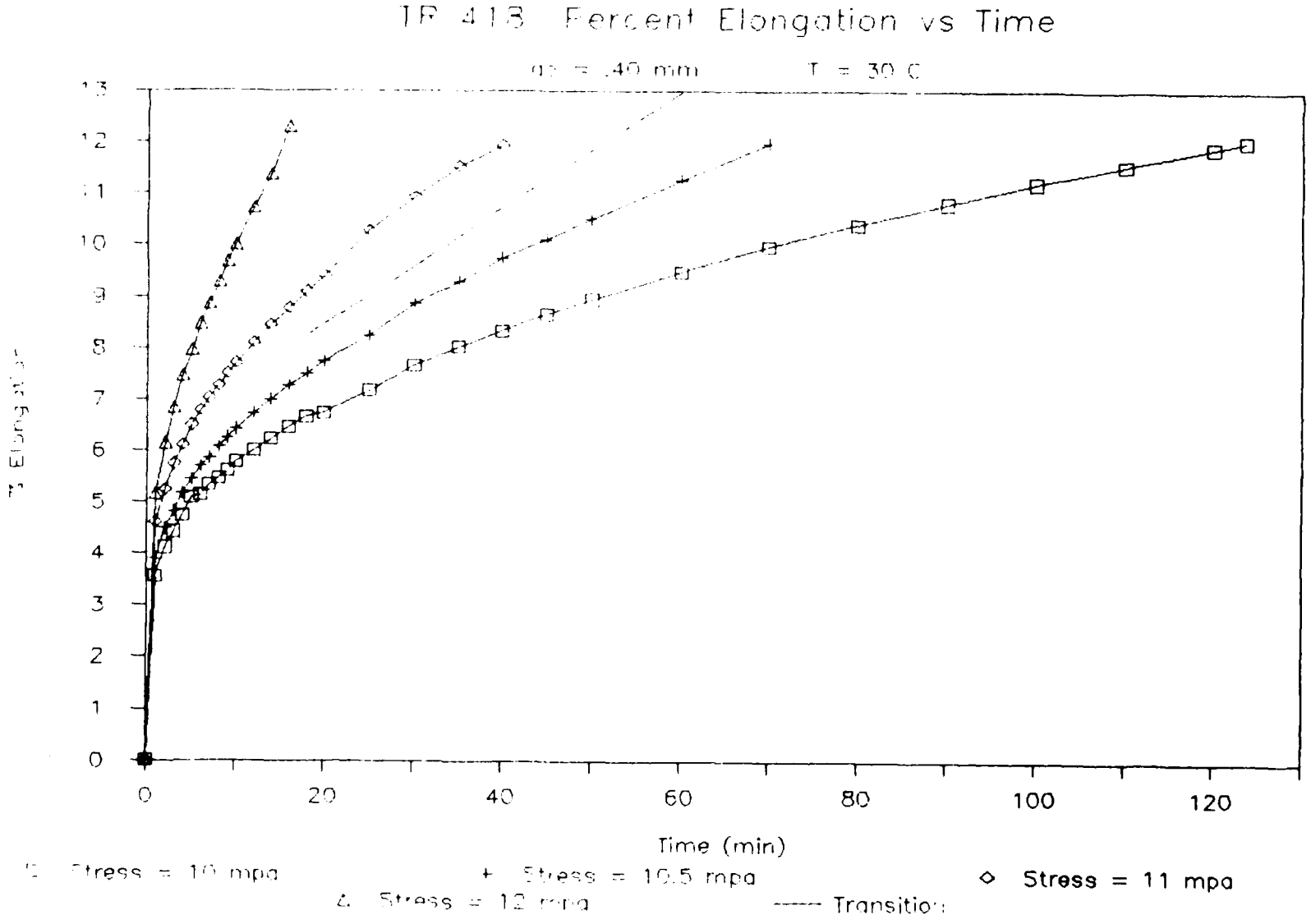
IR 413 Percent Elongation vs Time
T = 30 C
0
1
2
3
4
5
6
7
8
9
10
11
12
0
20
40
60
80
100
120
Time (min)
Stress = 11 mpa
Transition

Figure 40

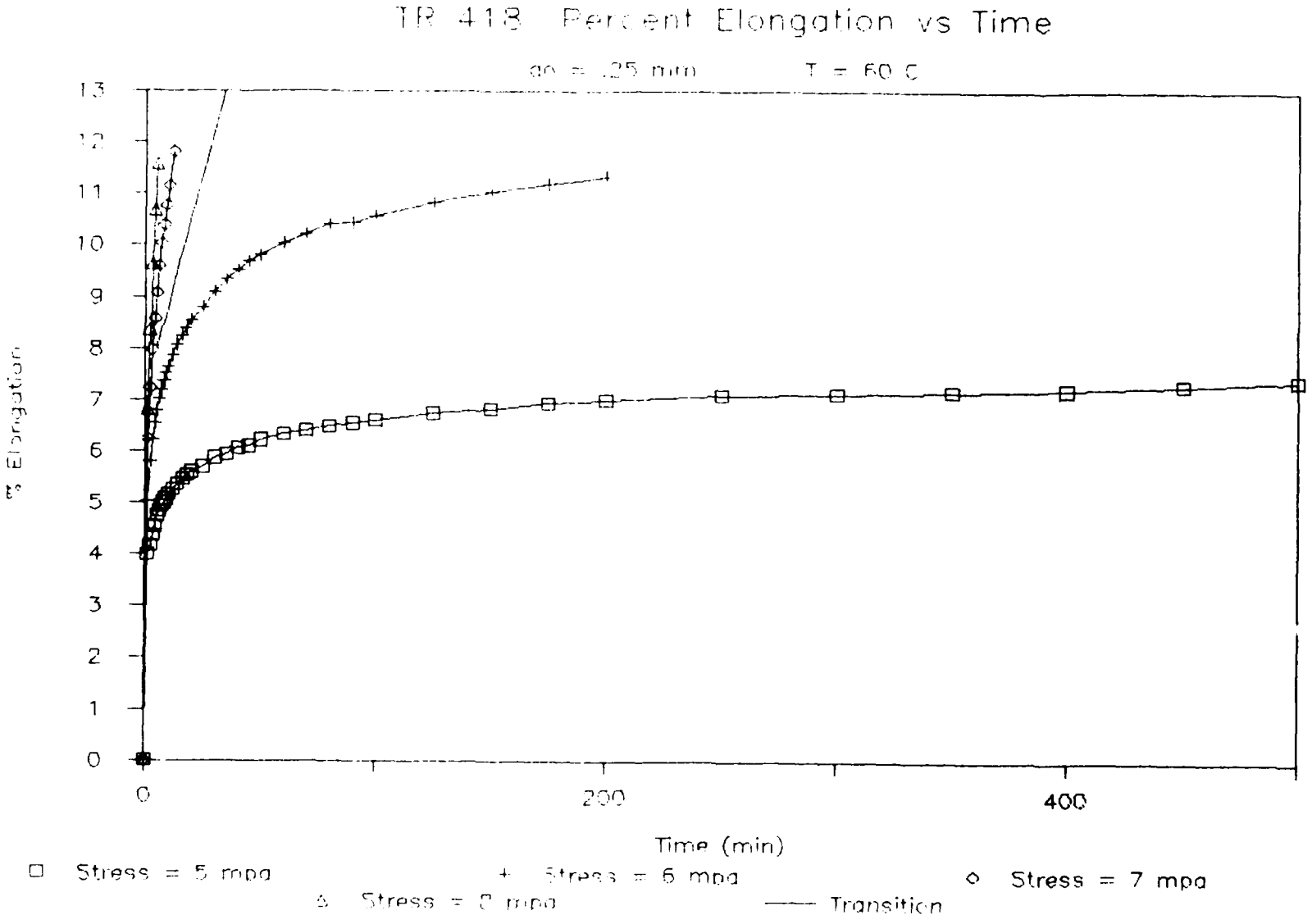
TR 418 Percent Elongation vs Time
T = 60 C
% Elongation
0
1
2
3
4
5
6
7
8
9
10
11
12
13
0
200
400
Time (min)
Stress = 5 mpa
Stress = 6 mpa
Stress = 7 mpa
Stress = 8 mpa
Transition

Figure 41A

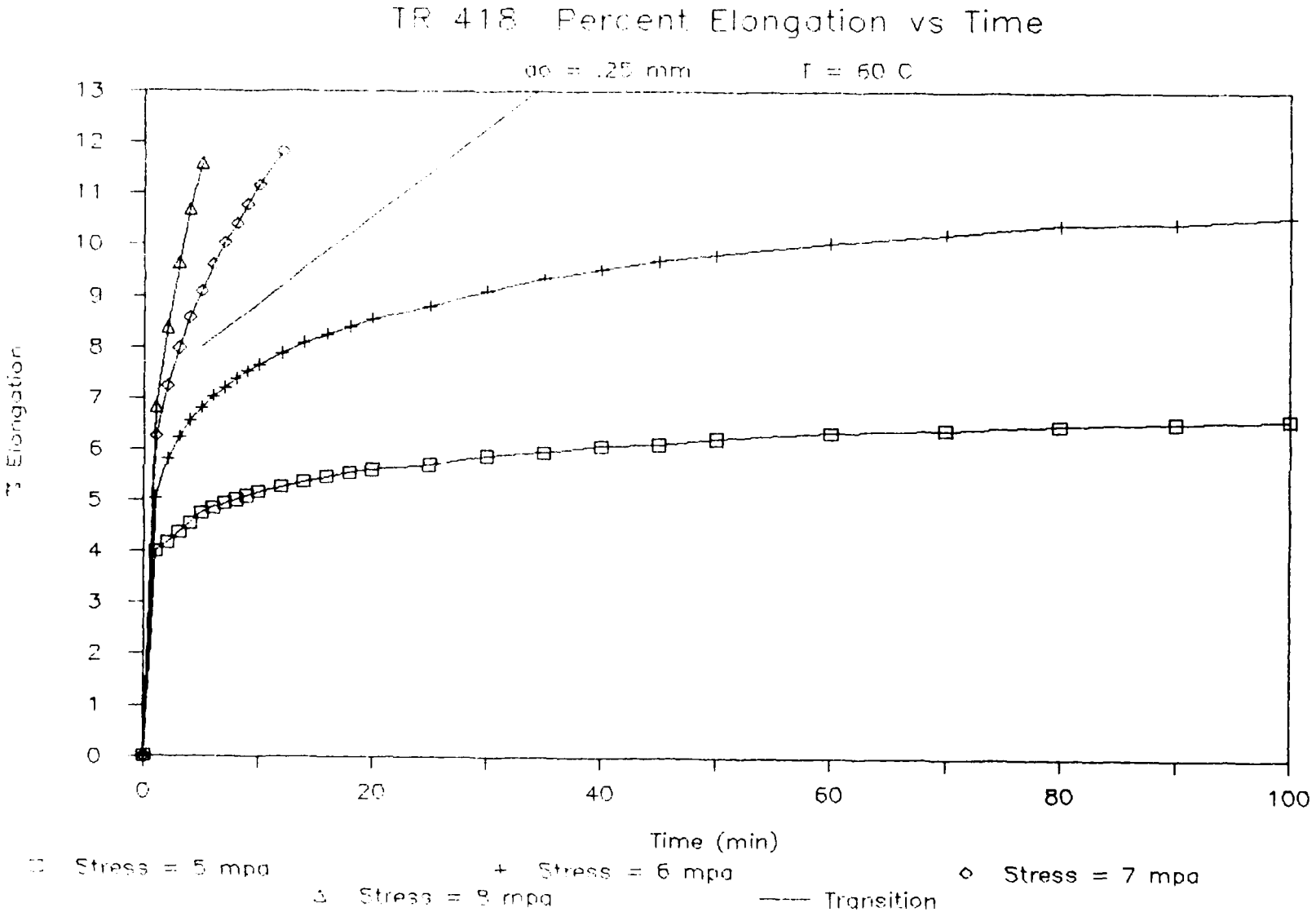
TR 418 Percent Elongation vs Time
do = .25 mm
T = 60 C
% Elongation
0
1
2
3
4
5
6
7
8
9
10
11
12
13
0
20
40
60
80
100
Time (min)
Stress = 5 mpa
Stress = 6 mpa
Stress = 7 mpa
Stress = 8 mpa
Transition

Figure 41B

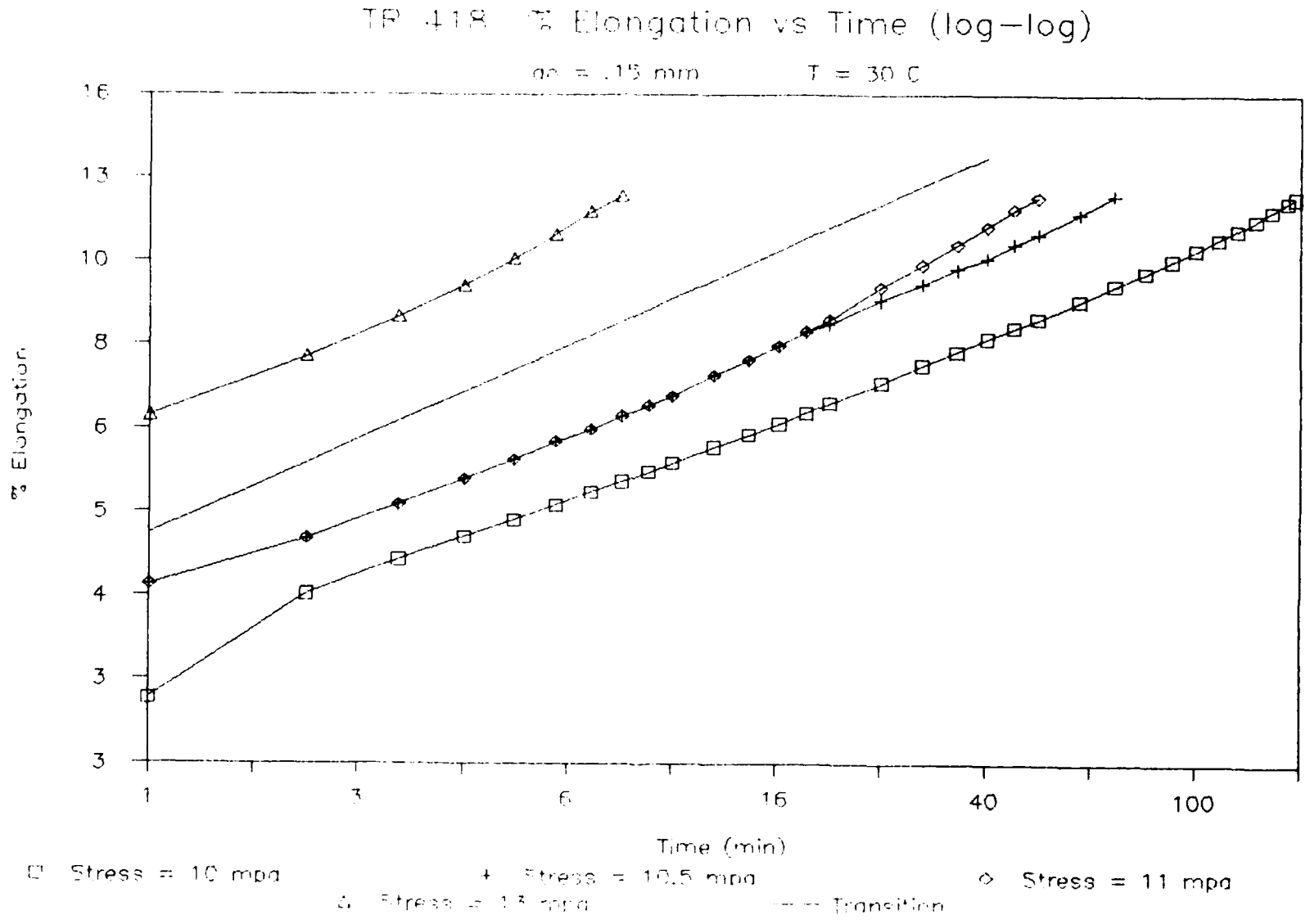
TP 418 % Elongation vs Time (log–log)
ao = .15 mm
T = 30 C
16
13
10
8
6
5
4
3
3
1
3
6
16
40
100
% Elongation
Time (min)
□ Stress = 10 mpa
+ Stress = 10.5 mpa
◇ Stress = 11 mpa
△ Stress = 13 mpa
— — Transition

Figure 42

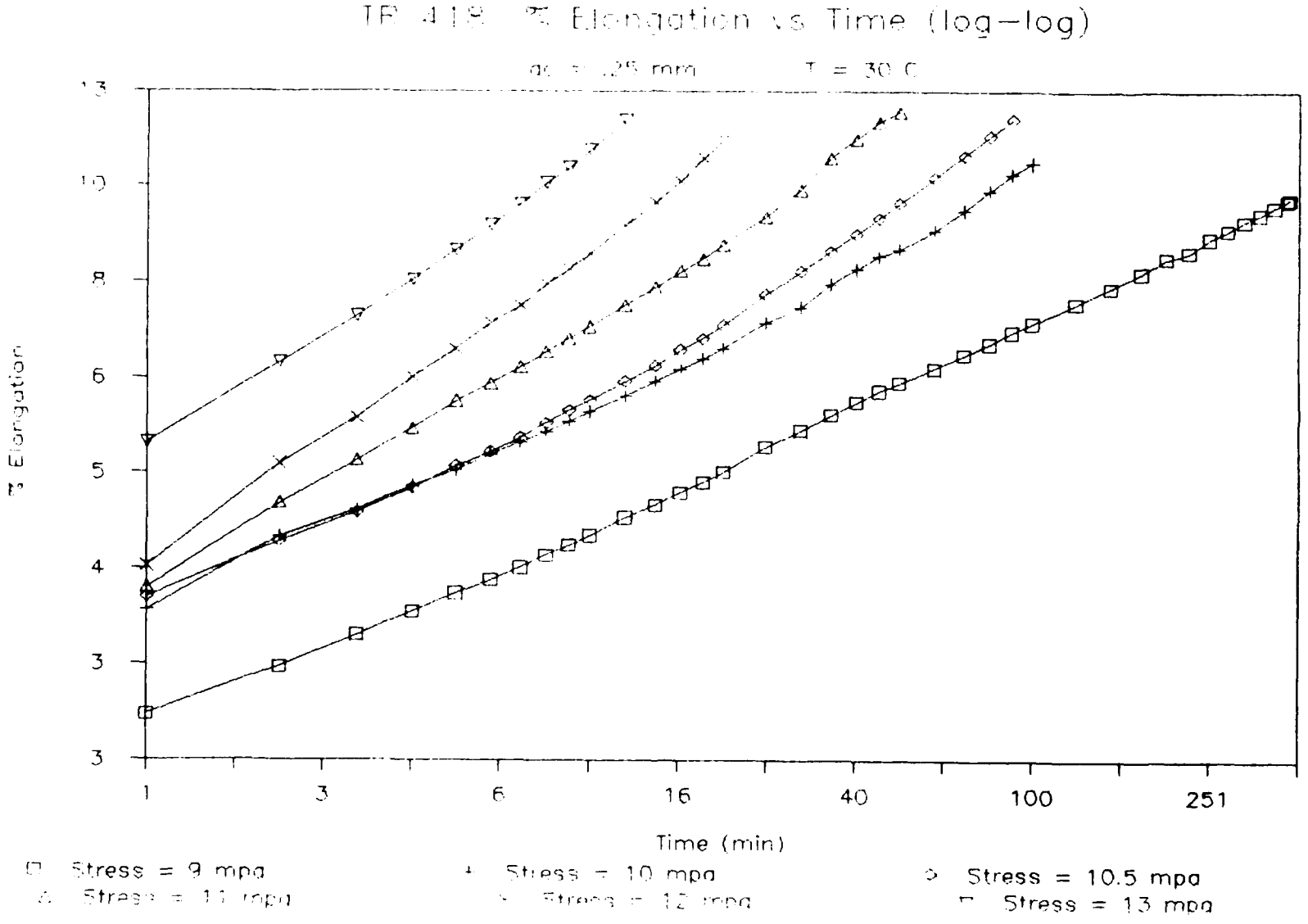
TR 418 % Elongation vs Time (log–log)
T = 30 C
% Elongation
13
10
8
6
5
4
3
1
3
6
16
40
100
251
Time (min)
Stress = 9 mpa
Stress = 10 mpa
Stress = 10.5 mpa
Stress = 11 mpa
Stress = 12 mpa
Stress = 13 mpa

Figure 43

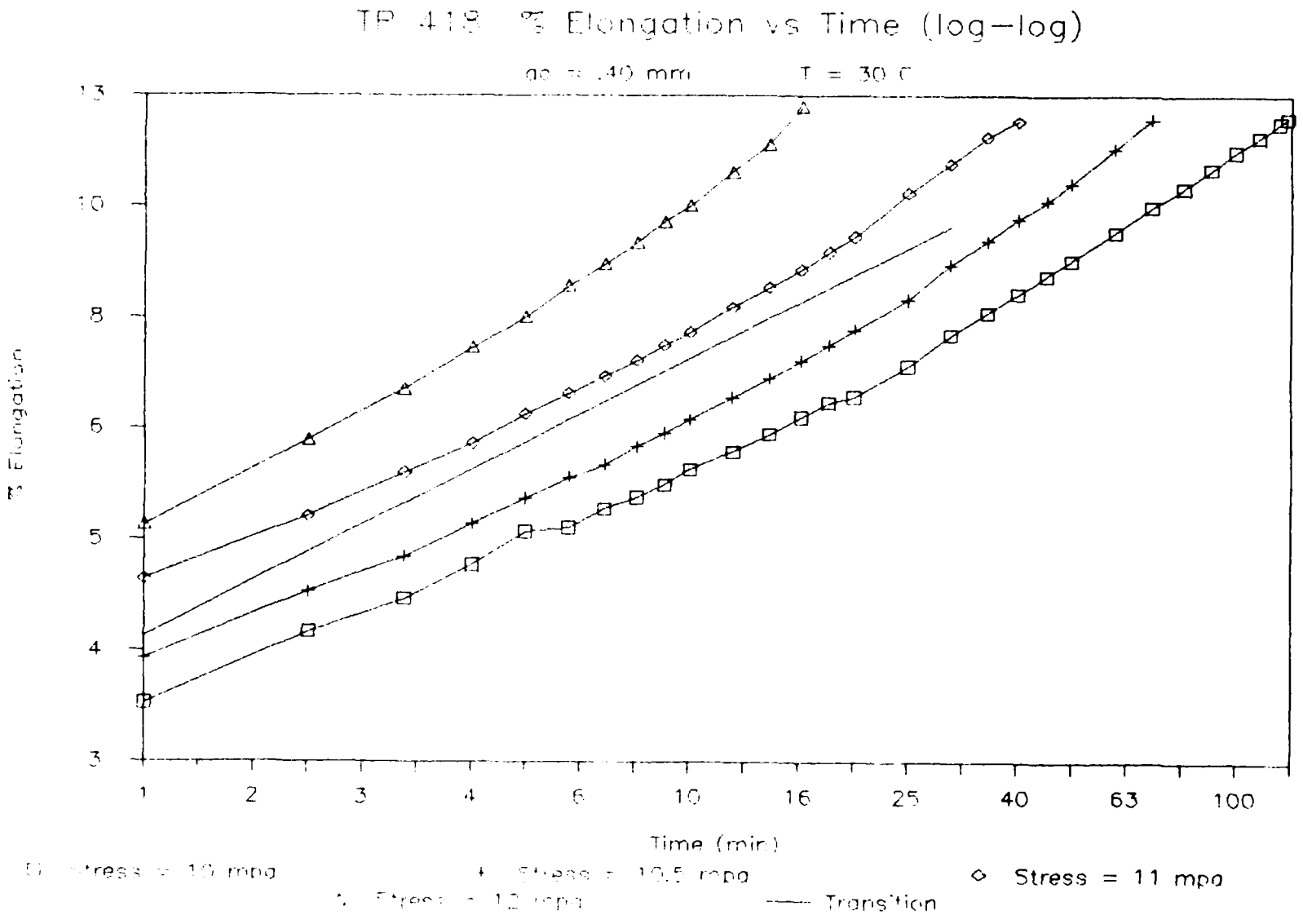
TP 418 % Elongation vs Time (log–log)
T = 30 C
% Elongation
13
10
8
6
5
4
3
1
2
3
4
6
10
16
25
40
63
100
Time (min)
Stress = 11 mpa
Transition

Figure 44

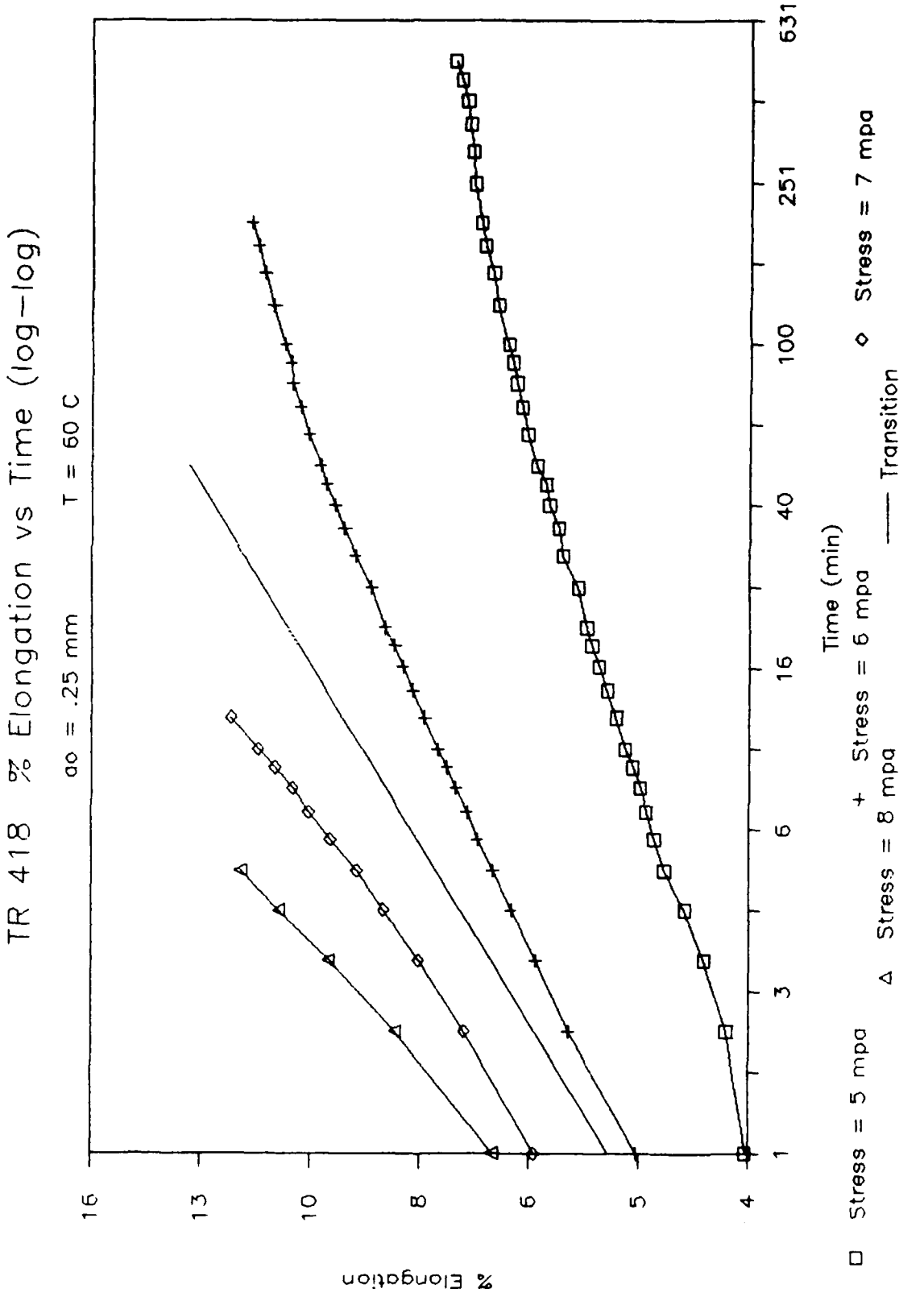
TR 418 % Elongation vs Time (log-log)
ao = .25 mm
T = 60 C
% Elongation
16
13
10
8
6
5
4
1
3
6
16
40
100
251
631
Time (min)
□ Stress = 5 mpa
+ Stress = 6 mpa
◇ Stress = 7 mpa
△ Stress = 8 mpa
—— Transition

Figure 45

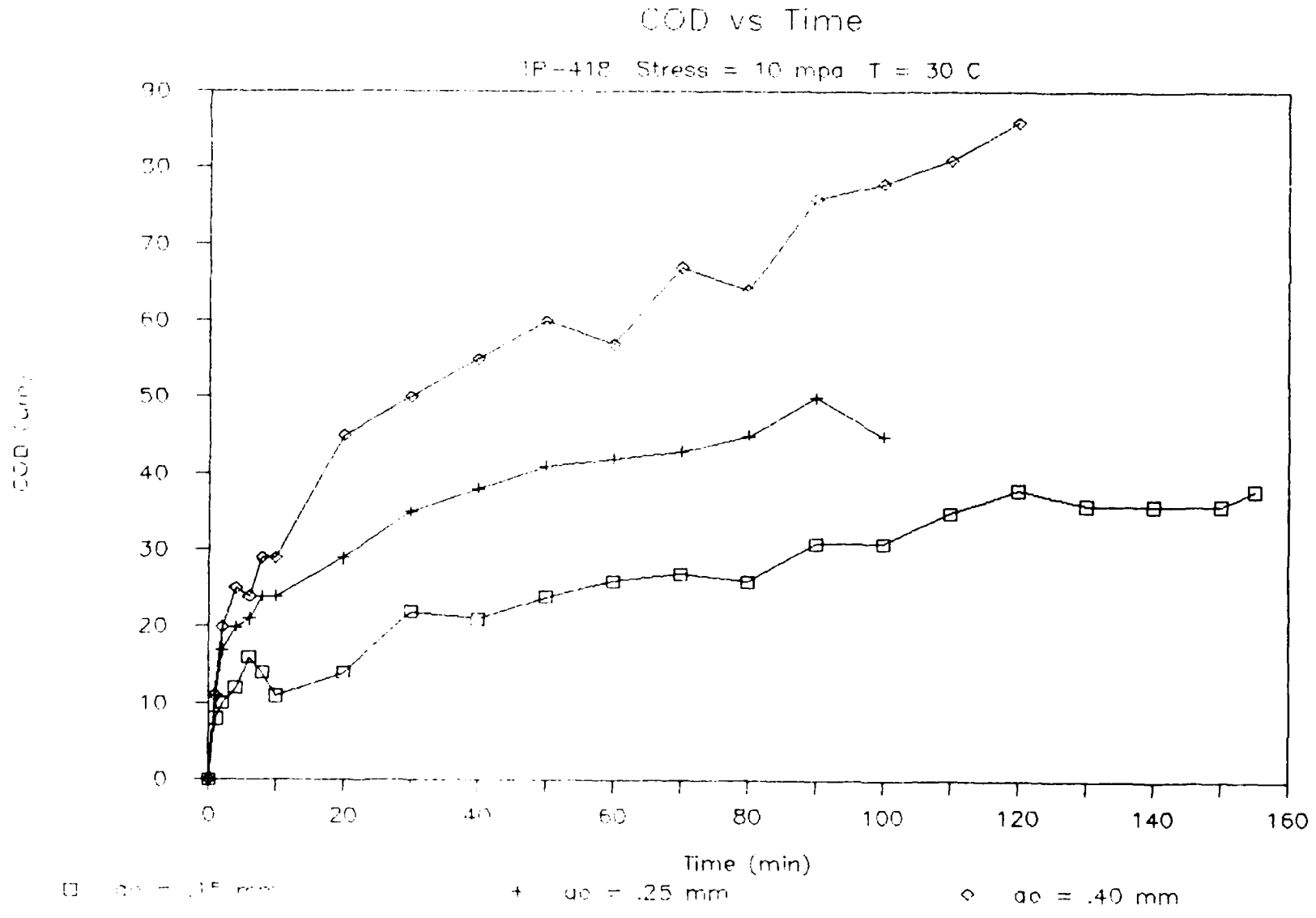
COD vs Time
IP-418 Stress = 10 mpa T = 30 C
COD (cm³)
0
10
20
30
40
50
60
70
80
0
20
40
60
80
100
120
140
160
Time (min)
□ ao = .15 mm
+ ao = .25 mm
◇ ao = .40 mm

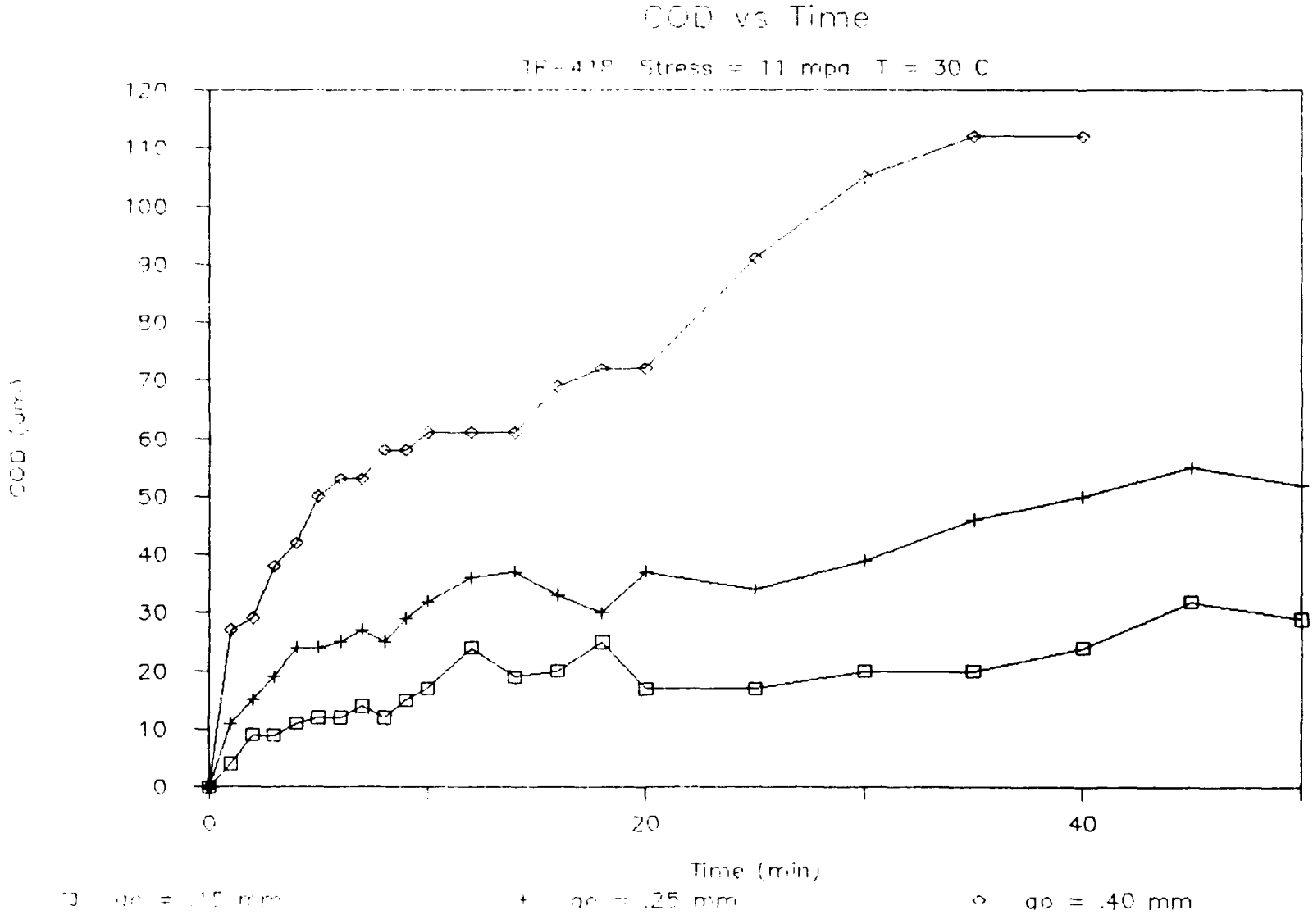
COD vs Time
Stress = 11 mpa T = 30 C
120
110
100
90
80
70
60
50
40
30
20
10
0
0
20
40
Time (min)
COD (um)
go = .25 mm
go = .40 mm

Figure 47

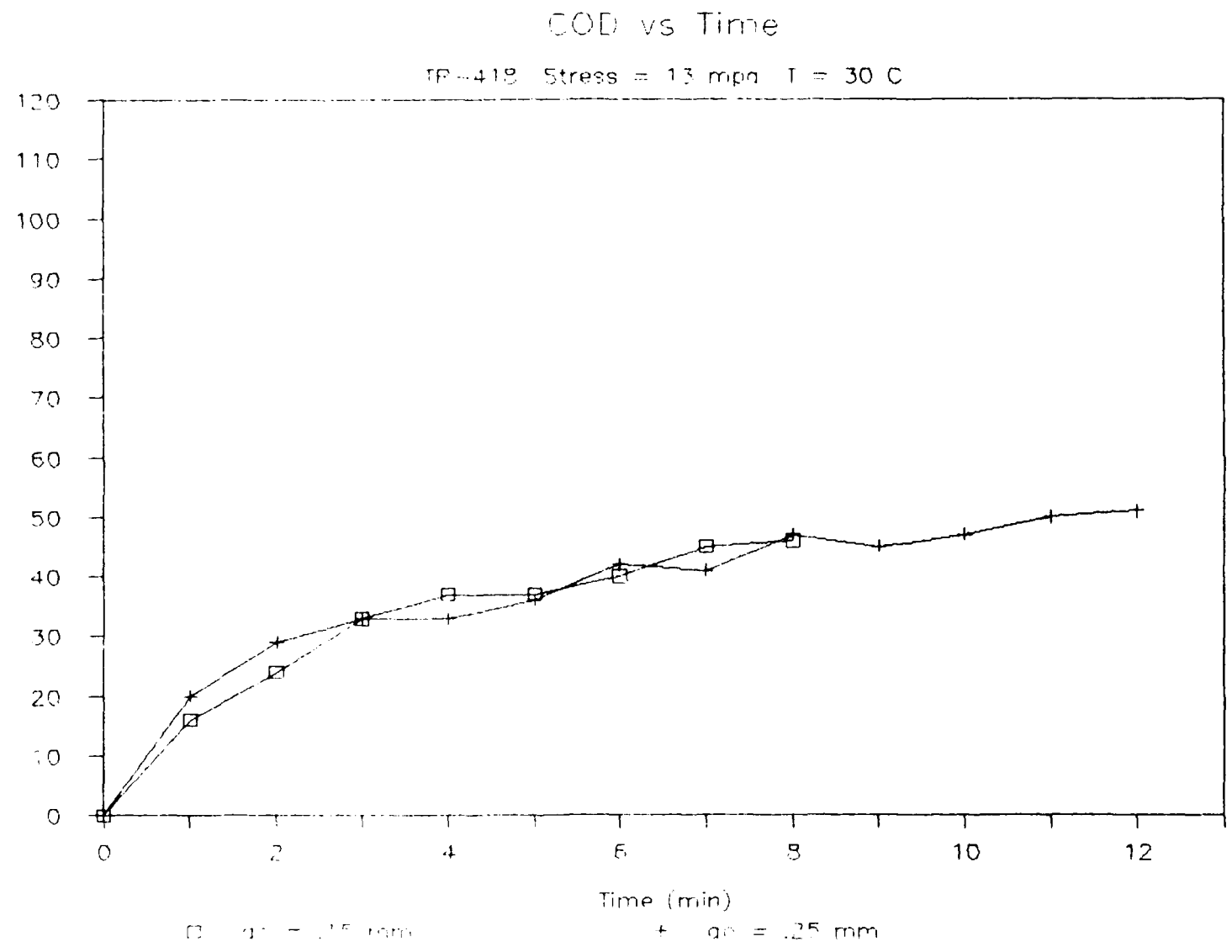
COD vs Time
TP-418 Stress = 13 mpa T = 30 C
COD (um)
120
110
100
90
80
70
60
50
40
30
20
10
0
0
2
4
6
8
10
12
Time (min)
+ = .25 mm

Figure 48

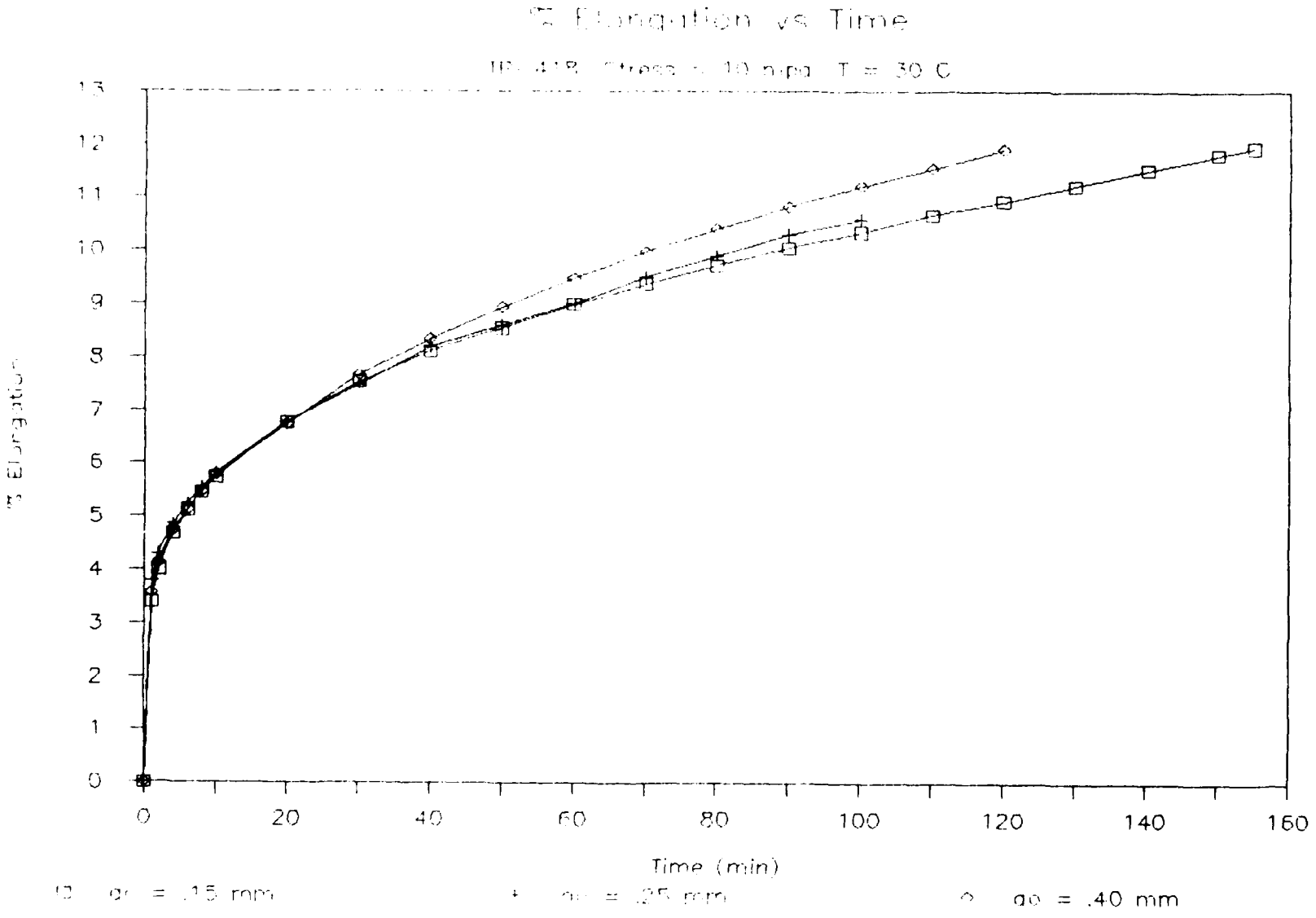
% Elongation vs Time
T = 30 C
% Elongation
Time (min)
0
20
40
60
80
100
120
140
160
0
1
2
3
4
5
6
7
8
9
10
11
12
13
go = .40 mm

Figure 49

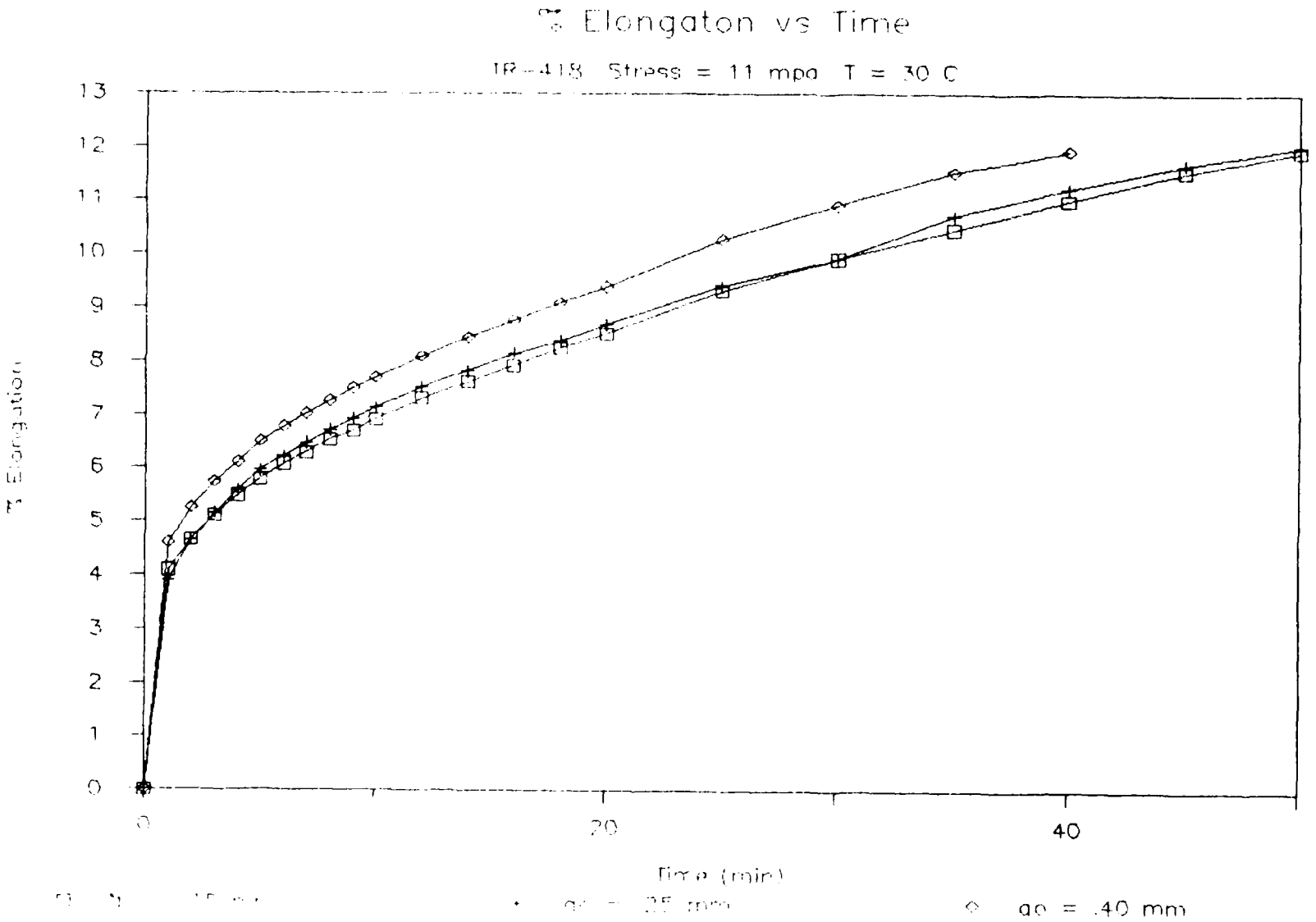
% Elongaton vs Time
IP-418 Stress = 11 mpa T = 30 C
% Elongation
13
12
11
10
9
8
7
6
5
4
3
2
1
0
0
20
40
Time (min)
go = .40 mm

Figure 50

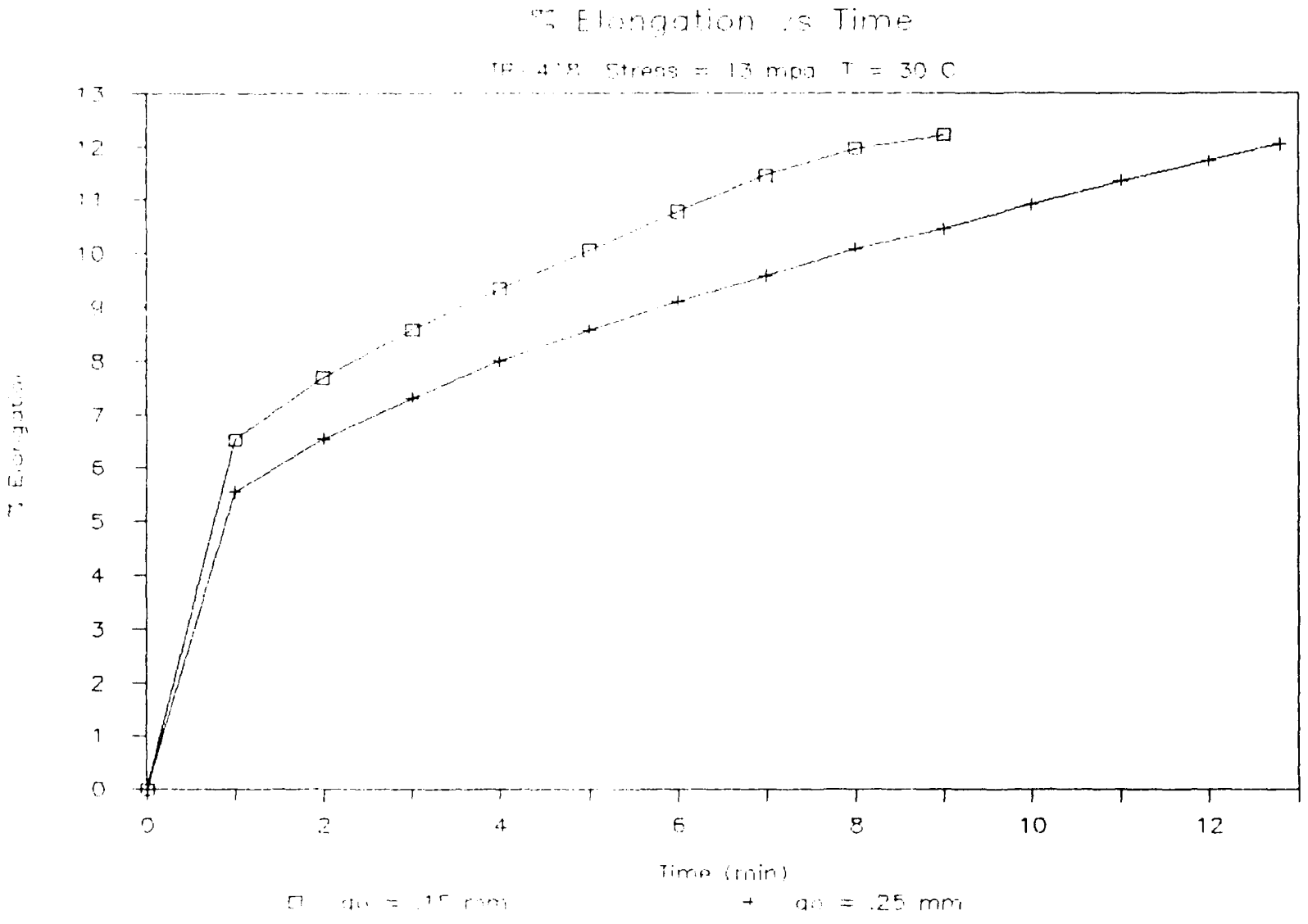
% Elongation vs Time
Stress = 13 mpa T = 30 C
% Elongation
0
1
2
3
4
5
6
7
8
9
10
11
12
13
0
2
4
6
8
10
12
Time (min)
+ .25 mm

Figure 51

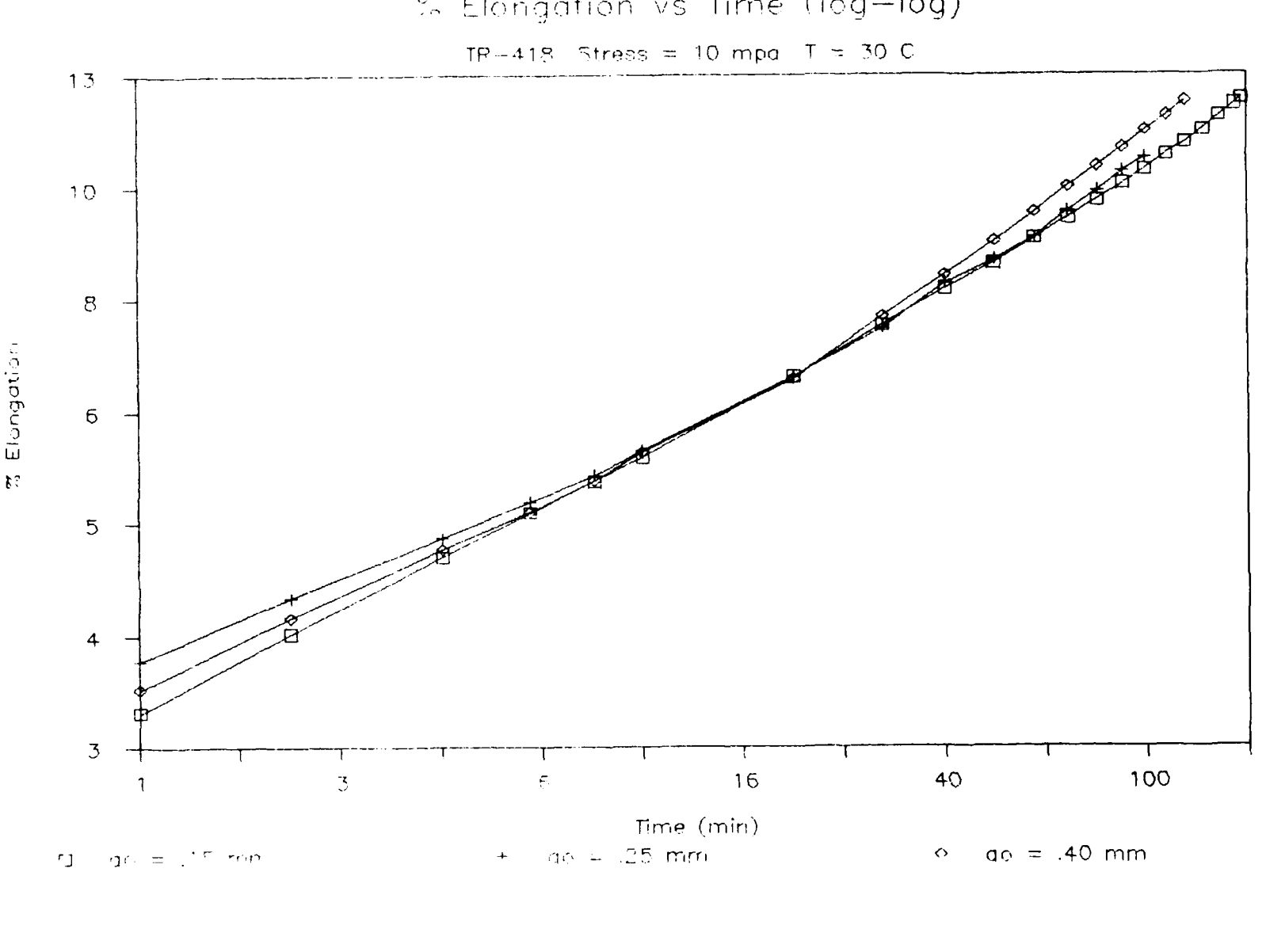
% Elongation vs Time (log–log)
TR–418 Stress = 10 mpa T = 30 C
% Elongation
13
10
8
6
5
4
3
1
3
5
16
40
100
Time (min)
+ ao = .25 mm
◇ ao = .40 mm

Figure 52

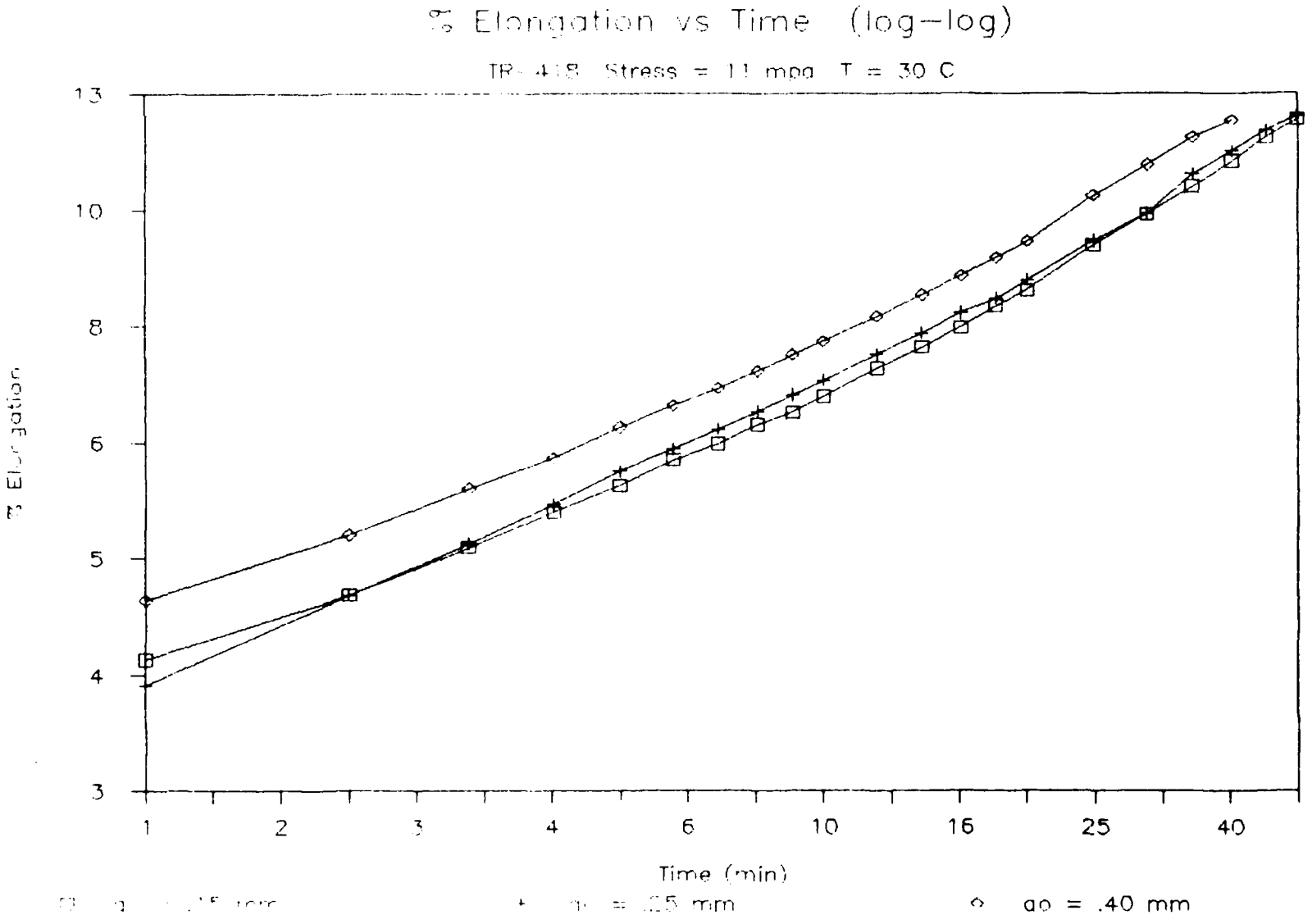
% Elongation vs Time (log–log)
TR- 418 Stress = 11 mpa T = 30 C
% Elongation
13
10
8
6
5
4
3
1
2
3
4
6
10
16
25
40
Time (min)
ao = .40 mm

Figure 53

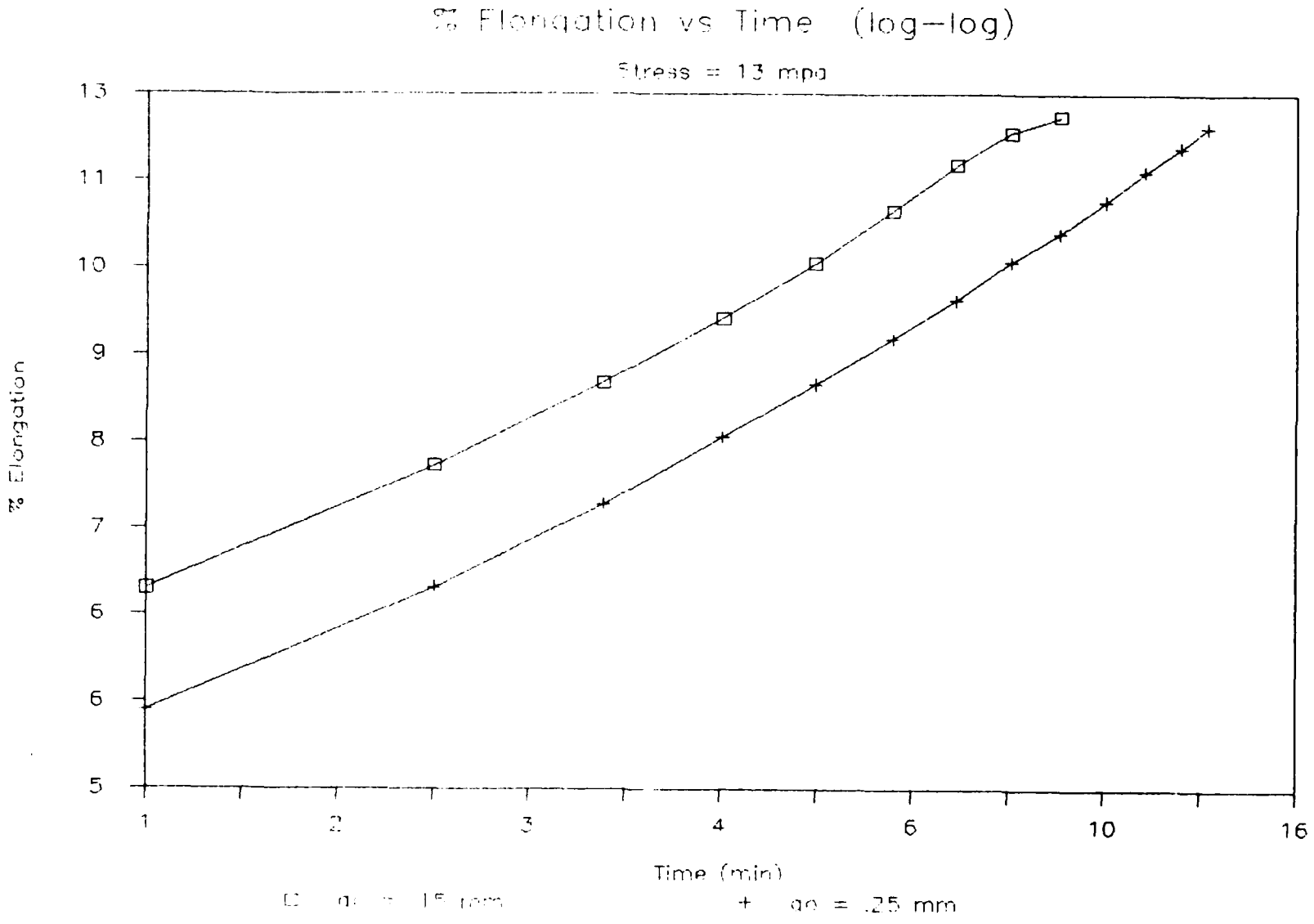
% Elongation vs Time (log-log)
Stress = 13 mpa
% Elongation
13
11
10
9
8
7
6
6
5
1
2
3
4
6
10
16
Time (min)
+ ao = .25 mm

Figure 54

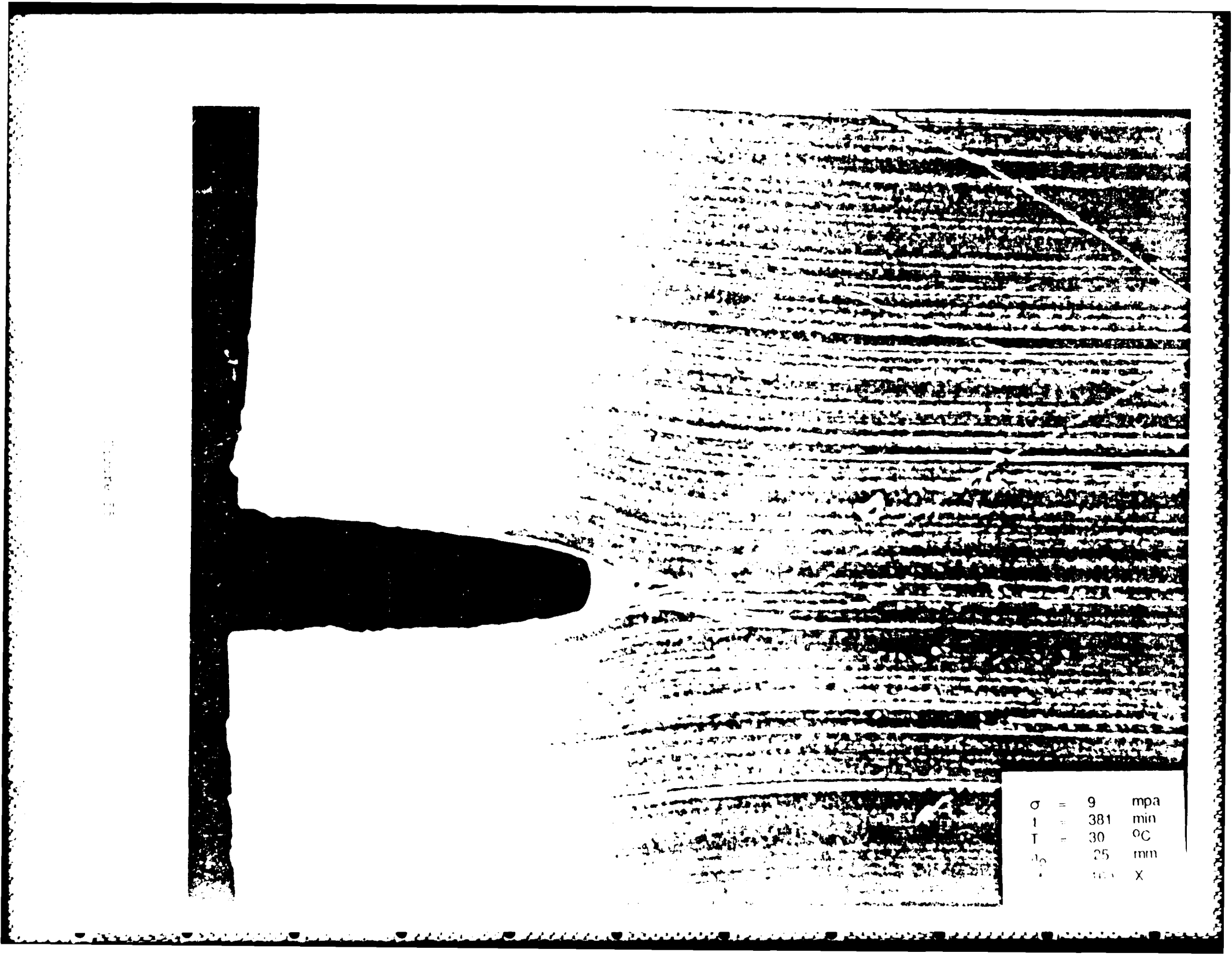
σ = 9 mpa
t = 381 min
T = 30 °C
25 mm
X

Figure 56

Figure 57

Figure 58

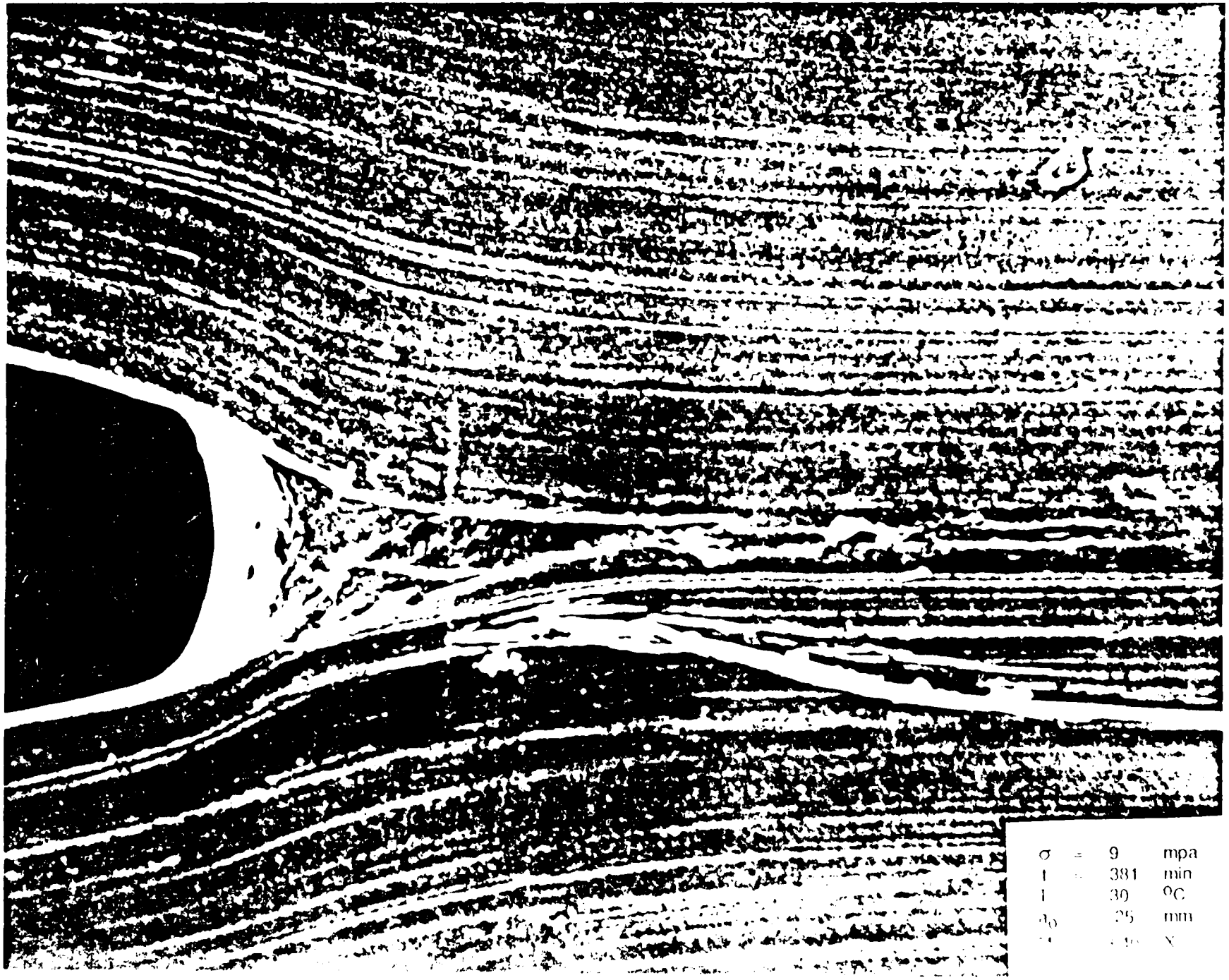
σ = 9 mpa
t = 381 min
T = 30 °C
d_0 = 25 mm

Figure 60

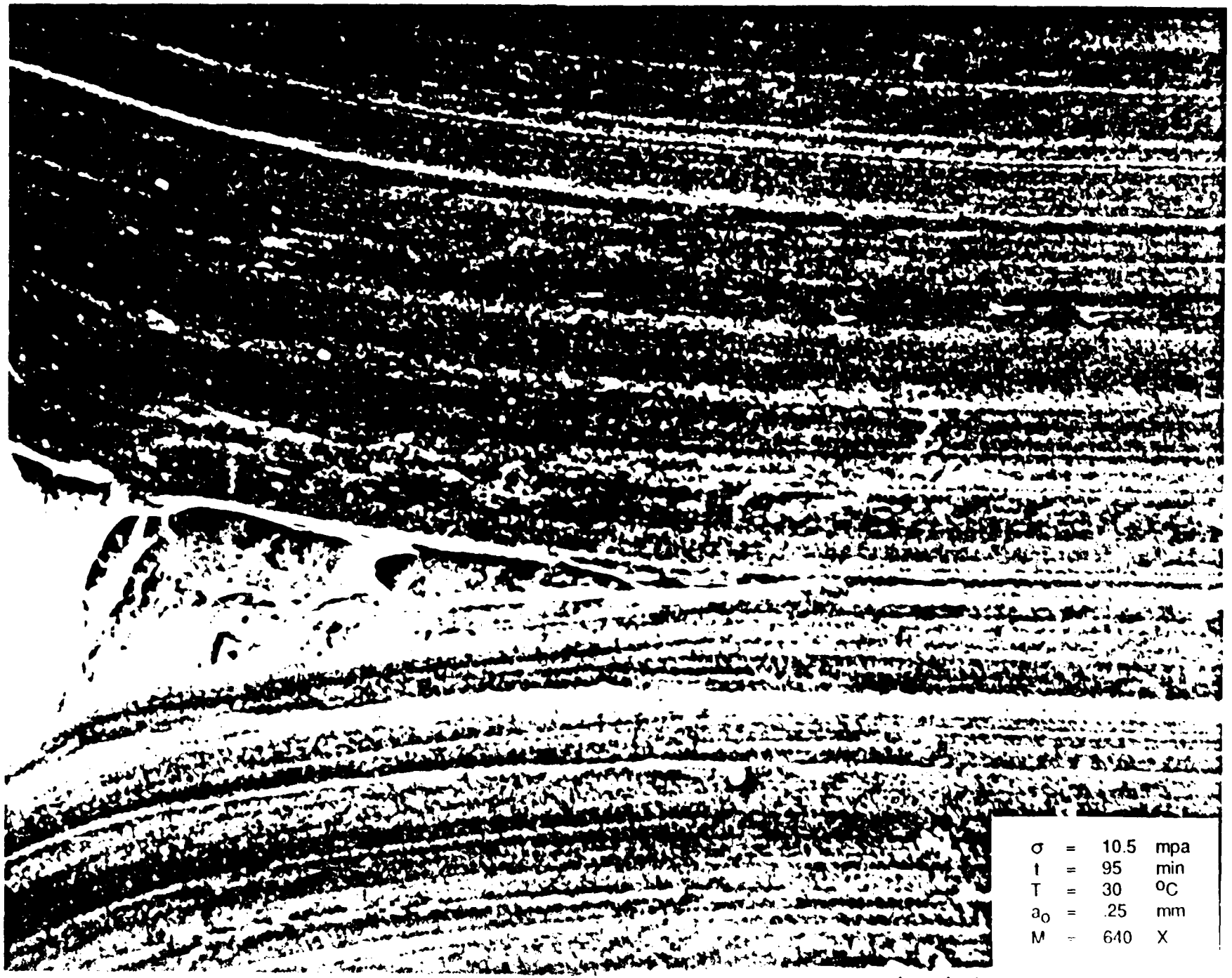
σ = 10.5 mpa
t = 95 min
T = 30 °C
a_o = .25 mm
M = 640 X

σ = 11 mpa
t = 48 min
T = 30 °C
ao = 25 mm

Figure 63

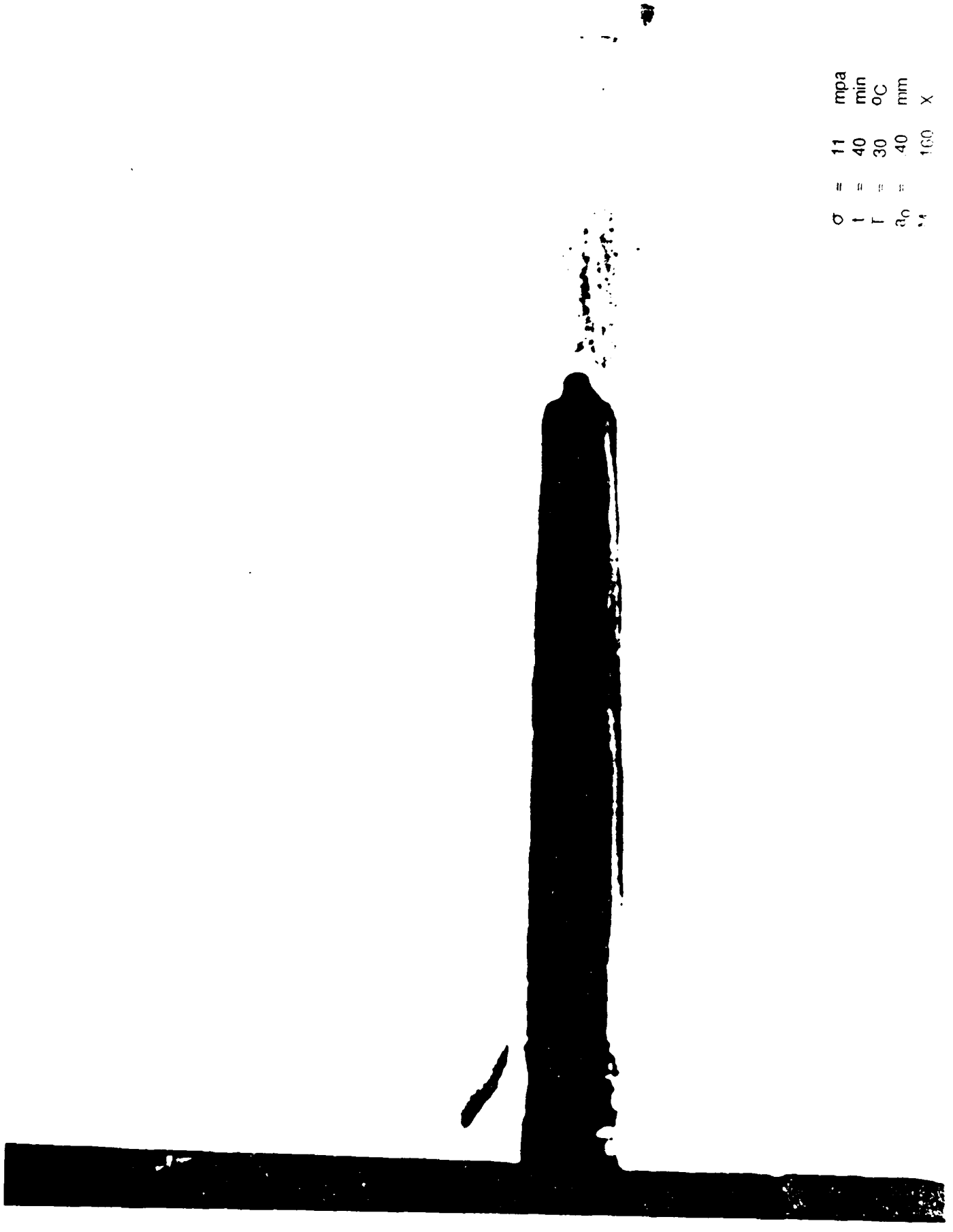

Figure 64

Figure 65

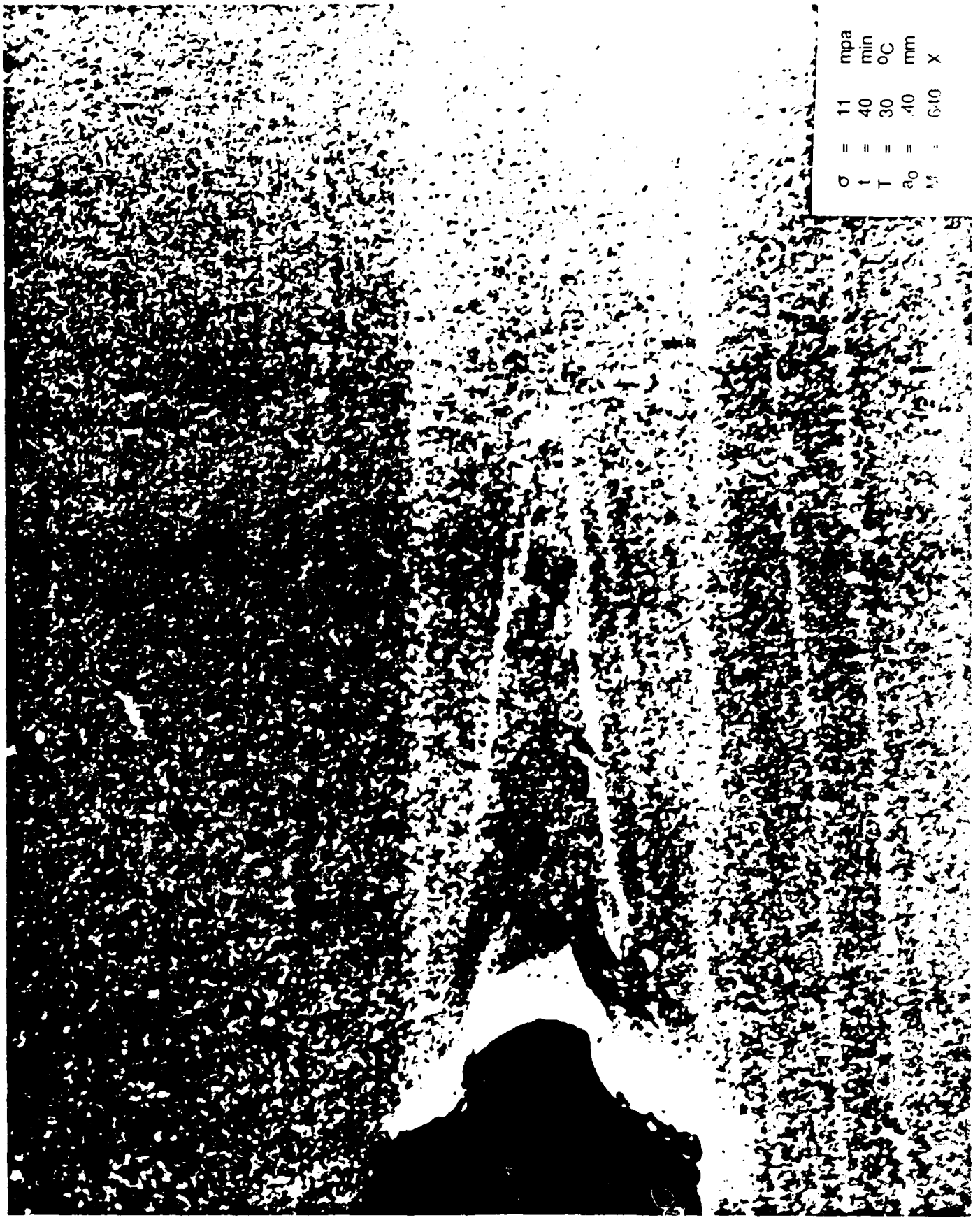

Figure 66

Table 7 [illegible] vs Stress

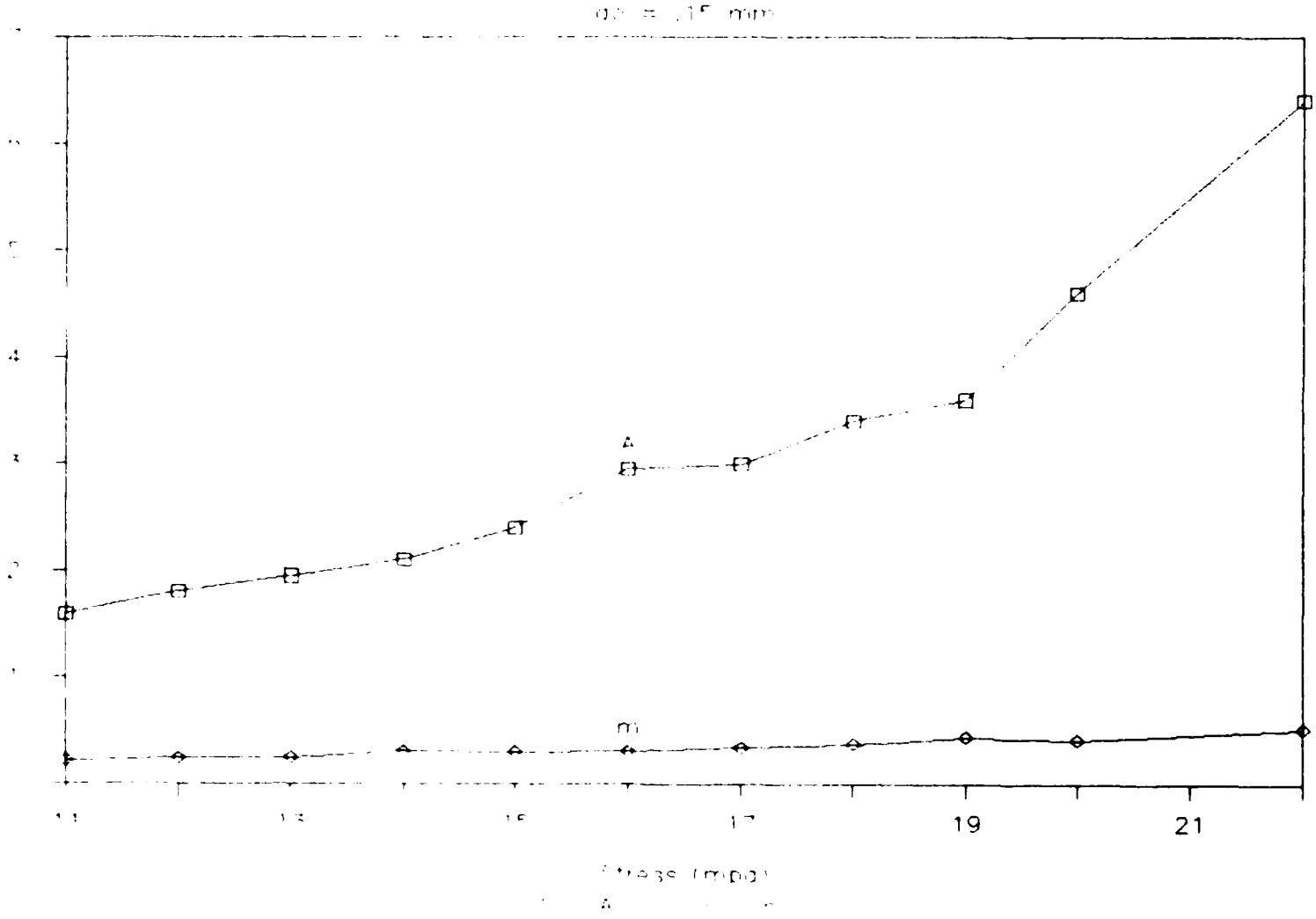

Figure 67

Table 4 A ; m vs Stress

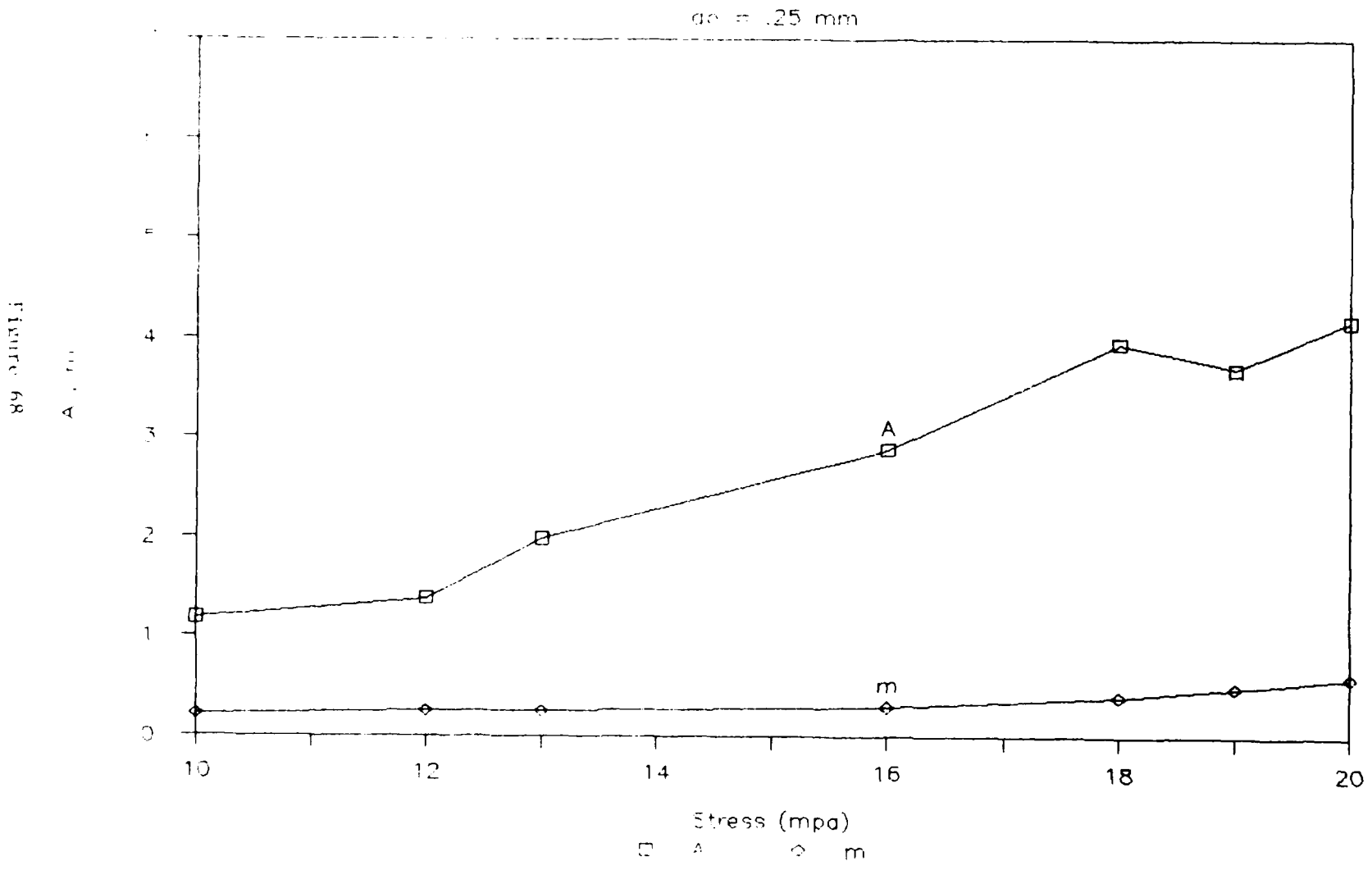

Table 5 A ; m vs Stress

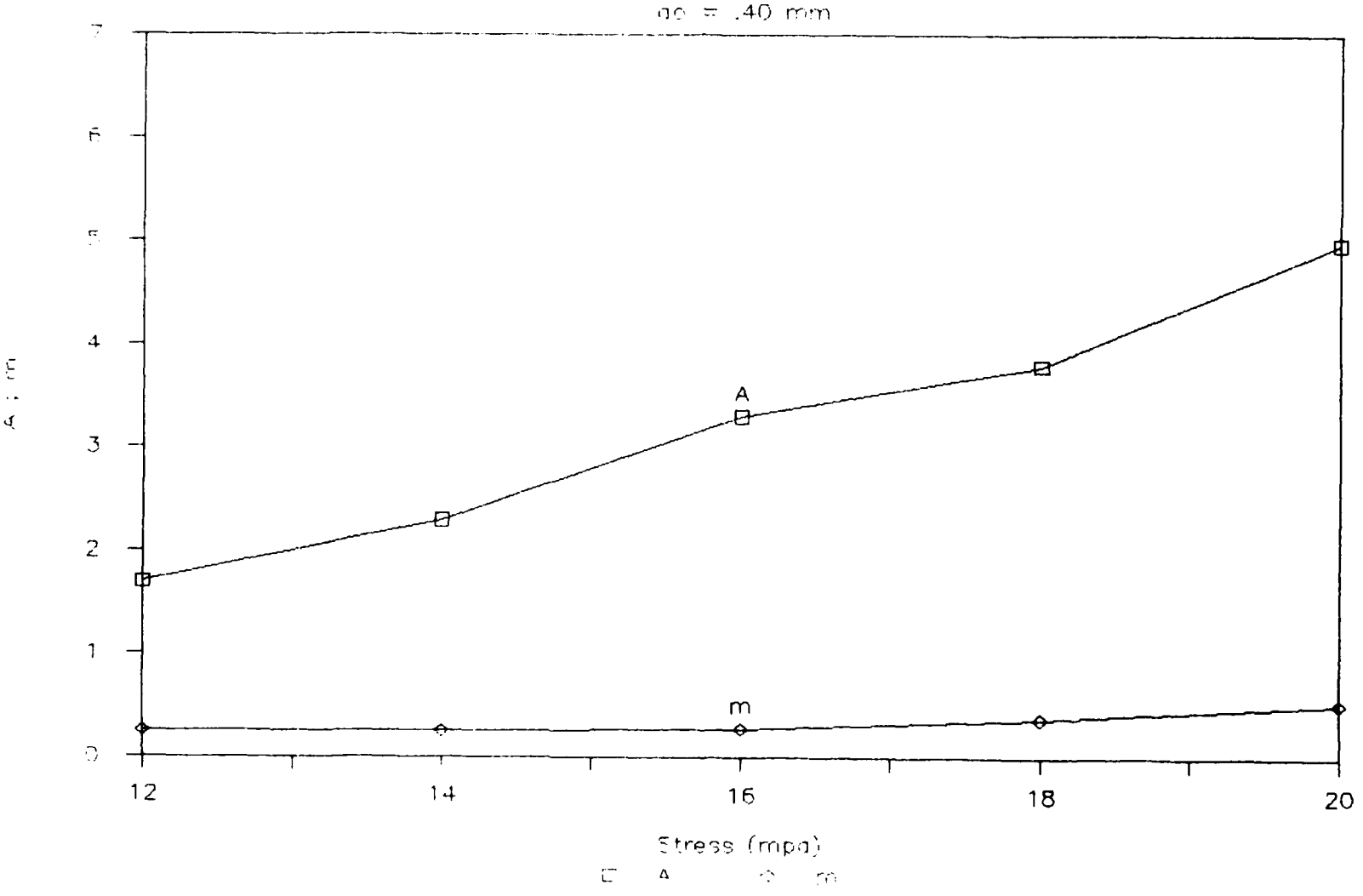

Figure 69

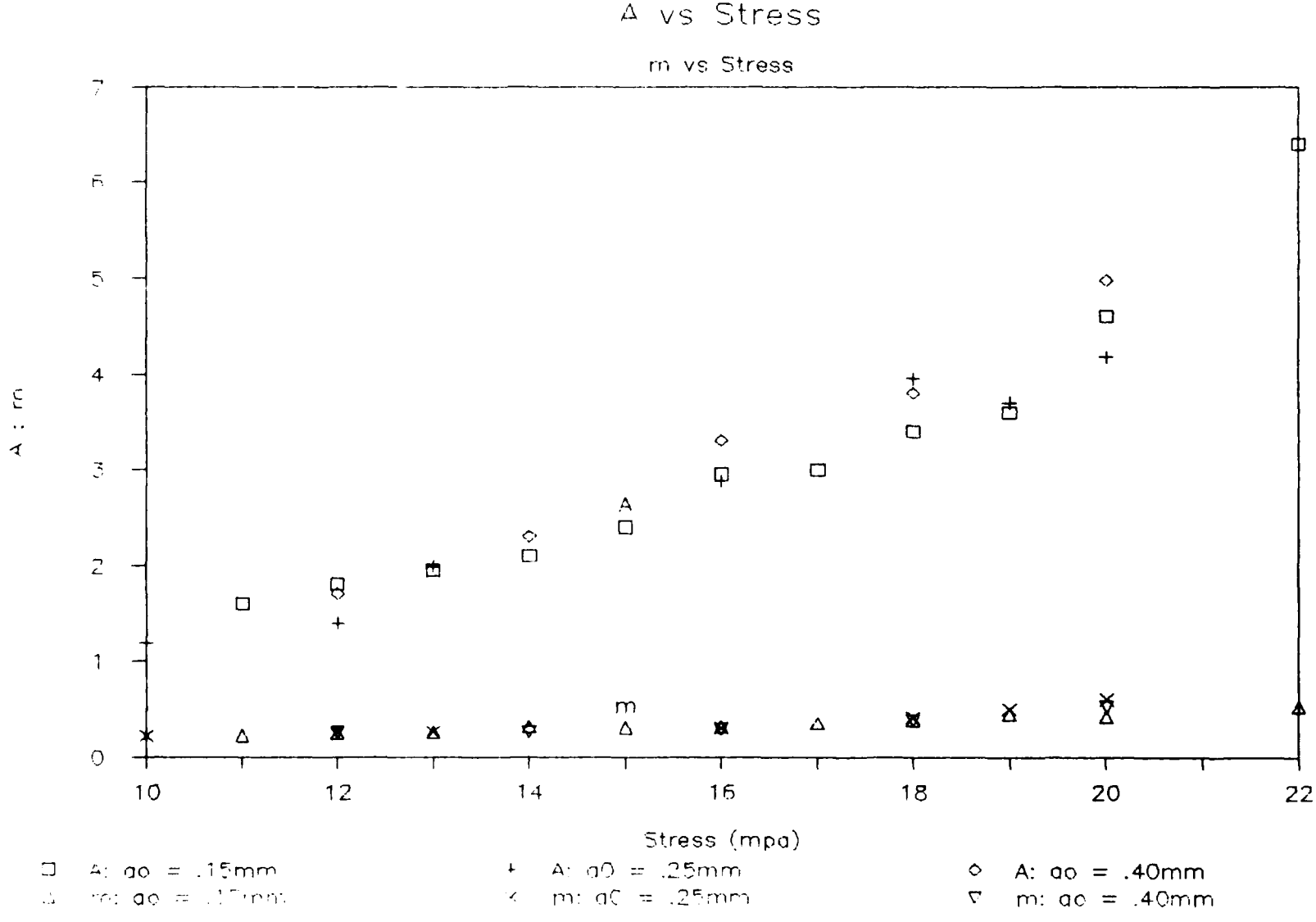
A vs Stress
m vs Stress
A : m
Stress (mpa)
10
12
14
16
18
20
22
0
1
2
4
5
7
A
m
A: ao = .15mm
A: ao = .25mm
A: ao = .40mm
m: ao = .25mm
m: ao = .40mm

Figure 70

Table 8 A ; m vs Stress

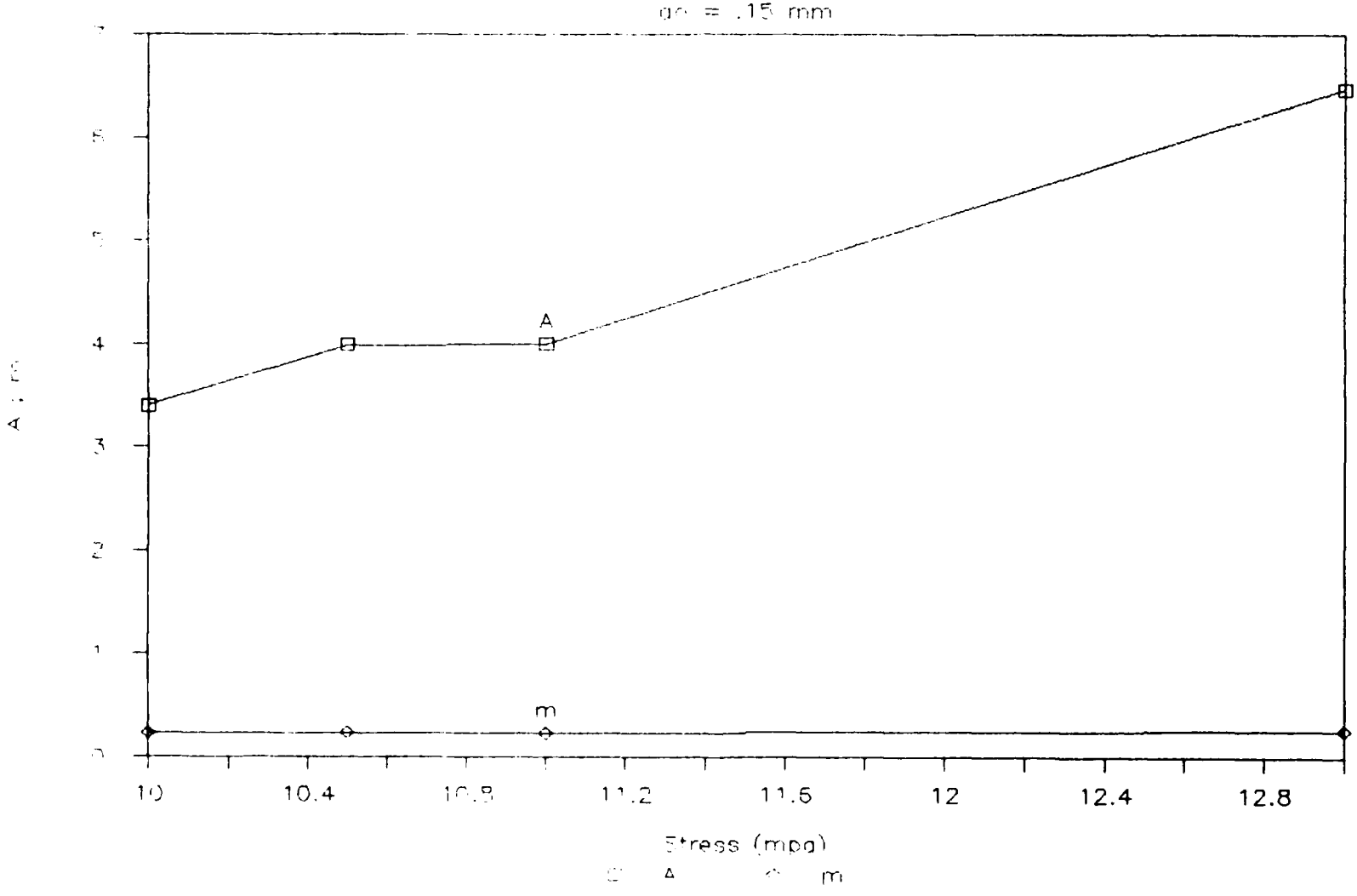

Figure 71

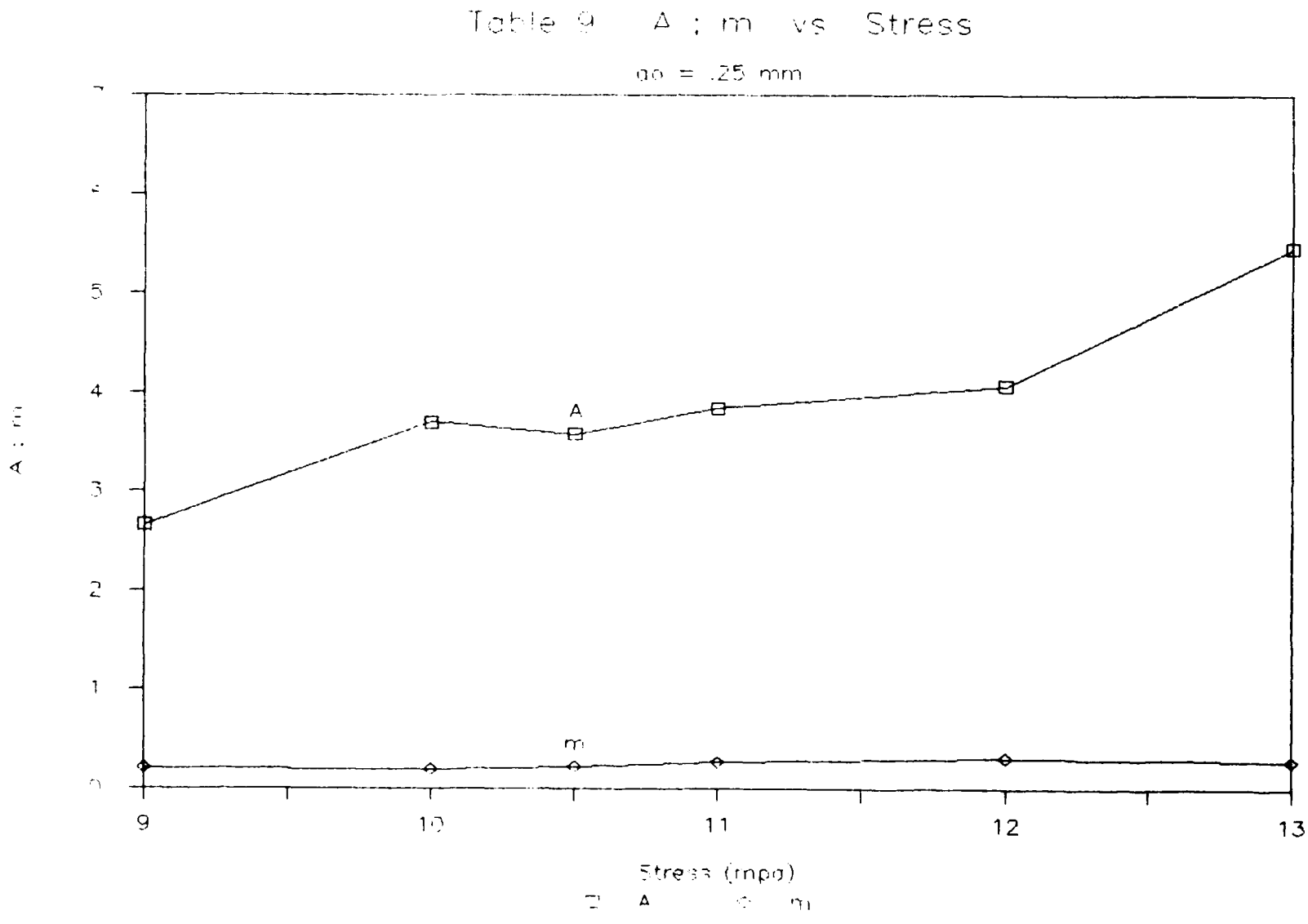

Figure 72

Table 10 A ; m vs Stress

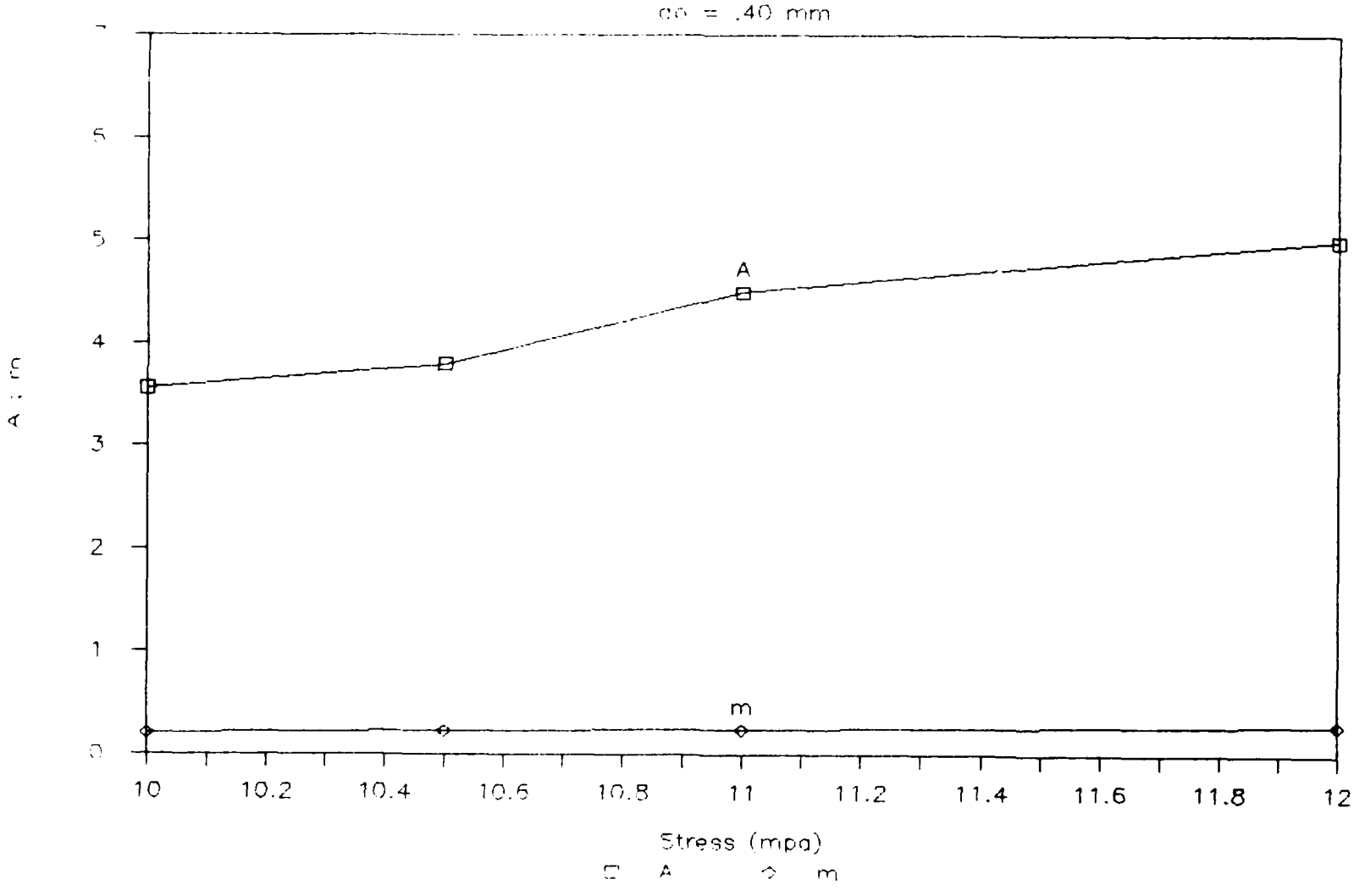

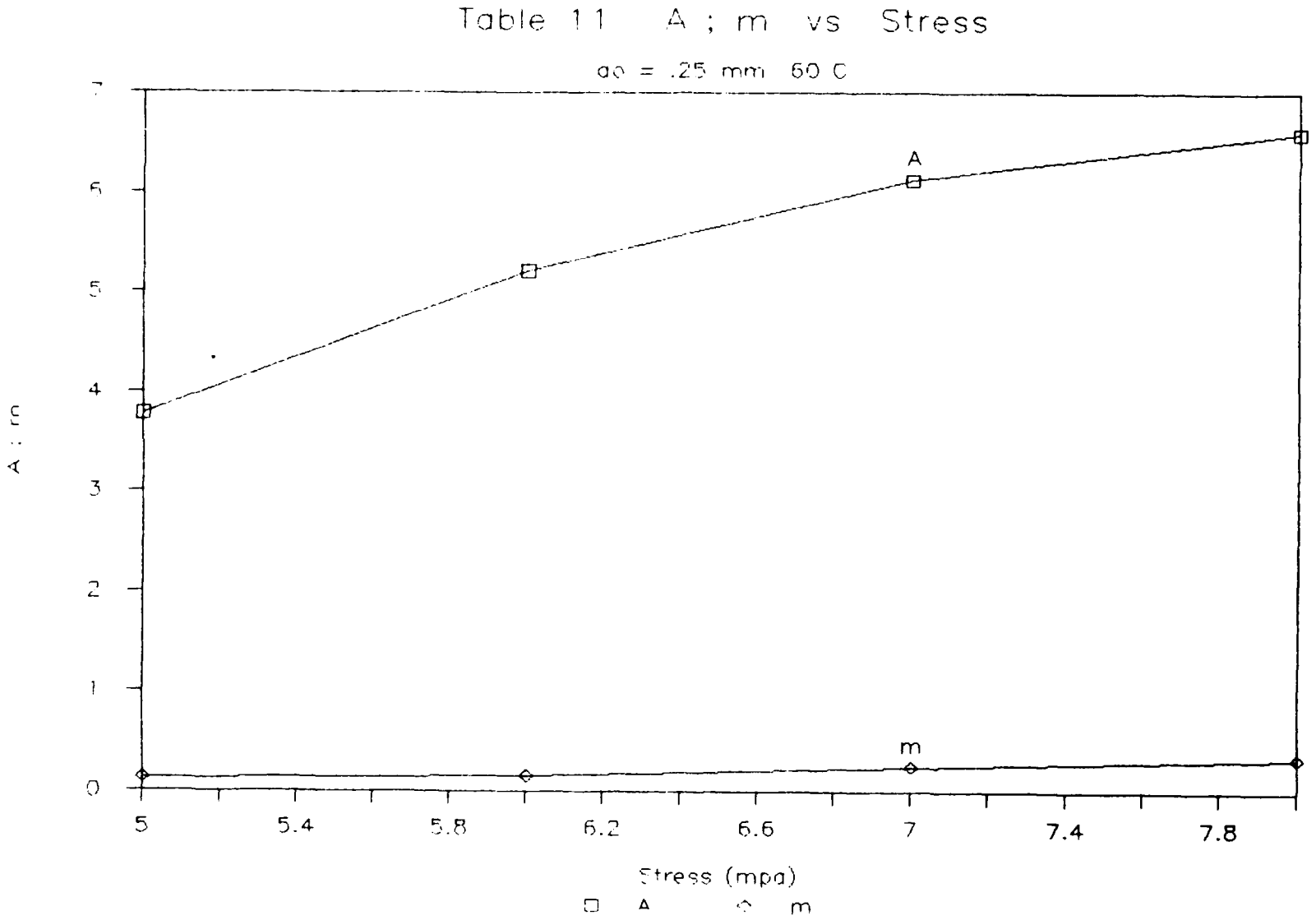
Table 11 A ; m vs Stress
ao = .25 mm 60 C
A ; m
7
6
5
4
3
2
1
0
A
m
5
5.4
5.8
6.2
6.6
7
7.4
7.8
Stress (mpa)
A
m

Figure 74

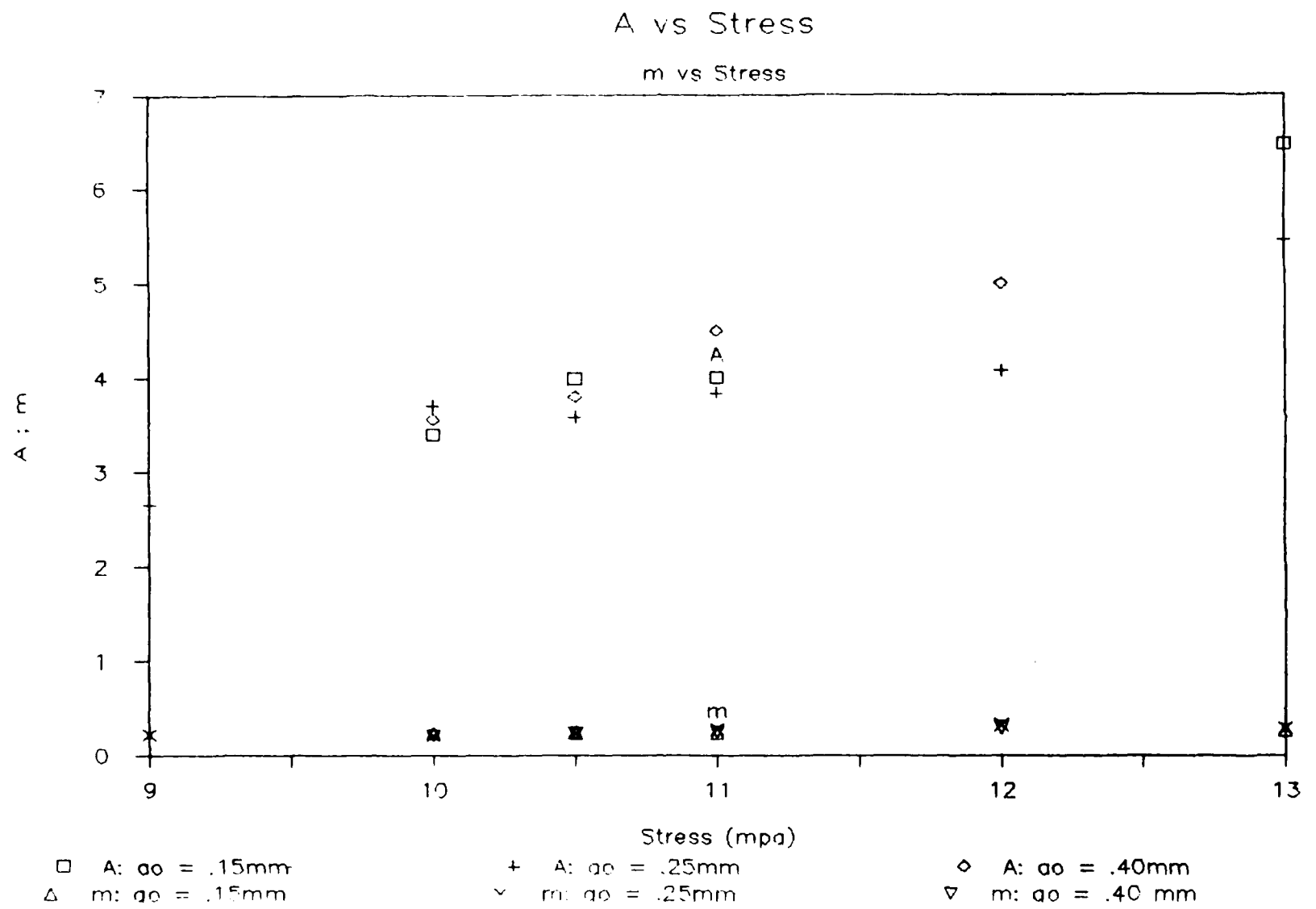
A vs Stress
m vs Stress
A ; m
0
1
2
3
4
5
6
7
9
10
11
12
13
Stress (mpa)
A
m
A: ao = .15mm
A: ao = .25mm
A: ao = .40mm
m: ao = .15mm
m: ao = .25mm
m: ao = .40 mm

Figure 75

END

9-87

DTIC